Hewson, Simon Andrew John (1996) ***A structural examination of the Telfer gold-copper deposit and surrounding region, northwest Western Australia: the role of polyphase orogenic deformation in ore-deposit development and implications for exploration.*** **PhD thesis, James Cook University.**

A Structural Examination of the Telfer Gold-Copper Deposit and Surrounding Region, northwest Western Australia: The Role of Polyphase Orogenic Deformation in Ore-deposit Development and Implications for Exploration.

VOLUME 2

Thesis submitted by
Simon Andrew John HEWSON **BSc** (Hons) (Curtin)
in October, 1996

for the degree of Doctor of Philosophy in the
Department of Earth Sciences at
James Cook University of North Queensland.

CONTENTS of VOLUME 2

APPENDICES

CONTENTS of MAP CASE

MAPS

MAP 1 - Structural Geology of the Telfer Mine (1:7,500)

MAP 2 - Structural Geology of the Telfer region (1:100,000)

MAP 2B - Structural Geology of the O'Callaghans Corridor (1:50,000)

ENCLOSURES: Laminated full A4 size versions of figures that are regularly referred to in the text (*e.g.* deformation chronology tables, regional maps etc.) are also enclosed in the Map Case. A number of regularly referred to figures are also enclosed in the Map Case. These have been included for the reader to hold/place in front of themselves so as to negate the need to search backwards through the Figure volume for reference to these figures.

ENCLOSURE 1 - Summary Table of the Deformation History in the Telfer Region (For use with Sections A, C, D & E).

ENCLOSURE 2 - Geology of the Rudall Metamorphic Complex and Lower Yeneena Group, Paterson Province, and field locations. (For use with Section B).

ENCLOSURE 3 - Stratigraphic Distribution of Stratabound Mineralised Reefs in the Telfer Dome. (For use with Sections C & D).

ENCLOSURE 4 - Structural Geology of the Telfer Dome/Mine. (For use with Section D).

ENCLOSURE 5 - Regional Geological Map of the Telfer District (For use with Section E, and Section A).

TWO GENERAL USE ENCLOSURES:

1. Orientation of Unoriented Drill Core Utilising Cleavage-Bedding Relationships.
2. Conceptual Exploration Models for the Telfer Region/Paterson Province - schematic flow chart.

SECTION A

Multiple Orthogonal Overprinting Deformation Events in the Telfer Region, W.A.: Preservation of a Complex Tectonic History in Weakly Deformed Rocks.

(FIGURES)

Figure 1: Simplified geological map of the Paterson Province, northwest Western Australia. This province, located at the SW margin of the Paterson Orogen, comprises two major litho-tectonic units; the early to middle Proterozoic Rudall Metamorphic Complex and the middle to late-Proterozoic Yeneena Basin that unconformably overlies it. The province is surrounded by various Archean (Pilbara Craton), Proterozoic (Savory, Bangemall and Karara Basins) and Phanerozoic (Officer Basin) rock units. The Yeneena Basin is divided into three geographic divisions (Williams, 1990a). The study area (outlined) comprised rocks of the North-western Zone surrounding the Telfer deposit, and immediately adjacent (SW side) to the Karakutikati Range. (Redrawn from fig. 3-67 - Williams, 1990a).

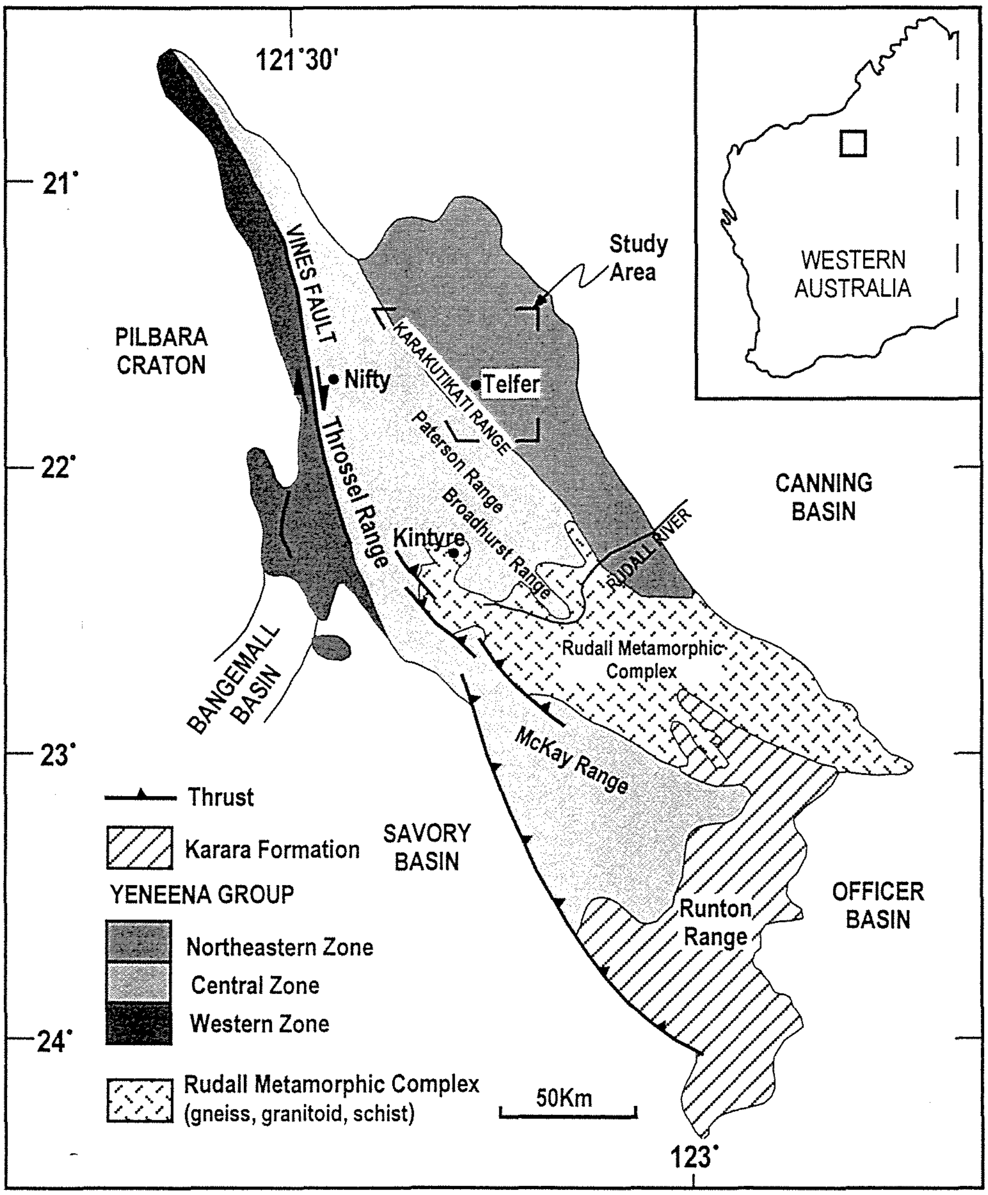
121°30'
21°
22°
23°
24°
123°
WESTERN AUSTRALIA
Study Area
PILBARA CRATON
VINES FAULT
Nifty
Telfer
KARAKUTIKATI RANGE
Paterson Range
Throssel Range
Broadhurst Range
Kintyre
RUDALL RIVER
CANNING BASIN
Rudall Metamorphic Complex
BANGEMALL BASIN
McKay Range
SAVORY BASIN
OFFICER BASIN
Runton Range
Thrust
Karara Formation
YENEENA GROUP
Northeastern Zone
Central Zone
Western Zone
Rudall Metamorphic Complex (gneiss, granitoid, schist)
50Km

***Figure** 2*: Photograph of centimetre-scale monoclinal D_1 folding within an interbedded siltstone unit in the Telfer Gold Mine. The hinge and NE dipping short limb are thickened relative to the SW dipping long limbs, which are attenuated. A coarsely spaced cleavage, S_1, is axial plane to the fold and preferentially developed in siltstone laminae. The photograph is looking NW, and the fold lies on the SW limb of West Dome in the Telfer Dome. (Location: NW face of Pit 11, Telfer Gold Mine; Mine Grid: 15010N, 8850E / see Map 1).

***Figure** 3*: Photomicrographs of S_1 from a micaceous bed in the Telfer Mine. (**A**) S_1 lies at a low angle to bedding and is penetratively developed in micaceous units, such as that in the lower half of the picture. The thin section was cut in the vertical plane and trends 020-200°; the scale bar at the bottom right represents 0.2mm, and the box outlines the area shown in (B); (**B**) S_1 is a coarsely spaced and weakly differentiated crenulation/seamy cleavage that crenulates a micaceous bedding fissility. The orientation is as for (A), and the scale bar at bottom right represents 0.04mm. (*JCU Catalogue No. 48341*)


OLYMPUS
S1

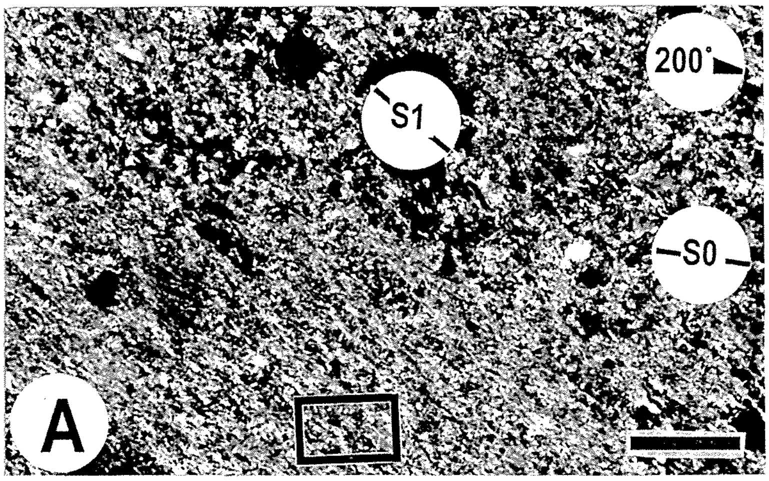
200°
S1
S0
A

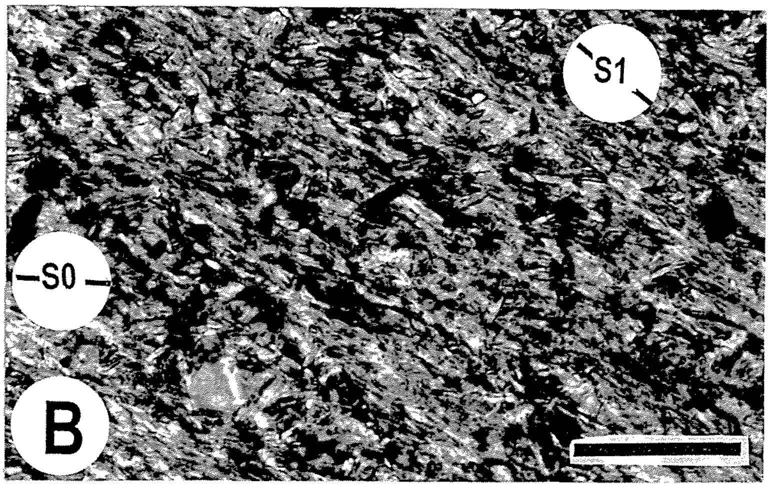
S1
S0
B

Figure 4: Cross-sectional field sketch (looking NW) illustrating D_1-S_1 fold-cleavage relationships (main figure) and cleavage-bedding relationships along the long limbs of D_1 folds (inset). S_1 lies axial plane to the D_1 monoclines and exhibits a top-to-the-SW shear sense, locally producing an extensional crenulation (*e.g.* Platt & Vissers, 1980) geometry against bedding on the SW limbs. This is consistent with the apparent attenuation (extensional thinning) of the SW limbs during D_1.

Figure 5: Field sketch (looking NW - redrawn from photograph) of centimetre-scale parasitic D_1 folding illustrating the SW directed shear sense indicated by fold asymmetry. The shorter NE fold limbs retain an original sedimentary thickness, whilst the longer SW limbs are attenuated along shear planes that parallel the axial plane. The deflection of bedding through these shear planes indicates a top-to-the-SW shear sense consistent with other indicators. The folds are located on the shallow NE dipping limb of a macroscale D_1 fold (see inset; see also fig. 4 - Section D). (Location: NW face of Pit 7, Telfer Gold Mine; Mine Grid: 12500N 10250E / see Map 1).

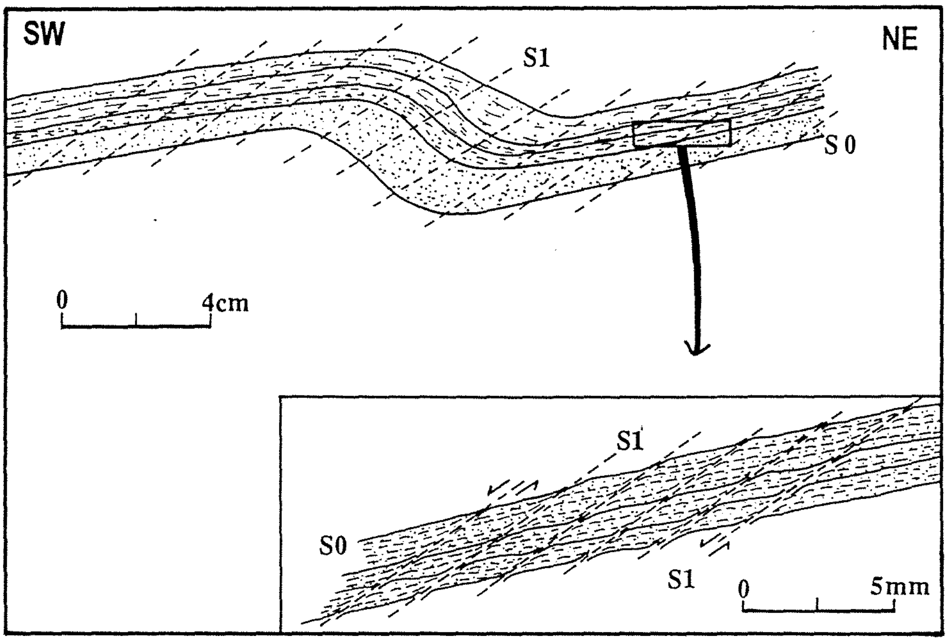
SW
NE
S1
S 0
0
4cm
S1
S0
S1
0
5mm

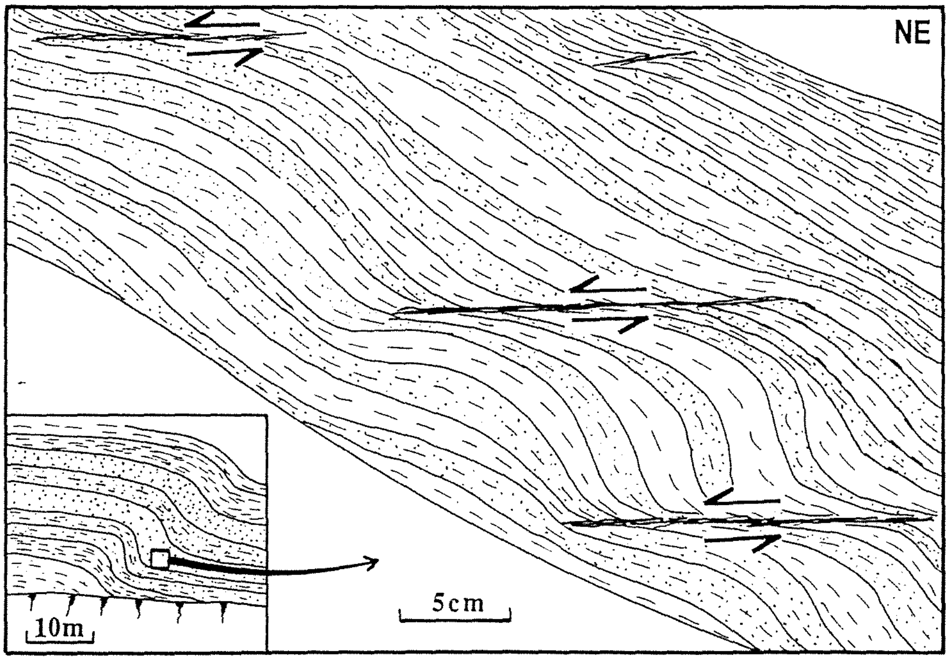
NE
10m
5cm

Figure 6: Photograph of small symmetric intrafolial isoclinal folds on the SE limb of Trotmans Dome (see Map 2 for location of Trotmans Dome). The isoclinal folds formed within finely laminated units and commonly exhibit a low-angle truncation of the long limbs against the enveloping bedding surface. Note the presence of smaller asymmetric folds in the lower left corner of the photograph, the vergence of which is opposite to that of the larger folds suggesting local coaxiality in the deformation. (Location: *AMG* - 7584000mN, 436000mE - see Map 2).

Figure 7: Photographs of isoclinal fold styles at Trotmans Dome. (**A**) Metre-scale isoclinal folding (F_I) that is refolded by D_2 (F_2). The isocline has a steeply NW dipping (to the right in the photograph) axial plane suggesting that it either formed vertical (prior to D_2), or was folded into this orientation post-D_2. The photograph is looking WSW. The small box indicates the location of; (**B**) Parasitic F_I folding in the hinge of the mesoscale isocline. The photograph is looking SW. The folds are at the same location as Fig. 6.

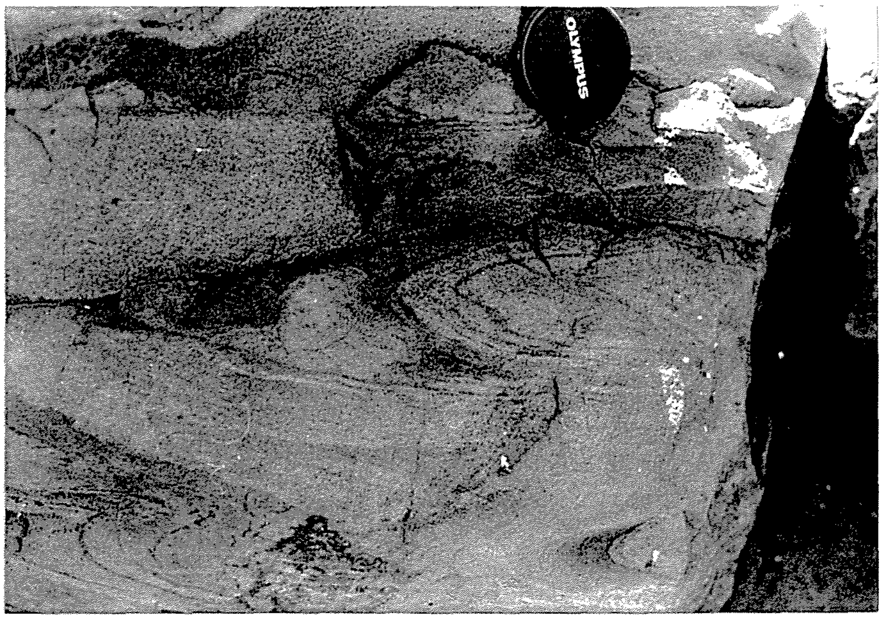
OLYMPUS

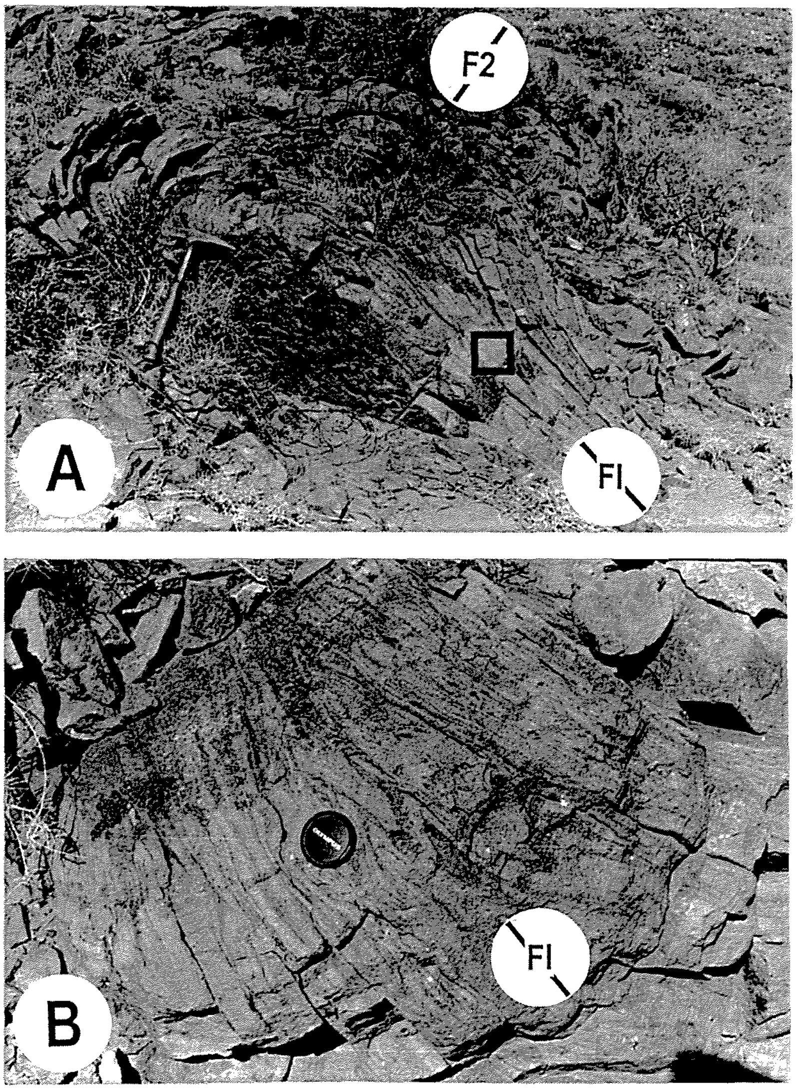
F2
A
Fl
B
Fl

***Figure** 8*: Summary sketches of different intrafolial isoclinal fold styles observed in deep core from the Telfer Dome. (**A**) Tight asymmetric folding of a finely laminar dolomite layer. The fold asymmetry suggests a potential shear sense across the fold as shown. (**B**) Symmetric intrafolial isoclinal folds that exhibit well formed parasitic folds along their limbs, and appear to be slightly discordant against the enveloping laminae. The laminae between the two symmetric folds are asymmetrically drag folded, with an opposite sense to that of the isoclinal folds, suggesting post-isocline layer-parallel shearing and disruption. (**C**) Symmetric isoclinal folds that lie within faulted and disrupted laminae. (All examples observed in the Lower Limy Unit, Main Dome (see Section D). Diamond Drill Hole: *MRC* 185-30; Depth, 1023m).

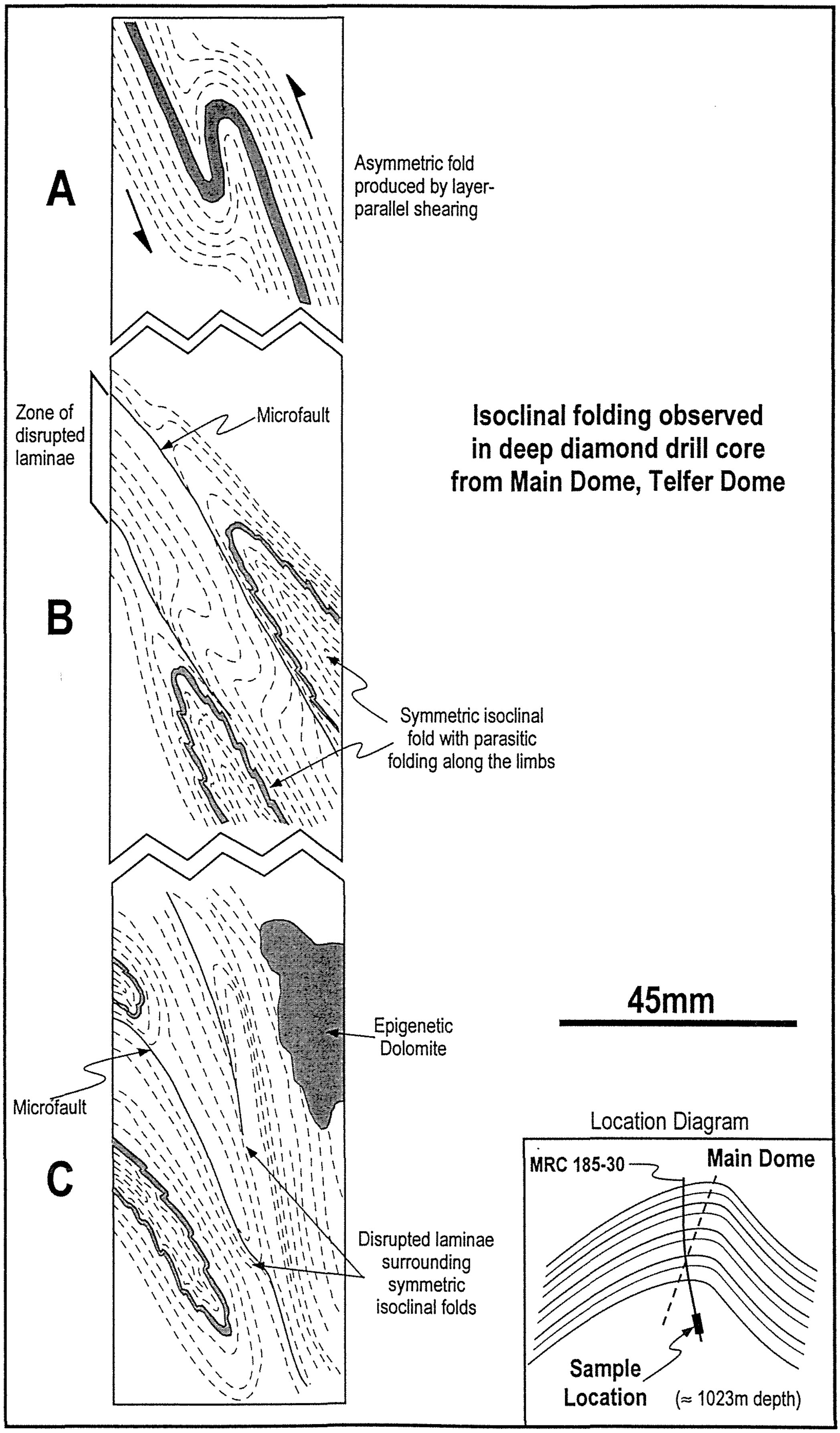

A
Asymmetric fold produced by layer-parallel shearing
Zone of disrupted laminae
Microfault
B
Symmetric isoclinal fold with parasitic folding along the limbs
Isoclinal folding observed in deep diamond drill core from Main Dome, Telfer Dome
45mm
Epigenetic Dolomite
Microfault
C
Disrupted laminae surrounding symmetric isoclinal folds
Location Diagram
MRC 185-30
Main Dome
Sample Location
(≈ 1023m depth)

Figure 9: Sketch map and schematic development models for isoclinal folding on the NE limb of Trotmans Dome. (**A**) Sketch map of a metre-scale isoclinal fold (**F_I** - illustrated in Fig. 7A), which is refolded by D_2, illustrating the orientations of minor folds of different generations in the outcrop. The isoclinal fold also appears to have been refolded by D_5 (axis marked on page). Trotmans Dome is located approximately 10-15kms SE of Telfer (see fig. 1 in Section E; Map 2, 2B). (**B**) Schematic flow-diagram (cross sectional - looking NW) illustrating potential development paths (large arrows) for the isoclinal fold. The isoclinal fold may have initially formed pre-D_1 as an upright fold, which was subsequently rotated into a recumbent orientation during D_1 (**I**); or may have formed during D_1 as a recumbent asymmetric fold (**ii**). Either (i) or (ii) could then have been refolded by D_2 onto the NE limb of Trotmans Dome (**iii**).

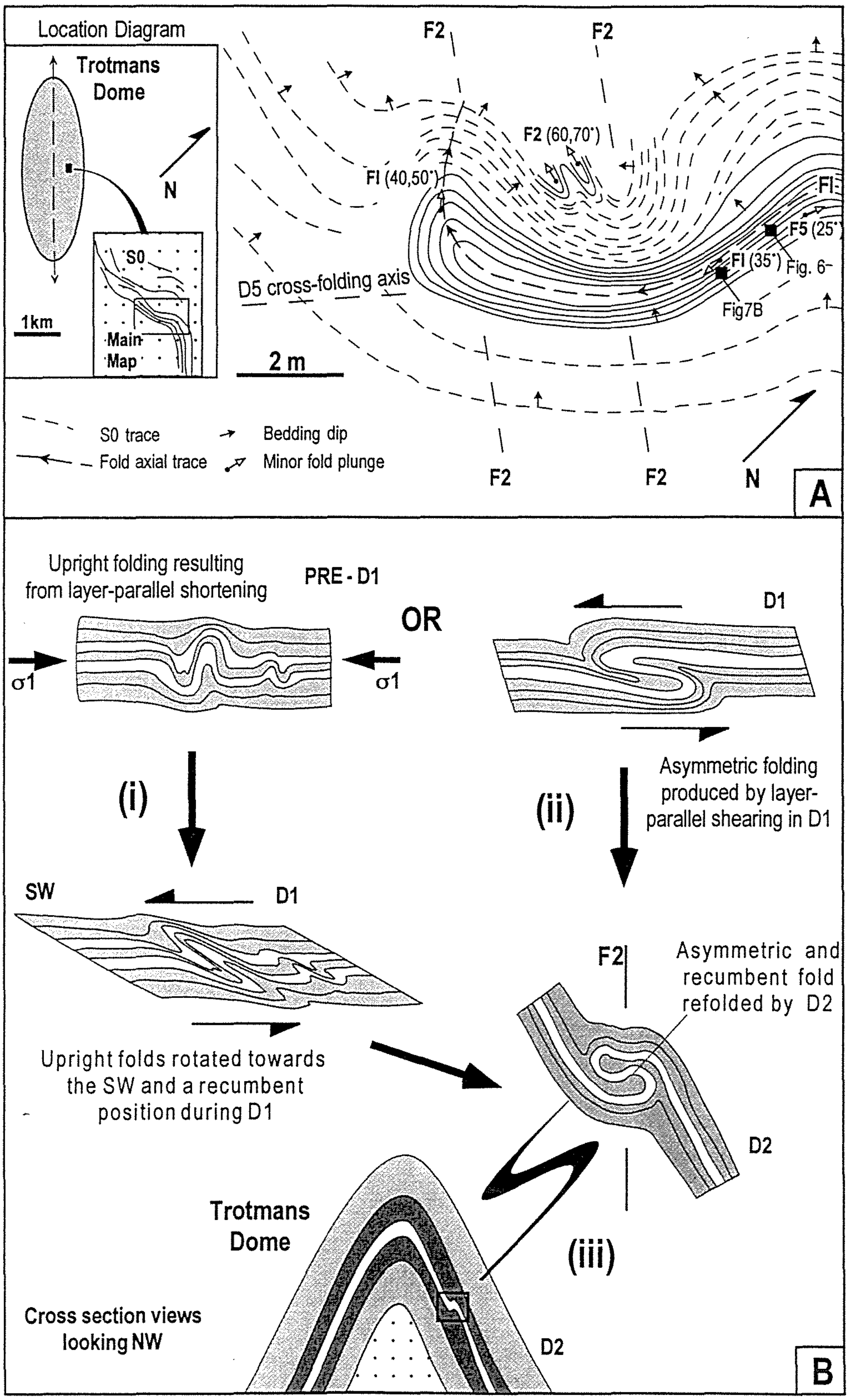
Location Diagram
Trotmans Dome
N
S0
1km
Main Map
2 m
F2
F2 (60,70°)
FI (40,50°)
FI
F5 (25°)
FI (35°)
Fig. 6
Fig7B
D5 cross-folding axis
S0 trace
Fold axial trace
Bedding dip
Minor fold plunge
F2
F2
N
A
Upright folding resulting from layer-parallel shortening
PRE - D1
OR
D1
σ1
σ1
Asymmetric folding produced by layer-parallel shearing in D1
(i)
(ii)
SW
D1
F2
Asymmetric and recumbent fold refolded by D2
Upright folds rotated towards the SW and a recumbent position during D1
D2
Trotmans Dome
(iii)
Cross section views looking NW
D2
B

Figure 10: Schematic cross section through a D_2 fold showing S_1/S_2 cleavage-bedding and vergence relationships. On the SW limb both S_1 and S_2 exhibit the same cleavage-bedding vergence, whilst on the NE limb the two are opposite. The insets illustrate the overprinting (crenulation) relationships between S_1 and S_2 (**C**), and crenulation of S_2 by bedding reactivation (Bell, 1986; **R**). For (C) note the changing shear sense of S_2 crenulations on either side of the dome (observed in outcrop and thin section for S_2 against S_0/S_1 foliations).

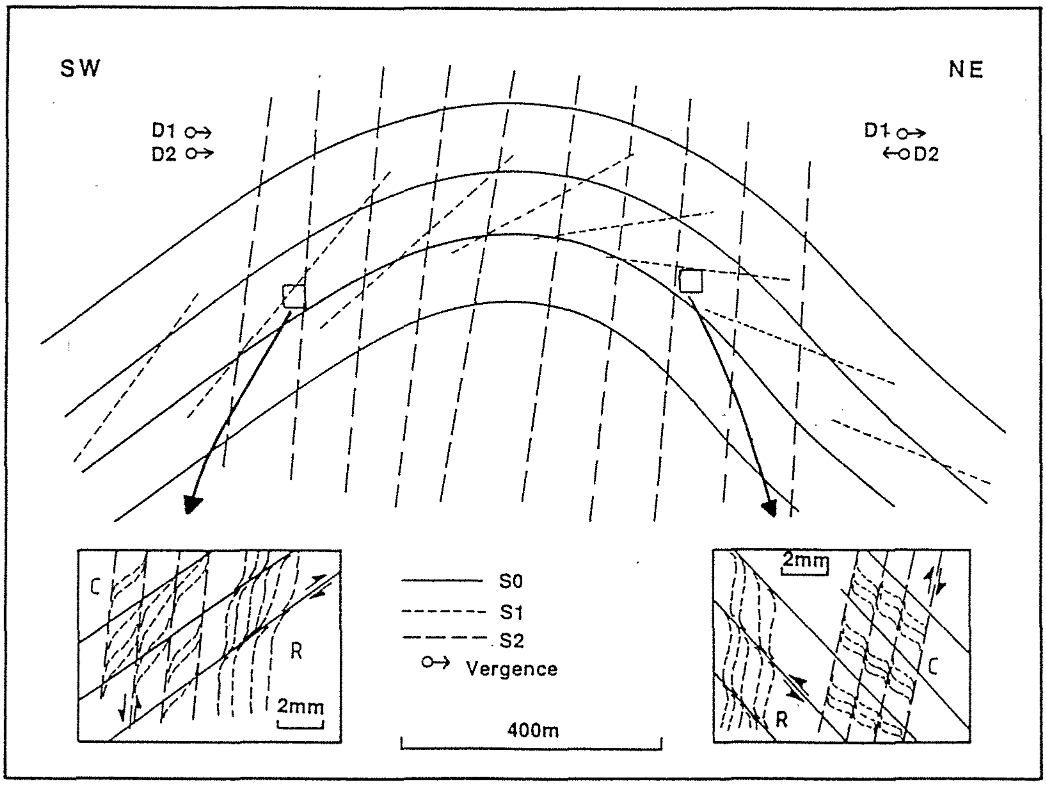

SW
NE
D1
D2
D1
D2
C
R
2mm
S0
S1
S2
Vergence
400m
2mm
C
R

Figure 11: Photograph of a mesoscale D_3 fold in finely laminar units of the Isdell Formation, SW of Telfer (view looking NW along the axial trend of regional D_2 folding). A fine-scale semi-discontinuous fracture/crenulation surface (parallel to the pencil) marks the axial plane, the asymmetry of which indicates a top-to-the-NE shear sense/movement direction for D_3 in this locality (Location: *AMG* - 7591102mN 407508mE - see Map 2B).

Figure 12: Field sketch of discrete sub-horizontal spaced S_3 crenulation cleavage (horizontal) overprinting S_2 (vertical). S_2 is evident as fine discontinuous traces, and the S_3 crenulation asymmetry indicates a top-to-the-NE shear sense for D_3 in this location. S_3 is only sporadically preserved at this locality owing to the extensive obliteration of the rock matrix through subsequent metasomatic alteration that accompanied skarn mineralisation (albite porphyroblast formation) and weathering (Location: Minyari Test Pit; *AMG* - 7634000mN 422300mE - see Map 2).

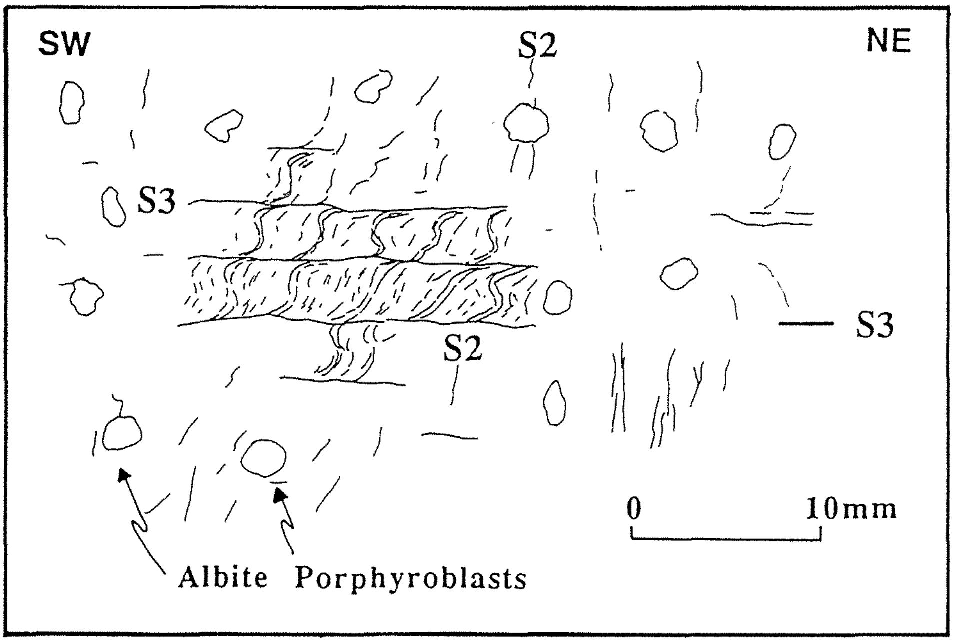
SW
S2
NE
S3
S3
S2
0
10mm
Albite Porphyroblasts

Figure 13: Field sketches (presented schematically) illustrating the various stages of D_2 and D_3 folding that were observed in a laminar bedding-concordant quartz vein in the Telfer Mine. Insets illustrate the location of the quartz vein within siltstones (**i**), at the SE corner of Main Dome (**ii** - filled box). (**A**) Parasitic D_2 folding (exhibiting a SW vergence). The range of D_3 styles, which exhibit an opposite (NE) vergence, includes: (**B**) A weak D_3 perturbation with no axial plane cleavage; (**C**) Moderately tight D_3 fold with no axial plane cleavage; (**D**) Tight D_3 fold with a weakly developed axial plane fabric defined by limited shearing/dissolution; (**E**) Fully formed D_3 fold with shearing/dissolution across the axial plane. (Location: NW face of old Pit 1 Ramp, SE corner of Main Dome, Telfer Gold Mine; Mine Grid: 10450mN 11350mE - see Map 1).

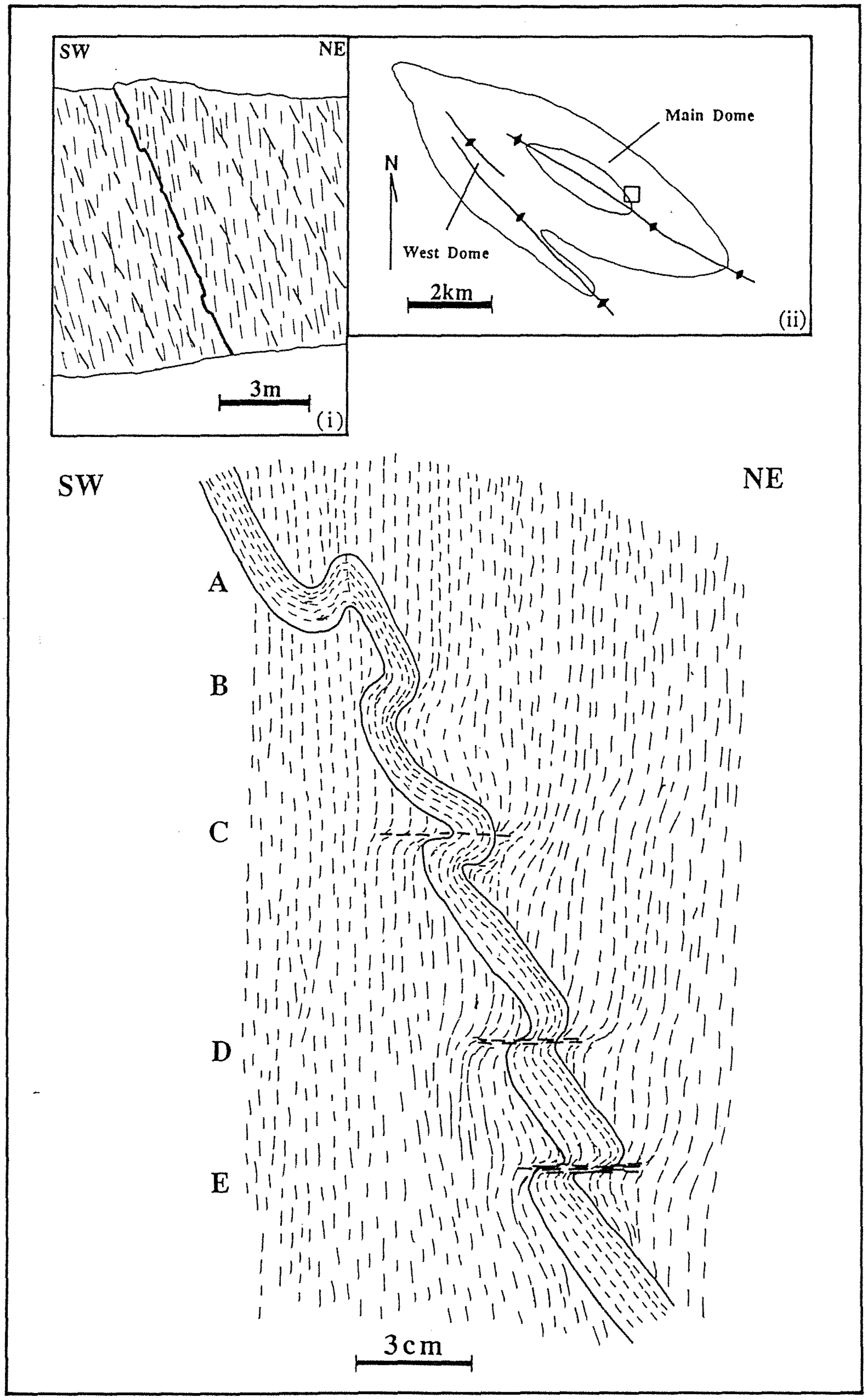
SW
NE
3m
(i)
Main Dome
N
West Dome
2km
(ii)
SW
NE
A
B
C
D
E
3cm

Figure 14: Open D_4 cross-folding of a D_2 fold in a sandy carbonate unit of the Isdell Formation near the Grace prospect (see Map 2, 2B), SW of Telfer. View is to the ENE and the D_2 axial plane lies parallel to the plane of the page. D_4 folding is of limited amplitude (3-5m) and cross-folded D_2 folds where the angular difference between the two was sufficiently high (see text for discussion). The small box marks the location of Fig. 15. (Location: *AMG* 7573560mN 427125mE - see Map 2, 2B).

Figure 15: Photograph of coarsely spaced sub-vertical S_4 crenulation cleavage lying axial plane to the D_4 fold illustrated in Fig. 14. Photograph is looking ENE, and the D_2 axial plane is parallel to the plane of the page. (Location - as for Fig. 14)

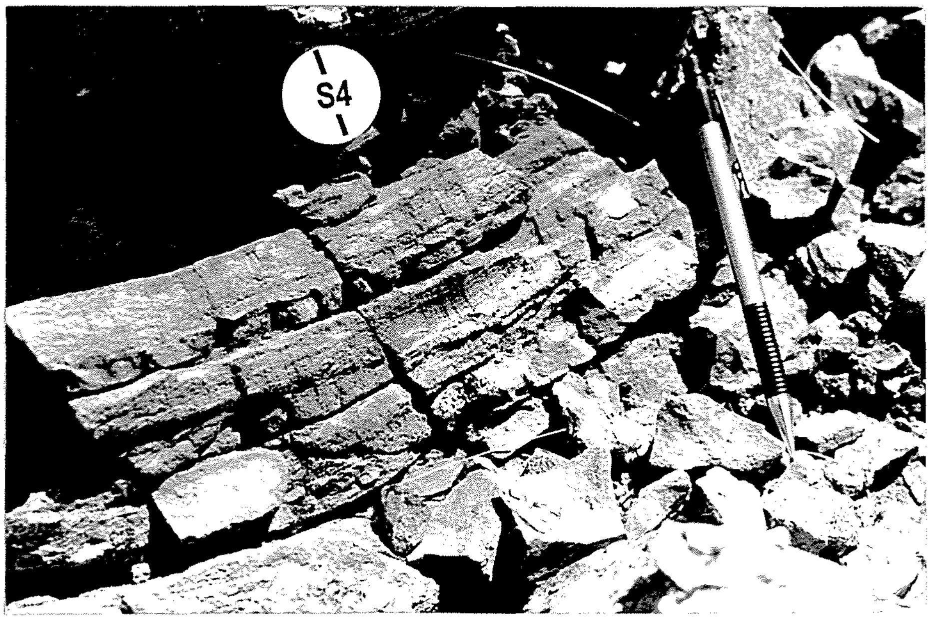
S4

Figure 16: D_5 kink folding styles observed in finely laminated calc-arenite and dolomitic units of the Isdell Formation, immediately adjacent to, but south of, the Karakutikati Range (see Fig. 1). (**A**) Monoclinal kink folding, which commonly terminates in rounded monoclinal folds/flexures. The kinks occasionally exhibit fine-scale dissolution seams along the axial plane. (**B**) Angular kink/crenulation fold that exhibits strong dissolution along the axial plane. The shear sense across the axial plane for both samples is dextral, the photographs are in plan-view and the arrows mark true north. (Location (both A & B): *AMG* 7590000mN 408300mE - see Map 2, 2B).

Figure 17: Equal area plot (contoured) illustrating the orientational distribution of D_5-style kink folds throughout the Telfer region. Two major groups are evident; the D_5 trend (sub-vertical -> 290°) and a further group clockwise from this (sub-vertical -> NNW), with a minor spread between the two. The majority of readings come from the Isdell Formation immediately SW of the Karakutikati Range.

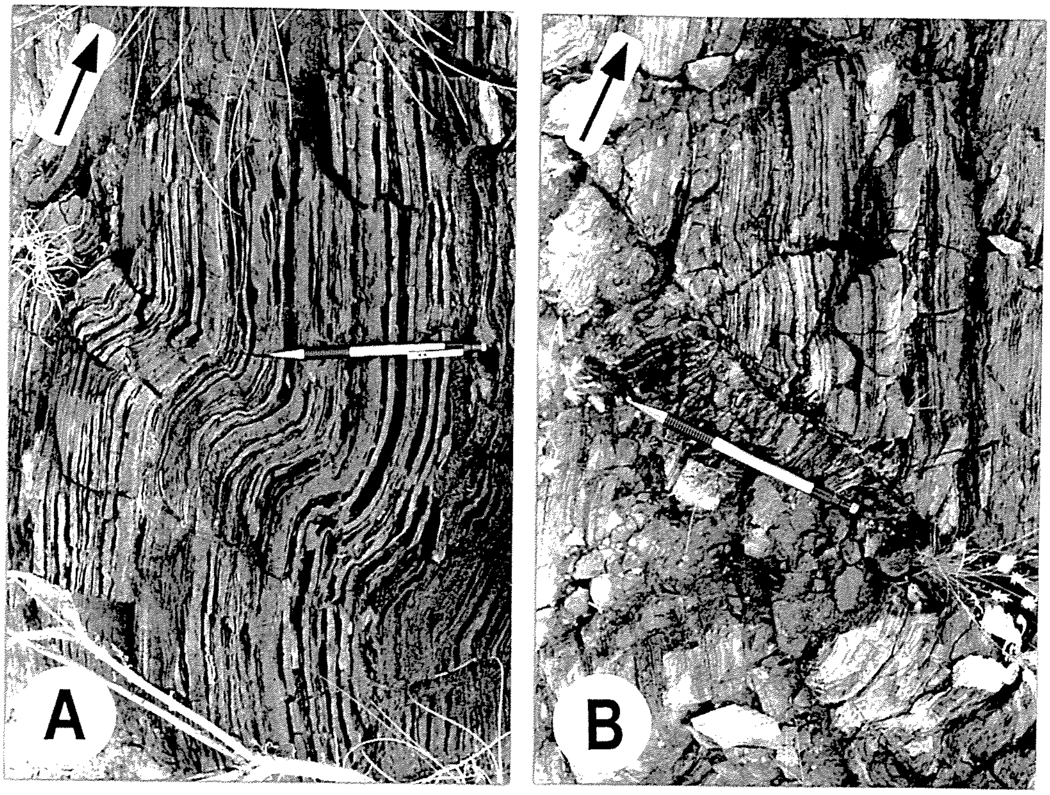
A
B

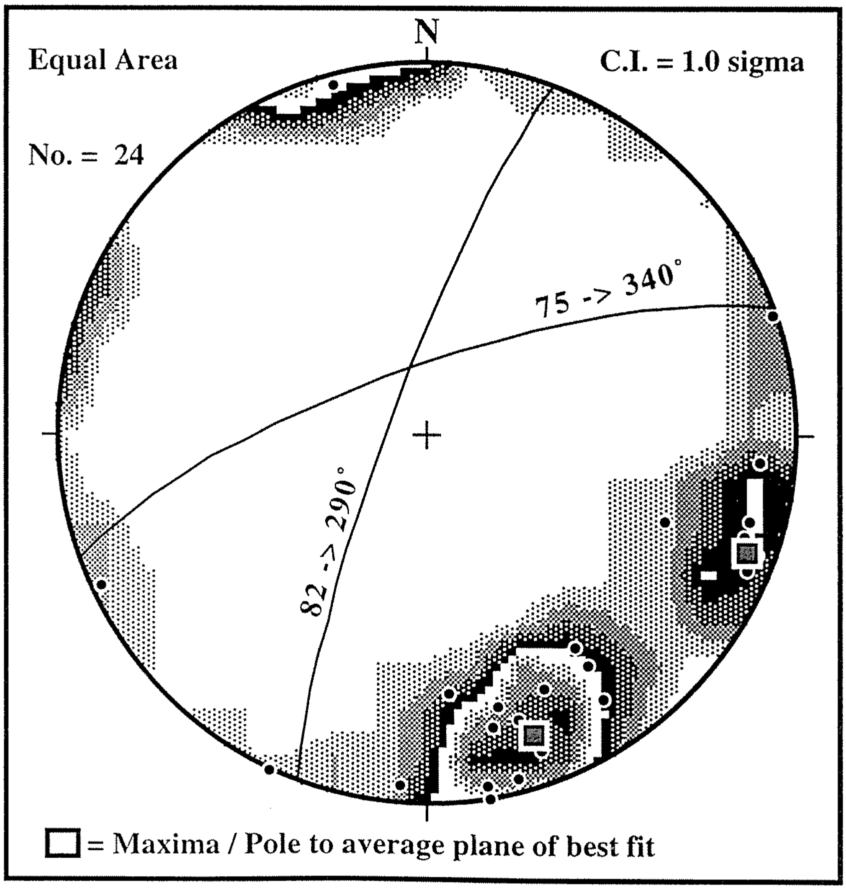
N
Equal Area
C.I. = 1.0 sigma
No. = 24
75 -> 340°
82 -> 290°
= Maxima / Pole to average plane of best fit

Figure 18: Summary table of the proposed deformation sequence for the Telfer region including schematic illustrations of the overprinting relationships. D_{EF} refers to an interpreted period of early horizontal shortening producing upright folds (see text for discussion). D_5 encompasses two separate episodes of compression, D_5 and D_{5b}.

Event	*Style*	*Orientation*	*Tectonic Regime*	*Schematic Overprinting Relations*
D_{EF}	Upright open to tight and isoclinal folding; most examples now recumbent.	NW-SE trending fold axes (no axial plane foliation)	*NE-SW directed tectonic shortening*	
D_1	Recumbent monoclinal folding; locally overturned NE (short) limbs; coarsely spaced axial plane cleavage (S_1), which exhibits a top-to SW shear sense.	S_1 : 15,30° → SW,W F_1^0 : 2,15° → NW,N (both strongly refolded by D_2)	*South-west directed sub-horizontal thrusting/ vertical shortening; locally extensional*	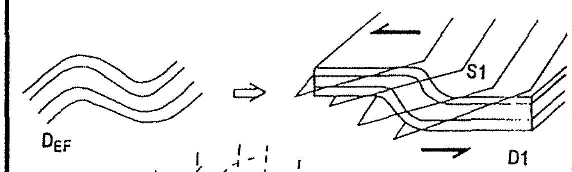
D_2	Upright open to tight NW-SE trending regional folds, with a penetrative axial plane cleavage (S_2).	S_2 : 70,90° → SW, SSW F_2^0 : 0,50° → NW,SE L_2^2 : steep pitch on S2	*NE-SW directed bulk inhomogeneous tectonic shortening (230-050°)*	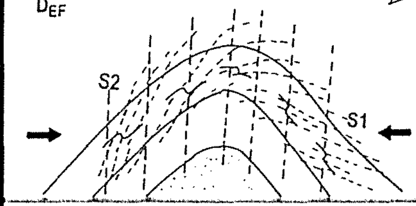
D_3	Recumbent asymmetric monoclinal folding and discrete sub-horizontal crenulations. Most examples are meso-scale; rare axial plane cleavage (S_3).	S_3 : 10,20° → 315,340° F_3^0 , F_3^2 : 0,5° → NNW, NNE	*NE directed sub-horizontal thrusting/differential movement and vertical shortening. Gravity-induced collapse post-D_2.*	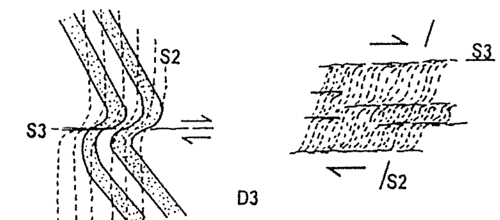
D_4	Upright cross folding of D_2 folds with a rare coarsely spaced axial plane crenulation cleavage (S_4); generally meso-scale folding.	S_4 : 70,85°→ 255, 265 F_4^0 : 40,45° (variable) → 320°	*WSW-ENE directed inhomogeneous tectonic shortening (255-075°)*	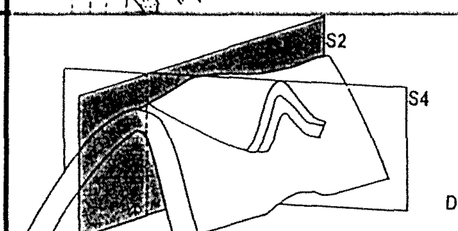
D_5	Upright kink folds, cross folds with associated weak coarsely spaced cleavage (cf. Chin et al, 1982).	S_5: 70,85° → 290,300° (incl. kink fold axial plane)	*WNW-ESE directed inhomogeneous tectonic shortening (290-110°)*	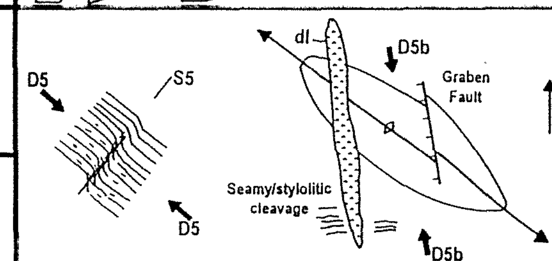
	(b) Mainly brittle structures including veining, dolerite dikes, fault reactivation and kink folds.	S_5: 75,85° → 350, 355° (incl. kink axial plane) *σ_1 = 345-165° to N-S.*	*NNW-SSE / N-S directed tectonic compression (350,000-170,180°)*	

Figure 19: Schematic illustration of two possible ways of forming D_1 monoclines from an earlier fold phase. (**A**) Initial upright open folding, with an associated axial plane cleavage, is overprinted by NE directed sub-horizontal thrusting/ shearing. This produces an asymmetric flexure through bodily rotation of the initial upright fold. Rotation of the axial plane cleavage causes it to be reactivated (antithetic cleavage reactivation - **ACR**), producing a local top-to-the-SW shear sense that is antithetic to the bulk tectonic movement. (**B**) Initial upright open folds, with or without an axial plane cleavage, are overprinted by a SW directed thrusting/ shearing deformation and associated sub-horizontal cleavage (S_1). Bulk movement, accommodated along S_1, causes attenuation of the long limbs of the now monoclinal folds. Cleavage shear sense (top-to-the-SW) is synthetic with respect to the bulk tectonic movement. (B) is the preferred model for D_1 fold formation - see text.

Figure 20: Horizontal D_3 kink folding in the Isdell Formation that is suggestive of vertical crustal shortening. The kinks developed with a markedly inclined axial plane (**F_k**) in sub-vertical finely laminar units (**i**), with the axial plane crenulation asymmetry suggesting top-to-the-NE shearing/movement. Two possible ways to produce this are; (**ii**) synthetic shearing along a shear band/micro-fault plane, inclined NE, during NE directed D_3 movement. *or* (**iii**) vertical shortening of the sub-vertical bedding/laminae producing a kink fold, whose axial plane was inclined with respect to the layering and the prevailing compression. The latter (iii) is the preferred development history given the kink-like character of the crenulation plane and its occurrence in finely laminated units (see text); this implies vertical crustal shortening during D_3.

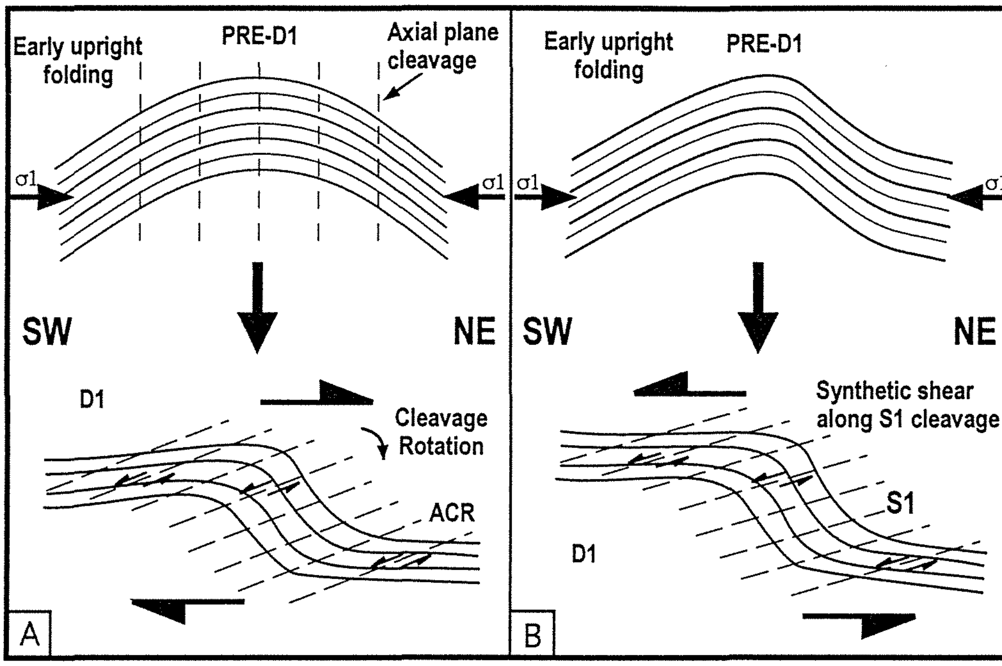

Early upright folding
PRE-D1
Axial plane cleavage
σ1
σ1
SW
NE
D1
Cleavage Rotation
ACR
A
Early upright folding
PRE-D1
σ1
σ1
SW
NE
Synthetic shear along S1 cleavage
S1
D1
B

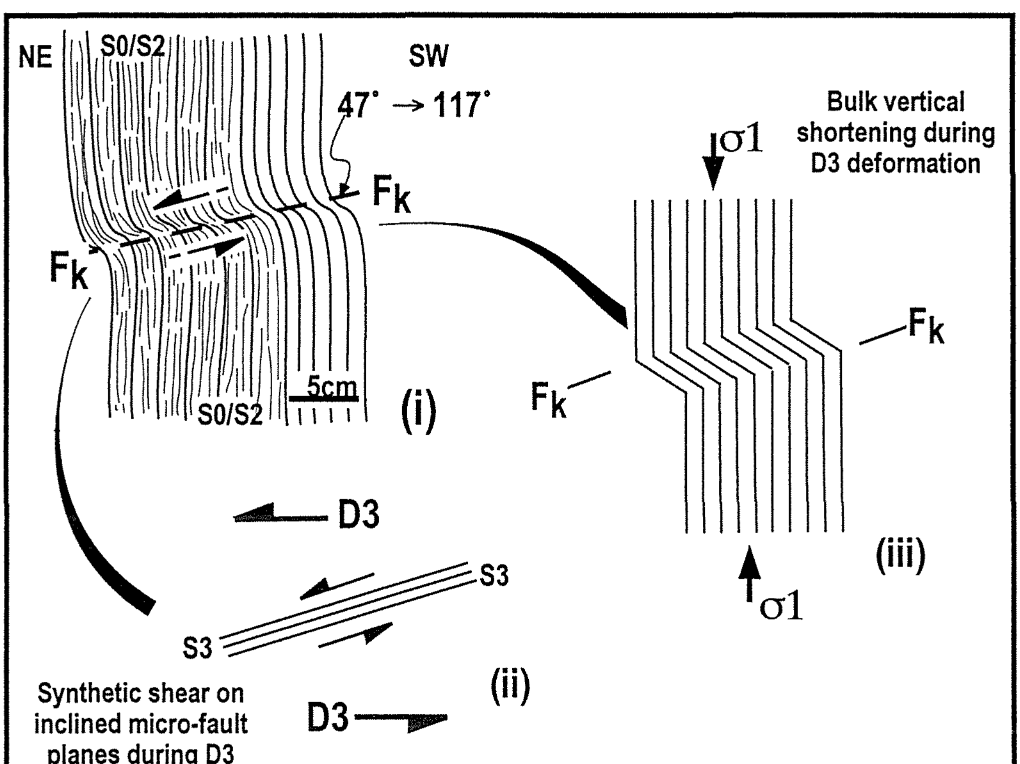

NE
S0/S2
SW
47° → 117°
Fk
Fk
5cm
S0/S2
(i)
Bulk vertical shortening during D3 deformation
σ1
Fk
Fk
(iii)
σ1
D3
S3
S3
Synthetic shear on inclined micro-fault planes during D3
D3
(ii)

Figure 21: Schematic diagram illustrating the variable effects (observed/interpreted) of NE directed D_3 deformation on a D_2 fold. The main diagram illustrates a D_2 fold where D_3 has refolded the hinge and axial plane cleavage (S_2), and the insets illustrate the mesoscale effects around this fold: (**A**) The SW limb is more likely to be antithetically reactivated (bedding), rather than deformed, by D_3 given its trailing orientation with respect to NE directed tectonic movement. S_3 may form in zones of high D_3 strain; where this occurs it will have an extensional crenulation geometry. (**B**) In contrast, the NE limbs, which are oriented against the bulk D_3 movement, are more likely to be deformed resulting in sub-horizontal crenulation folding of bedding and S_2. The crenulation asymmetry should mimic the larger bulk movement (Bell & Johnson, 1992). (**C**) In regions of steeply oriented bedding, sub-vertical D_3 shortening may produce symmetrical crenulations (*ie.* coaxial deformation), in addition to asymmetric crenulations/folds as in (B).

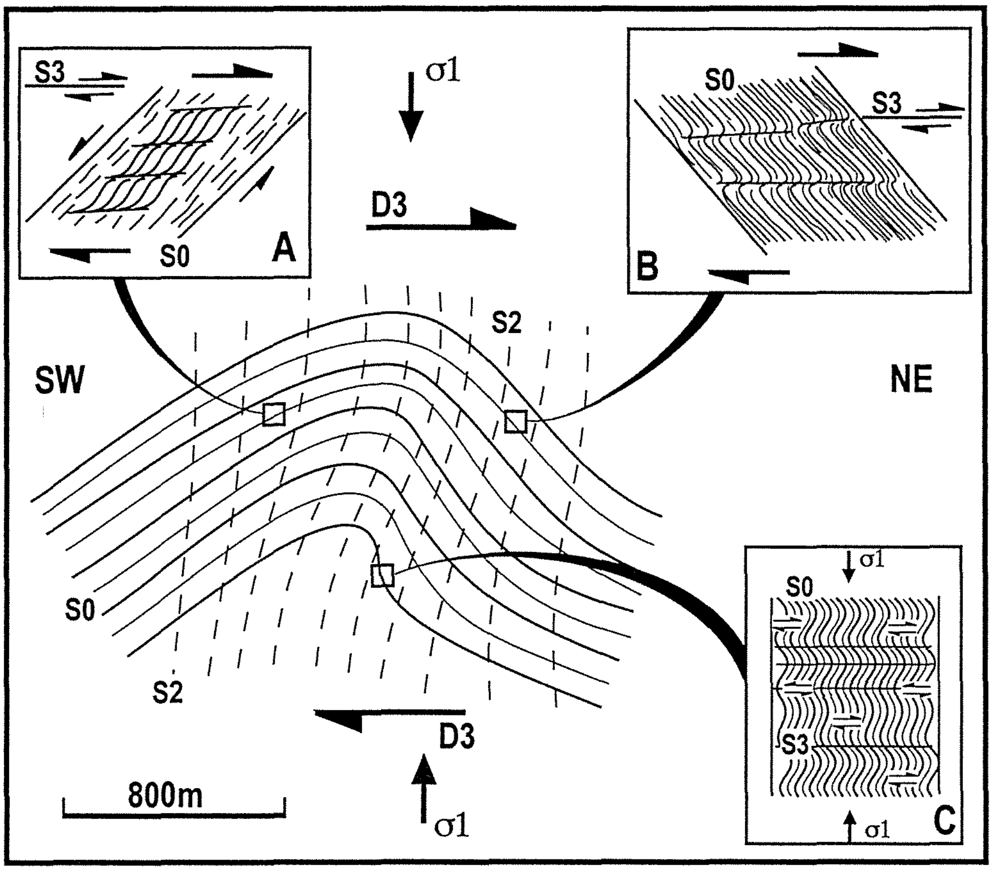

S3
S0
A
σ1
D3
S0
S3
B
SW
S2
NE
S0
S2
σ1
S0
S3
σ1
C
D3
800m
σ1

SECTION B

Structural Reconnaissance of the Lower Yeneena Group, Paterson Province, W.A.; Overprinting of an Ensialic Intracratonic Basin by Migrating late-Proterozoic Collisional Orogenesis and Resolution of Conflicting Tectonic Indicators.

(FIGURES)

Figure 1: Map of western and central Australia showing the location of the Paterson Province and Paterson Orogen with respect to other Archean and Proterozoic terranes. The Paterson Orogen trends NW-SE across northern and central Australia, lies marginal to the West Australian Shield (Myers & Hocking, 1988), and truncates the Albany-Fraser Orogen. A large gravity ridge under much of its length (the Anketell Gravity Ridge - Fraser, 1976) indicates continuity to central Australian orogens and sedimentary basins (*e.g.* Musgrave Complex, Amadeus Basin). The orogen is bounded to the east by the Archean Pilbara Craton, and the southwest by the middle Proterozoic Capricorn Orogen (*e.g.* Tyler & Thorne, 1990). It is covered to the north by the Canning Basin, and to the southeast by the Officer Basin (both Phanerozoic in age). The inset illustrates the geology of the Paterson Province (also shown in Fig. 2). The Yeneena Group (light stipple) overlies the basement Rudall Metamorphic Complex (cross stipple). Both are overlain by the Karara Basin (dark stipple).

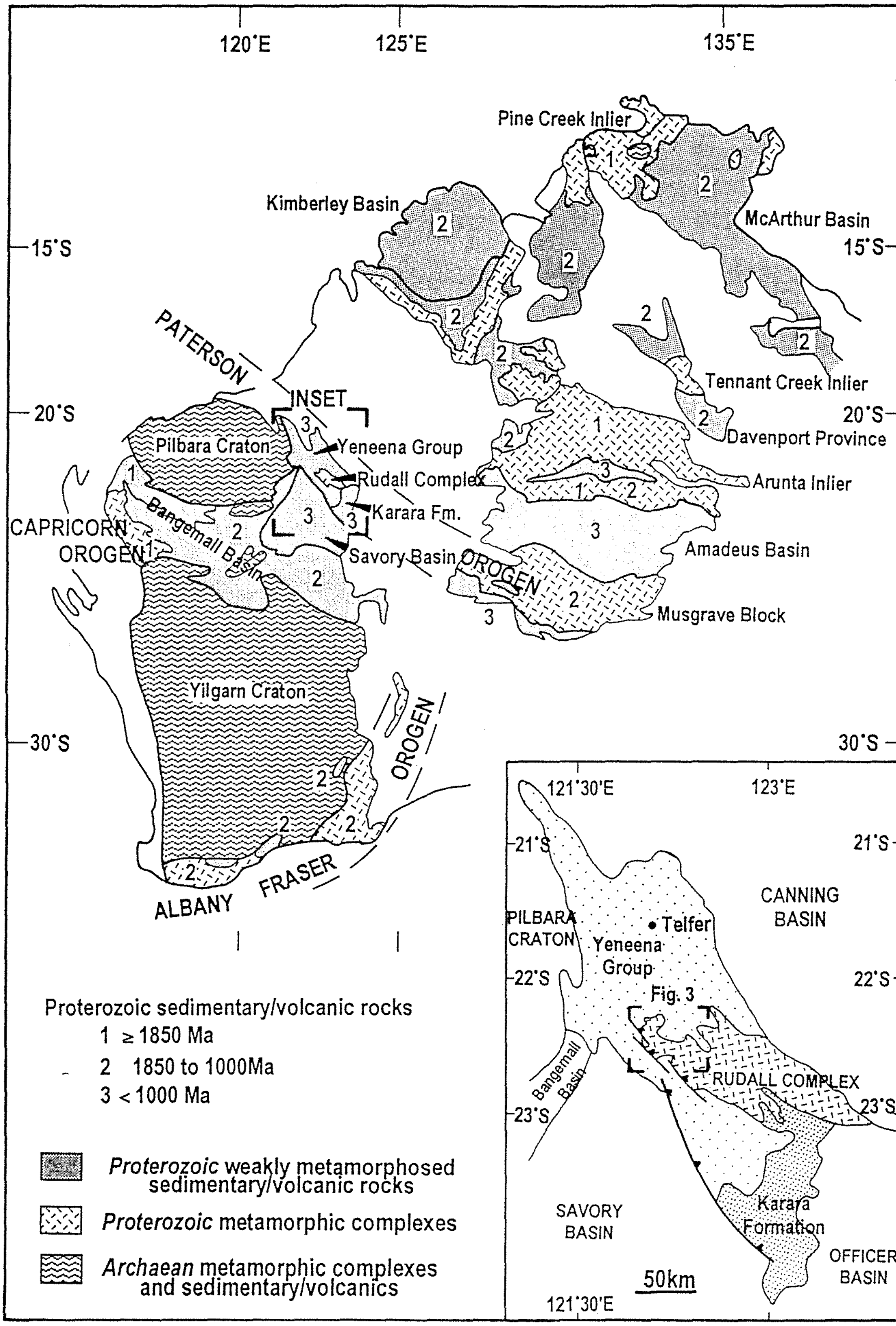
120°E
125°E
135°E
15°S
20°S
30°S
Pine Creek Inlier
Kimberley Basin
McArthur Basin
PATERSON
INSET
Tennant Creek Inlier
Davenport Province
Pilbara Craton
Yeneena Group
Rudall Complex
Arunta Inlier
Karara Fm.
CAPRICORN OROGEN
Bangemall Basin
Savory Basin
OROGEN
Amadeus Basin
Musgrave Block
Yilgarn Craton
OROGEN
ALBANY
FRASER
121°30'E
123°E
21°S
22°S
23°S
CANNING BASIN
PILBARA CRATON
Telfer
Yeneena Group
Fig. 3
Bangemall Basin
RUDALL COMPLEX
SAVORY BASIN
Karara Formation
OFFICER BASIN
50km
Proterozoic sedimentary/volcanic rocks
1 ≥ 1850 Ma
2 1850 to 1000Ma
3 < 1000 Ma
Proterozoic weakly metamorphosed sedimentary/volcanic rocks
Proterozoic metamorphic complexes
Archaean metamorphic complexes and sedimentary/volcanics

Figure 2: Simplified map of the Paterson Province illustrating the two main lithostratigraphic units, the Rudall Metamorphic Complex and the Yeneena Basin/Group. The Yeneena Group is divided into three geographic zones (after Williams, 1990a) whose stratigraphic succession is summarised in the table below the diagram. The Karara Basin unconformably overlies the Yeneena Basin.

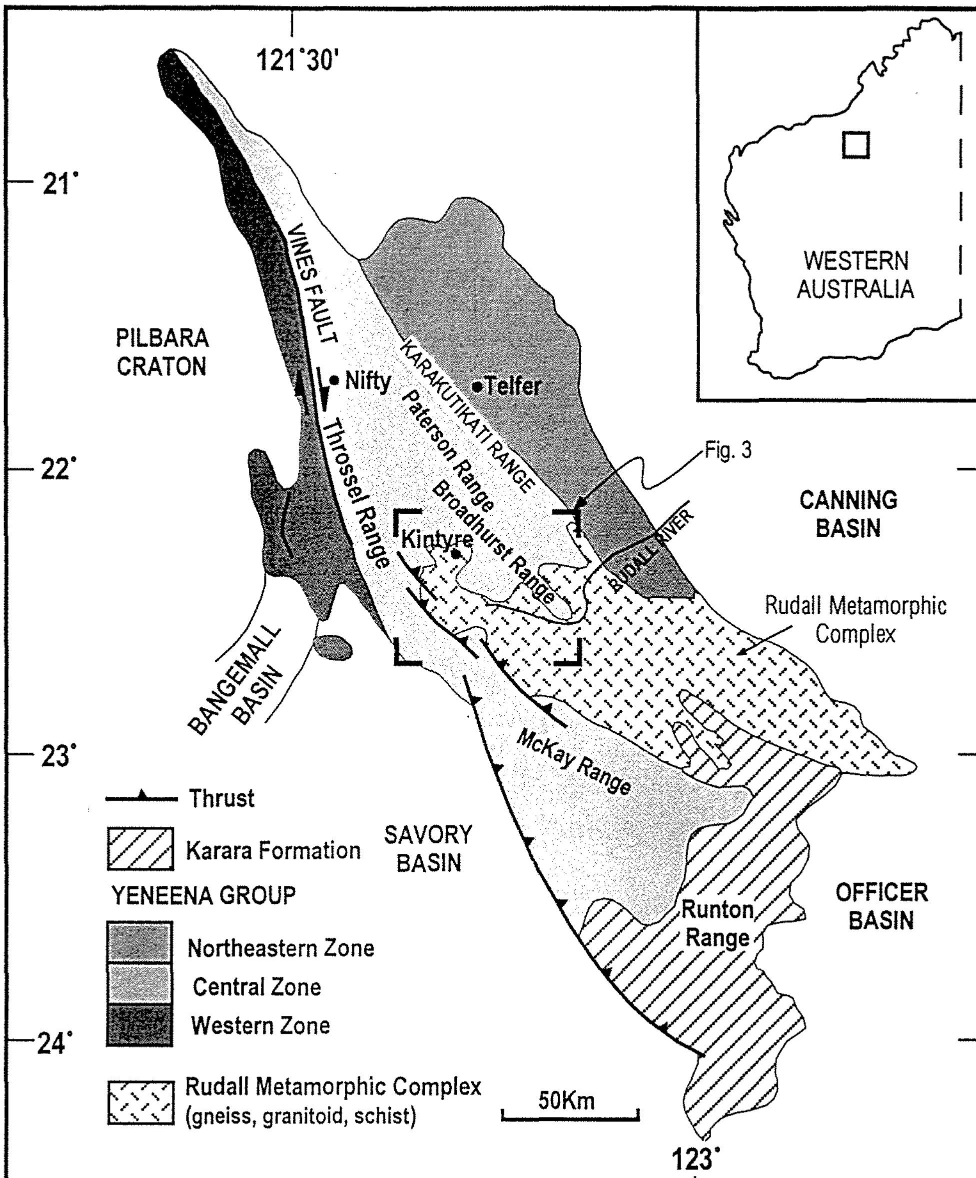

Western Zone	*Central Zone*	*Northeastern Zone*
		Kaliranu Beds Wilki Quartzite Puntapunta Fm. Telfer Fm. Malu Quartzite
Isdell Formation	Isdell Formation	Isdell Formation
-DISCONFORMITY-	*-DISCONFORMITY-*	? ?
Choorun Formation Yandanunyah Fm. Brownrigg Sandstone Waroongunyah Fm. Googenama Fm.	Choorun Formation Broadhurst Formation Coolbro Sandstone	**Basement not known**
-UNCONFORMITY-	*-UNCONFORMITY-*	
Hamersley-Fortescue Gp. Manganese Subgroup	Rudall Metamorphic Complex	

Figure 3: Summary map of the geology of the Rudall River area (see Figs 1 & 2 for location), and the field locations in this study (see Appendix 2 for structural data at each location). Basement rocks (Rudall Metamorphic Complex) are unconformably overlain by lower units of the Yeneena Group (Coolbro Sandstone and Broadhurst formations). Numerous thrust faults along the southwest margin interleaved gneissic basement and Yeneena Group sediments. The Broadhurst Formation in this location is tightly folded, with closely spaced axial planes commonly inclined/overturned to the SW. In the Broadhurst Range area, the large Sunday Creek Syncline contains numerous parasitic antiformal and synformal folds, many exhibiting thrust/lag faulting along their limbs (Hickman & Clarke, 1993).

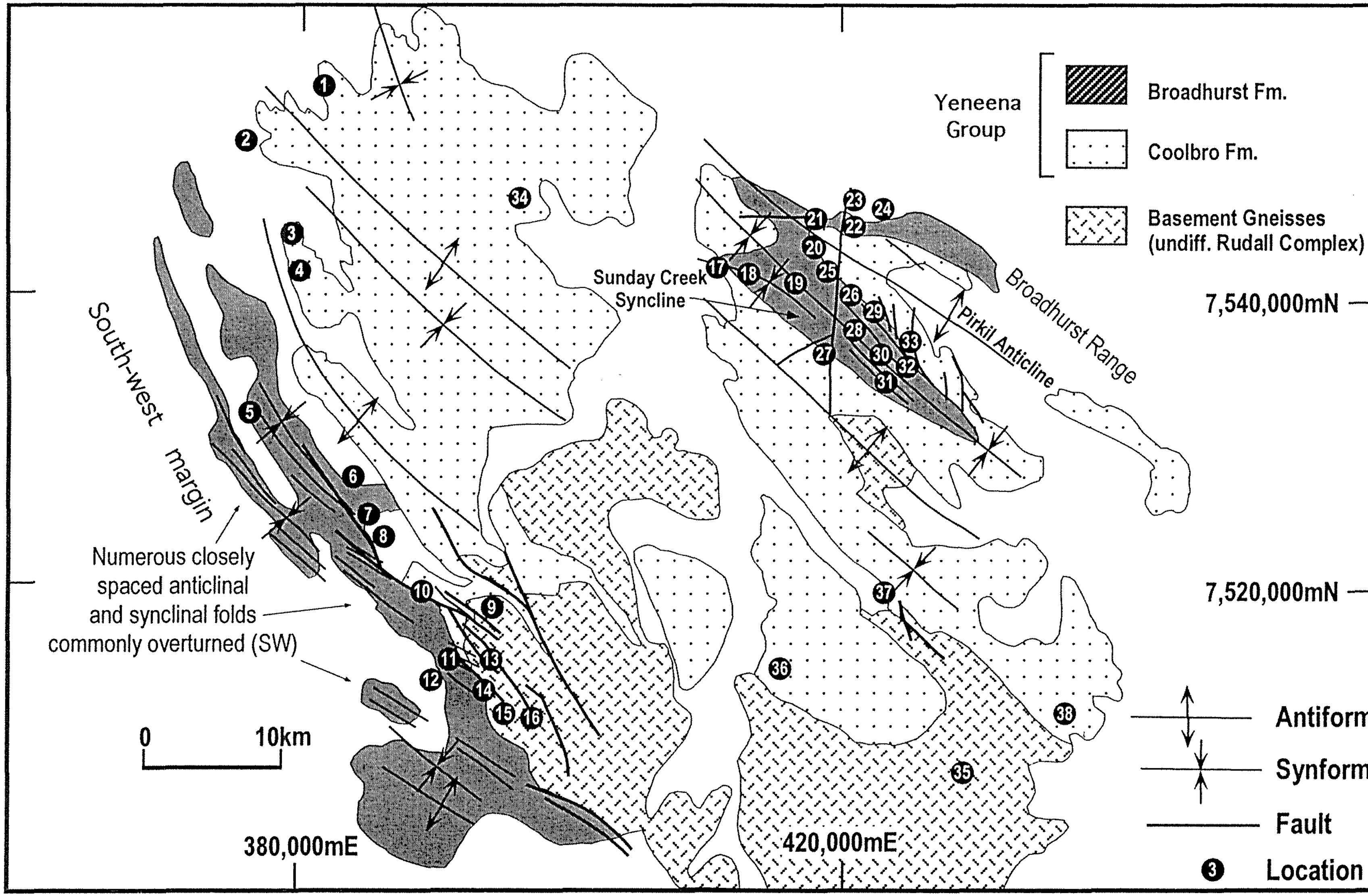

Yeneena Group
Broadhurst Fm.
Coolbro Fm.
Basement Gneisses (undiff. Rudall Complex)
South-west margin
Numerous closely spaced anticlinal and synclinal folds commonly overturned (SW)
Sunday Creek Syncline
Pirkil Anticline
Broadhurst Range
7,540,000mN
7,520,000mN
380,000mE
420,000mE
0
10km
Antiform
Synform
Fault
Location

Figure 4: Photograph of highly-strained boulder-conglomerate containing boudinaged gneissic cobbles. The rock is the basal erosional unit of the Yeneena Group, and the present fissility is the old S_0 surface. Photograph is taken looking NW. The zone now dips at 50°NE and movement was parallel to the dip direction (based on slickenside lineations on quartzose cobbles) and reverse (based on shear sense from porphyroclastic cobbles and grit grains). (*Location No. 13*)

Figure 5: D_1 intrafolial isocline preserved in finely fissile Broadhurst Formation and overprinted by S_3. Photograph is looking SE on the moderately SW dipping limb of an anticline. These isoclines may commonly be sheared/attenuated along their limbs indicating bedding-parallel shear post-D_1. This could have occurred during D_2 (see text) or from antithetic bedding reactivation during D_3. (*Location No. 19*)

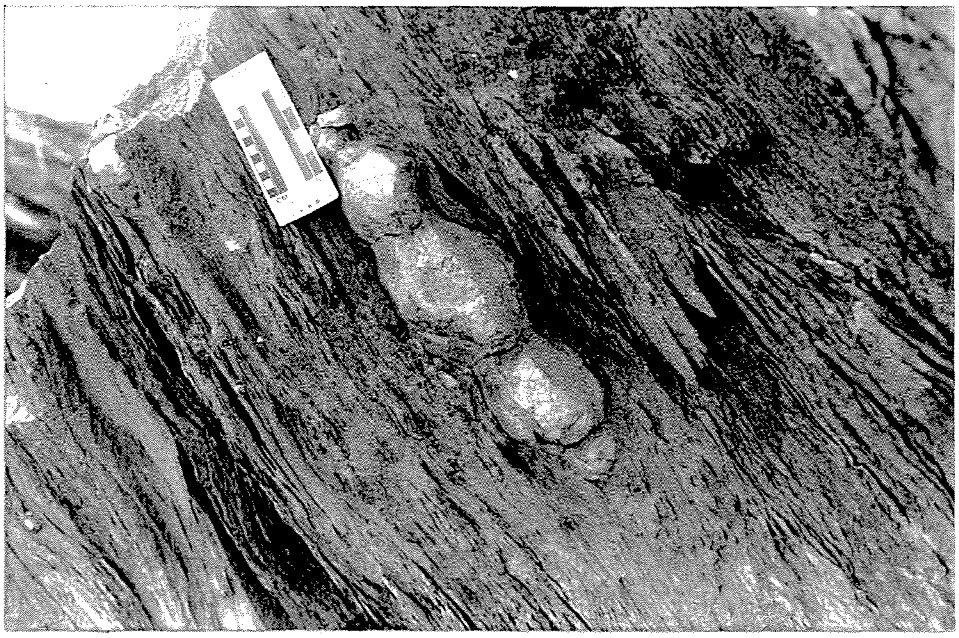

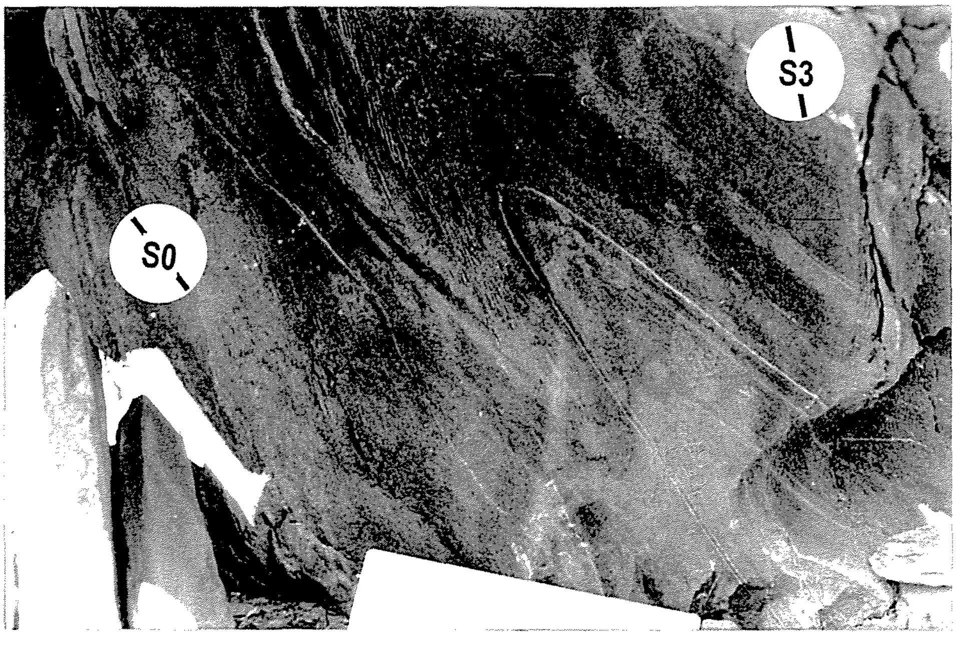
S0
S3

Figure 6: Photograph and line diagram illustrating the formation of D_2 monoclinal folding along the long limb of a tight D_1 fold. The D_1 fold was rotated during D_2 such that the trailing limb was attenuated along discrete high strain zones, producing a D_2 monocline. The short limb (low strain) of these monoclines may represent a relict sub-vertical bedding orientation produced by D_1 folding. S_2 is a coarsely spaced crenulation cleavage that lies axial plane to the monoclines and is well developed in D_2 high strain zones. Note the relative intensity of bedding attenuation along the long limbs (high-strain zones) of the monocline, with little or no thinning on the short limb (low-strain zones). This sample comes from the upper limb of a larger thrust-faulted D_1 isocline illustrated in Fig. 7. (*JCU Catalogue No. 48342; Location No. 22*)

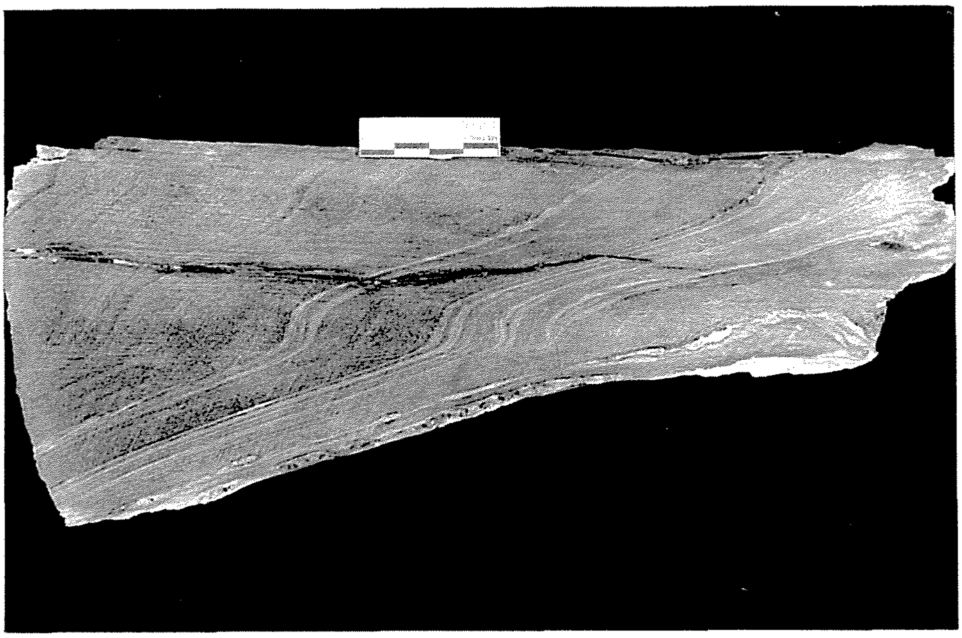

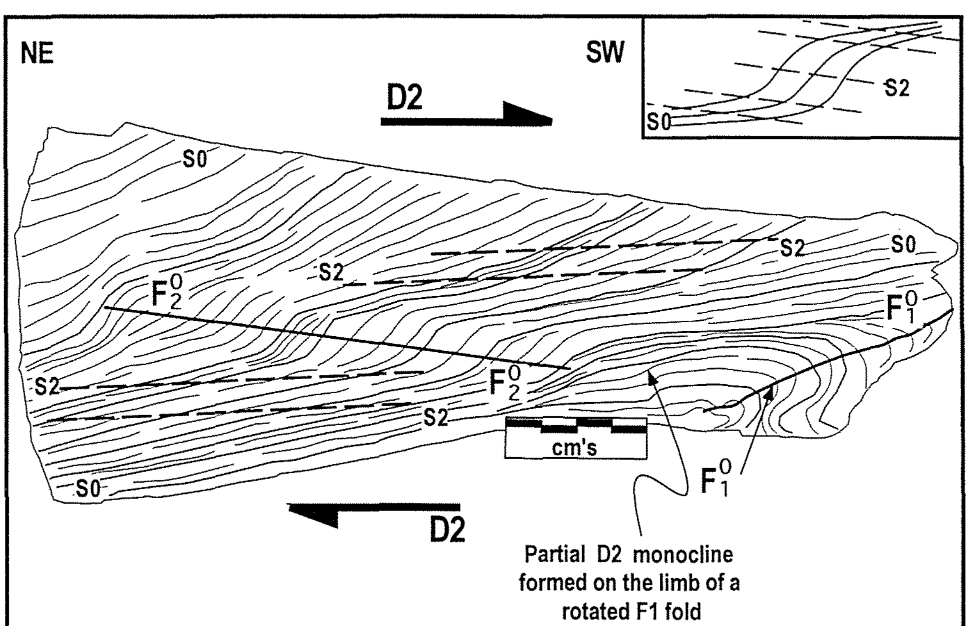
NE
SW
D2
S2
S0
S0
S2
S0
S2
F_2^0
F_1^0
S2
F_2^0
S2
cm's
S0
F_1^0
D2
Partial D2 monocline formed on the limb of a rotated F1 fold

Figure *7*: Field sketch of a recumbent isoclinal fold with a thrust-faulted lower limb. The structure is interpreted to be a D_1 fold that was rotated towards the southwest into a recumbent orientation during D_2, with associated thrusting along the lower limb. The fold and the basal fault plane are refolded by D_3 (regional folding). The location of Fig. 6 is indicated by the box. (*Location No. 22*)

Figure *8*: Photograph of small rootless monoclinal folds in which coarsely spaced S_2 cleavage overprints the steeper short limb. These are overprinted by S_3, and the long limbs have been subsequently unfolded by antithetic bedding reactivation during D_3 (see Fig. 9). Note the small inclined asymmetric folds in the lower-central left of the photograph (**IFF**). Photograph is looking SE at moderately SE-S dipping Broadhurst Formation on the SW side of a D_3 anticline hinge. (*Location No. 18*)

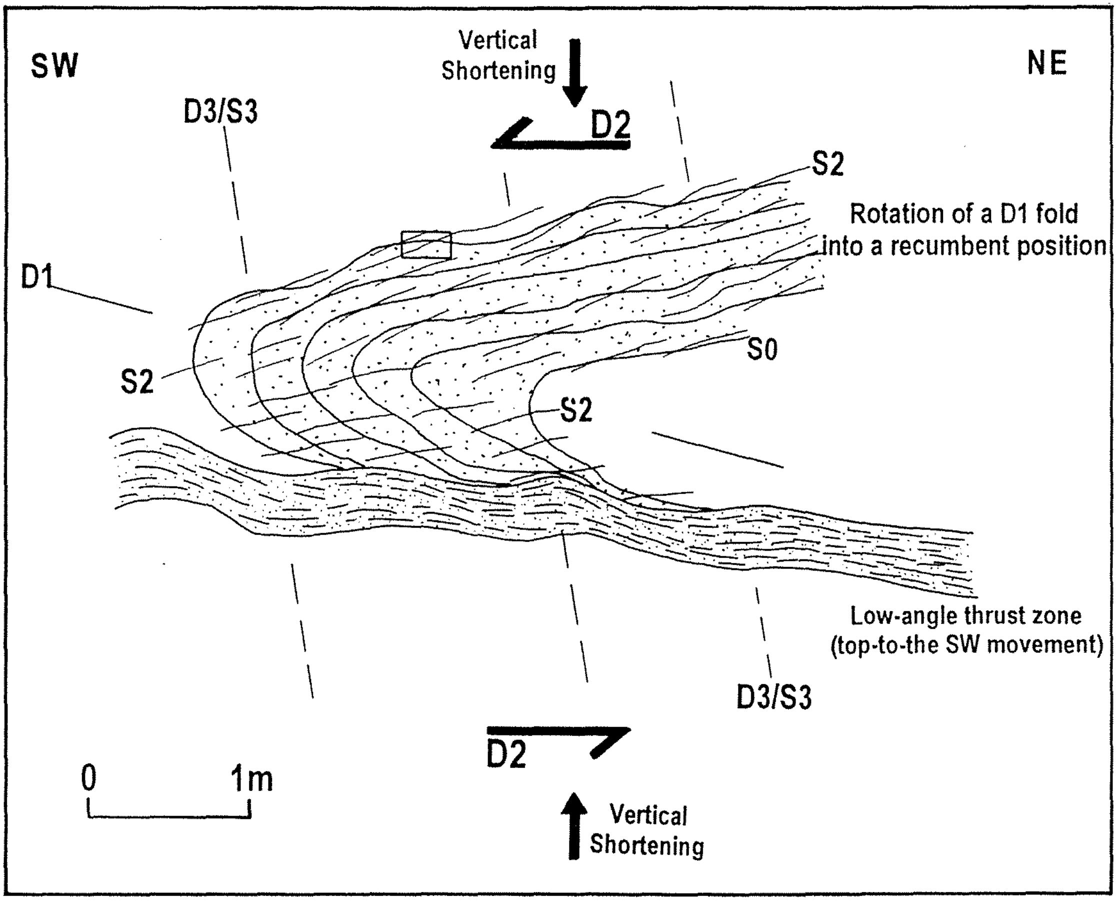
SW
NE
Vertical
Shortening
D2
D3/S3
S2
Rotation of a D1 fold
into a recumbent position
D1
S2
S0
S2
Low-angle thrust zone
(top-to-the SW movement)
D3/S3
D2
0
1m
Vertical
Shortening

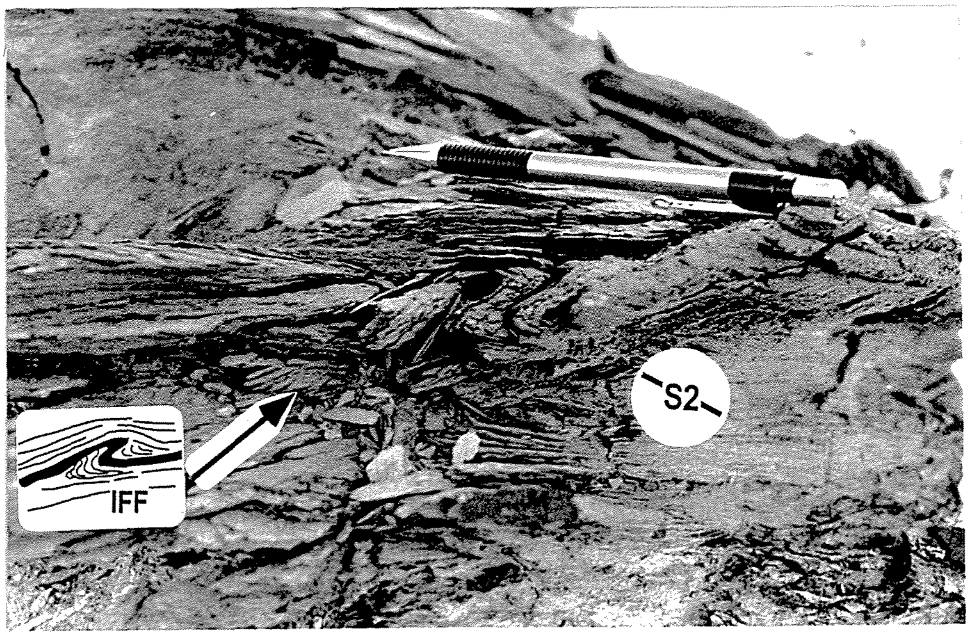
S2
IFF

Figure 9 : Schematic diagram illustrating potential development of structures observed in Fig. 8. (**A**) Initial D_1 folds formed through layer-parallel shortening, in an upright or weakly SW inclined orientation. (**B**) These were subsequently rotated by SW directed horizontal movement and vertical shortening during D_2 that produced a coarsely spaced overprinting cleavage (S_2). (**C**). The latter was well developed on the short limb as this lay parallel to the compressional direction (*ie*. sub-vertical). (**D**) D_2 folds were overprinted by S_3 during subsequent D_3 folding. Bold arrows mark the bulk fold movement. (**E**) Antithetic bedding reactivation (**B_R**) late in D_3 caused layer-parallel shearing that unfolded the relict D_1-D_2 folds obliterating the long limbs, which lay at a low-angle to bedding.

Figure 10: Field sketch (drawn from photograph) of the timing relationships between high-angle reverse faulting and D_3 fold formation. The main diagram illustrates D_3 folding and S_3 cleavage development during bulk horizontal shortening with synthetic bulk fold movement (**BFM**) across bedding in the fold limb, which lies on the NE limb of a regional fold (inset). The shear sense on S_3 is also synthetic (**1**), however late in the folding, as the limb steepens, antithetic shearing of bedding (reactivation) crenulates S_3 along the bedding plane (**2**). This is overprinted by the high-angle reverse faults (**3**) indicating these formed late- or post-D_3 (*Location No. 21*)

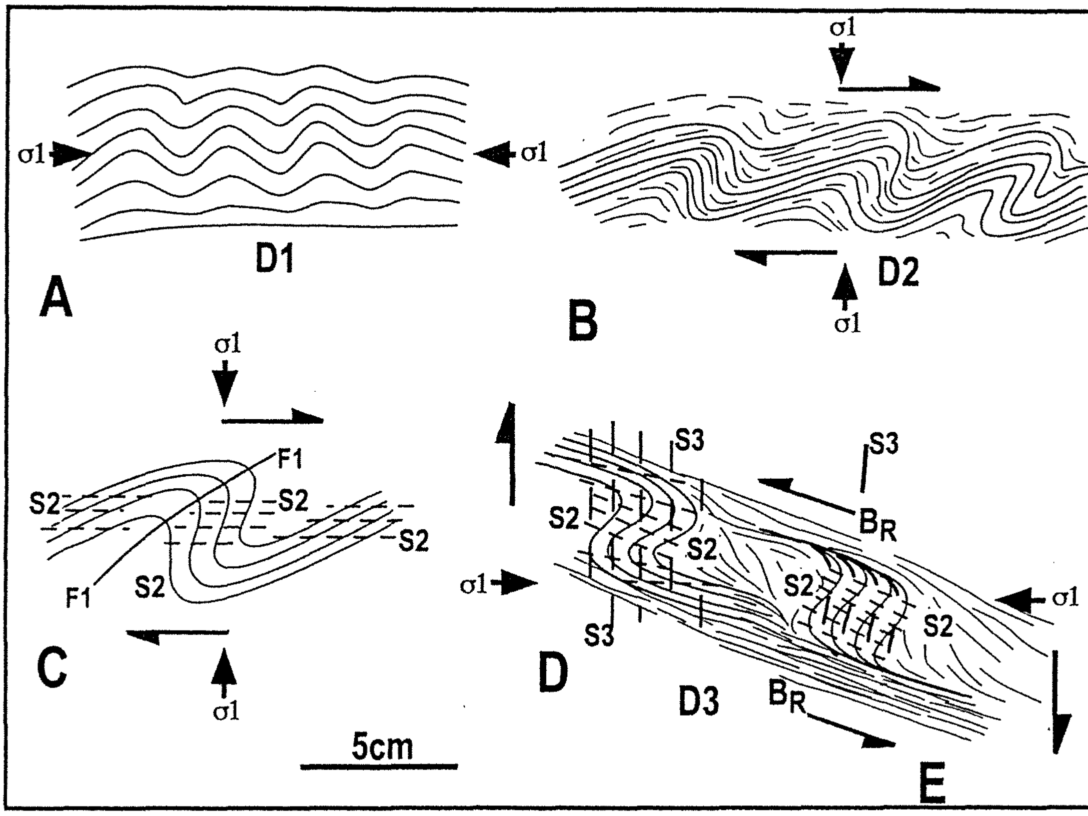
σ1
σ1
σ1
D1
A
σ1
D2
σ1
B
σ1
F1
S2
S2
S2
F1
S2
σ1
C
S3
S3
S2
BR
S2
σ1
S2
σ1
S2
S3
D
D3
BR
E
5cm

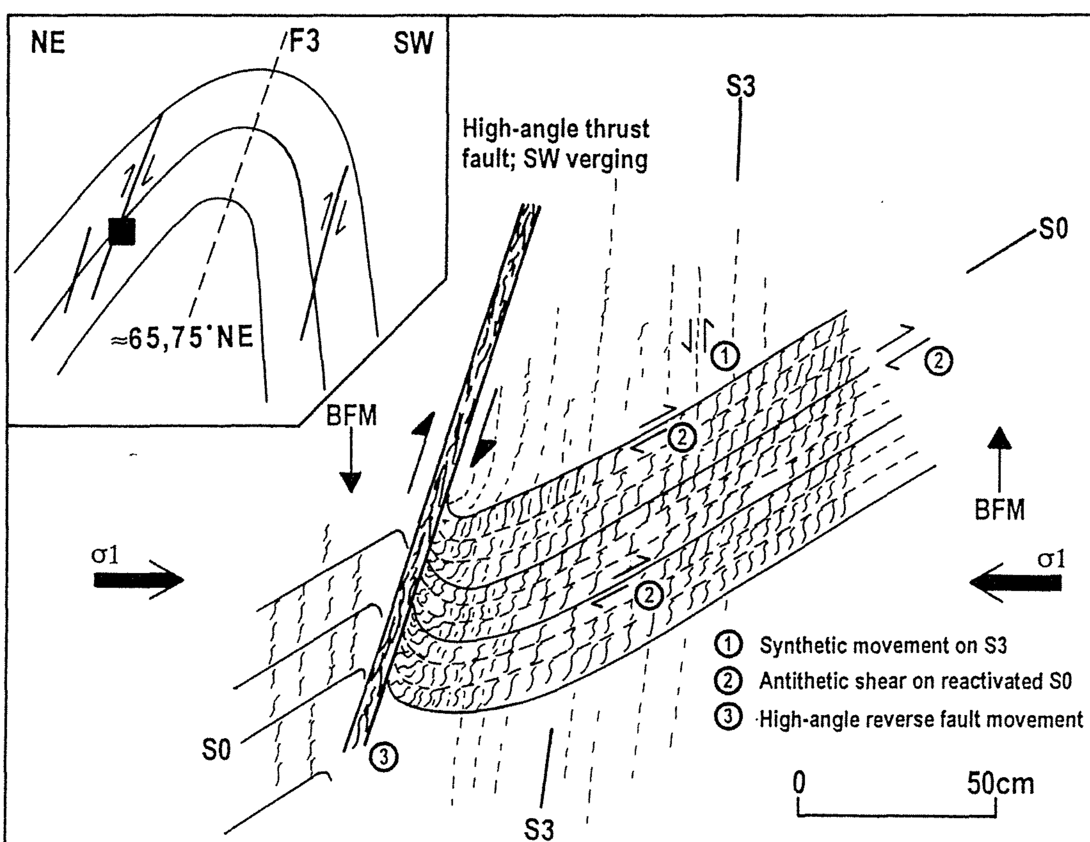
NE
F3
SW
≈65,75°NE
High-angle thrust fault; SW verging
S3
S0
BFM
BFM
σ1
σ1
S0
S3
① Synthetic movement on S3
② Antithetic shear on reactivated S0
③ High-angle reverse fault movement
0
50cm

Figure 11: Photograph of a D_4 fold in finely schistose Broadhurst Formation The sub-vertical fabric is S_3, which is coarsely crenulated (asymmetric) by D_4. The F_4 axial plane is sub-horizontal (parallel to the head of the hammer) where S_3 is horizontal. In this locality S_4 is marked by local and extremely fine dissolution of foliated (S_3) country rock in high D_4 strain zones. The photograph is looking south-east on the SW dipping limb of a D_3 anticlinal fold. (*Location No. 6*)

Figure 12: Field sketch of a metre scale F_4 fold on the SW dipping limb of a D_3 anticline. Bedding, S_3 and syn-D_3 quartz veins are folded about a horizontal D_4 axial plane. The fibrous quartz veins formed during D_3 with their fibres parallel to S_3 (**a**). However, D_4 folding has rotated S_3 in the matrix (**b**), with the vein preserving the initial vertical S_3 orientation. The location of Fig. 14 is indicated by the small box marking the lower right inset. The section is drawn looking NW and both F_3 and F_4 verge NE. This locality is approximately 2.5kms SE of Fig. 11 (see Fig. 3) illustrating the potential for localised D_4 vergence reversals. (*Location No. 7*)

F4
S3

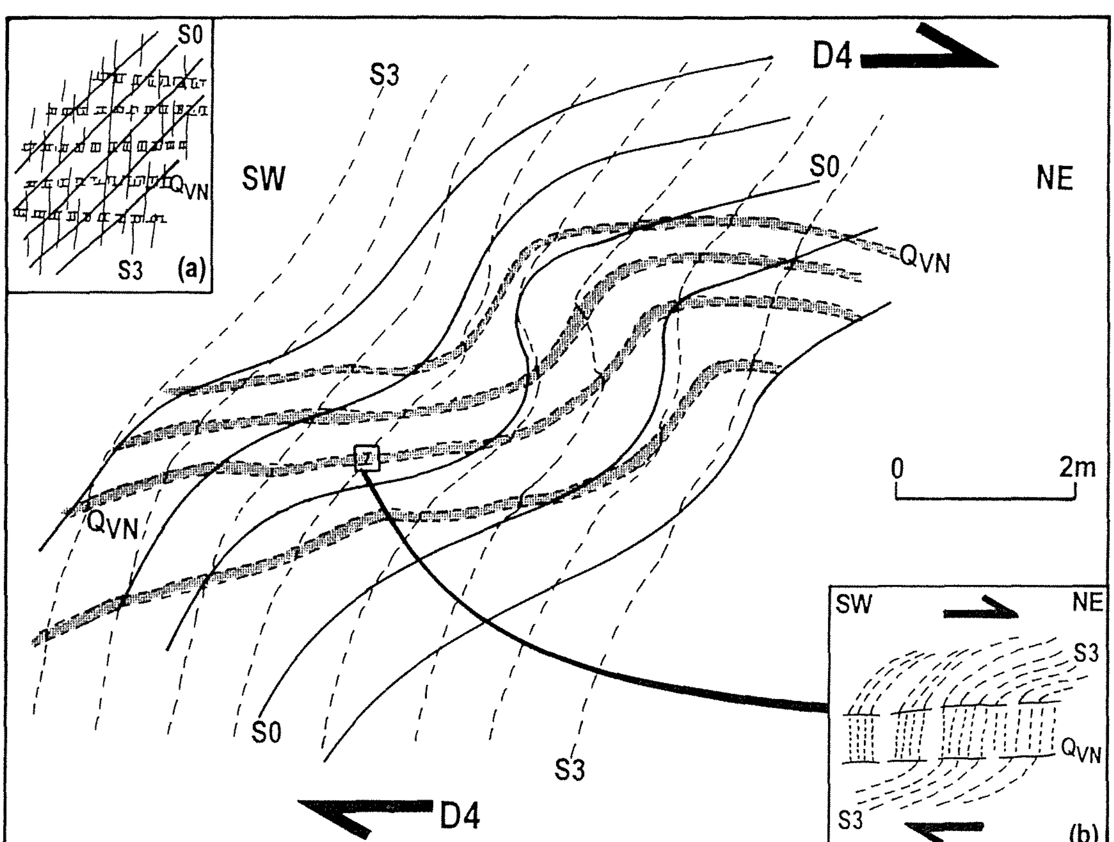

S0
QVN
S3
(a)
S3
D4
SW
S0
NE
QVN
QVN
0
2m
S0
S3
D4
SW
NE
S3
QVN
S3
(b)

Figure 13: Photomicrographs illustrating various styles of S_4. (**A**) S_4 is a coarsely spaced asymmetric crenulation cleavage (horizontal) overprinting sub-vertical S_3 in highly fissile Broadhurst Formation. The thin section is vertical and oriented as shown. In this location the differentiated S_4 crenulation asymmetry indicates a top-to-the-SW shear sense on the F_4 axial plane. The scale bar is 4mm long. (*JCU Catalogue No. 48343; Location No.* 24). (**B**) S_4 is a coarsely spaced symmetric crenulation of S_0/S_3 with weak differentiation along the fabric plane. Symmetric S_4 crenulations are generally observed only in fabrics that are vertical/sub-vertical, suggesting shortening perpendicular to the layers (*ie.* vertical shortening). The thin section is vertical and oriented as shown. The scale bar is 3mm long. (*JCU Catalogue No. 48344; Location No. 7*)

Figure 14: Field photograph illustrating the preservation of S_3 within quartz veins, and its subsequent folding in the matrix by D_4. Large fibrous quartz veins formed with their fibres parallel to, and preserving, S_3. In the rock matrix, where S_3 was not protected by the quartz, it was subsequently rotated/flattened during D_4. Photograph is looking NW, and the movement sense for F_4 is top-to-the-NE. The sample comes from the limb of the D_4 fold illustrated in Fig. 12 (inset ***b*** in Fig. 12). (*Location No. 7*).

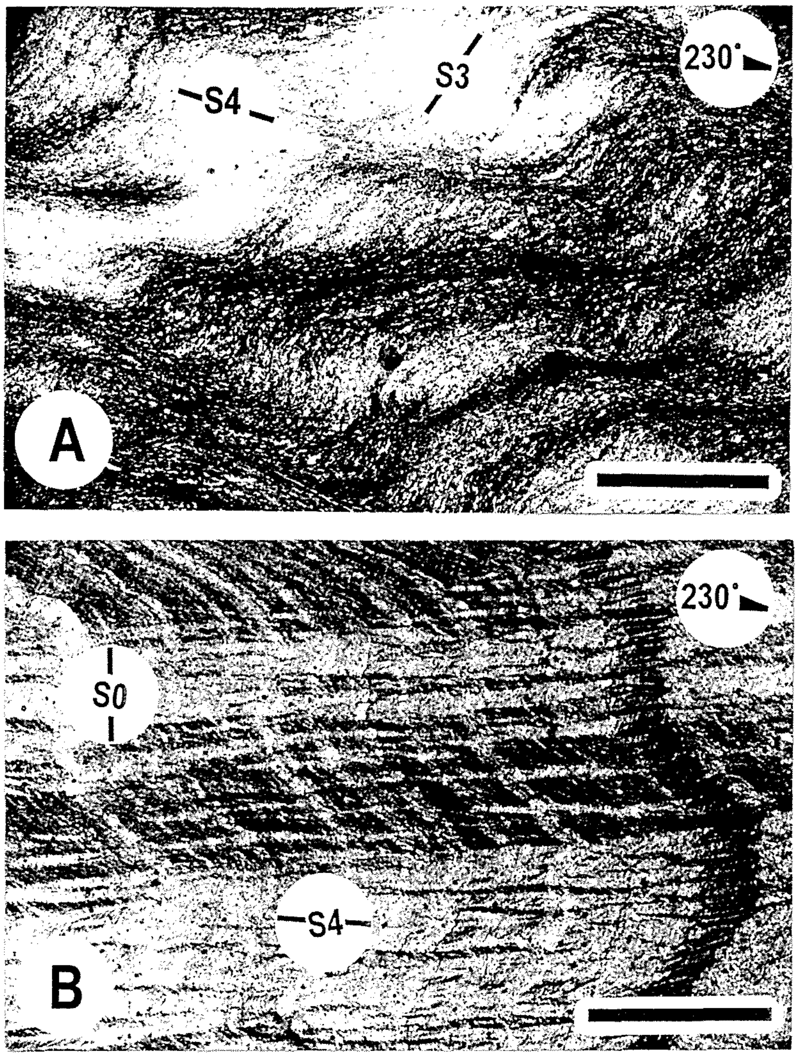
230°
S4
S3
A
230°
S0
S4
B

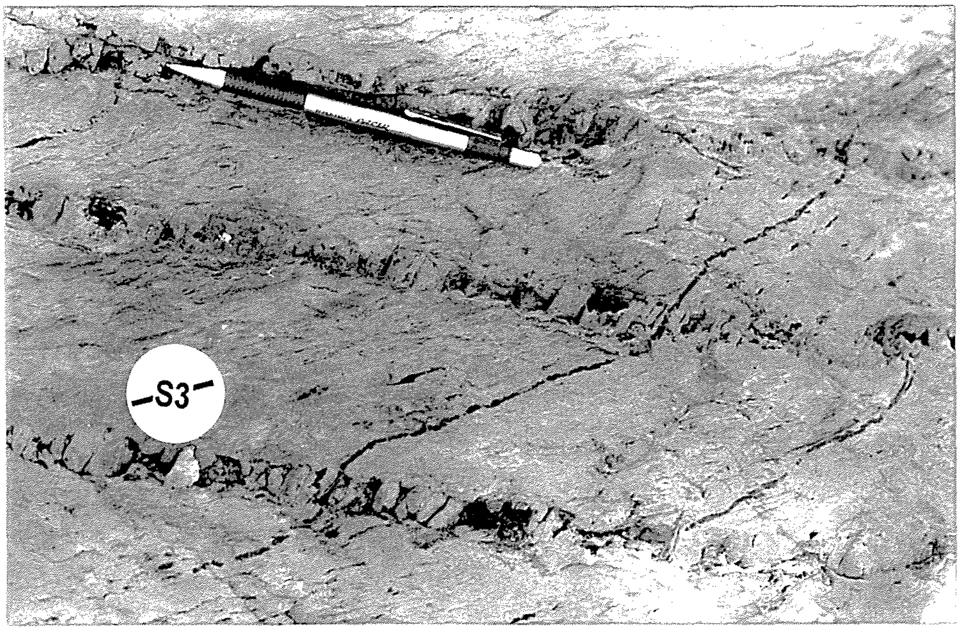
S3

Figure 15: Summary diagram of the effects and structures produced by D_4 and D_5 deformation in the Lower Yeneena Group. Main figure is a schematic D_3 anticline-syncline pair illustrating the macroscale refolding effects of D_4, which include flattening and rotation of F_3 hinges. Mesoscale (centimetre) effects include; **(i)** - S_3, in the hinge of an F_3 fold is rotated into a horizontal orientation by D_4. This flattened zone, an F_4 hinge, is subsequently overprinted by D_5 crenulations. **(ii)** - Crenulation of S_3 along bedding arising from antithetic reactivation of the F_3 limb by D_4. Note the sense of crenulation is the reverse of that expected for bedding reactivated during D_3 (*cf. Fig.* 10). **(iii)** - D_4 folding of sub-vertical S_3. The F_4 hinges were subsequently overprinted by D_5 crenulations (this is a cross sectional view of the crenulation geometries shown in Fig. 16). **(iv)** - Asymmetric D_4 crenulation of S_0 and S_3; these occur predominantly on the SW dipping limbs of D_3 folds, which were favourably inclined for deformation during top-to-the-SW shear in D_4. **(v)** - Symmetric D_4 folding of S_3 is observed in the central hinge regions of F_3 folds where asymmetric crenulation formation was restricted. **(vi)** - Symmetric D_4 folds developed in sub-vertical bedding (and S_3) suggesting vertical shortening.

Figure 16 : Plan view photograph showing D_5 crenulations overprinting D_4 folds of S_3 cleavage. The prominent fracture direction (N-S on the page) marks the trace of sub-vertical S_3 that is sub-horizontally crenulated by D_4 (see Fig. 15iii for section). These areas of sub-horizontal S_3 were favourably oriented for overprinting by D_5 crenulations. The latter lie at an acute angle to S_3 (NNE-SSW on page) indicating that D_5 shortening was approximately 20-25° anticlockwise from that of D_3. Photograph is looking SE up the page. (*Location No. 24*)

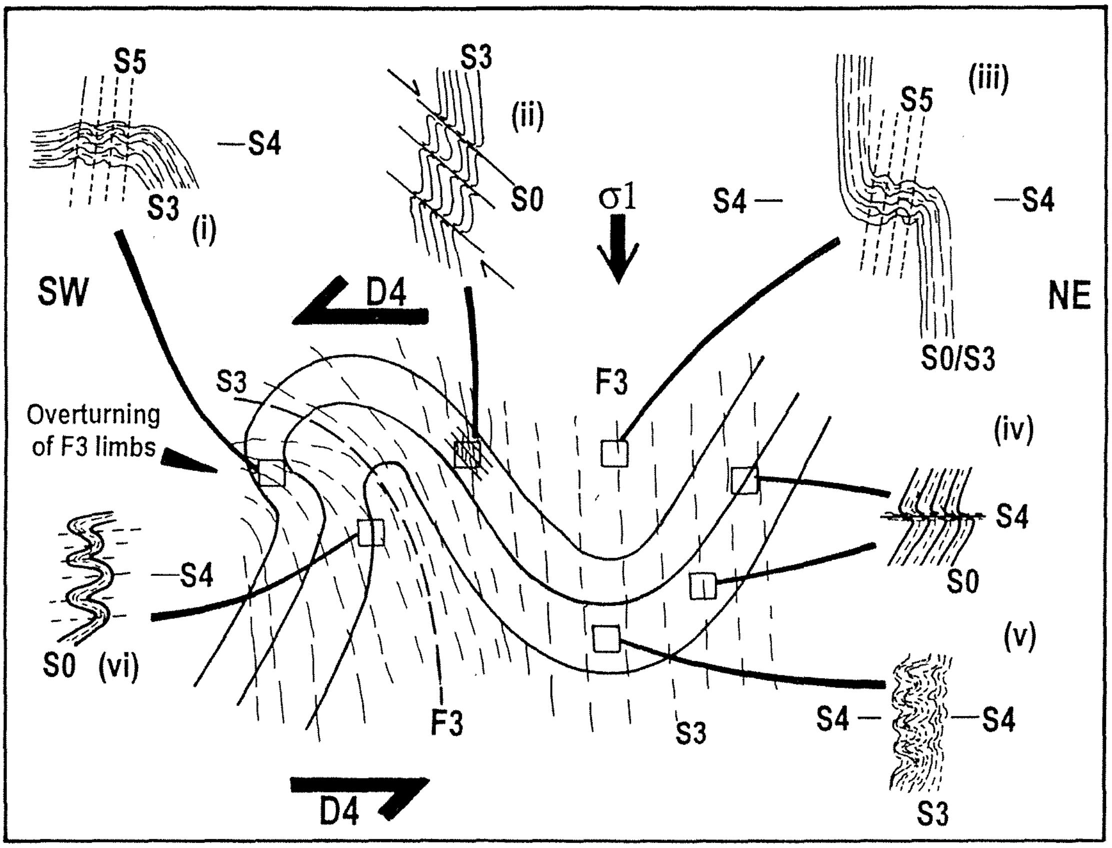
S5
S4
S3
(i)
S3
(ii)
S0
σ1
S4
(iii)
S5
S4
SW
D4
NE
S0/S3
S3
F3
Overturning
of F3 limbs
(iv)
S4
S0
S4
S0
(vi)
(v)
F3
S3
S4
S4
S3
D4

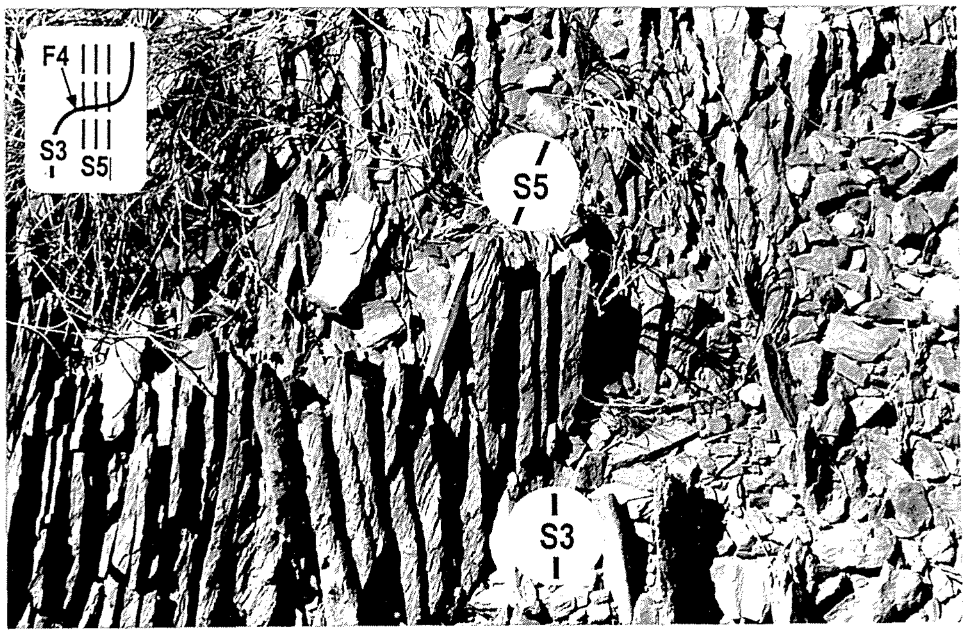
F4
S3
S5
S5
S3

Figure 17: Photomicrograph of coarse F_5 crenulation folding and localised differentiated S_5 development in schistose Broadhurst Formation. The main schistosity is a composite S_0/S_3 foliation that is lying horizontal in the hinge of a D_4 fold. The thin section is vertical and oriented as shown. The scale bar is 1.5mm long. (*JCU Catalogue No. 48345; Location No. 7*)

Figure 18: Photographs of D_6 kink folding styles. (**A**) Coarsely developed D_6 kinks within finely cleaved Broadhurst Formation. The prominent fabric (N-S on page) is S_3. Associated with the kinks are fine discontinuous and continuous fracture planes that define a rough axial plane fracture cleavage (S_6). The photograph is a plan view and NW is to the top. The scale bar is 6cm long. (*Location No. 20*). (**B**) D_6 kinking of S_0/S_3. Photograph is looking sideways at an intermediate angle to the NE. S_0 and S_3 are roughly parallel in trend. Note the local weak development of dissolution seams along the axial planes of the kinks. (*Location No. 9*)

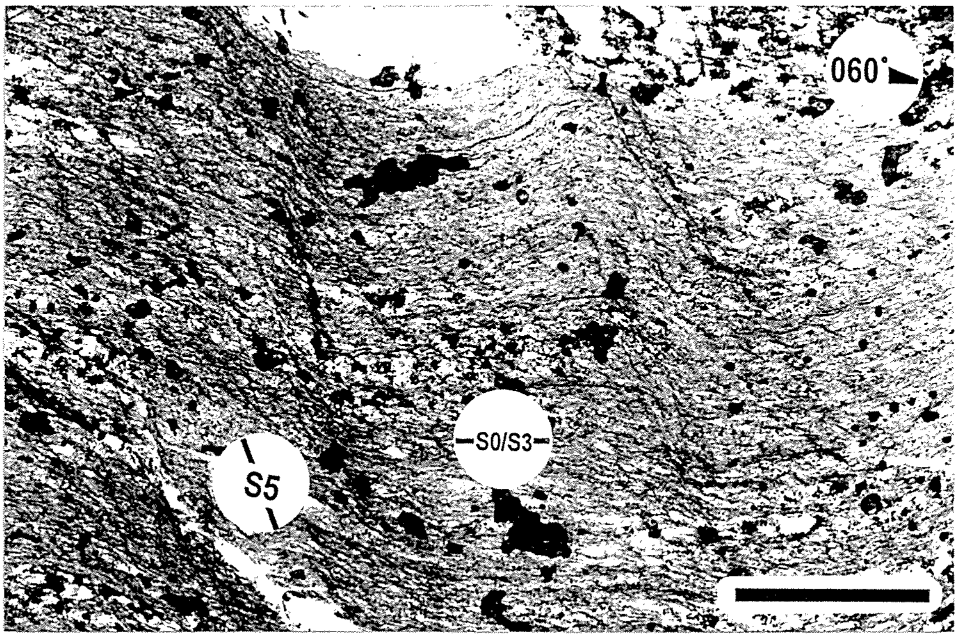
060°
S5
S0/S3


S3
F6/S6
A

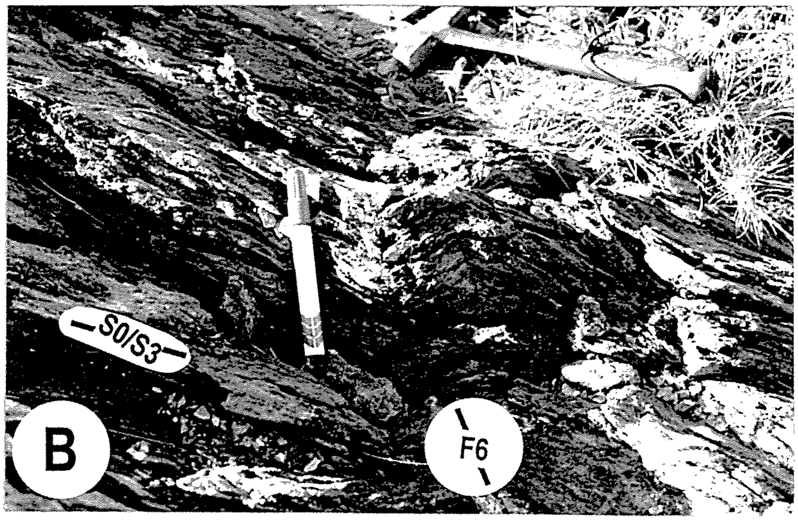
S0/S3
B
F6

Figure 19: Summary map of gravity and magnetic data for the Paterson Province (data sourced from regional surveys carried out by the Western Australian Geological Survey (GSWA - 1:250,000)). The map illustrates the major gravity divisions across the province and prominent magnetic linears. The clear overlay illustrates the broad lithological divisions of the Paterson Province and shows the positions of the two study areas (Rudall Inlier and Telfer district). The broad Anketell Gravity Ridge is clearly visible, and in the SW corner large gravity depressions mark the edge of the Karara and Savory Basins. In the Throssell Range and Anketell regions major magnetic linears define complex patterns suggestive of transpressive (*e.g.* Mitchell & Reading, 1986, p. 503; Sylvester, 1988; Woodcock & Schubert, 1994) and faulted-fold geometries. Larger discordant linears are also evident in the NE area of the Paterson Province.

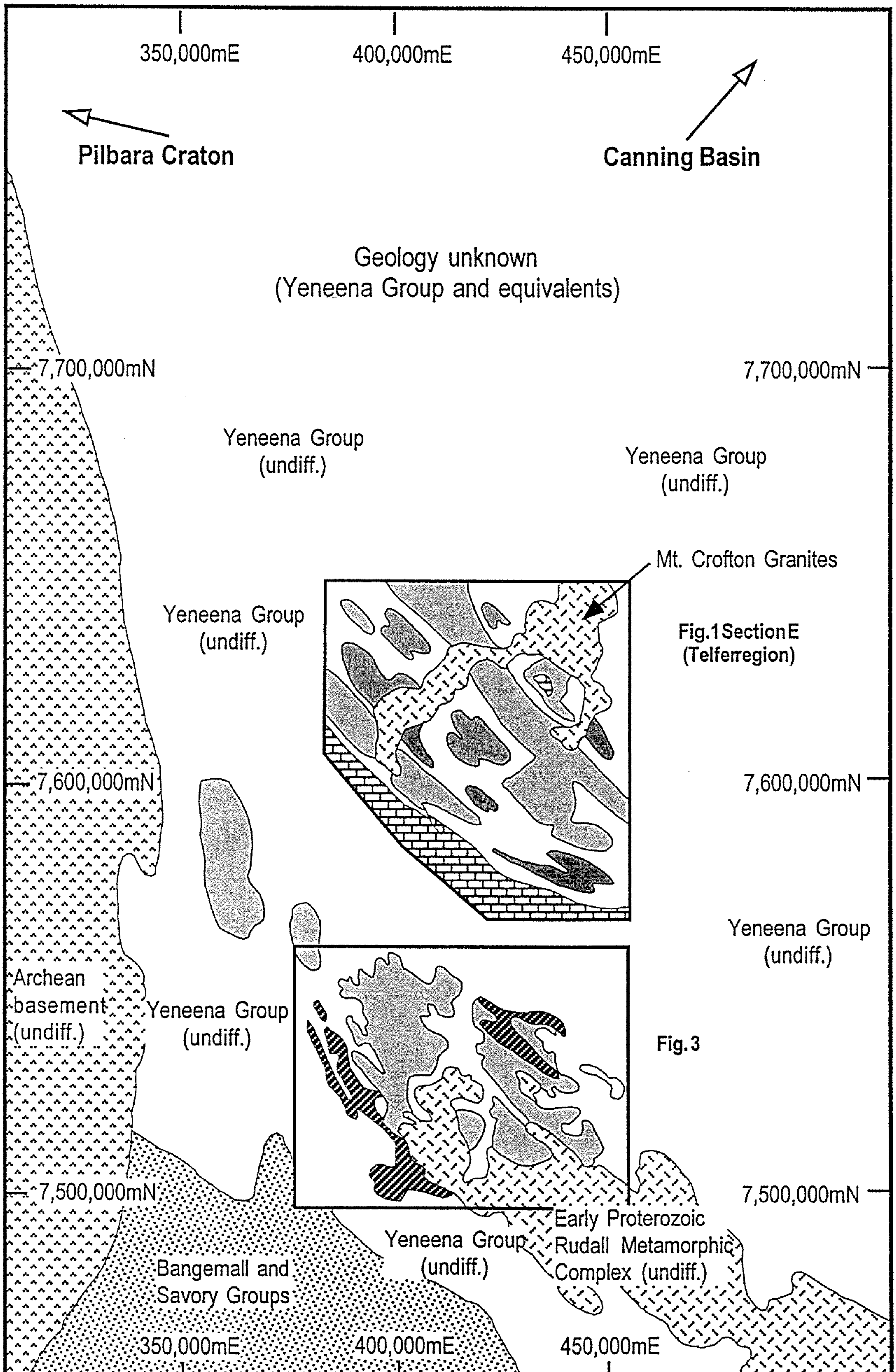

350,000mE
400,000mE
450,000mE
Pilbara Craton
Canning Basin
Geology unknown
(Yeneena Group and equivalents)
7,700,000mN
7,700,000mN
Yeneena Group
(undiff.)
Yeneena Group
(undiff.)
Mt. Crofton Granites
Yeneena Group
(undiff.)
Fig.1 Section E
(Telferregion)
7,600,000mN
7,600,000mN
Yeneena Group
(undiff.)
Archean
basement
(undiff.)
Yeneena Group
(undiff.)
Fig.3
7,500,000mN
7,500,000mN
Early Proterozoic
Rudall Metamorphic
Complex (undiff.)
Yeneena Group
(undiff.)
Bangemall and
Savory Groups
350,000mE
400,000mE
450,000mE

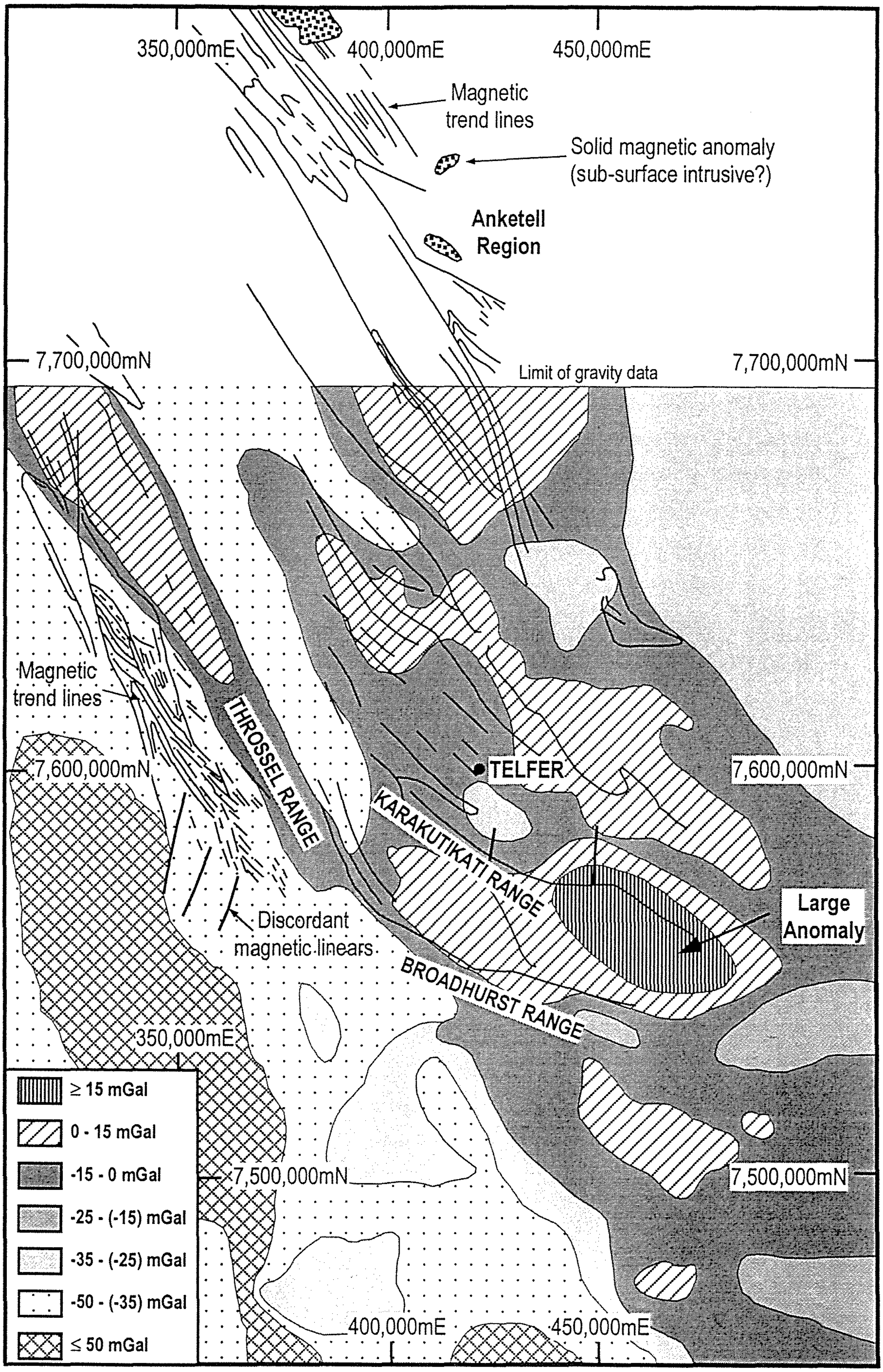

350,000mE
400,000mE
450,000mE
Magnetic trend lines
Solid magnetic anomaly (sub-surface intrusive?)
Anketell Region
7,700,000mN
Limit of gravity data
7,700,000mN
Magnetic trend lines
THROSSEL RANGE
7,600,000mN
TELFER
7,600,000mN
KARAKUTIKATI RANGE
Large Anomaly
Discordant magnetic linears
BROADHURST RANGE
350,000mE
≥ 15 mGal
0 - 15 mGal
-15 - 0 mGal
-25 - (-15) mGal
-35 - (-25) mGal
-50 - (-35) mGal
≤ 50 mGal
7,500,000mN
7,500,000mN
400,000mE
450,000mE

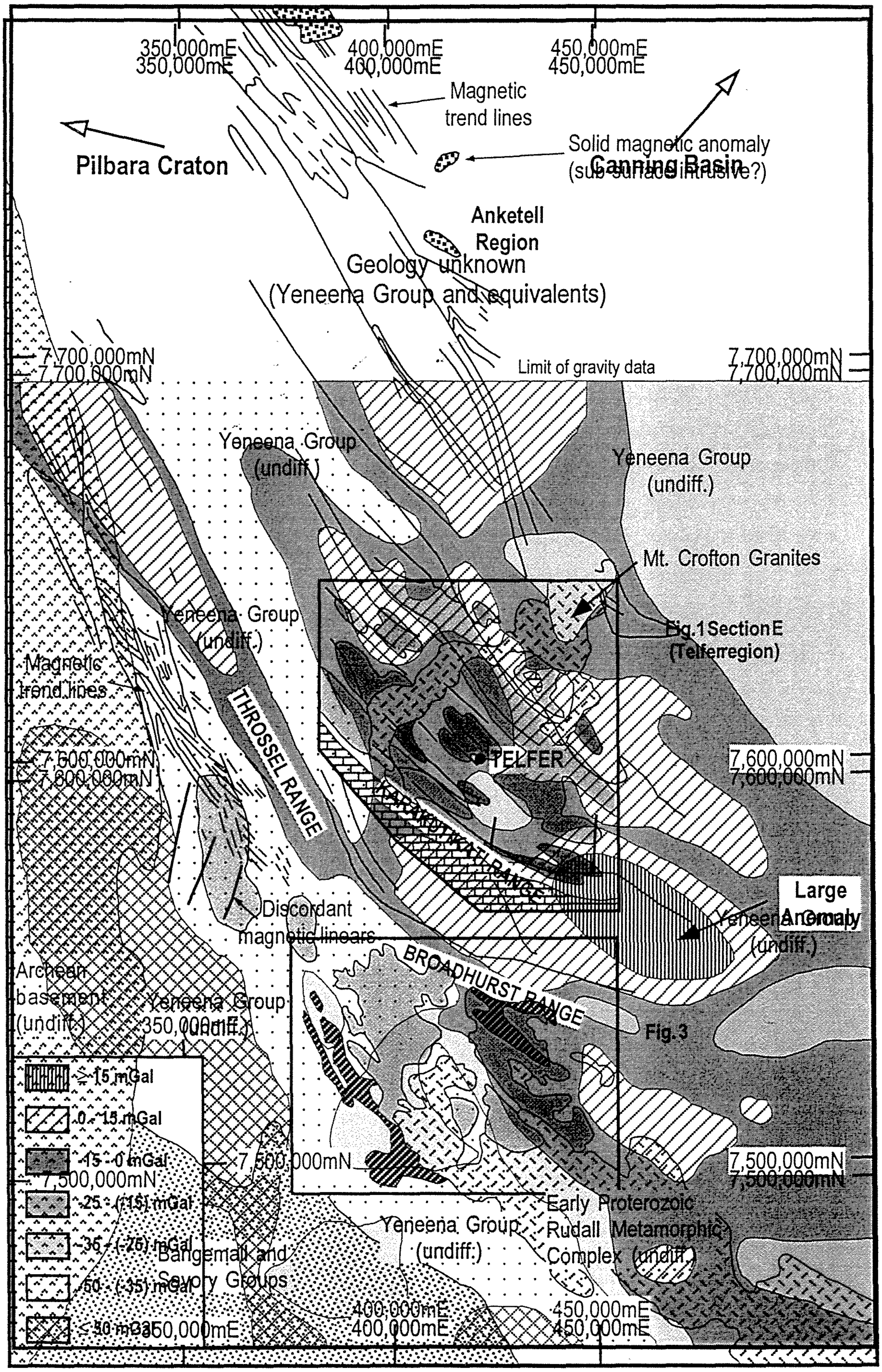
350,000mE
400,000mE
450,000mE
Magnetic trend lines
Pilbara Craton
Solid magnetic anomaly (sub-surface intrusive?)
Canning Basin
Anketell Region
Geology unknown (Yeneena Group and equivalents)
7,700,000mN
Limit of gravity data
Yeneena Group (undiff.)
Mt. Crofton Granites
Fig.1 Section E (Telfer region)
Magnetic trend lines
THROSSEL RANGE
7,600,000mN
TELFER
Large Anomaly
Discordant magnetic linears
BROADHURST RANGE
Archean basement (undiff.)
Fig.3
≥ 15 mGal
0 - 15 mGal
-15 - 0 mGal
-25 - (-15) mGal
-35 - (-25) mGal
-50 - (-35) mGal
< -50 mGal
7,500,000mN
Early Proterozoic Rudall Metamorphic Complex (undiff.)
Bangemall and Savory Groups

Figure 20: Schematic summary of the progressive development, and migration of the core, of the Paterson Orogeny during the late-Proterozoic. (**A**) Initial shortening during D_1, with the orogen core lying NE of the Paterson Province, produced weak folding of the sequence (F_1). (**B**) Gravity induced collapse of the core during D_2 produced SW directed thrusting across the Paterson Province. (**C**) Progressive widening of the orogen, and migration of it's core, produced stronger shortening in the Paterson Province during D_3. (**D**) Continued SW migration of the orogen core and subsequent collapse during D_4 resulted in the inflection line (see text) lying between Telfer and the Rudall inlier, thus explaining the development of opposite D_4 vergence directions in either area. (**E**) The accretionary wedge model of Platt (1986) illustrating the various structural styles (extension and thrusting), and inferred bulk shear senses, in different levels of the wedge. The inferred position of the inflection line of Bell & Johnson (1989) is also illustrated. Such a wedge, encompassing the Paterson Province, may have lain on the foreland side of a collisional/subduction driven orogen (Inset). (**F**) Granite intrusion in the NE part of the Paterson Province may have induced local gravitational collapse causing coaxiality in D_4 deformation; a situation akin to a changing inflection line position. (**G**) Alternative explanations for the changing shear sense geometries between D_2 and D_4 across the Paterson Province, whereby the orogen core initally lay SW of the presently exposed province and Telfer and the Rudall Inlier were initially (D_1-D_2) located in the upper NE quadrant of the orogen. Over time the orogen core may have migrated SW (**i**) or NE (**ii**) with burial of the province. These explanations are considered less likely (see text).

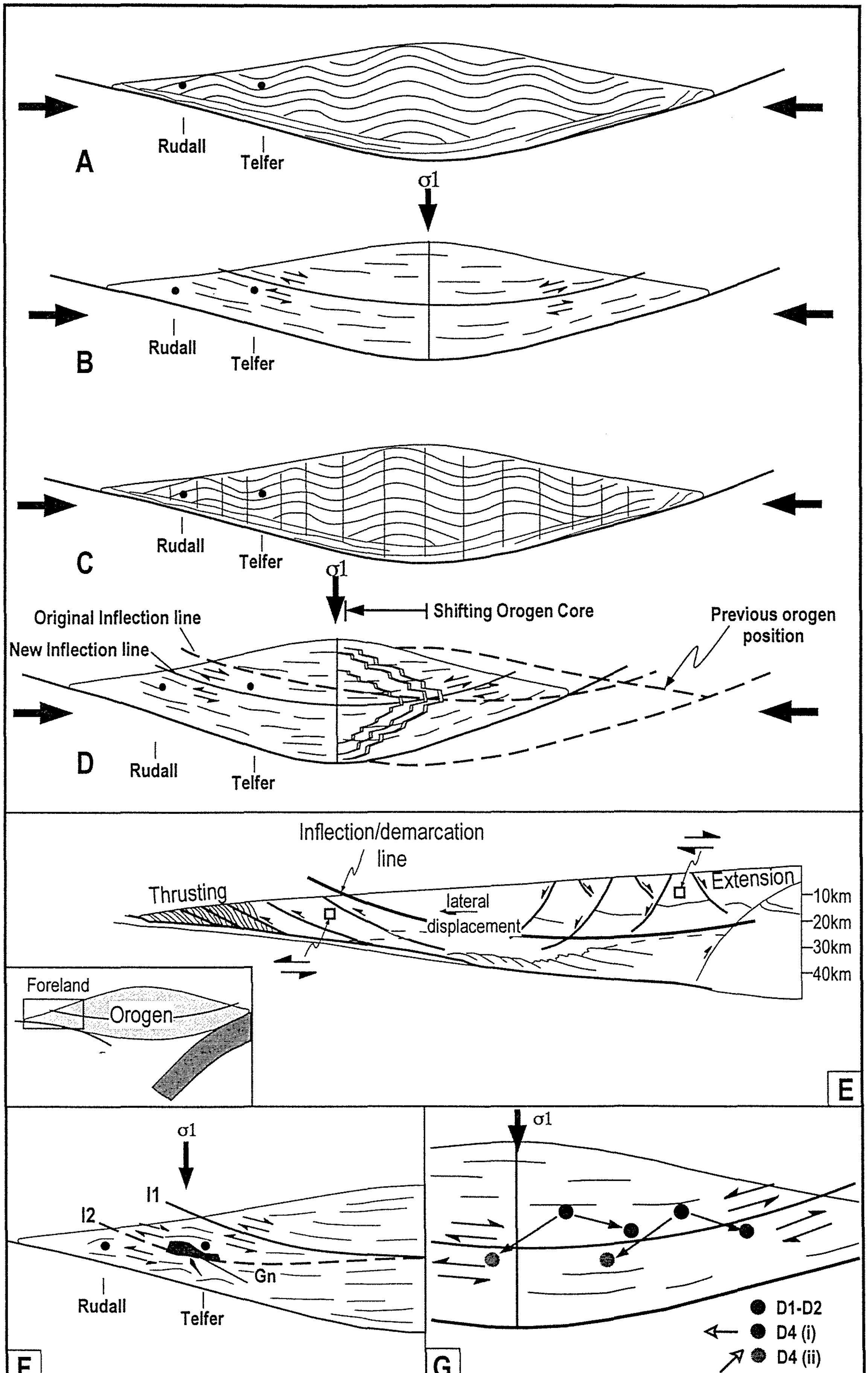

Rudall
Telfer
A
σ1
Rudall
Telfer
B
Rudall
Telfer
C
σ1
Shifting Orogen Core
Original Inflection line
New Inflection line
Previous orogen position
D
Rudall
Telfer
Inflection/demarcation line
Thrusting
lateral displacement
Extension
10km
20km
30km
40km
Foreland
Orogen
E
σ1
I1
I2
Gn
Rudall
Telfer
F
σ1
D1-D2
D4 (i)
D4 (ii)
G

Figure 21: Summary map of the effects of NE-SW convergence across the Paterson Orogen during the period 750-550Ma (redrawn from Myers, 1990a,b). These effects included deformation of earlier deposited sediments, and the formation of new sedimentary basins in response to thrust-loading of the foreland. The latter occurred over most of the length of the Paterson Orogenic belt during this time.

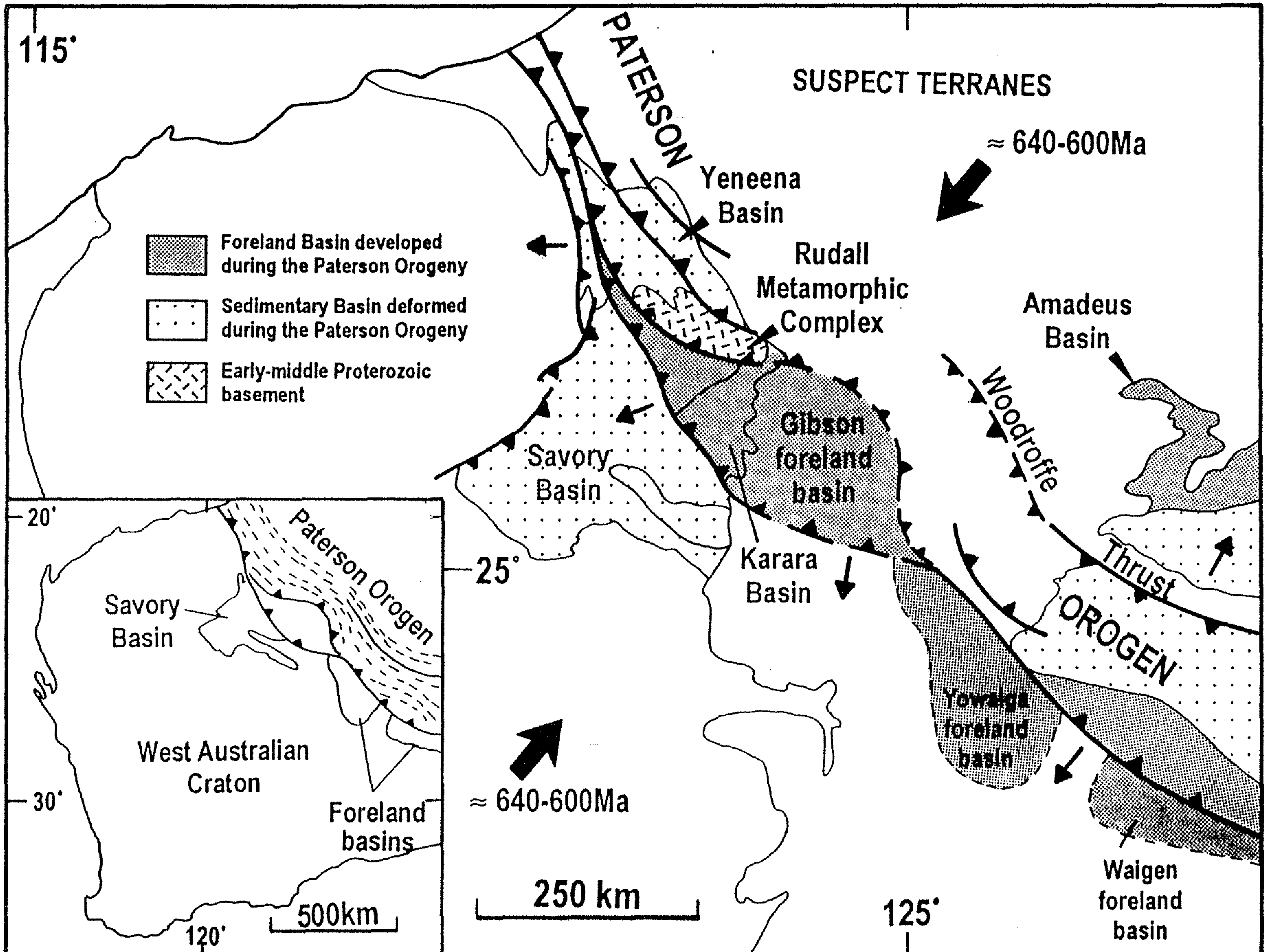

115°
PATERSON
SUSPECT TERRANES
≈ 640-600Ma
Yeneena
Basin
Rudall
Metamorphic
Complex
Foreland Basin developed
during the Paterson Orogeny
Sedimentary Basin deformed
during the Paterson Orogeny
Early-middle Proterozoic
basement
Amadeus
Basin
Woodroffe
Gibson
foreland
basin
Savory
Basin
Thrust
Karara
Basin
25°
OROGEN
20°
Paterson Orogen
Savory
Basin
West Australian
Craton
Foreland
basins
30°
500km
120°
Yowalga
foreland
basin
≈ 640-600Ma
250 km
125°
Waigen
foreland
basin

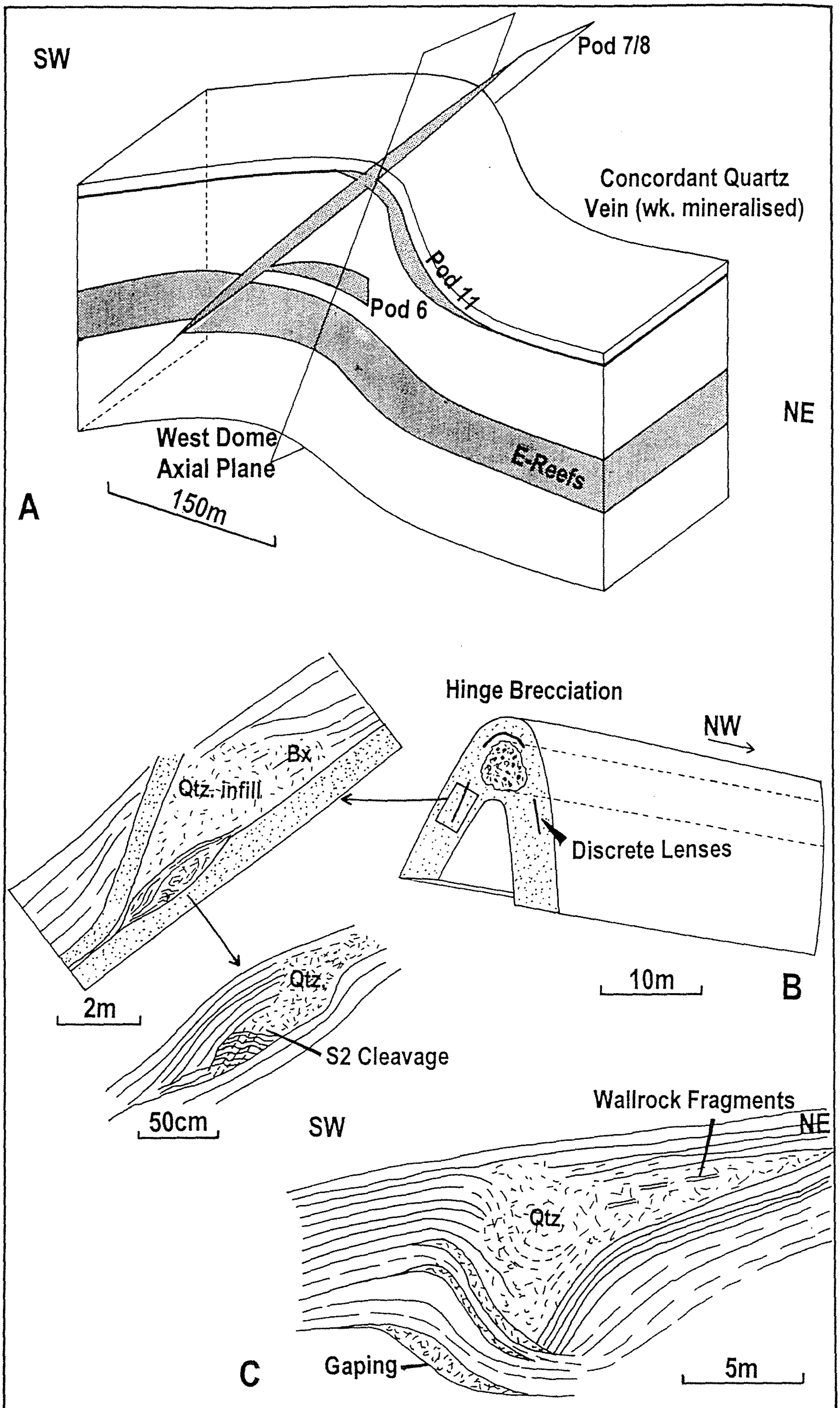
SW
Pod 7/8
Concordant Quartz
Vein (wk. mineralised)
Pod 11
Pod 6
NE
West Dome
Axial Plane
E-Reefs
A
150m
Hinge Brecciation
NW
Bx
Qtz. infill
Discrete Lenses
10m
B
2m
Qtz.
S2 Cleavage
50cm
SW
Wallrock Fragments
NE
Qtz.
C
Gaping
5m

Figure 28: Summary diagram of different styles of "pod" mineralisation in West Dome. (**A**) Large fault-parallel pod mineralisation (stippled - Pod 7/8) occurs within a moderate SW dipping reverse fault in the northern section of West Dome. E-reef mineralisation (also stippled) is offset along this fault, and subsidiary pods have developed in the footwall (Pod 6). Additionally hinge-parallel pods have developed in steepened asymmetric fold hinges (Pod 11). (**B**) A linear pod hosted within the hinge of a shallowly plunging antiformal fold. Insets (cross-sections looking NW) show the nature of smaller faulted bodies that occur on the limbs of the fold. These generally comprised local ramping of the strata by curviplanar reverse faults, which produced zones of dilation/gaping with resultant quartz infill and brecciation. This faulting post-dates S_2 development. (**C**) Large pod structure formed within bedding that developed through local disharmonic folding/flexing of bedding. This caused gaping of the strata with resultant implosive brecciation that is now evident as a zone of massive quartz infill/replacement supporting large clasts/blocks of bedding.

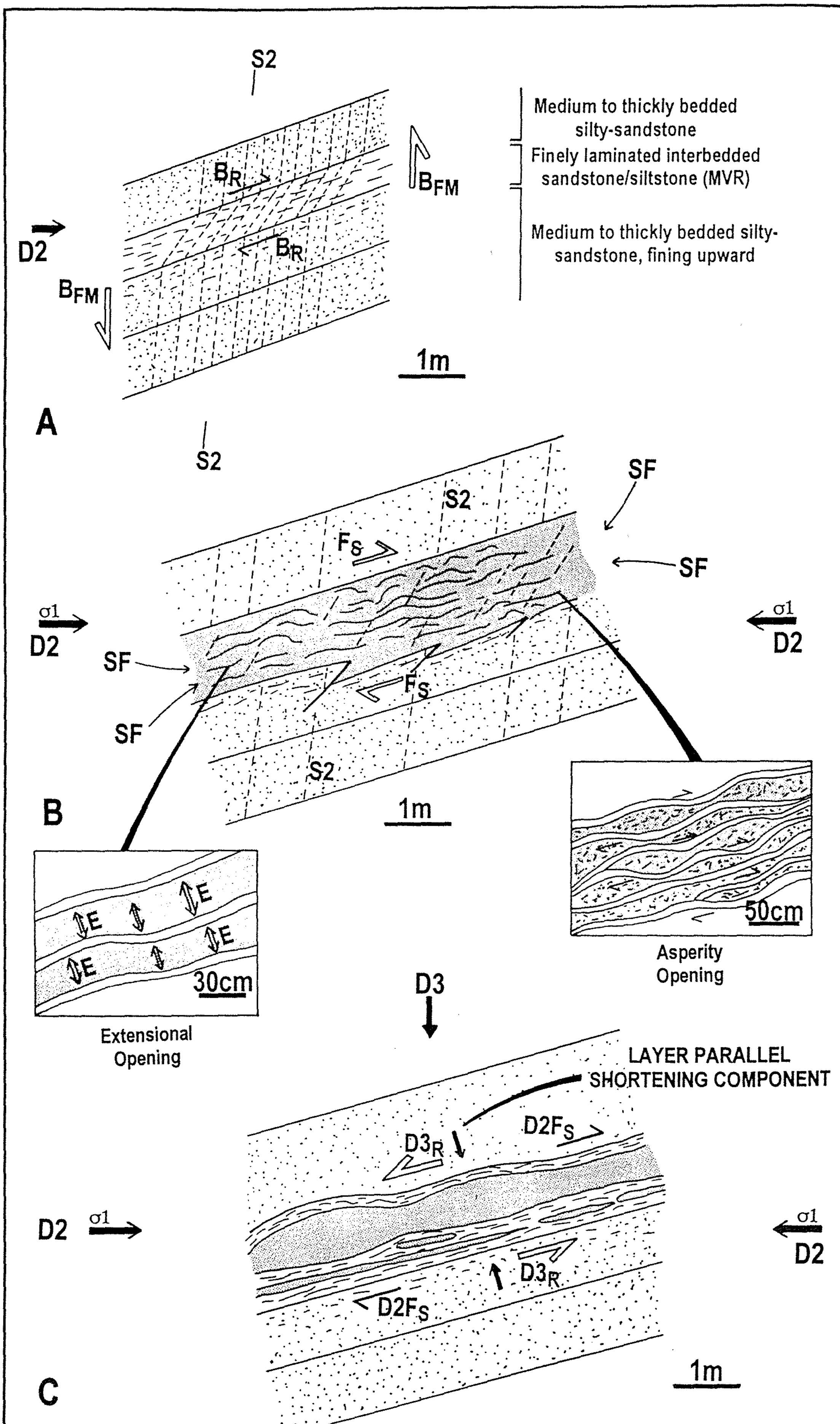

S2
Medium to thickly bedded silty-sandstone
Finely laminated interbedded sandstone/siltstone (MVR)
Medium to thickly bedded silty-sandstone, fining upward
B_R
B_FM
D2
1m
A
S2
SF
F_S
σ1
D2
B
1m
E
30cm
Extensional Opening
50cm
Asperity Opening
D3
LAYER PARALLEL SHORTENING COMPONENT
D3_R
D2F_S
C

Figure 34: Schematic diagram summarising the formation of the massive quartz veining component of the Telfer reefs. (**A**) Compressive strain produced flexural flow/slip deformation that was partitioned into a mechanically favourable horizon that consisted of finely laminated sediments lying between more massive units. **BFM** = bulk fold movement during D_2 developing an antiform to the right and a synform to the left. $\mathbf{B_R}$ = bedding reactivation arising from folding during horizontal shortening. (**B**) Partitioning of D_2 flexural slip ($\mathbf{F_S}$) deformation into this horizon enhanced structural permeability through gaping and microcracking that assisted the infiltration of high-pressure siliceous fluids (**SF**) and resultant silicification. Gaping mechanisms may have included extensional opening of laminae (assisted by elevated fluid pressures) and asperity opening, both enhancing structural permeability. Brittle faulting along the base will also have been enhanced by elevated fluid pressures, and would have provided a pathway for siliceous fluids to enter the reef horizon. (**C**) Continued flexural slip deformation ($\mathbf{D_2Fs}$) and layer-parallel shortening would have caused the quartz veins to pinch and swell, producing smooth reef margins, quartz lenses and further silica addition (particularly along the upper contact). Layer-parallel shear, but with a reverse sense to that for flexural slip, may also have occurred through antithetic reactivation of bedding during D_3 ($\mathbf{D_{3R}}$), initiating further fracturing and fluid infiltration. (All diagrams are cross-sections looking NW).

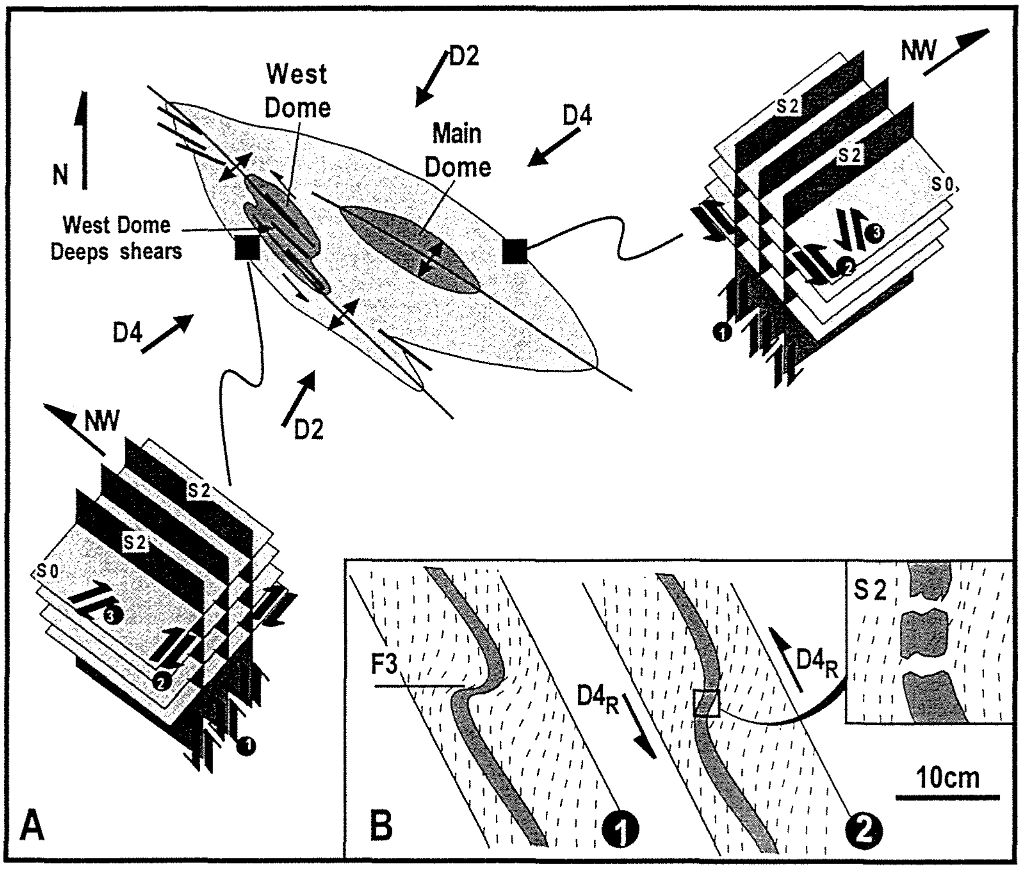

West Dome
Main Dome
D2
D4
N
West Dome Deeps shears
D4
D2
NW
S2
S2
S0
NW
S2
S2
S0
F3
D4R
D4R
S2
10cm
A
B

Figure *33*: Schematic diagram illustrating the effects of D_4 shortening across the Telfer Dome. (**A**) D_4 horizontal shortening was slightly oblique to the Telfer Dome and is thus likely to have reactivated and re-used pre-existing domal structures, including bedding and axial plane cleavage (block diagrams). These effects include synthetic reactivation of S_2 (1), and antithetic reactivation of bedding, with both dip-slip (2) and oblique slip (3) movement components. Because of the obliquity of D_4 stresses these effects would have been strongest in both the NW and SE corners of the Telfer Dome. Large axial plane parallel shears (West Dome Deeps) have a left-stepping arrangement suggesting they were reactivated and further developed during weak sinistral transpression produced by the oblique D_4 stress. (**B**) Unfolding of D_3 folds by bedding reactivation during D_4. Recumbent D_3 folds, which were observed in the SE corner of Main Dome (1), were progressively unfolded and fractured by reactivation of the enveloping bedding surface during D_4 (2). This reactivation was strongest along the SE limb of Main Dome as a result of D_4 strain intensification into this corner of the Telfer Dome (as illustrated in A).

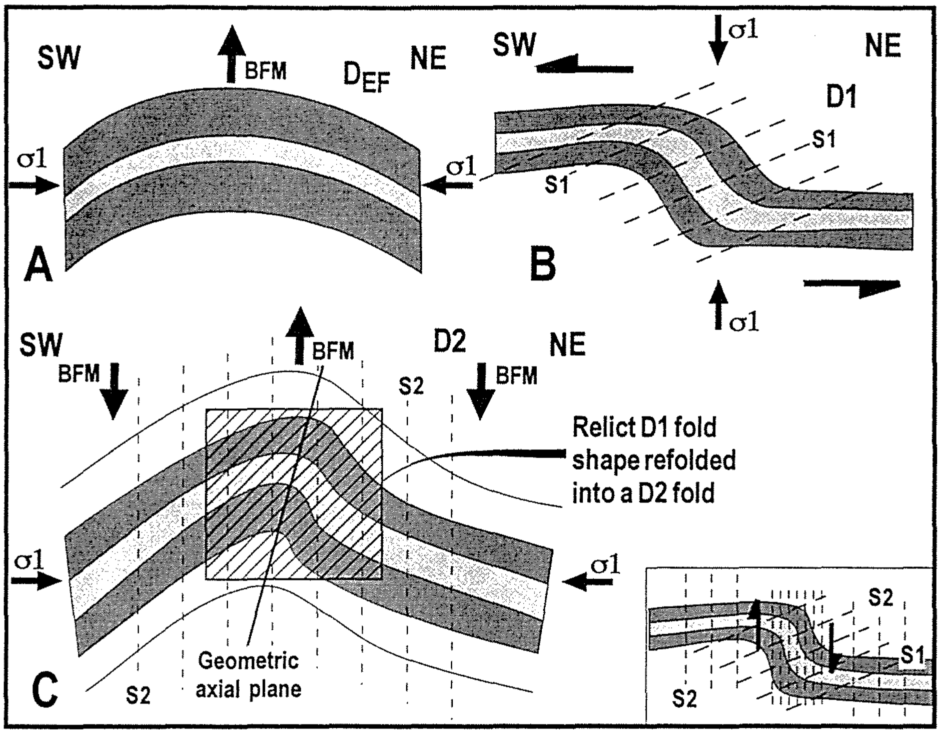
SW
BFM
D_{EF}
NE
σ1
σ1
A
SW
σ1
NE
D1
S1
σ1
S1
B
σ1
SW
BFM
BFM
D2
NE
BFM
S2
Relict D1 fold shape refolded into a D2 fold
σ1
σ1
S2
S2
S1
C
S2
Geometric axial plane
S2

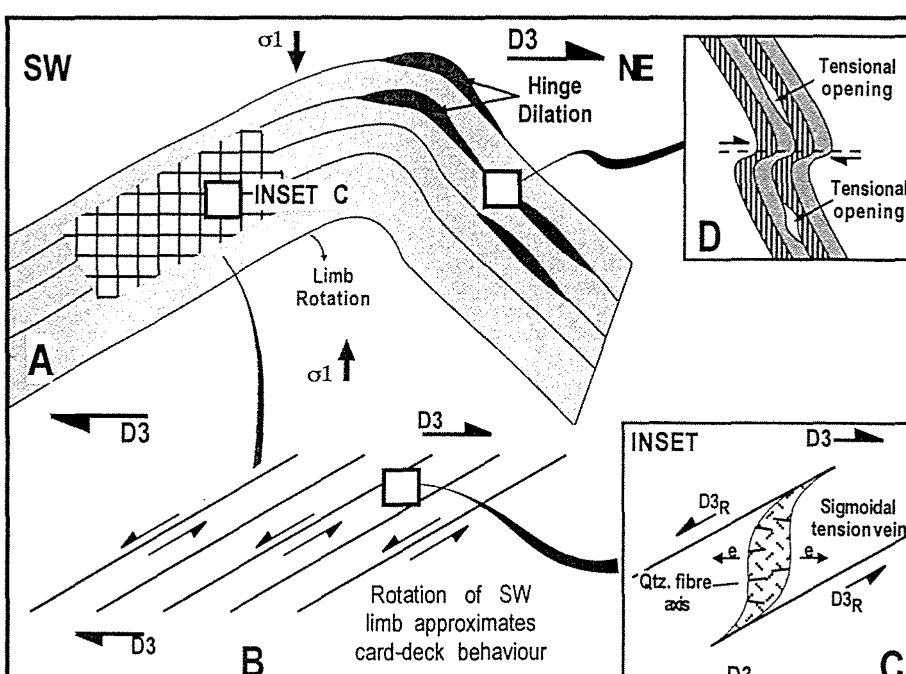
SW
σ1
D3
NE
Hinge Dilation
Tensional opening
INSET C
Tensional opening
D
Limb Rotation
A
σ1
D3
D3
INSET
D3
D3R
Sigmoidal tension vein
e
e
Qtz. fibre axis
D3R
Rotation of SW limb approximates card-deck behaviour
D3
B
D3
C

Figure 31: Schematic development of a D_2 dome by re-folding of earlier folds. Early orogenic shortening (D_{EF} - see Section A) forms broad flexures (**A**) that subsequently become the nucleus for D_1 fold development (**B** - see also Section A). Refolding of the F_1 folds by D_2 results in an antiformal fold with a characteristic asymmetry in the hinge, and a geometric axial plane that is not parallel to S_2 (**C**). The small inset illustrates the potential for preferential D_2 strain intensification along the pre-existing steep limb of a D_1 fold, thus further steepening this limb and increasing the asymmetric character of D_2 folds. This may occur in the Telfer Dome to enhance the domal asymmetry. Large full arrows marked **BFM** in all diagrams indicate the bulk fold movements.

Figure 32: Schematic diagram illustrating the potential effects of D_3 on the Telfer Dome, and other D_2 folds. Main diagram (**A**) illustrates the D_2-formed Telfer dome with D_3 (consisting of vertical shortening and NE directed horizontal movement) acting on it. Rotation of the SW limb during D_3 would have caused antithetic layer-parallel shear (reactivation) along bedding (**B**), a situation analogous to rotation of a card deck model (*e.g.* Bell, 1986). This shearing produced intra-bedding tensional gashes (**C** - observed in Pit 14) whose asymmetry is opposite that of those developed during D_2 flexural slip deformation. In contrast the NE limb and domal hinge would have been gaped (A) and refolded (**D**). Gaping would have been greatest where the limb and hinge were markedly rotated towards the NE by refolding during D_3 (*e.g.* the I-reefs)

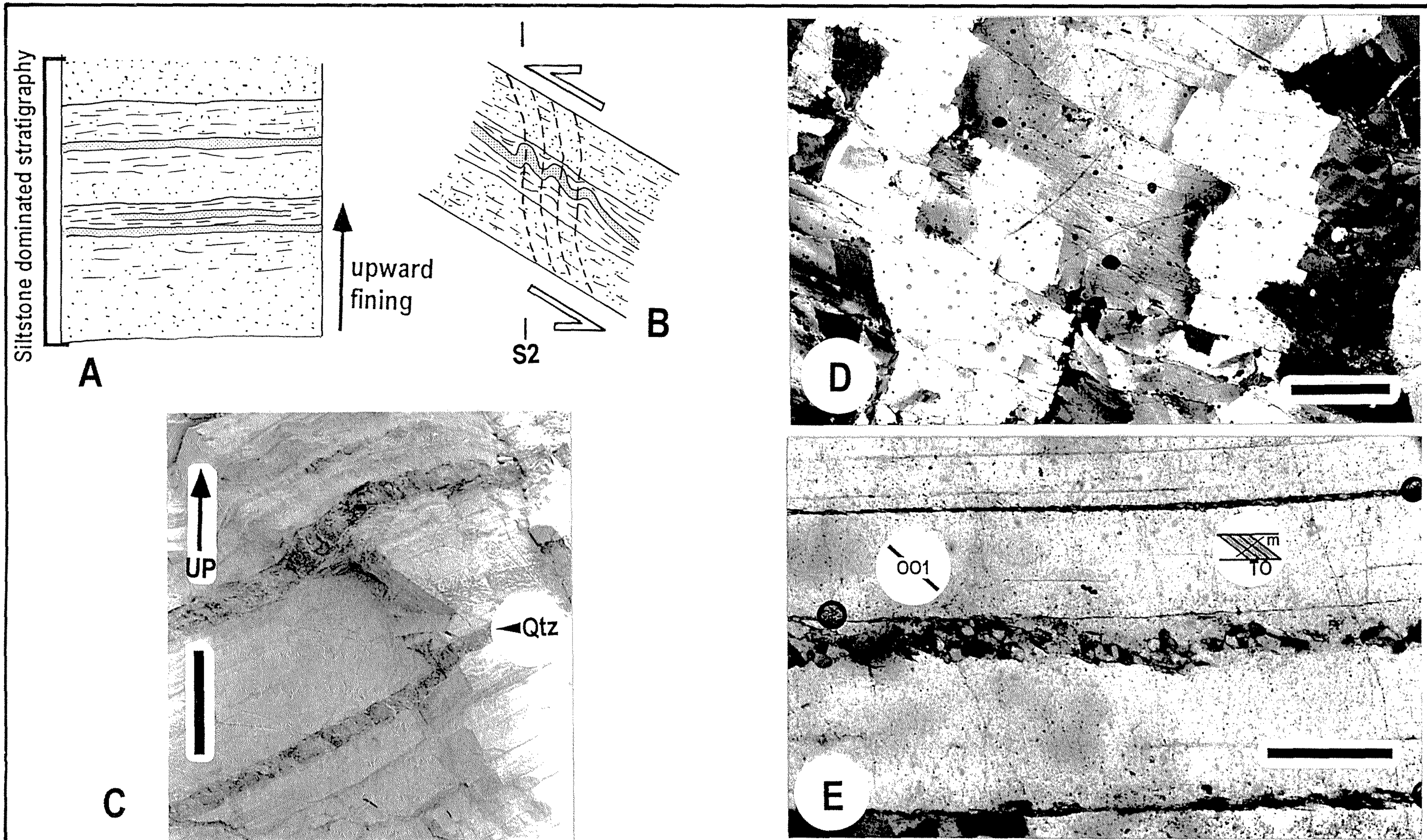
Siltstone dominated stratigraphy
upward fining
A
S2
B
UP
Qtz
C
D
001
m
TO
E

Figure 30: Characteristics of bedding-concordant laminar veins within the Telfer Dome. (**A**) Field relationships of the veins, which occur within siltstone laminae towards the top of upward fining sequences. (**B**) The veins are folded (F_2) suggesting either pre- or syn D_2 vein formation. However, S_2 is steeper in the vein horizon suggesting that it's orientation was preserved by silicification associated with the veining, whereas in the matrix S_2 was rotated by D_2 reactivation of bedding; thus implying the veins developed syn-D_2. (**C**) Field photograph of laminar and massive quartz veins within finely laminar/bedded siltstones of the Outer Siltstone Formation (scale bar represents 30cm; Location: NW face of Pit 9R, Telfer Mine; Mine Grid - 13840mN 8665mE). (**D**) Photomicrograph of laminar veins illustrating the coarse blocky and optically continuous character of quartz crystals. The crystals are offset along fine fractures that define the laminar form of the vein; these pass diagonally NW-SE across the photograph. The scale bar represents 2mm, and the view is in cross polarised light. (*JCU Catalogue No*. 48358). (**E**) Photomicrograph of one of the lamination fractures illustrating the oblique mica growth along the fracture plane; the trace of the 001 mica crystal plane is marked. Note the small jog-like openings in which mica has precipitated. This suggests that the fractures formed through shearing, rather than dissolution. This would have had a top-to-the-right (in the photo) shear sense, resulting in tensional opening (**TO**) and oblique mica growth (**m**) along the shear plane. The scale bar represents 0.4mm, and the view is in cross polarised light. (*JCU Catalogue No*. 48358).

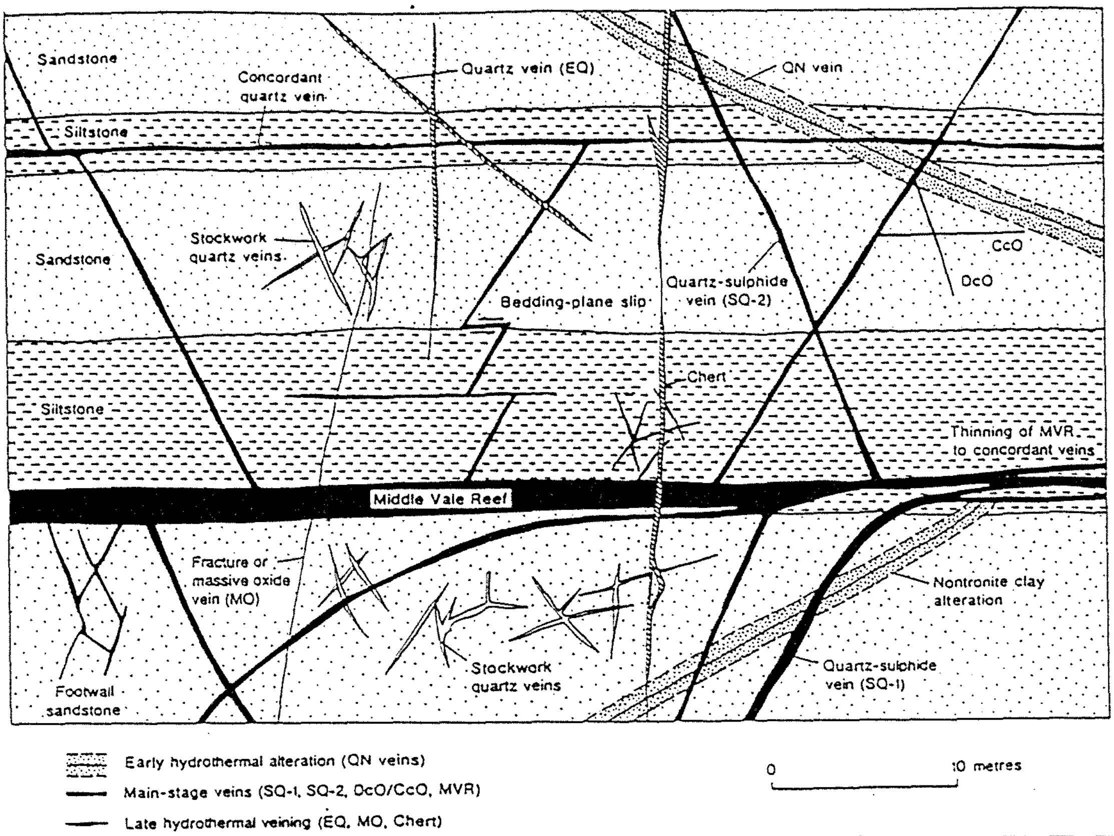

Class/Timing	Description	Orientation	Mineralogy	Associated Alteration
Qn veins(1)	Thin, irregular qtz veins up to 3cm thick, with a characteristic lime-green alteration halo; abundant	North-south trending, sub-concordant, discordant	Qtz (+ rare pyrite)	Nontronite, silica, sericite, trace pyrite
SQ-1 veins (2)	Massive qtz-sulphide, vuggy, < 30cm thick, planar-irregular; common	West-southwest - east-northeast trending, discordant	Qtz, pyrite, chalcopyrite, galena, sphalerite	Sericite, silica, Fe-staining, pyrite, adularia, albite, tourmaline
SQ-2 veins (2)	Massive qtz.-sulphide, oxide, <10cm thick, irregular, planar; common	North-south trending, sub-concordant to discordant	Massive pyrite, chalcopyrite, qtz., ankerite, fine gr. pyrite	
CcO/DcO veins (2)	Thin planar massive oxide veins; common	Sub-concordant (CcO), discordant (DcO)	Ankerite, qtz, pyrite, chalcopyrite, muscovite, trace albite	
Concordant quartz (2)	Continuous, <5cm thick, locally folded; abundant	Concordant	Quartz	
EQ - veins (3)	Thin planar (<3cm) qtz. veins, stockworks; common	Variable, discordant	Qtz (minor pyrite)	
MO veins (3)	Massive sulphide, oxide; rare	North-south trending, sub-vertical	Massive pyrite, chalcopyrite	
Chert dikes (3)	Grey or cream, stockwork like, locally brecciate wall rocks and MVR; rare	North-south trending, sub-vertical	Cryptocrystallin e silica	

Figure 29: Summary diagram and table of the various veining styles identified by Goellnicht (1987). The shaded portion of the table represents the main veining stage within the Telfer system. (adapted from Goellnicht, 1987)

Figure 22: Summary diagram of the major folding style (main diagram) and macroscale effects (observed and interpreted) of progressive deformation across the Paterson Province during the Paterson Orogeny. Prominent magnetic linears are also indicated. Boxes A - E represent schematic summaries of the macro-structural development and potential for re-use of pre-existing structures in the major regions of the Paterson Province. Cross section views are annotated ***X*** (all looking NW) and plan views are marked ***P*** (north is towards the top of the page). Deformation episodes are annotated with their respective numbers. (**A**) The Anketell region illustrating closely spaced magnetic linears and curvilinears, many of which are truncated suggesting thrust folding. These faults may also have been reactivated sinistrally during D_5, and dextrally during D_6. (**B**) Structural styles in the Telfer region, including doming during D_3 (**i**), refolding of these by D_4 (**ii**), and faulting of regional folds during D_5 (**iii**). (**C**) Transpressive structures in the Vines Fault - Nifty region (after Dare, 1994). These include dextral N-S trending faults that formed late-D_3 (**i**), truncating D_3 folds and producing subsidiary faults. During D_6 these faults may have been reactivated sinistrally, or new faults could have initiated truncating earlier ones (**ii**). (**D**) Structural development along the south-western margin and Broadhurst Range included thrust-faulted D_3 folding. Rotation and flattening of these folds during D_4 may have caused lag fault formation (**i**). These faults would have been reactivated with a sinistral sense during D_5 (**ii**), which was weakly transpressive. D_6 compression could also have reactivated these faults in a dextral manner (**iii**). (**E**) Fault truncated folding (ENE plunging) developed in the Karara Basin/Formation by D_6 deformation.

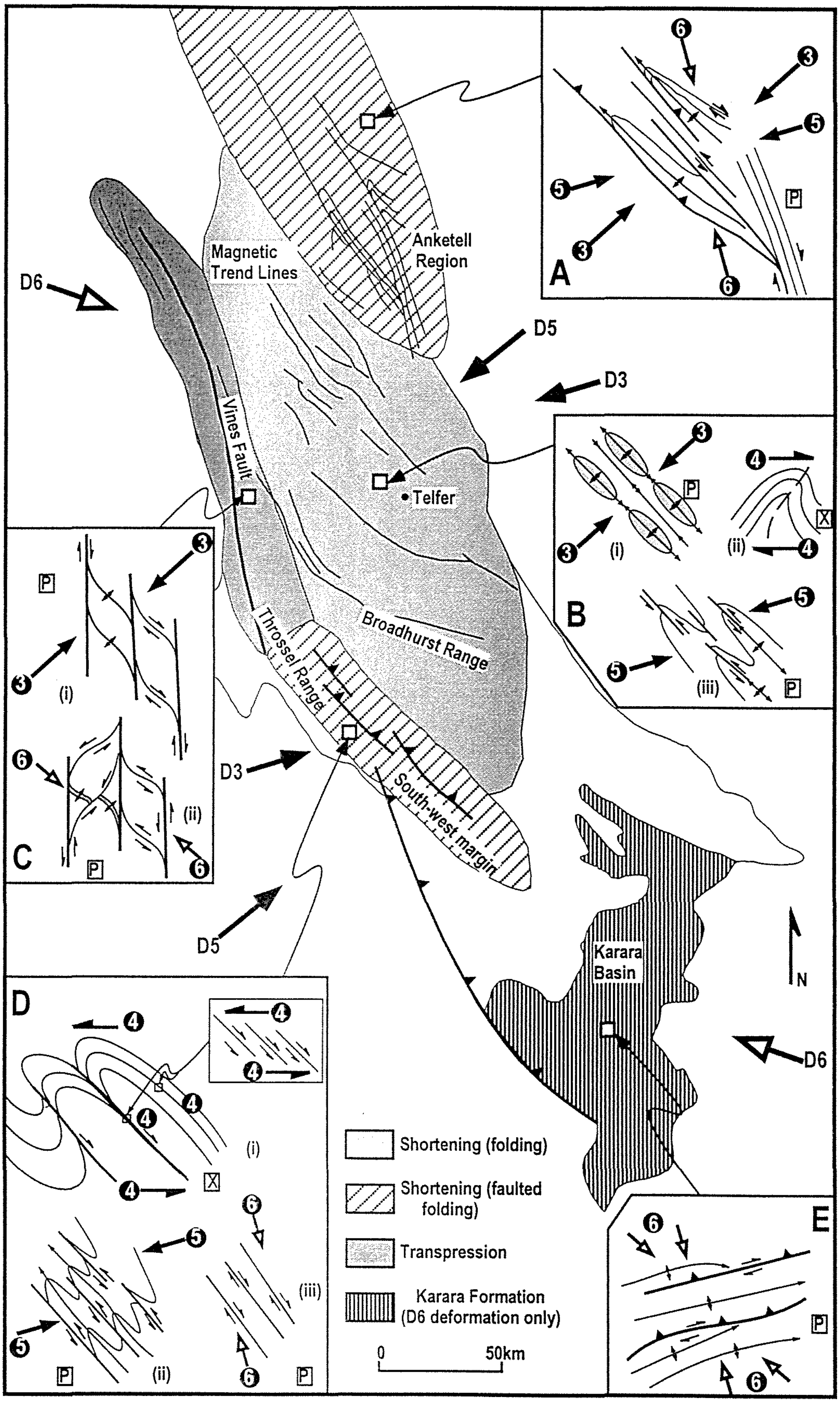

Magnetic Trend Lines
Anketell Region
D6
D5
D3
Vines Fault
Telfer
Broadhurst Range
Throssel Range
South-west margin
D3
D5
Karara Basin
N
D6
A
B
C
D
E
(i)
(ii)
(iii)
P
X
Shortening (folding)
Shortening (faulted folding)
Transpression
Karara Formation (D6 deformation only)
0
50km

Figure 23: Schematic diagram illustrating the potential tectonic setting of the Paterson Province as an ensialic (intracratonic) foreland/back-arc basin. Collisional orogenesis occurred to the NE, and may have involved oceanic crust subduction. The Paterson Province, along with this orogen, was accreted SW onto the Archean Pilbara Craton. Lithospheric delamination (**A**) may have produced asthenopheric upwelling (**B**) that resulted in magma underplating the Yeneena Basin (**C**). Such magma, and other crustal fluids, could have moved along deep basal thrusts and décollements towards the Paterson Province. Such fluids could have been sourced from subducting oceanic crust (**D**), or alternatively further inboard from broken pieces of oceanic crust that descended to deeper mantle levels (**E**). Similarly, metamorphic fluids, released from the core of the orogen, may have migrated SW to the Paterson Province (**F**).

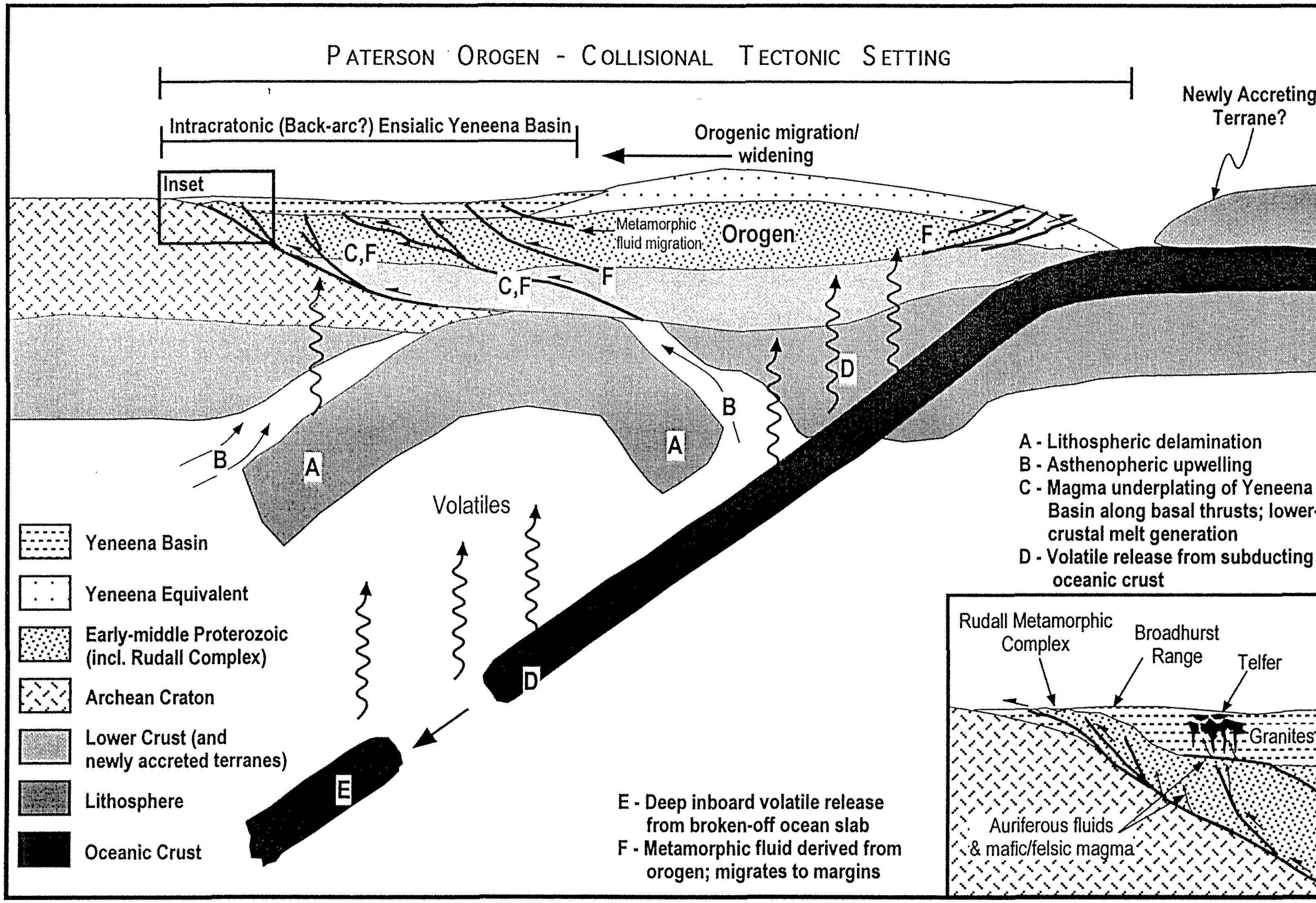

PATERSON OROGEN - COLLISIONAL TECTONIC SETTING
Intracratonic (Back-arc?) Ensialic Yeneena Basin
Orogenic migration/ widening
Newly Accreting Terrane?
Inset
Metamorphic fluid migration
Orogen
C,F
C,F
F
F
A
A
B
B
D
D
E
Volatiles
Yeneena Basin
Yeneena Equivalent
Early-middle Proterozoic (incl. Rudall Complex)
Archean Craton
Lower Crust (and newly accreted terranes)
Lithosphere
Oceanic Crust
A - Lithospheric delamination
B - Asthenopheric upwelling
C - Magma underplating of Yeneena Basin along basal thrusts; lower-crustal melt generation
D - Volatile release from subducting oceanic crust
E - Deep inboard volatile release from broken-off ocean slab
F - Metamorphic fluid derived from orogen; migrates to margins
Rudall Metamorphic Complex
Broadhurst Range
Telfer
Granites
Auriferous fluids & mafic/felsic magma

SECTION C

Late Structural Timing of Mineralisation in the Telfer Au-Cu deposit and the Role of Orogenic Deformation in Regional Fluid Flow and Mineralisation.

(FIGURES)

Figure 1: Geometry of the Telfer Dome and areas sampled in this study. (**A**) Plan view of the Telfer Dome illustrating the position of the two lower order sub-domes, Main and West Domes, and the distribution of stratabound reef mineralisation (MVR and E-Reefs). (**B**) Cross section of Main Dome (≈11,100mN - Mine Grid; NE-SW - magnetic; section line marked in A) illustrating the geology and distribution of stratabound reef mineralisation, as well as the location of the three sampled suites. Suite *1* , the Middle Vale Siltstone and Middle Vale Reef (**MVR**), was sampled from two locations; in drill core immediately SW of the domal hinge, and from underground workings on the NE limb. *Suite 2* was sampled from the newly discovered M-Reef series in an exploration decline and associated drives and cross-cuts. *Suite 3* was sampled from the newly discovered I-Reefs ("deeps") in diamond drill core from the deeper Main Dome hinge. These reefs commonly comprise extensive brecciation in the vicinity of the tightened and refolded Main Dome hinge. **NOTE**: the development of many of the deeper reefs away from the hinge is currently untested.

Figure 2: Photomicrograph of typical massive quartz veining in the Middle Vale Reef. Note the "dirty" appearance of the quartz (**Qtz**) resulting from numerous fine-grained silty inclusions, coupled with small clasts of wallrock (**Cr**) that were subsequently dolomitised (although much of this is now extremely weathered). The massive quartz was dynamically recrystallised during subsequent veining/deformation phases, and irregular sulphide aggregates (black) infilled along seriate quartz margins. The scale bar at the bottom right is 1.5mm long. (*JCU Catalogue No.* 48346)

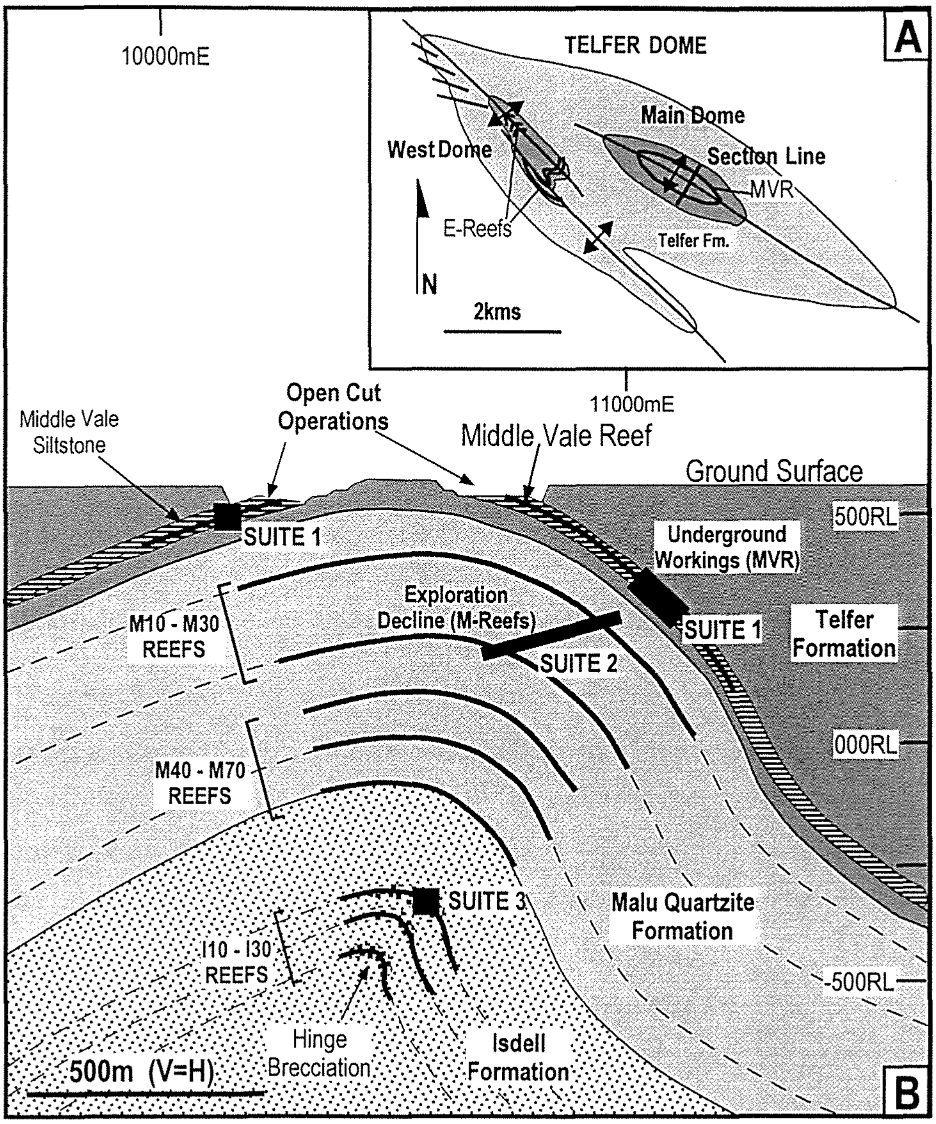

TELFER DOME
A
10000mE
Main Dome
West Dome
Section Line
MVR
E-Reefs
Telfer Fm.
N
2kms
11000mE
Middle Vale Siltstone
Open Cut Operations
Middle Vale Reef
Ground Surface
500RL
SUITE 1
Underground Workings (MVR)
Exploration Decline (M-Reefs)
M10 - M30 REEFS
SUITE 1
Telfer Formation
SUITE 2
000RL
M40 - M70 REEFS
SUITE 3
Malu Quartzite Formation
I10 - I30 REEFS
-500RL
Hinge Brecciation
Isdell Formation
500m (V=H)
B

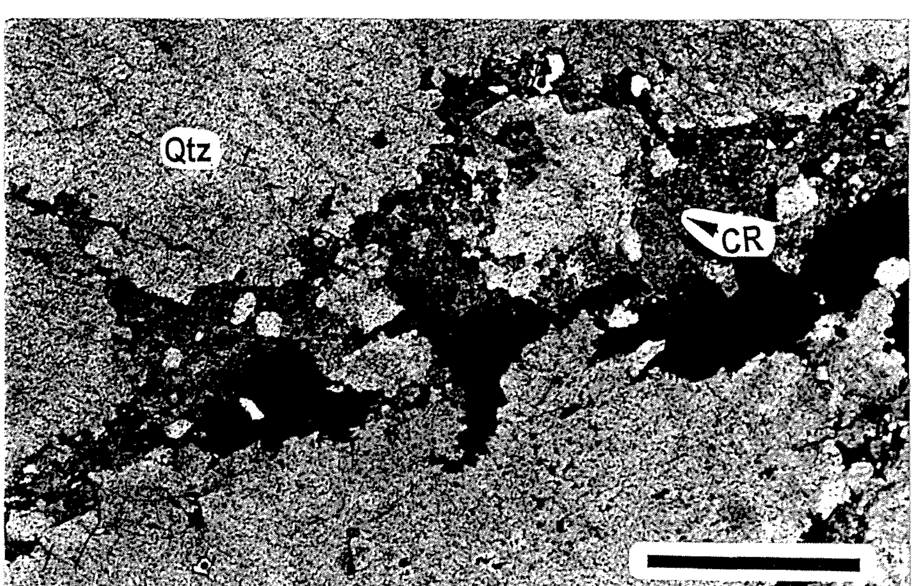

Qtz
CR

Figure 3: Photomicrograph of coarse-grained dolomite-quartz-sulphide veining and alteration in the Middle Vale Siltstone. Veining comprises coarse-grained ferroan dolomite (**Dol**), which exhibits rhombic twinning, with interstitial quartz. Finer grained quartz grew syntaxially along vein margins (**Qtz**) following reopening of the vein after dolomite growth. The matrix is altered to sericite, calcite and dolomite, with lesser chlorite and epidote. Small clumps of chlorite-sericite-epidote alteration occur marginal to the veins (**CS**), and pervasive sulphide (pyrite ± galena/chalcopyrite/gold inclusions) alteration/infill occurs through the matrix and along vein margins (**Py**). The scale bar at the bottom right is 3mm long. (*JCU Catalogue No.* 48347).

Figure 4: Photomicrograph of rhombic/rounded dolomite porphyroblast (**Dol**) alteration in the rock matrix. These porphyroblasts overgrew S_2, are ferroan and commonly show internal zoning. In this photo, the large, apparently well-zoned, porphyroblast is now altered to quartz-sericite in the core with a fine-grained sericite rim around the margin. The scale bar at the bottom right is 2mm long. (*JCU Catalogue No.* 48348).

Figure 5: Photomicrograph of strongly deformed Middle Vale Reef illustrating coarse-grained sulphide (mainly pyrite) growth (**Py**) associated with the first mineralisation phase, which was subsequently fractured and overgrown by fibrous quartz (**Qtz Fb.**). Relict pieces of "dusty" massive quartz (**Qtz**) lie in the matrix surrounded by newly recrystallised (and inclusion-free) quartz. The scale bar at the bottom right is 0.5mm long. (Sample MVR SM-1 - Newcrest Mining; Telfer Geology Dept., Telfer Gold Mine)

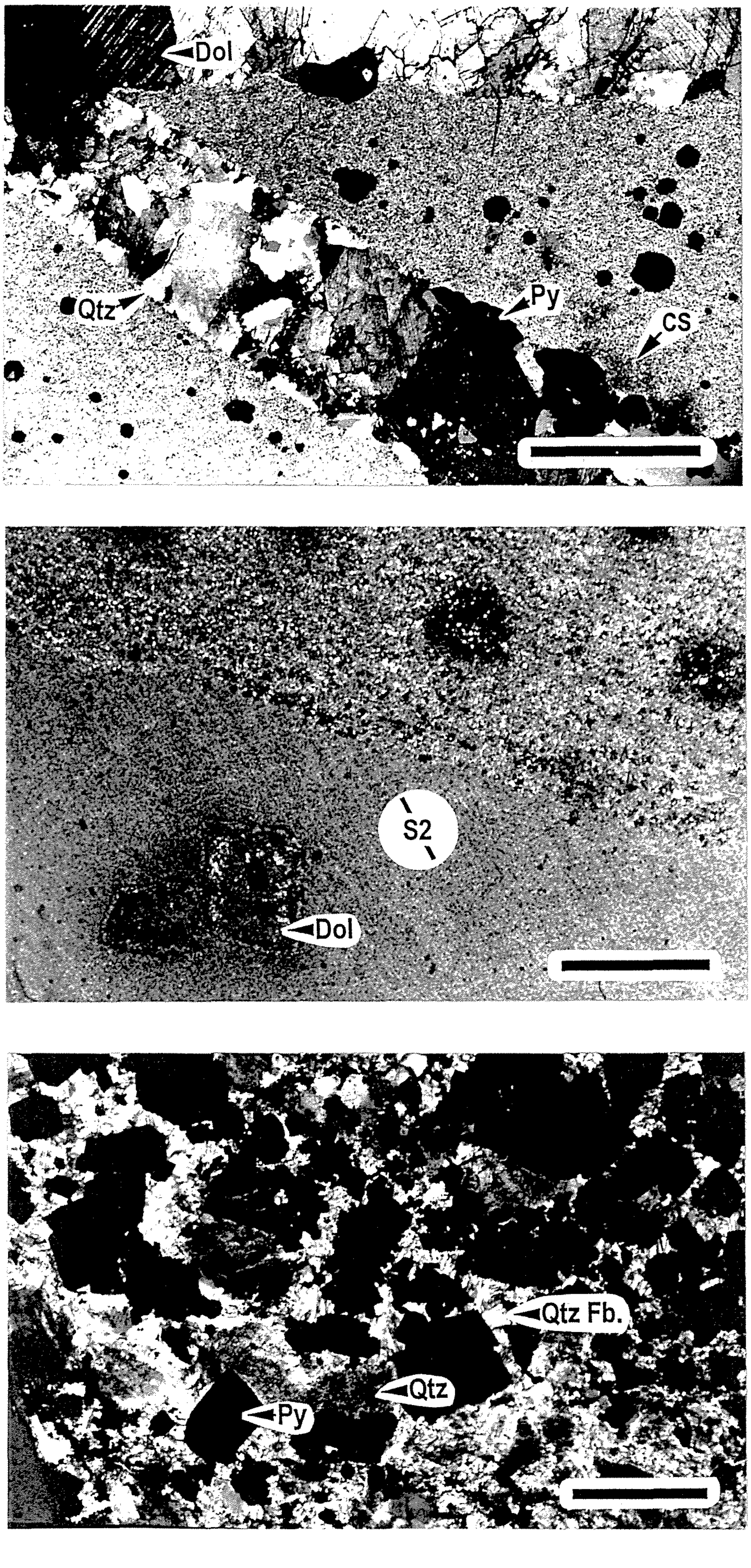

Dol
Qtz
Py
CS
S2
Dol
Qtz Fb.
Qtz
Py

Figure 6: Photomicrograph of a metasomatic aggregate within a fine-grained argillaceous unit. The aggregate consists of a cluster of coarse-grained quartz (**Qtz**), and occasionally albite, grains that exhibit a helicitic texture comprising fine-grained sericite, muscovite and dolomite inclusions, that parallel S_2. The aggregates were replaced and overgrown by dolomite (**Dol**), followed by sulphide grains and aggregates (Sulph). The scale bar at the bottom right is 0.5mm long. (*JCU Catalogue No.* 48349)

Figure 7: Photomicrograph of the lower margin of the M10 reef. Massive quartz veining (**Qtz**) is subsequently deformed (progressively intensifying towards the margin) and dynamically recrystallised. This was followed by grey ferroan dolomite (**Dol**), both as infill and replacement/alteration that overprints the recrystallised quartz boundaries and hence formed syn- to post-quartz deformation. Sulphide mineralisation (opaque) replaces the dolomite. Pervasive dolomite alteration also occurred in the wallrock (**Dol**). This was subsequently overprinted by further silicification (**Si**), coeval with chlorite-calcite alteration/veining, and resulted in textural destruction of the dolomite alteration front. The scale bar at the bottom right is 2mm long. (*JCU Catalogue No.* 48350)

Figure 8: Photomicrograph of coarse-grained grey ferroan dolomite (**Dol 1**) truncated by veinlets of a second white-pink coloured opaque dolomite phase (**Dol 2**). Note the dirty colouration of large euhedral rhombic grains, which represents the first dolomite phase being replaced (**RP**) by the second, particularly along grain boundaries. The scale bar at the bottom right is 4mm long. (*JCU Catalogue No.* 48351)

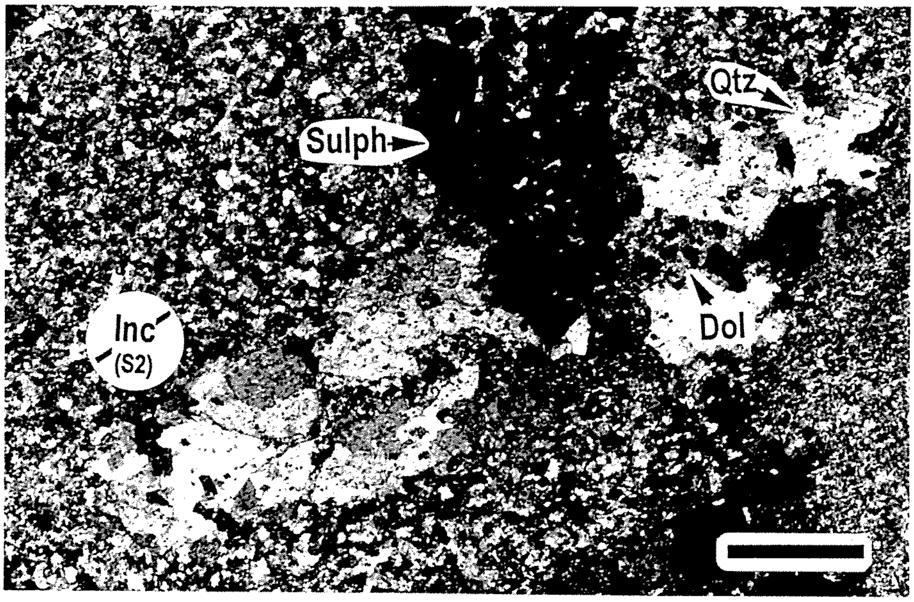
Qtz
Sulph
Dol
Inc
(S2)

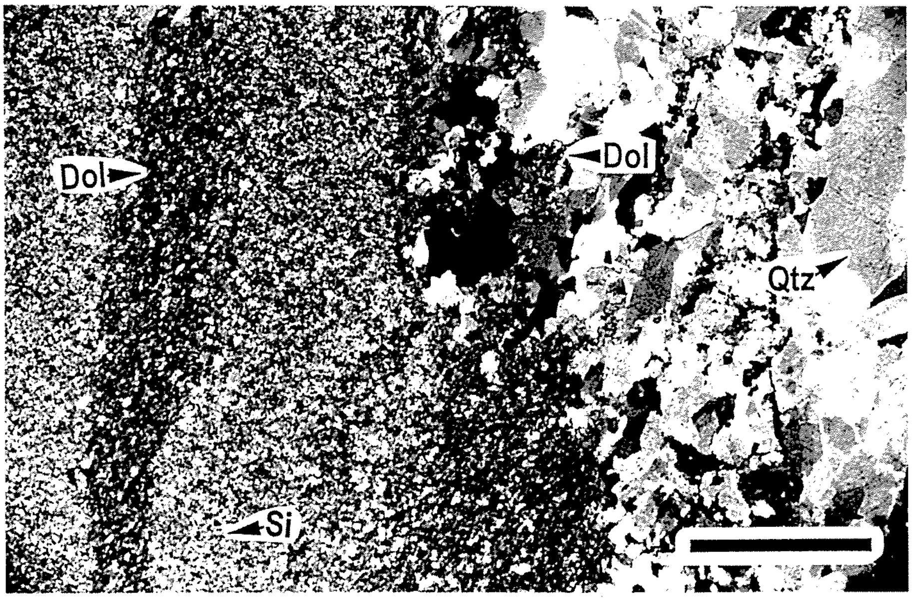
Dol
Dol
Qtz
Si

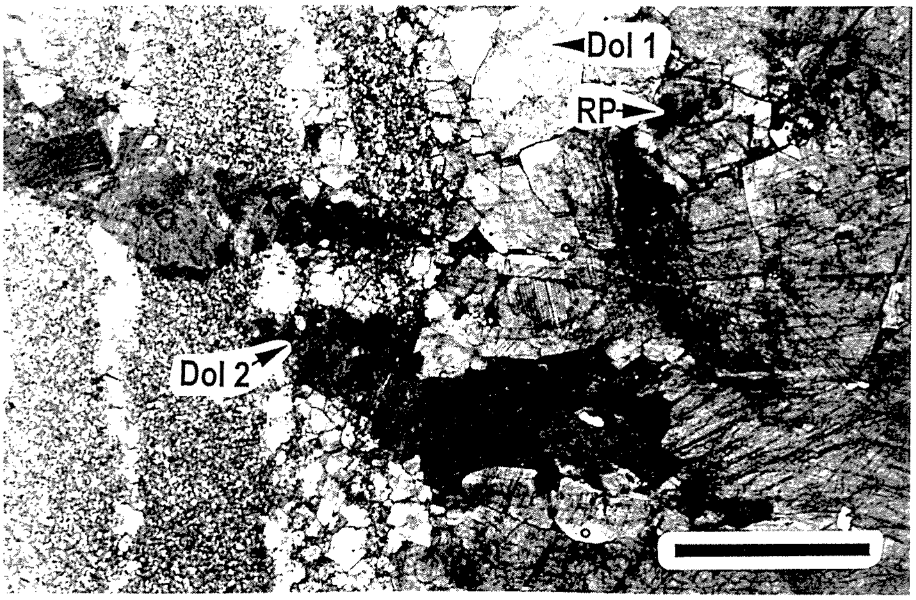
Dol 1
RP
Dol 2

Figure 9: Photomicrograph of an altered wallrock clast, within the massive quartz (**Qtz**) of the M10 illustrating the successive alteration history. The clast was initially altered to dolomite (**Dol**) and fine-grained epidote, which was subsequently altered (pervasively) to chlorite, calcite and muscovite (**Chl-Musc**) accompanying sulphide (mainly chalcopyrite) deposition. Fine-grained micas scattered across the clast and along its margins are related to the second alteration phase. Elsewhere, these occur as thick clusters at reaction fronts along chalcopyrite grain margins. The scale bar at the bottom right is 0.5mm long. (JCU Catalogue No. 48350)

Figure 10: Photomicrograph of coarse brecciation in the Telfer "deeps" illustrating angular breccia clasts supported in an exotic grey ferroan dolomite-quartz matrix. Note the fine-grained euhedral epidote crystals (**Ep**) that rim the clasts and precipitated just prior to the dolomite (**Dol**). The breccia clasts are pervasively altered to epidote-sericite-grey dolomite. "Dusty" areas within the matrix are a second opaque dolomite phase that replaces/infills the earlier grey ferroan dolomite, particularly along grain margins. This second dolomite phase was accompanied by chlorite-calcite alteration. The scale bar at the bottom right is 2mm long. (Sample ST 18 - Newcrest Mining; Telfer Geology Dept., Telfer Gold Mine)

Figure 11: Photomicrograph of coarse-grained ferroan grey dolomite veining (**Dol**) in the Telfer "deeps", which has been subsequently replaced by a second white opaque phase of dolomite (**Dol 2**). This second phase infilled/replaced along grain boundaries and as fine-grained veinlets that cross-cut the earlier coarse-grained dolomite matrix. The scale bar at the bottom right is 2mm long. (Sample ST 18 - Newcrest Mining; Telfer Geology Dept., Telfer Gold Mine).

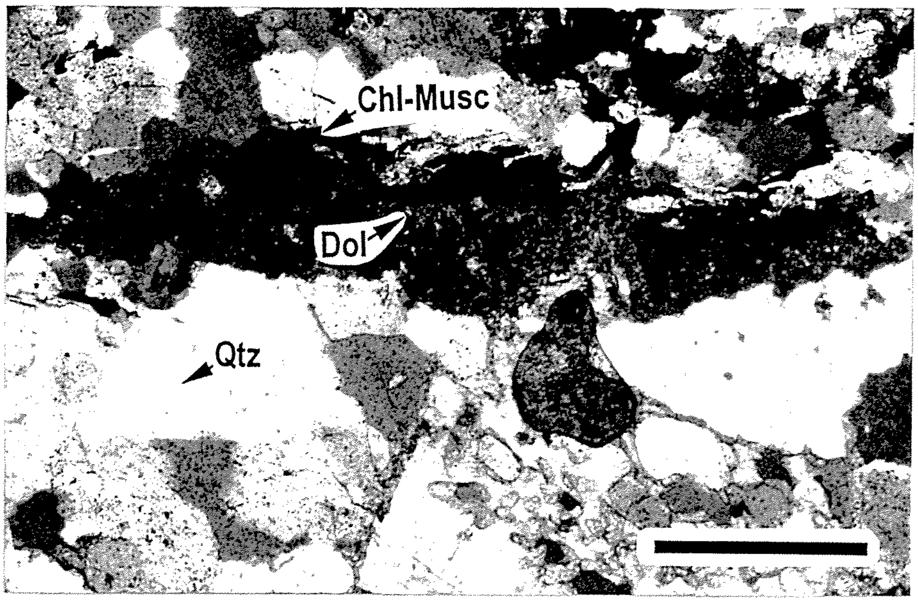
Chl-Musc
Dol
Qtz

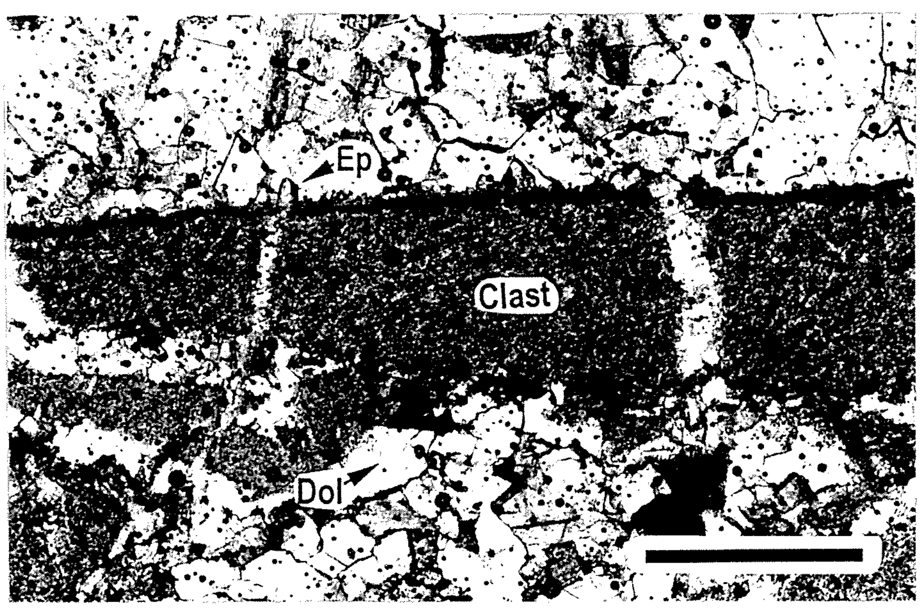
Ep
Clast
Dol

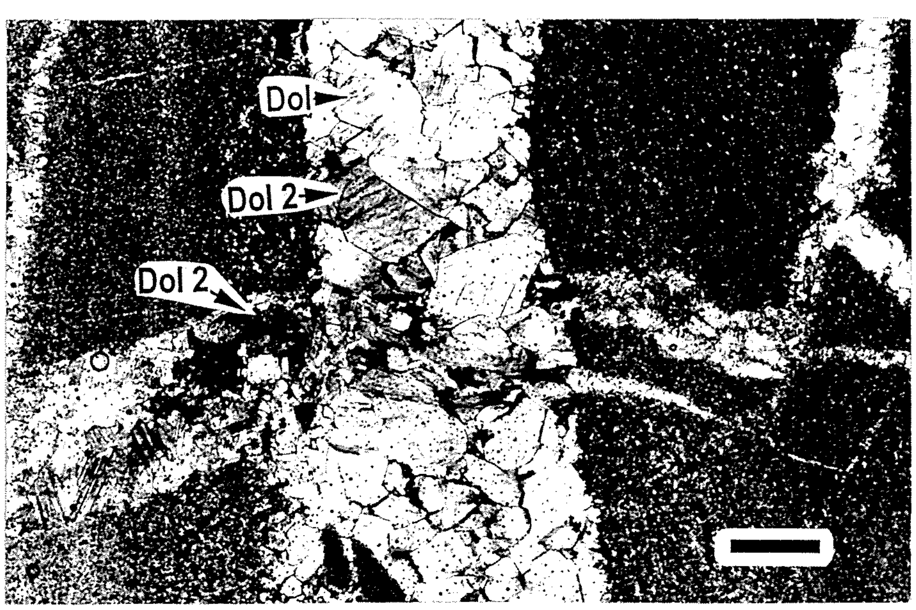
Dol
Dol 2
Dol 2

Figure 12: Photomicrograph of highly altered wallrock (first phase of dolomite-sericite-epidote) cut by fine-grained quartz (**Qtz**) veinlets that contain sulphides (**Sulph**). Associated with these are silica alteration halos (**Si**) that overprint the earlier wallrock alteration. Also associated with the silicification are fine-grained muscovite grains that grew within the silica, and along reaction fronts on sulphide grain margins. The scale bar at the bottom right is 2mm long. (Sample ST 17 - Newcrest Mining; Telfer Geology Dept., Telfer Gold Mine)

Figure 13: Photomicrograph of a coarse-grained rhombic grey ferroan dolomite aggregate (**DOL**) with infilling sulphides (mainly chalcopyrite - **Cpy**). The sulphides replaced dolomite along grain margins, and infilled interstices. Dusty opaque areas represent the second opaque-white dolomite phase that replaced the earlier grey ferroan dolomite. The scale bar at the bottom right is 2mm long. (Sample ST 16 - Newcrest Mining; Telfer Geology Dept., Telfer Gold Mine).

Figure 14: Photomicrograph illustrating the main phase of sulphide deposition in the "deeps" and associated alteration. Anhedral sulphides (**Sulph** - mainly pyrite with late chalcopyrite) infill fractures in the pervasively altered rock matrix. Associated with this, were silica alteration fronts (**Si**) and fine-grained muscovite-sericite growth (**Musc**) that were concentrated into reaction fronts along sulphide grain margins and which overprint the earlier wallrock alteration (grey dolomite veining phase). The scale bar at the bottom right is 2mm long. (Sample ST 11 - Newcrest Mining; Telfer Geology Dept., Telfer Gold Mine).

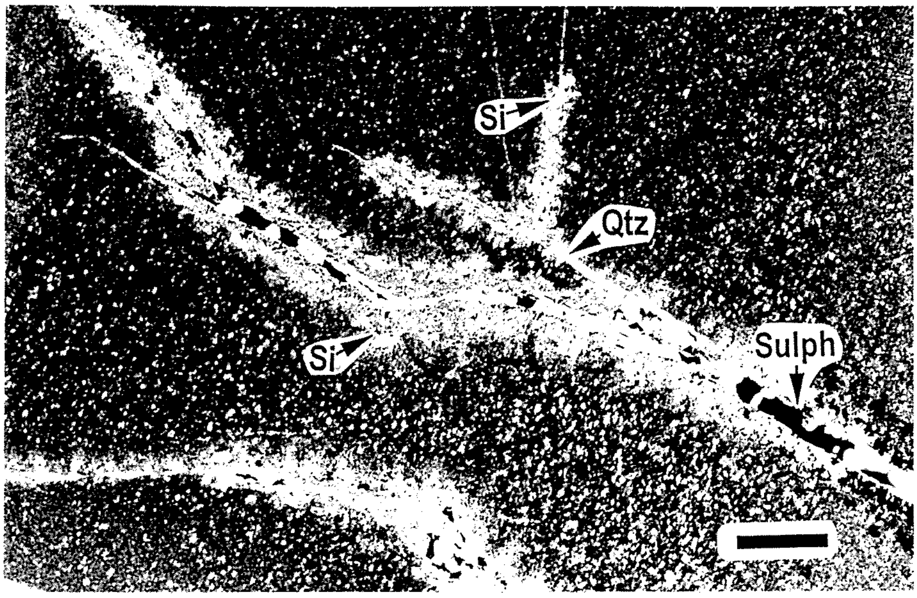
Si
Qtz
Si
Sulph

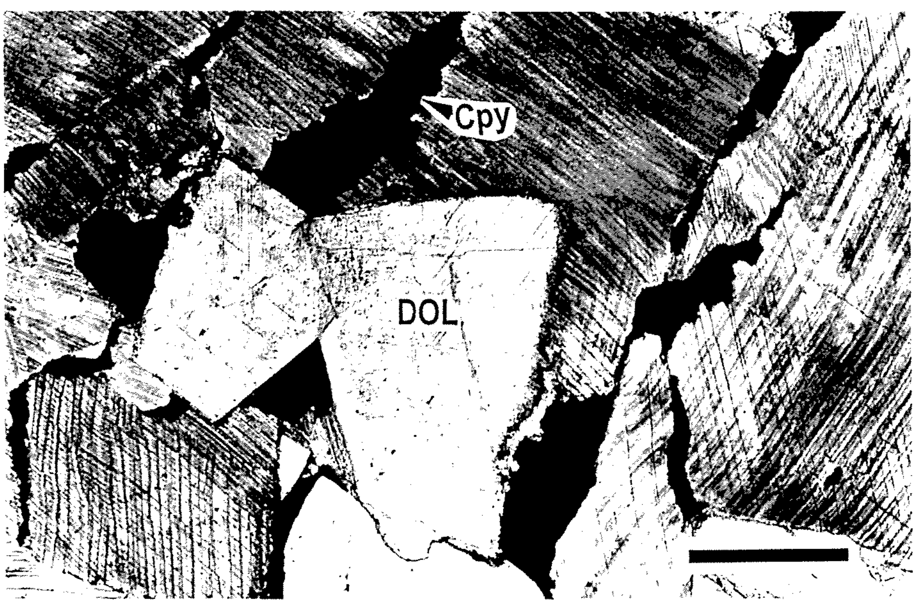
Cpy
DOL

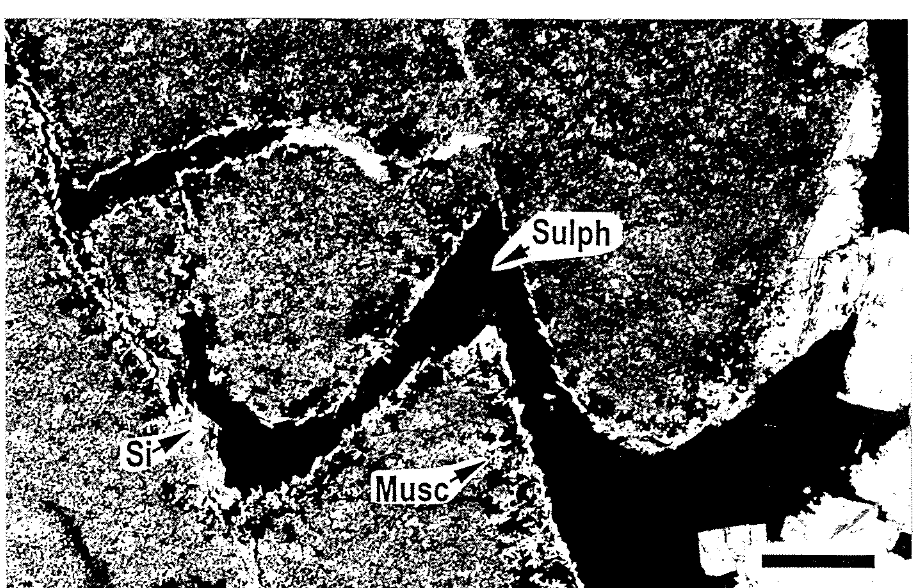
Sulph
Si
Musc

Figure 15: Line diagrams (drawn from colour 35mm slide) illustrating the textural relationships between galena and pyrite. (**A**) Euhedral pyrite grains (**Py**) are overgrown by galena (**Gn**), both on the margins and infilling fractures in the pyrite. Small aggregates of chalcopyrite (**Cpy**) infill fractures in pyrite and replace galena. (**B**) Large pyrite grain overgrown on the rim by slightly later galena (*JCU Catalogue No.* A- 48352; B- 48353).

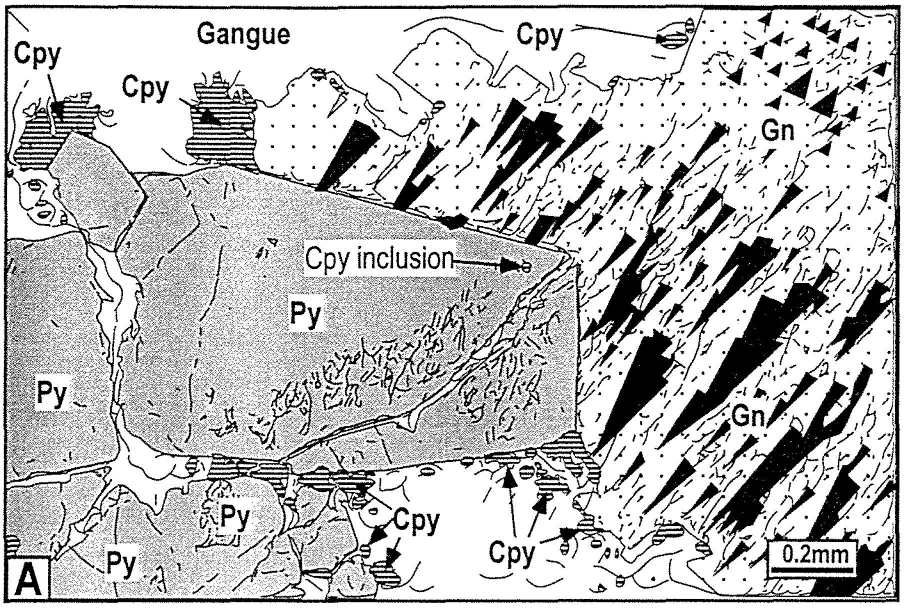
Gangue
Cpy
Cpy
Cpy
Gn
Cpy inclusion
Py
Py
Gn
Py
Cpy
Py
Cpy
A
0.2mm

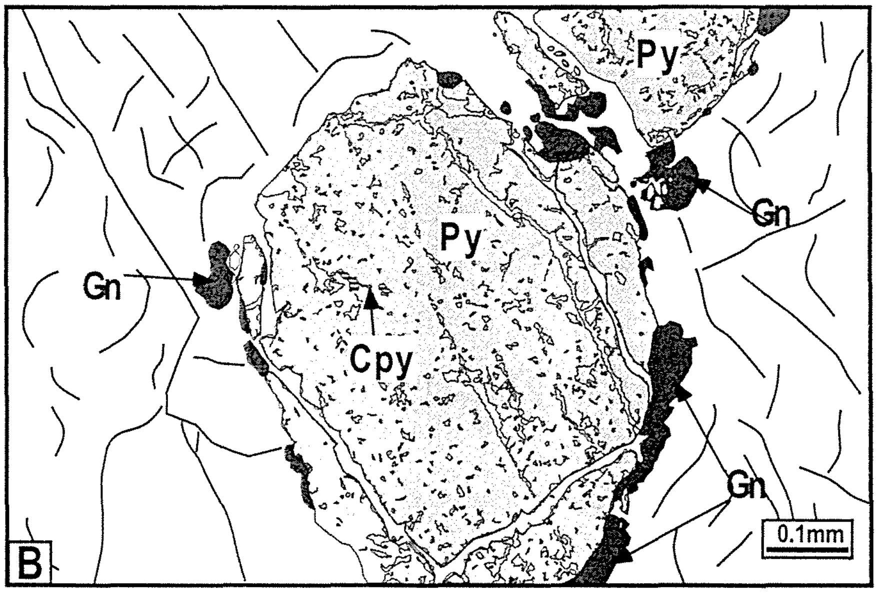
Py
Gn
Py
Gn
Cpy
Gn
0.1mm
B

Figure 16: Line diagrams (drawn from colour 35mm slide) illustrating the textural relationships between galena and chalcopyrite. (**A**) Large grains of galena (**Gn**), including cubic forms, lie within a matrix of gangue minerals. Later chalcopyrite (**Cpy**) replaces the galena, particularly along galena-gangue margins. Chalcopyrite is also scattered throughout the gangue material, suggesting that some gangue also replaced the galena, which is consistent with the prominent embayed boundaries on the large galena grain. (**B**) Massive galena is replaced by anhedral clusters of chalcopyrite. Note the curvature of cleavage pits in the galena suggesting syn- to post-precipitation deformation. Chalcopyrite also shows embayed boundaries suggesting it may also have been replaced by galena. (*JCU Catalogue No.* A - 48352; B- 48353)

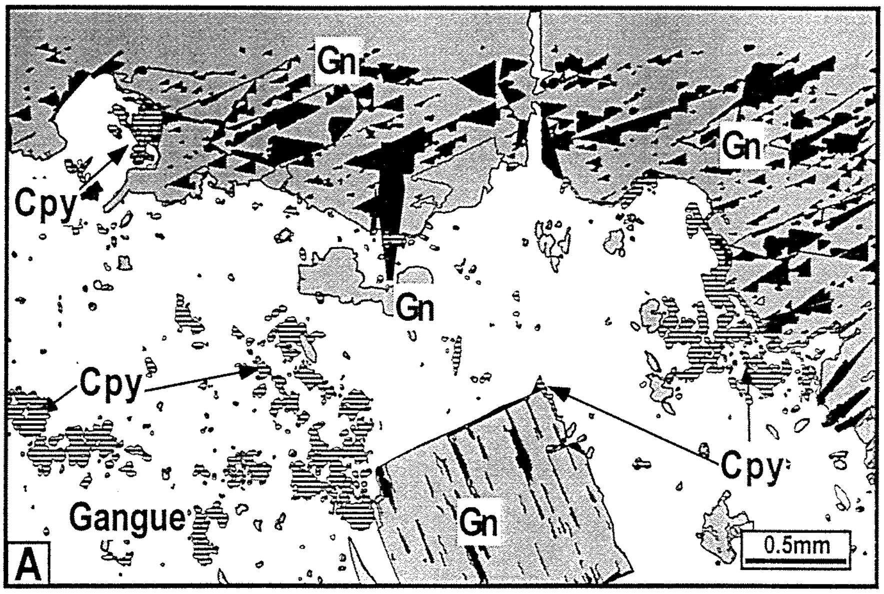
Gn
Gn
Cpy
Gn
Cpy
Cpy
Gangue
Gn
0.5mm
A

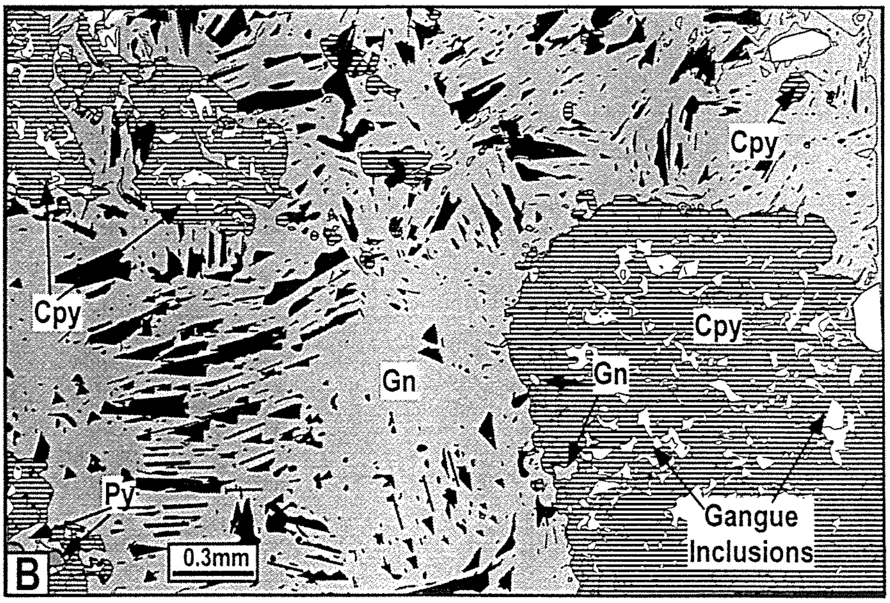
Cpy
Cpy
Cpy
Gn
Gn
Py
0.3mm
Gangue
Inclusions
B

Figure 17: Line diagram (drawn from colour 35mm slide) illustrating the textural relationship between pyrite and chalcopyrite. Early euhedral pyrite (**Py**) crystals contain small chalcopyrite (**Cpy**) inclusions, and are surrounded by anhedral chalcopyrite aggregates that also infilled fractures in the pyrite grains. (*JCU Catalogue No.* 48354)

Figure 18: Line diagram (drawn from colour 35mm slide) of gold mineralisation within the M10 reef. Large gold grains (**Au**), surrounded by chlorite (**Chl**), precipitated within fractures in the quartz-dolomite reef matrix of the reef and were associated with chalcopyrite (**Cpy**)-calcite-chlorite veining. (*JCU Catalogue No.* 48354)

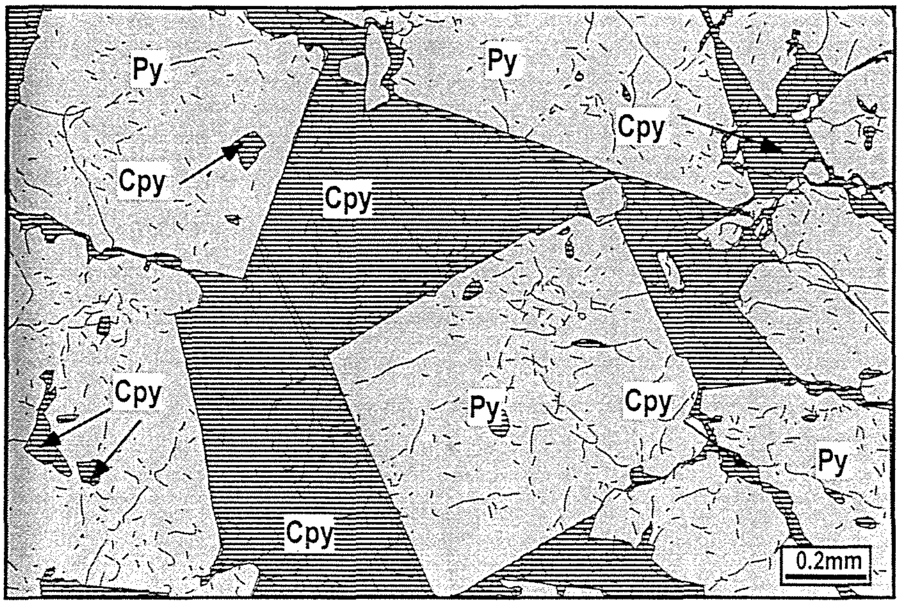
Py
Py
Cpy
Cpy
Cpy
Cpy
Py
Cpy
Py
Cpy
0.2mm

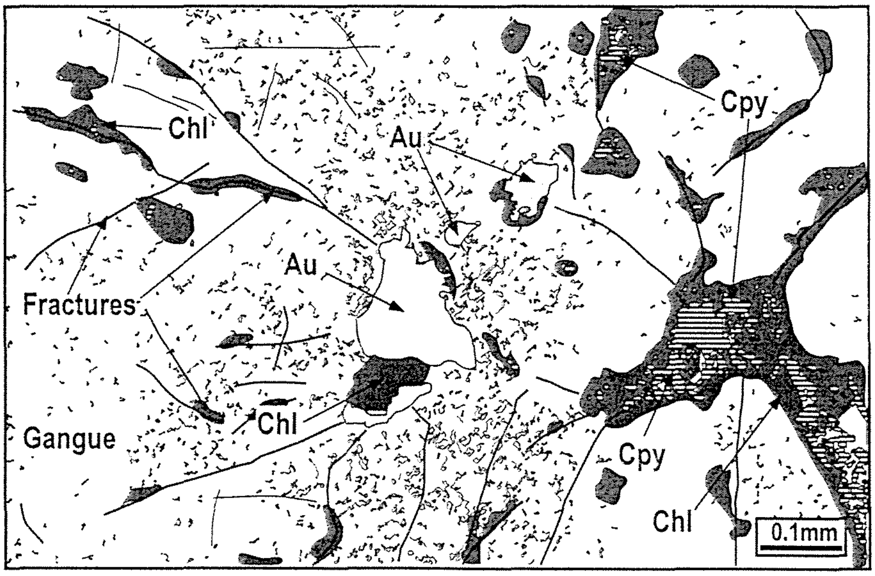
Chl
Au
Cpy
Au
Fractures
Gangue
Chl
Cpy
Chl
0.1mm

Figure 19: Paragenetic diagram summarising the mineral paragenesis across the three suites examined in Main Dome. The upper section represents gangue/silicate minerals, whilst the lower illustrates sulphide/gold relationships. Dolomite 1 is the grey rhombic ferroan phase that was proceeded by a second white-pink opaque ferroan dolomite phase (Dolomite 2). The interpreted timing-relationships to regional metamorphic/deformation events is given across the top with the X-axis indicating relative time (see text for discussion).

Figure 20: Timing relationships for Phase 1 massive quartz veining in the Middle Vale Reef. (**A**) Preservation of S_1 in quartz as fine-grained inclusions indicating late- to post-D_1 silicification. (**B**) Intensification of shearing strain in the Middle Vale Reef (MVR) horizon, also observed by Vearncombe & Hill (1993), that rotated S_2 and deformed round (now elliptical) carbonate spots that grew parallel to S_2. (**C**) If silicification occurred prior to the strain intensification, S_2 would have been prevented from being markedly rotated; instead it would have been deformed outside the MVR horizon. (**D**) Silicification post-dates strain intensification in the MVR thus preserving the deformed and rotated S_2.

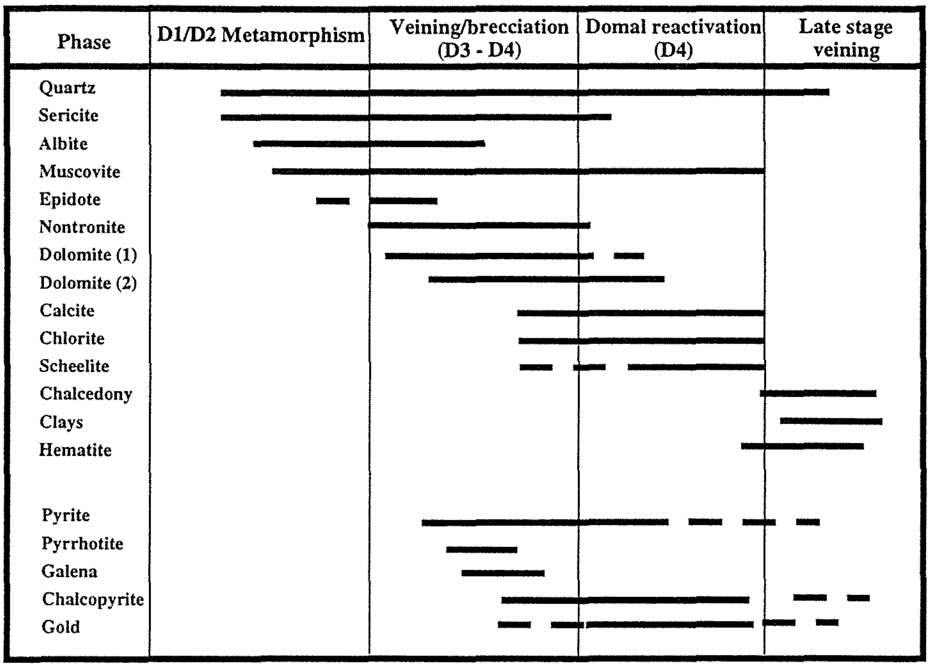
Phase
D1/D2 Metamorphism
Veining/brecciation (D3 - D4)
Domal reactivation (D4)
Late stage veining
Quartz
Sericite
Albite
Muscovite
Epidote
Nontronite
Dolomite (1)
Dolomite (2)
Calcite
Chlorite
Scheelite
Chalcedony
Clays
Hematite
Pyrite
Pyrrhotite
Galena
Chalcopyrite
Gold

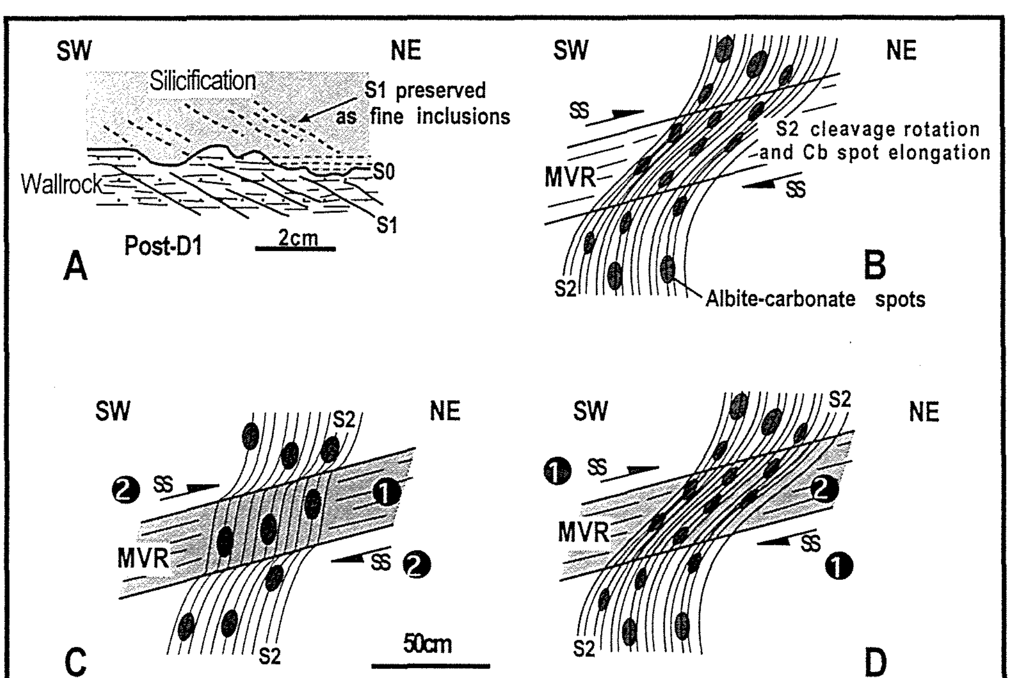
SW
NE
Silicification
S1 preserved as fine inclusions
Wallrock
S0
S1
Post-D1
2cm
A
SS
S2 cleavage rotation and Cb spot elongation
MVR
S2
Albite-carbonate spots
B
S2
MVR
50cm
C
D

Figure 21: Summary of microstructural mineralisation/vein timing criteria for the Telfer deposit (drawn from observations made in thin section). (**A**) Main stage veining in the country rock truncates S_2. Alteration halos associated with the veining, including coarse-grained muscovite, sulphide and carbonate rhombs overprint S_2. (**B**) Breccia clasts containing S_2 are rotated within the veins (*e.g.* van Dijk, 1986) thus veining is late- to post- S_2 formation. (**C**) Metasomatic aggregate exhibiting a weak curvature of inclusion trails within either end. These correspond with a very weak seamy cleavage overprinting S_2 at a high angle in the matrix; interpreted to be S_3. Aggregate growth therefore occurred early in D_3. (**D**) Aggregate growth parallel to a weak S_3 crenulation cleavage, which overprints S_2 at a high angle, indicating an early D_3 timing. The aggregates were subsequently altered to calcite (stippled area) and then replaced by sulphide, thus mineralisation is syn- post-D_3. (**E**) Weak wrapping (anastomosing) of matrix S_2 around the metasomatic aggregates is consistent with renewed shortening of the matrix during D_4. (**F**) Tensional cracking of the quartz, with subsequent deposition of calcite-dolomite (stippled) occurred during D_4 shortening and; (**G**) these effects were overprinted by further sulphide/gold mineralisation.

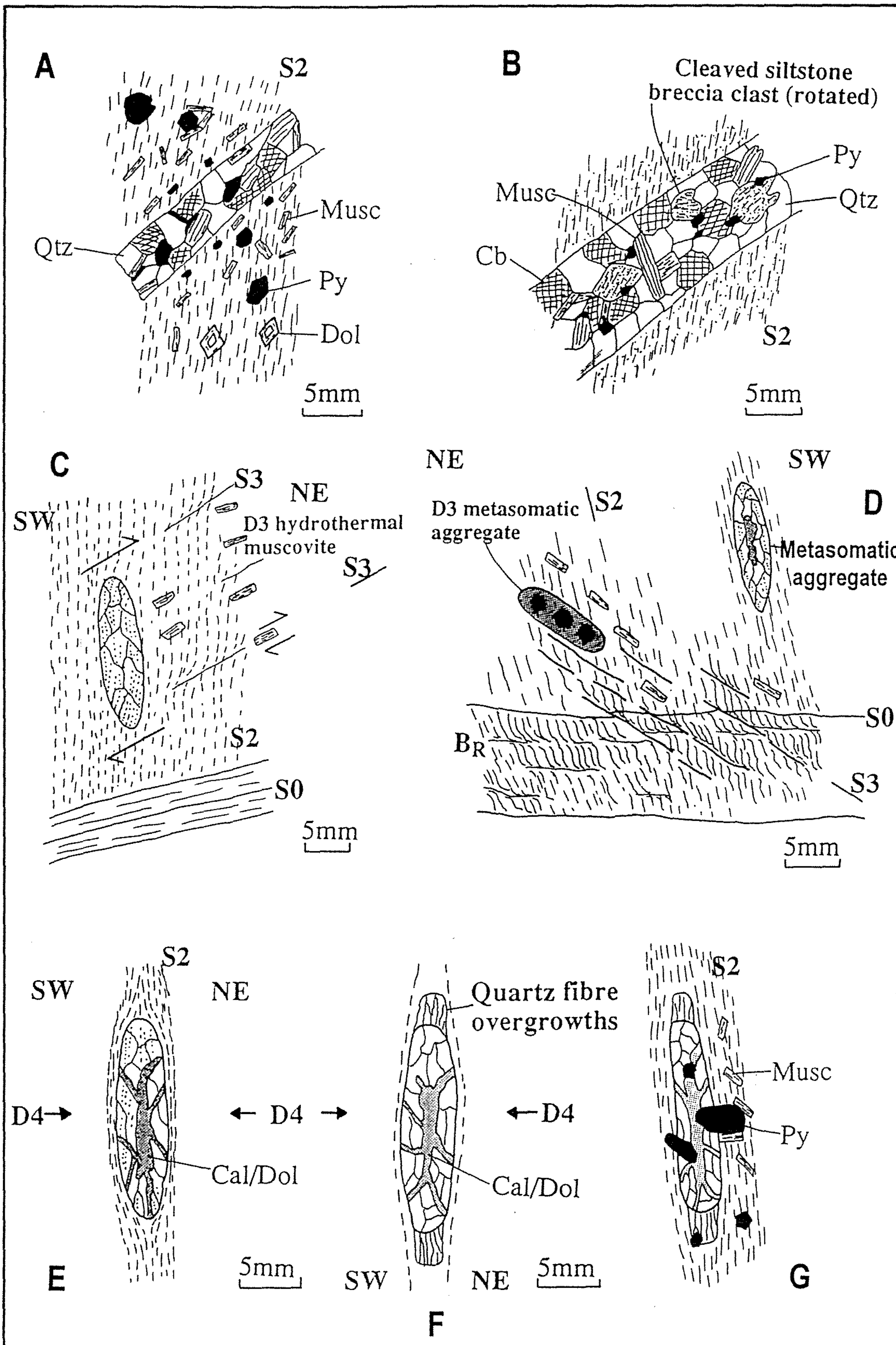
A
S2
Musc
Qtz
Py
Dol
5mm
B
Cleaved siltstone
breccia clast (rotated)
Py
Musc
Qtz
Cb
S2
5mm
C
S3
NE
SW
D3 hydrothermal
muscovite
S3
S2
S0
5mm
NE
SW
D
D3 metasomatic
aggregate
S2
Metasomatic
aggregate
S0
B_R
S3
5mm
S2
SW
NE
D4
D4
Cal/Dol
5mm
E
Quartz fibre
overgrowths
D4
Cal/Dol
SW
NE
5mm
F
S2
Musc
Py
G

Figure 22: Photomicrograph and line diagram of timing relationships between aggregate growth and S_0, S_2 & S_3 foliations. In this example S_2 in the matrix is overprinted by a shallow crenulation fabric (S_3) with a top-to-the-NE shear sense suggested by the crenulation asymmetry (inset **A** - line diagram). Strongly fissile bedding layers, cleaved by S_2, were overprinted and crenulated by the sub-horizontal S_3 foliation, which is coarsely spaced (inset **B** - line diagram). The metasomatic quartz aggregates overprint S_2 and grew parallel to S_3 suggesting a syn-D_3 timing. The aggregates were subsequently altered to carbonate (**Cb**) and pyrite (**Py**) indicating that mineralisation occurred syn- post-D_3 deformation. Locally, bedding and S_3 were reactivated by subsequent shortening during D_4. (*JCU Catalogue No*. 48355)

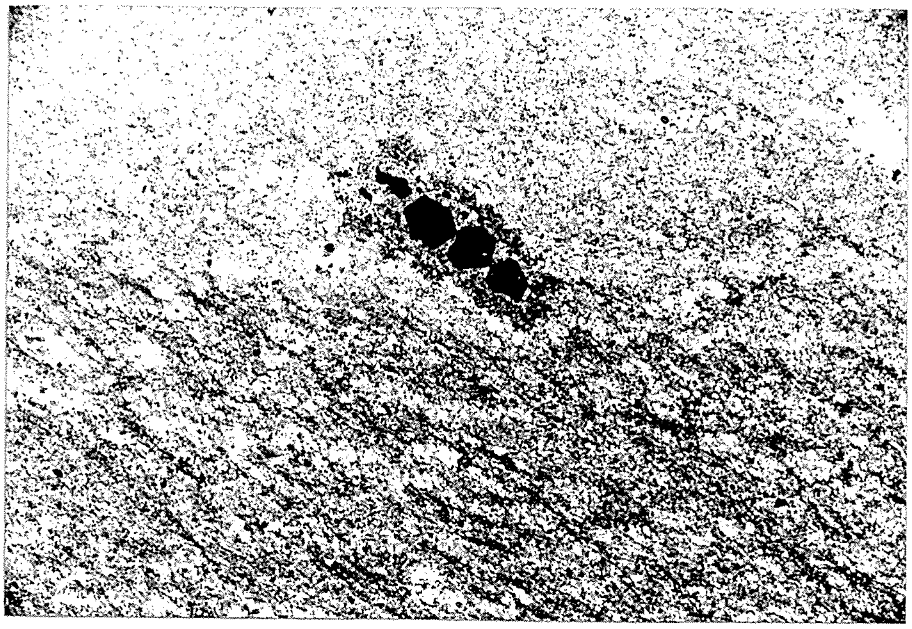

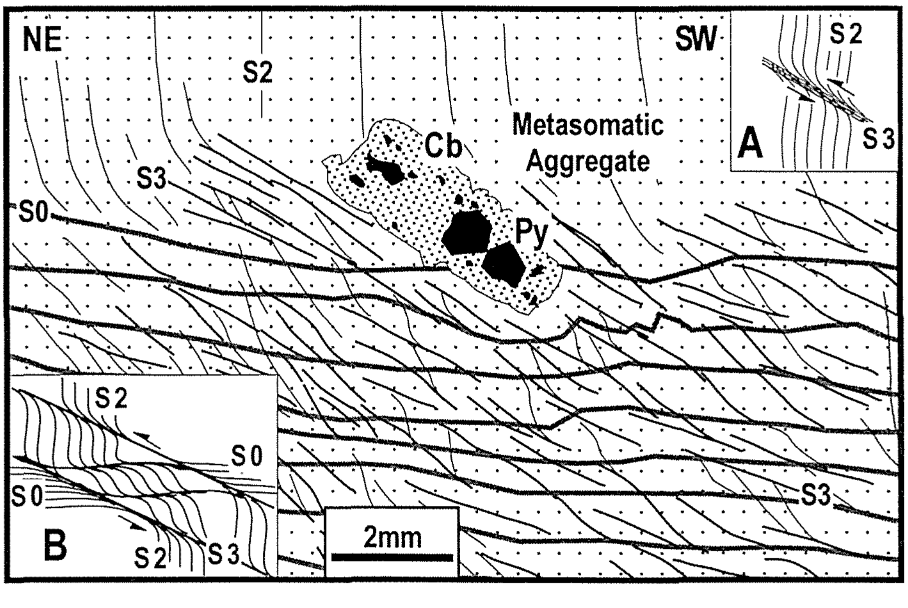
NE
SW
S2
Cb
Metasomatic
Aggregate
S3
S0
Py
A
S2
S3
B
S2
S0
S0
S2
S3
S3
2mm

Figure 23: Summary diagram of the macroscale structural indicators of mineralisation timing in the Telfer deposit. Small inset illustrates the general fold asymmetry and hinge tightening, with concomitant brecciation (**Bx**), in many fold hinges throughout the Telfer Dome. This rotation and tightening is interpreted to be the result of refolding during D_3. Other indicators are a set of right stepping shear zones in West Dome (West Dome Deeps) suggestive of late sinistral movement that is consistent with D_4 shortening that was oblique (≈25° clockwise from that during D_2) to the Telfer Dome. D_5 faults, such as the Graben Fault, overprint reef mineralisation, thereby constraining the development of reef mineralisation to between D_2 and D_5.

Figure 24: Summary plot of isotope data (data from Rowins et al., 1992; Rowins, 1994) for the Telfer deposit. The data were collected from hydrothermal carbonate veins in the Telfer Deposit, with a suite from regional carbonate formations for comparison.

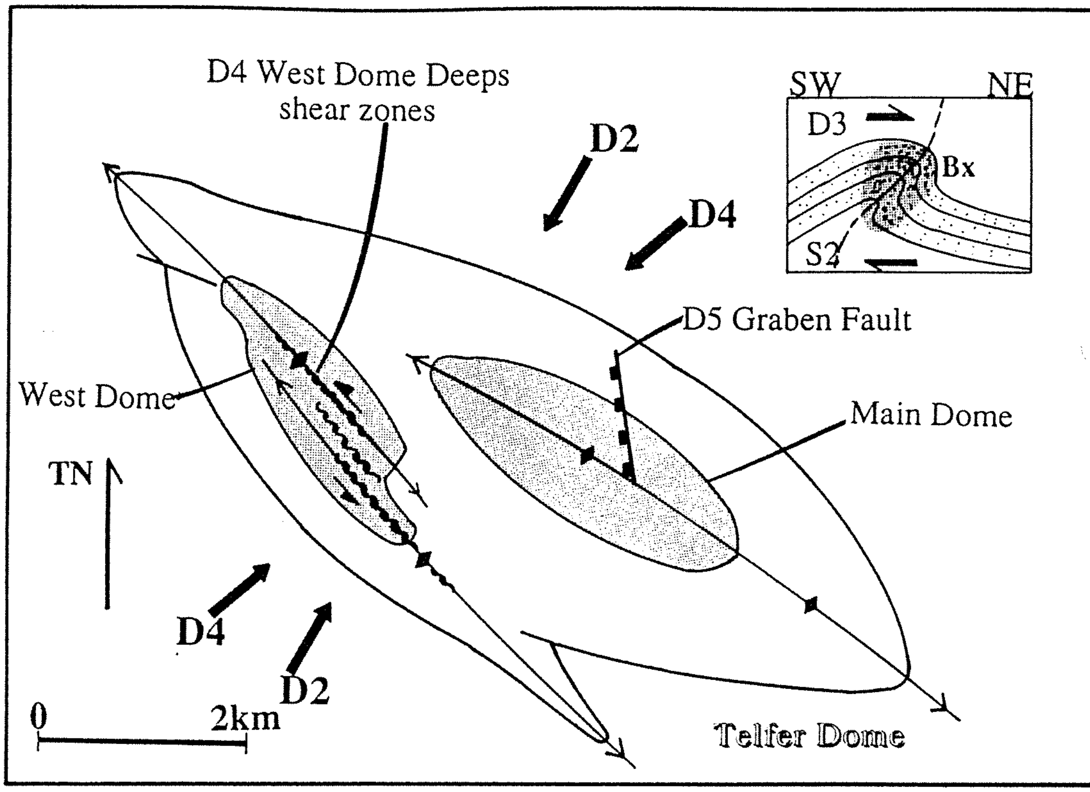
D4 West Dome Deeps
shear zones
D2
D4
SW
NE
D3
Bx
S2
D5 Graben Fault
West Dome
Main Dome
TN
D4
D2
0
2km
Telfer Dome

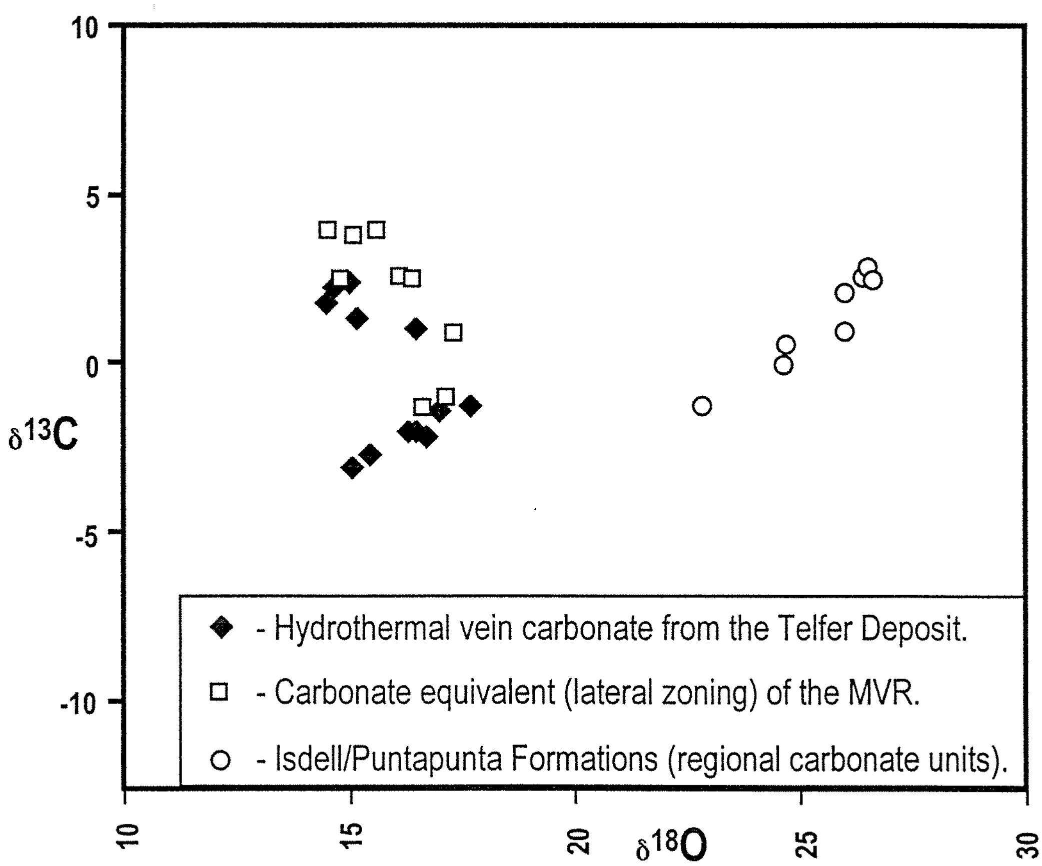
10
5
0
-5
-10
$\delta^{13}C$
10
15
20
$\delta^{18}O$
25
30
- Hydrothermal vein carbonate from the Telfer Deposit.
- Carbonate equivalent (lateral zoning) of the MVR.
- Isdell/Puntapunta Formations (regional carbonate units).

Figure 25: Schematic diagram illustrating the differences in fluid-flow mechanisms during different deformation events. (**A**) The major deformation, D_2, produced strong regional folding with an associated penetrative axial plane cleavage (S_2). Consequently, fluid was distributed pervasively throughout the rock moving along grain contacts (opaque blobs) in both quartzites and pelites as well as cleavage (particularly in pelites). Fluid movement along axial plane cleavage would have been assisted by shearing on this foliation during D_2. (**B**) In contrast to the D_2 event, late weaker deformations were less pervasive throughout the rock sequence and produced only localised structural permeability through D_3 gaped fold limbs (stippled; see Section D), veins and reactivated bedding/faults. Therefore, fluid movement (opaque blobs) would have been highly partitioned into these discrete zones.

Figure 26: Schematic representation of potential alteration zoning in Main Dome. The upper regions (hinge) of the dome are characterised by strong silicification of the reef horizons, whilst further away down the limbs carbonate alteration was prevalent. Silicification (early) in the upper regions probably prevented massive carbonate infiltration (subsequent) in these areas due to the reduction of permeability arising from silicification, thus producing structurally controlled hydrothermal zoning. This implies that ore-fluid flow was strongly channelled into individual reef horizons. Additionally, the silicification appears to have controlled sulphide-gold deposition as the best grades of mineralisation correspond with thick quartz veining in these horizons.

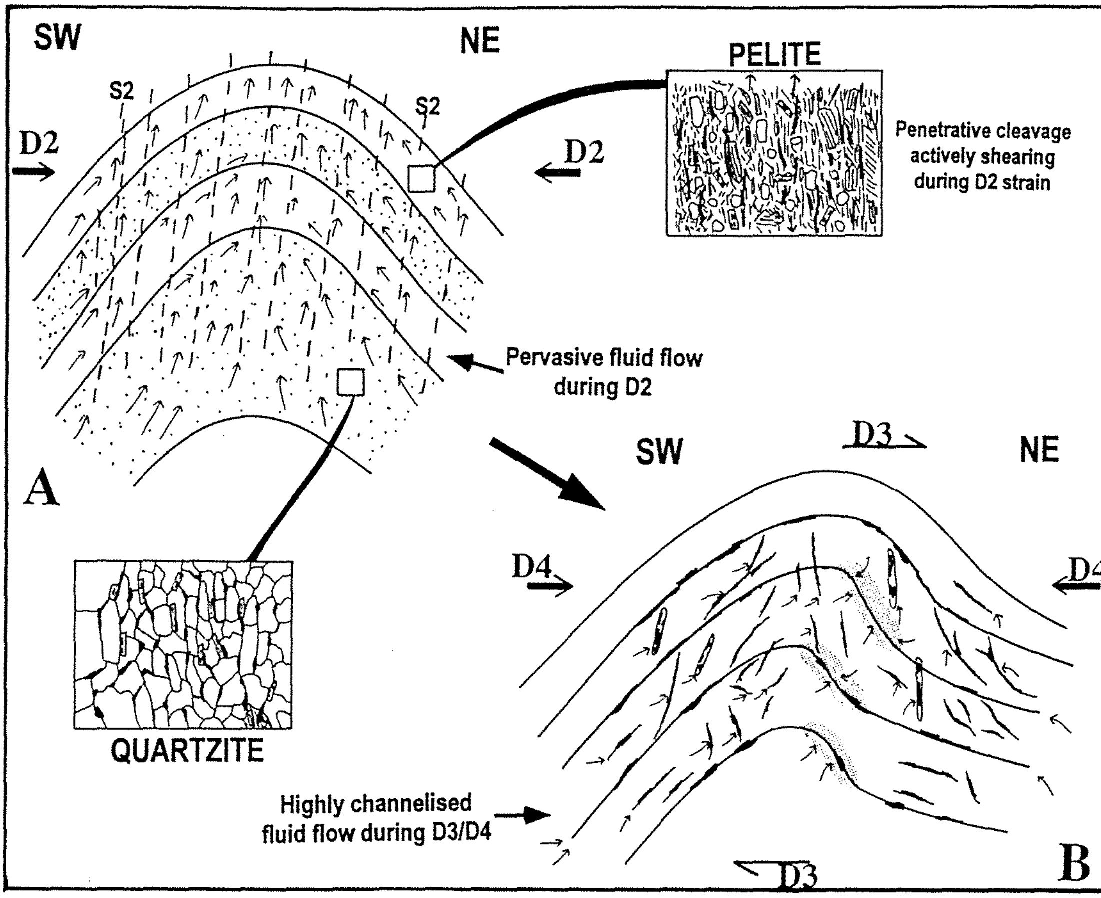
SW
NE
S2
S2
D2
D2
PELITE
Penetrative cleavage actively shearing during D2 strain
Pervasive fluid flow during D2
A
QUARTZITE
SW
D3
NE
D4
D4
Highly channelised fluid flow during D3/D4
D3
B

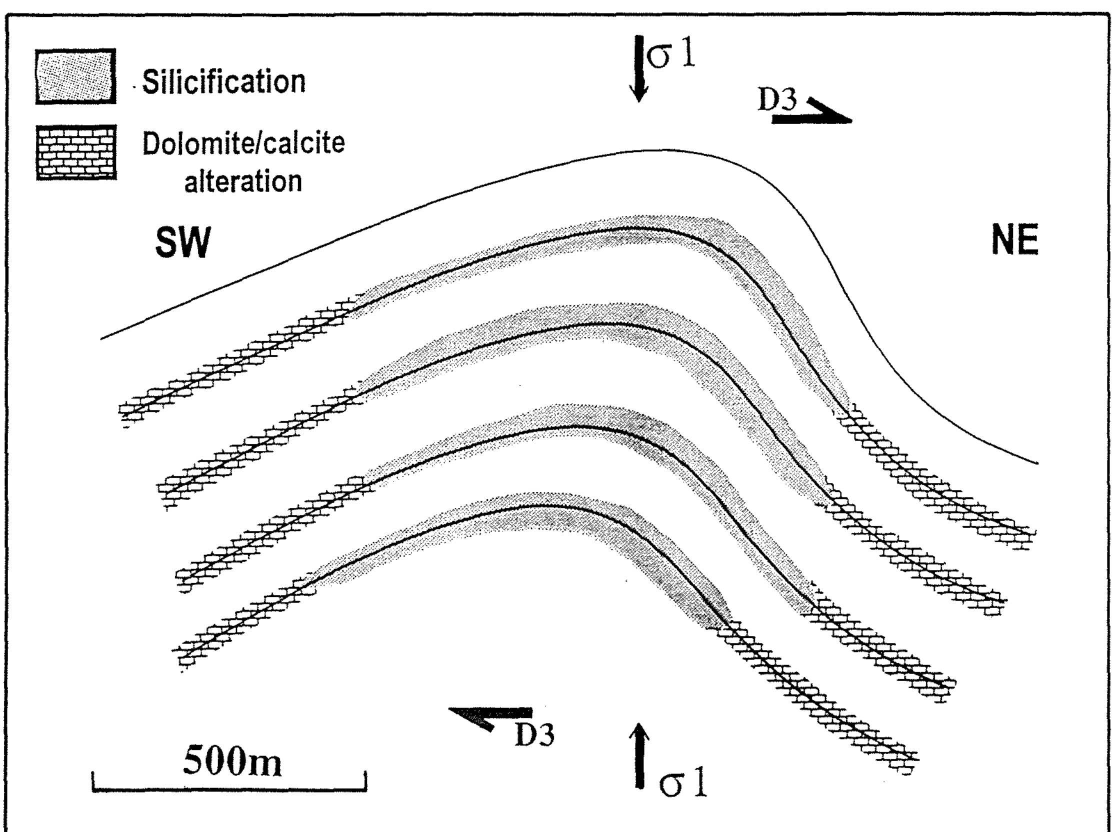
Silicification
Dolomite/calcite alteration
σ1
D3
SW
NE
D3
500m
σ1

SECTION D

Progressive Structural Development of the Telfer Dome and Controls on Gold-Copper Mineralisation.

(FIGURES)

Figure 1: Summary of the distribution and stratigraphic setting of the major mineralised reefs in the Telfer deposit. (**A**) Plan view of the Telfer Dome illustrating the distribution of mineralised reefs that are exposed in surface mining (Middle Vale Reef (**MVR**) and **E-Reefs**). (**B**) SW-NE cross section through Main Dome (section line indicated in A) illustrating the distribution and stratigraphic setting of the Middle Vale Reef, M-Reefs and I-Reefs. (**C**) Summary of the stratigraphy in the Telfer Deposit. The Telfer Formation is exposed at the surface in the Telfer Dome.

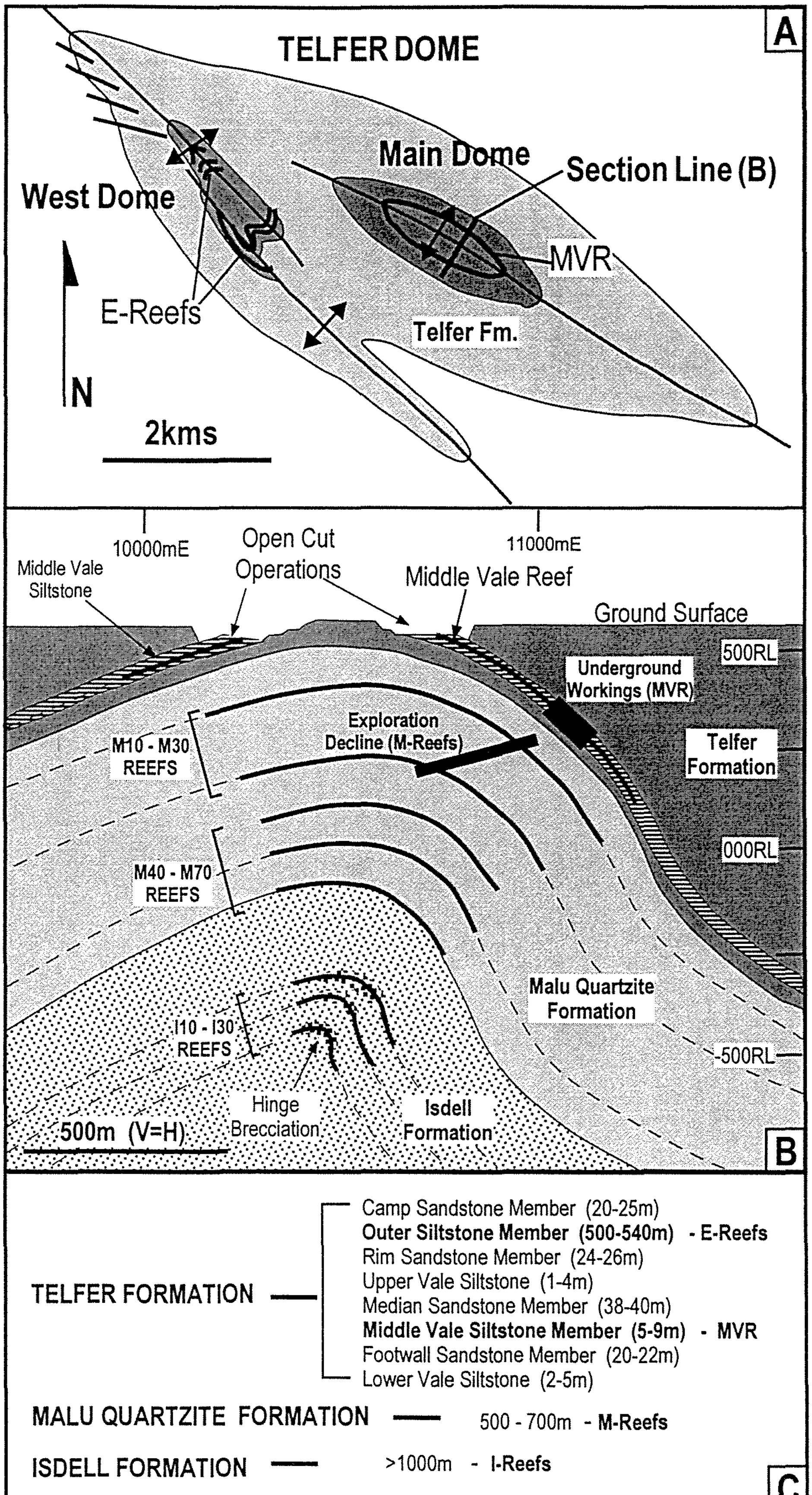

A
TELFER DOME
Main Dome
Section Line (B)
West Dome
MVR
E-Reefs
Telfer Fm.
N
2kms
B
10000mE
11000mE
Open Cut Operations
Middle Vale Siltstone
Middle Vale Reef
Ground Surface
500RL
Underground Workings (MVR)
Exploration Decline (M-Reefs)
Telfer Formation
M10 - M30 REEFS
000RL
M40 - M70 REEFS
Malu Quartzite Formation
I10 - I30 REEFS
-500RL
Hinge Brecciation
Isdell Formation
500m (V=H)
C
TELFER FORMATION
Camp Sandstone Member (20-25m)
Outer Siltstone Member (500-540m) - E-Reefs
Rim Sandstone Member (24-26m)
Upper Vale Siltstone (1-4m)
Median Sandstone Member (38-40m)
Middle Vale Siltstone Member (5-9m) - MVR
Footwall Sandstone Member (20-22m)
Lower Vale Siltstone (2-5m)
MALU QUARTZITE FORMATION
500 - 700m - M-Reefs
ISDELL FORMATION
>1000m - I-Reefs

***Figure** 2*: Simplified geological map of the Telfer Dome (reduced data from Map 1) showing lithology, structure and the distribution of current mining activity. The Telfer Dome is divided into two lower-order sub-domes, Main Dome and West Dome, which are arranged en-echelon (left stepping). Large faults, average bedding, cleavage and vein orientations and prominent joint directions are also indicated.

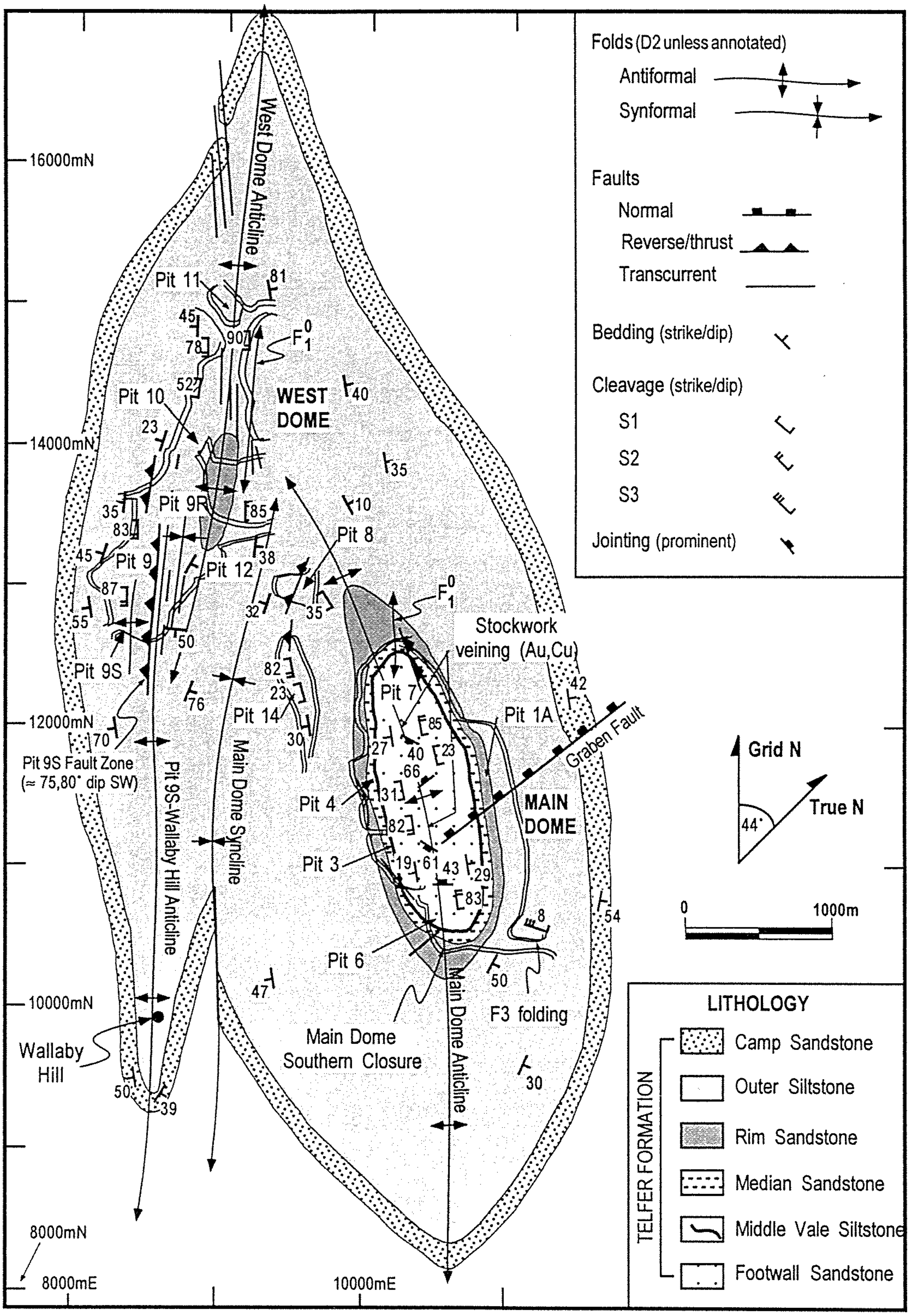

Folds (D2 unless annotated)
Antiformal
Synformal
Faults
Normal
Reverse/thrust
Transcurrent
Bedding (strike/dip)
Cleavage (strike/dip)
S1
S2
S3
Jointing (prominent)
Grid N
True N
44°
0
1000m
LITHOLOGY
TELFER FORMATION
Camp Sandstone
Outer Siltstone
Rim Sandstone
Median Sandstone
Middle Vale Siltstone
Footwall Sandstone
West Dome Anticline
WEST DOME
MAIN DOME
Main Dome Syncline
Main Dome Anticline
Pit 9S-Wallaby Hill Anticline
Graben Fault
Stockwork veining (Au,Cu)
Main Dome Southern Closure
F3 folding
Pit 9S Fault Zone (≈ 75,80° dip SW)
Wallaby Hill
Pit 11
Pit 10
Pit 9R
Pit 9
Pit 9S
Pit 12
Pit 8
Pit 14
Pit 7
Pit 1A
Pit 4
Pit 3
Pit 6
16000mN
14000mN
12000mN
10000mN
8000mN
8000mE
10000mE

Figure 3: Schematic NE-SW cross section of Main Dome illustrating the fold geometry at depth based on recent diamond drilling. The dome has an overall weak asymmetry with a steeper NE dipping limb and an inclined (SW) axial plane. Axial plane (S_2) cleavage is generally sub-vertical where observed at the surface in the mine. However, on the SW limb it has been locally rotated into a shallower orientation during antithetic bedding reactivation (see Section A). At deeper levels the cleavage is commonly inclined (75°SW) suggesting that it may have been refolded during subsequent deformation. Further evidence for refolding is indicated in the vicinity of the I-Reefs where the fold hinge and S_2 are rotated towards the NE, an effect interpreted to arise from D_3. The inset shows the nature of fold-hinge rotation with overturning of the NE limb and S_2, causing individual mineralised reefal horizons to be multiply intersected in sub-vertical drill-holes. Vertical scale = horizontal scale.

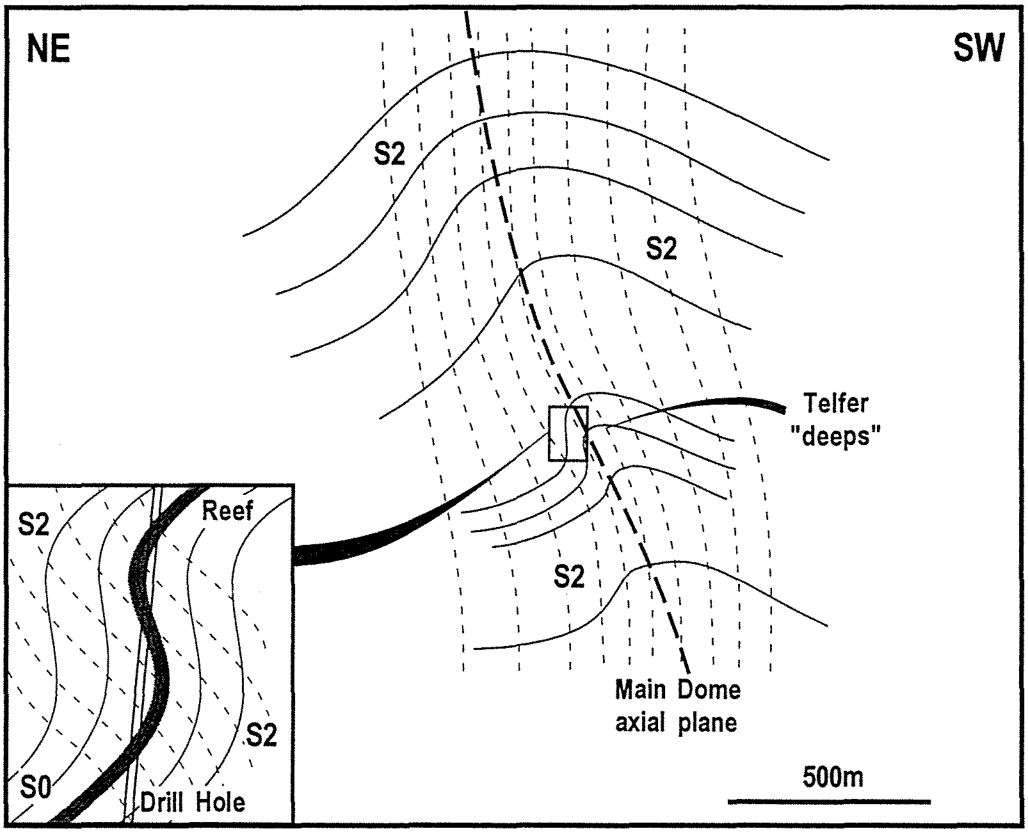
NE
SW
S2
S2
S2
Telfer
"deeps"
S2
Reef
S2
S0
Drill Hole
S2
Main Dome
axial plane
500m

Figure 4: Photograph of a D_1 fold immediately NE of the northern closure of Main Dome. Previous studies had interpreted this to be related to the domal closure. However, the fold is of an earlier deformation phase (D_1; Section A) and is overprinted by the domal axial plane cleavage (**S_2** - annotated for reference). S_2 - bedding relationships indicate an F_2 vergence to the left (SW) in the photo. NOTE: the prominent shallow-dipping vein sets that lie parallel to the F_1 axial plane. These veins overprint S_2 and formed within fractures that developed parallel to the F_1 axial plane/axial plane cleavage (**S_1** - annotated for reference). The scale bar at the bottom right represents approximately 7m. (Location: NW face of Pit 7, Telfer Mine; Mine Grid - 12460mN 10200mE)

Figure 5: Field diagram (drawn from photograph) illustrating the geometry and cleavage-bedding relationships on the NE limb (**i**), hinge (**ii**) and SW limb (**iii**) of the southern closure of Main Dome. The asymmetry evident in (ii), which is opposite to that observed near the northern closure (Fig. 3), is interpreted to be due to heterogeneous D_2 strain during folding. This is evident from the refolding of S_1, and the relatively constant vertical/sub-vertical S_2 orientation across the closure. If the asymmetry was due to post-D_2 refolding then S_2 would also have been folded and would have a variable orientation across the closure. The prominent faulting is interpreted to have occurred either late in D_2, as a result of accommodation of tightening of the strata, or as a result of further horizontal shortening of the D_2 closure during D_4. (Location: SE face of Pit 6, Telfer Mine; Mine Grid - 10385mN 10620mE)

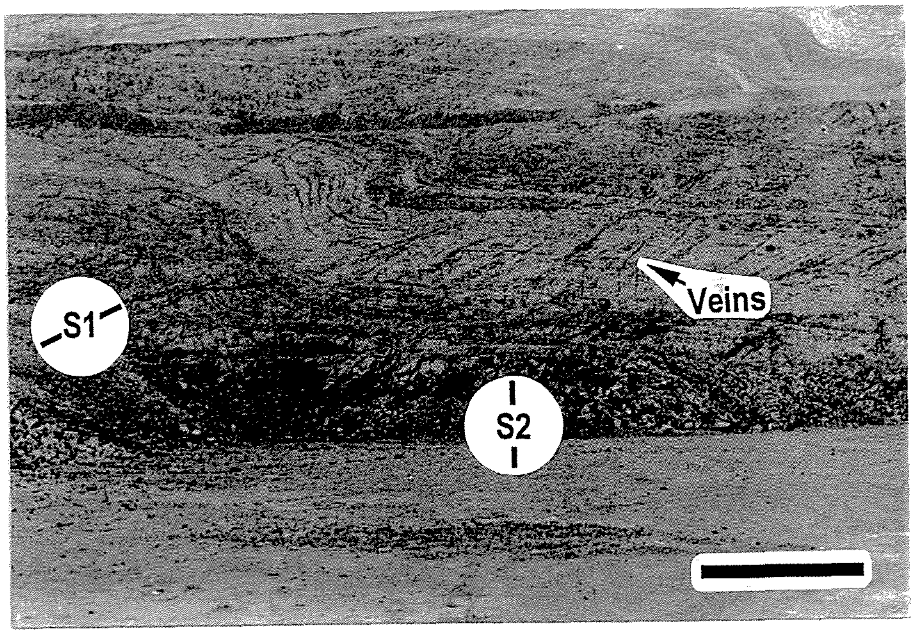

S1
Veins
S2

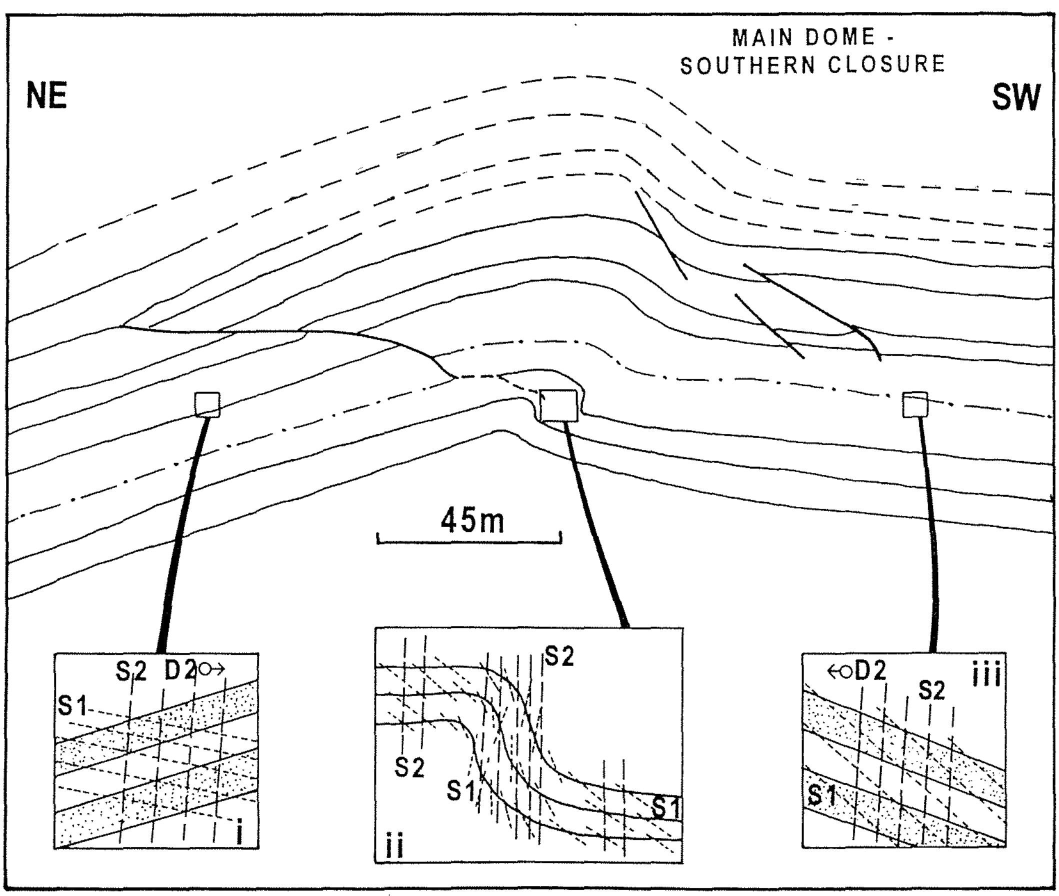

MAIN DOME -
SOUTHERN CLOSURE
NE
SW
45m
S2
D2
S1
i
S2
S2
S1
S1
ii
D2
S2
iii
S1

Figure 6: Schematic three-dimensional block diagram illustrating folding style and mesoscale fold-related structures throughout Main Dome in both cross-section (NE-SW) and longitudinal section (NW-SE). Many of these are equally applicable for West Dome and were produced during local flexural slip deformation along bedding within the dome.

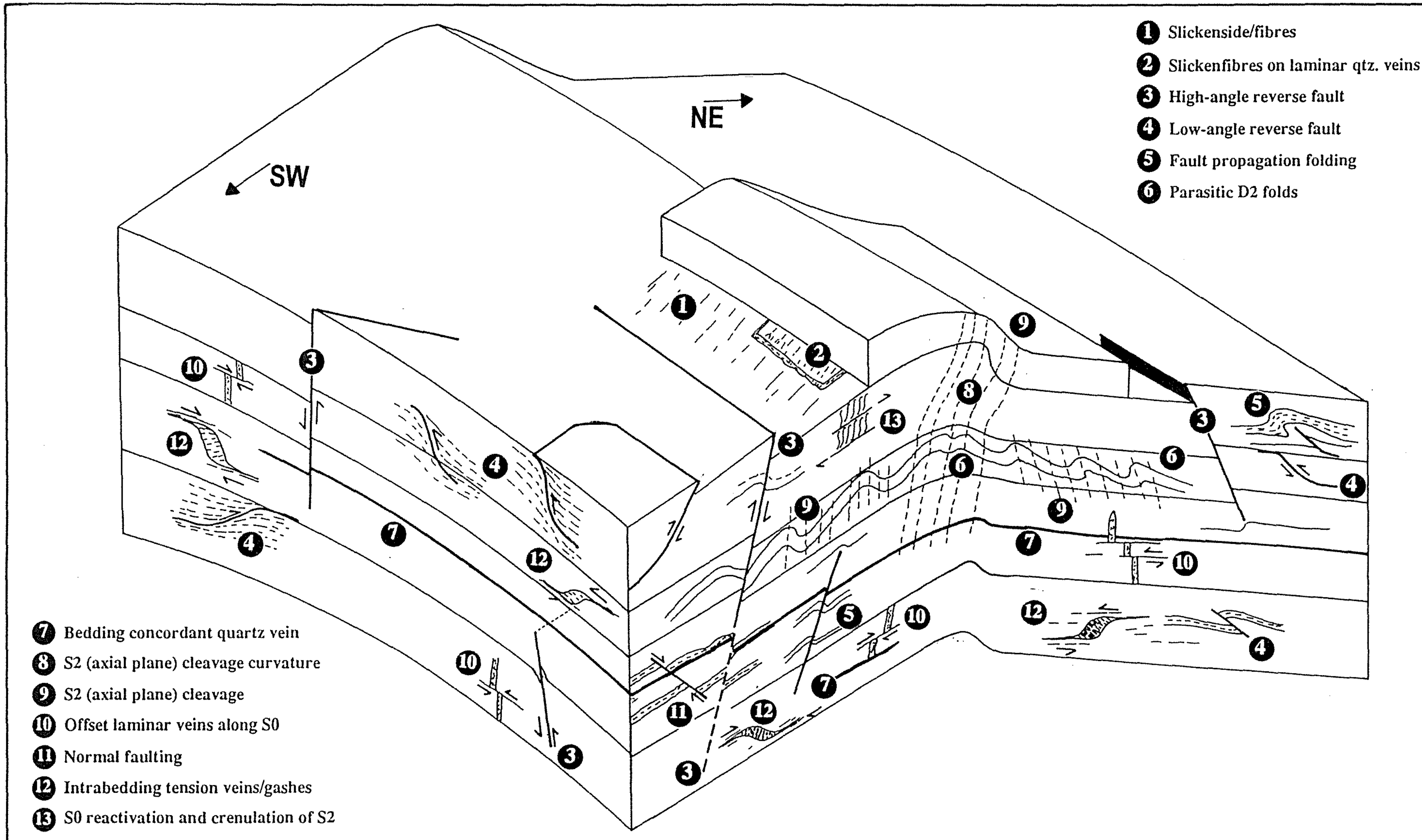

SW
NE
1 Slickenside/fibres
2 Slickenfibres on laminar qtz. veins
3 High-angle reverse fault
4 Low-angle reverse fault
5 Fault propagation folding
6 Parasitic D2 folds
7 Bedding concordant quartz vein
8 S2 (axial plane) cleavage curvature
9 S2 (axial plane) cleavage
10 Offset laminar veins along S0
11 Normal faulting
12 Intrabedding tension veins/gashes
13 S0 reactivation and crenulation of S2

Figure 7: Stereographic summary of joint orientations (unpub. data from I. Kirchner, 1991 - Newcrest Mining Pty Ltd) in the core of Main Dome. (**A**) 1% area contour plot, contoured in 1% intervals. (**B**) Directional rose diagram of major joint strike trends (left-hand convention). Major joint trends include N-S and E-W, with subsidiary NE-SW values. A near orthogonal set that is symmetric with respect to the domal axis has a sub-vertical intersection axis (illustrated in A) suggesting that rapid swapping between $\sigma 2$ and $\sigma 3$ occurred (Dunne & Hancock, 1994), consistent with local stresses in the core of an actively forming fold.

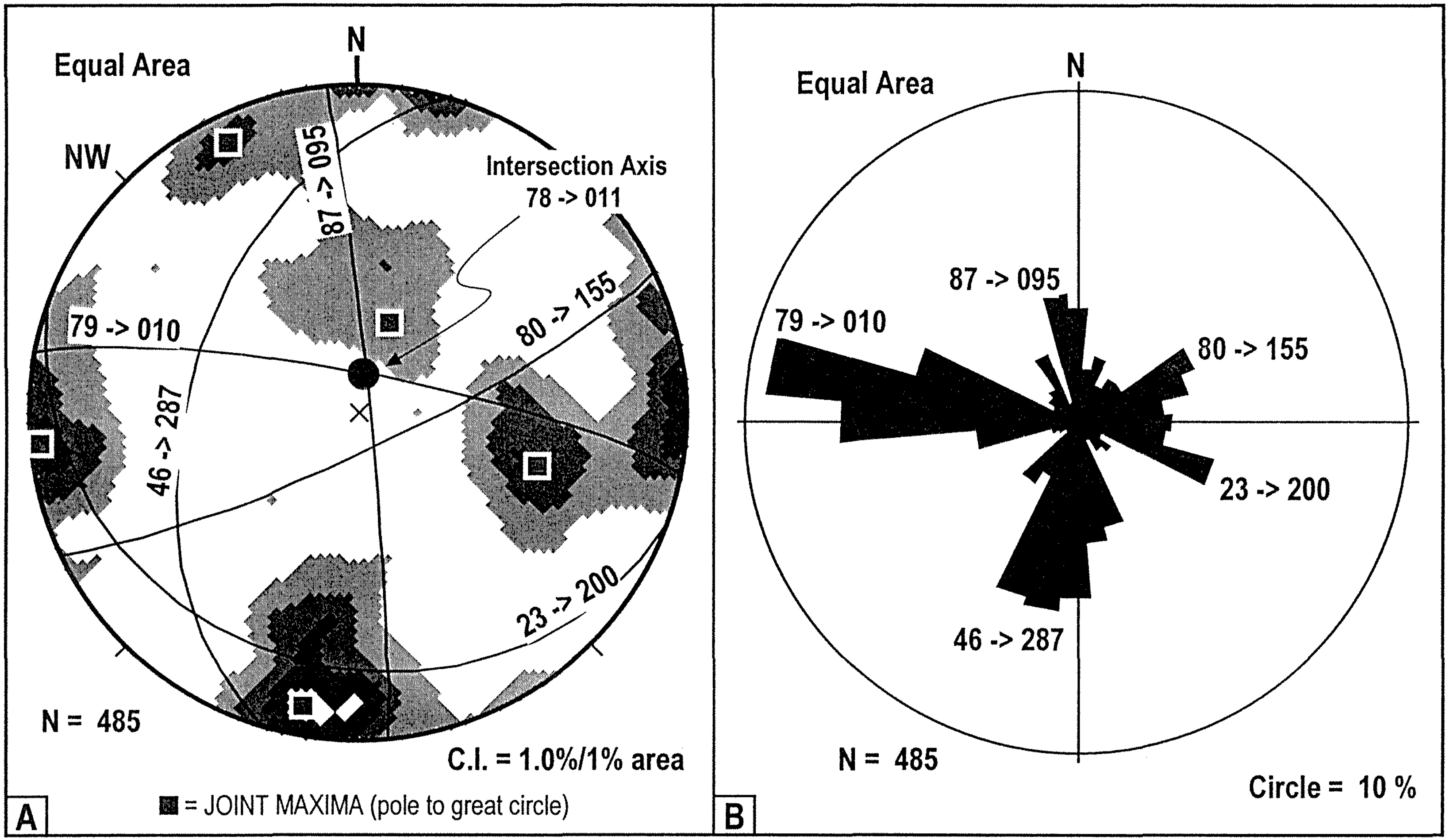
Equal Area
N
NW
87 -> 095
Intersection Axis
78 -> 011
80 -> 155
79 -> 010
46 -> 287
23 -> 200
N = 485
C.I. = 1.0%/1% area
= JOINT MAXIMA (pole to great circle)
A
Equal Area
N
87 -> 095
79 -> 010
80 -> 155
23 -> 200
46 -> 287
N = 485
Circle = 10 %
B

Figure 8: Fault styles exhibited in the NE corner of Pit 7, Main Dome (see Fig. 1 for location). The line-diagram (**A**), drawn from a photo-mosaic, illustrates a large sub-vertical sinistral-reverse fault that terminates in a "complex zone" of contorted bedding and smaller faults that resembles a thrust duplex (**B** - position in A illustrated by the brackets). However, bedding-cleavage relationships within this zone suggest that it is a parasitic D_2 fold that was sliced up by the smaller faults late in D_2. Scale Bar in (B) represents approximately 10m, and the photograph is looking NNW-N. (Location: N wall of Pit 7, Telfer Mine: Mine Grid - 12450mN 10365mE)

Figure 9: Field photographs of faulting styles in Main Dome; (**A**) Large sub-vertical reverse/transcurrent fault (F) cutting the SW limb in Pit 3 (see Fig. 1 for location). The fault dips 55-65° towards the SW (into the page) giving an apparent low-angle thrust geometry. Photograph is looking SW, and the scale bar represents 5m. (**B**) Lateral extension of the N-S trending Graben Fault in the SW corner of Pit 6 that exhibits brittle-ductile effects along the margin, including drag folding and small scale graben formation. Photograph is looking SW, and the scale bar represents 10m. (Location: **A**; SW face of Pit 3, Telfer Mine; Mine Grid - 10860mN 10410mE. **B**; SW face of Pit 6, Telfer Mine; Mine Grid - 10440mN 10600mE).

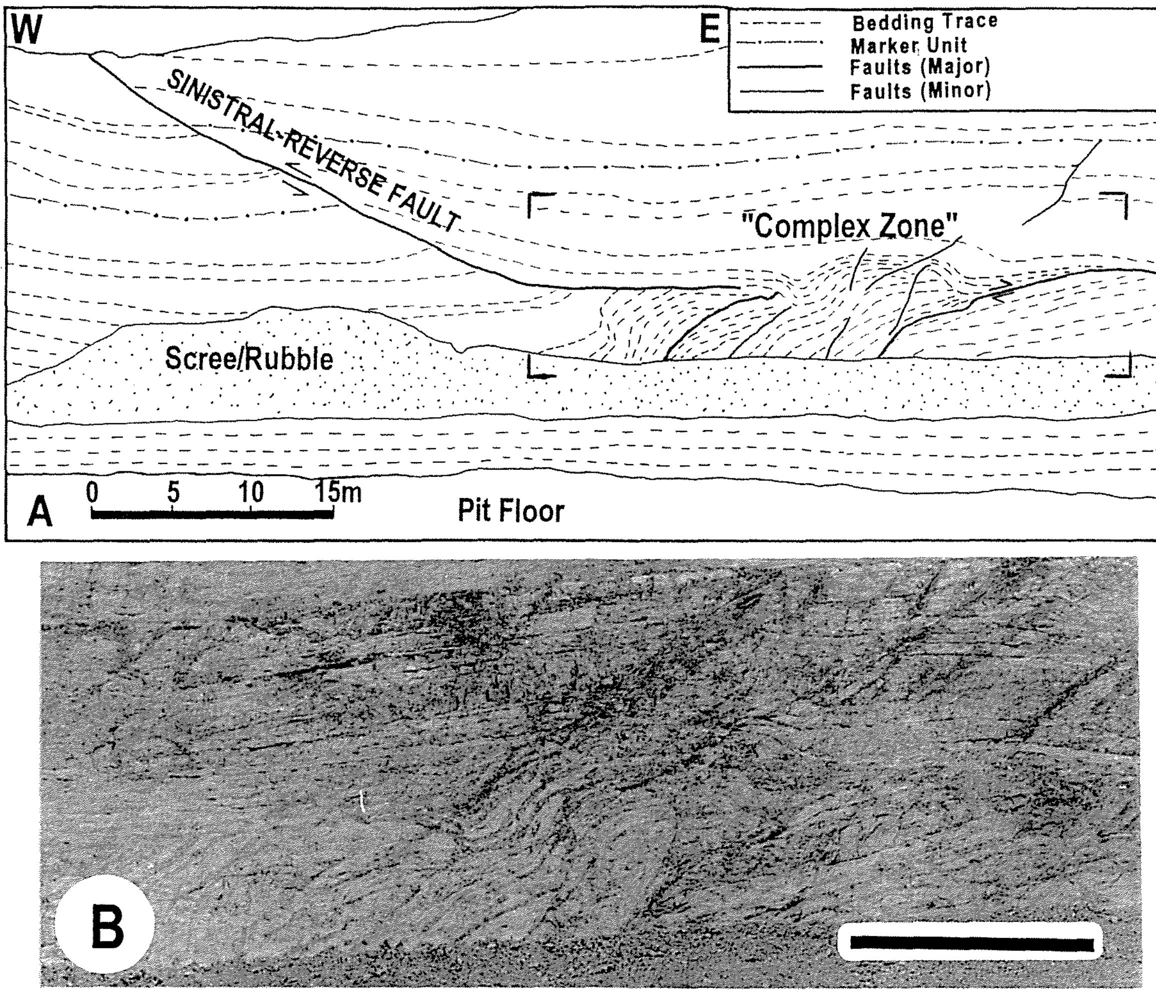
W
E
Bedding Trace
Marker Unit
Faults (Major)
Faults (Minor)
SINISTRAL-REVERSE FAULT
"Complex Zone"
Scree/Rubble
A
0
5
10
15m
Pit Floor
B

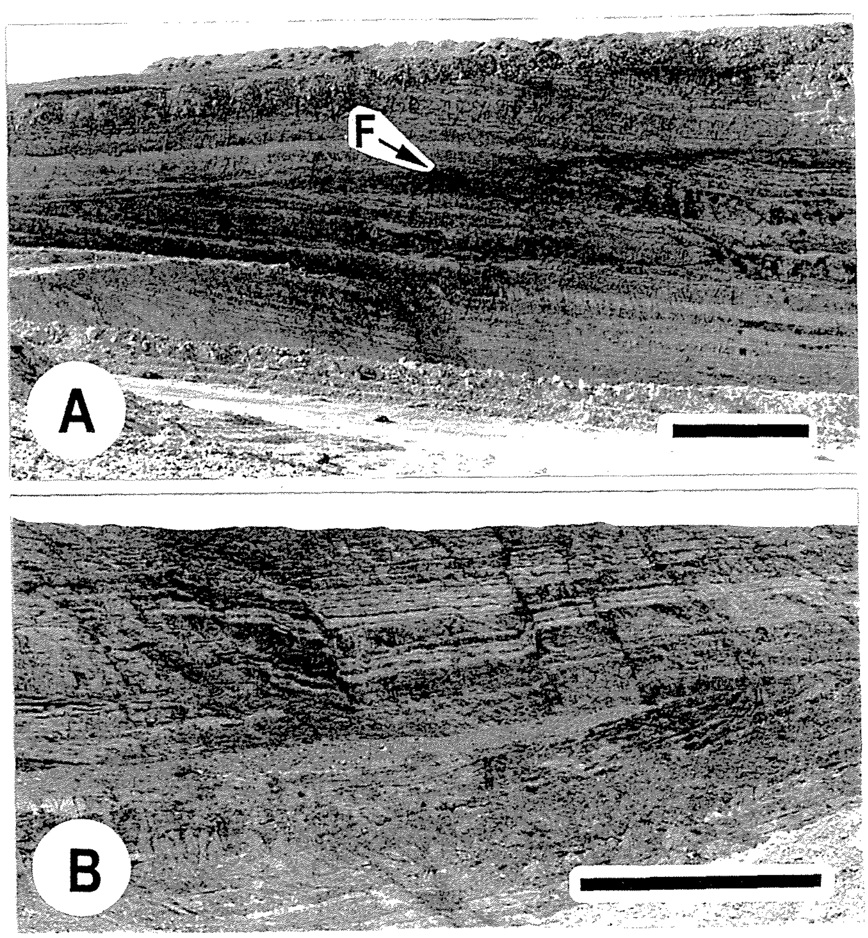
F
A
B

Figure 10: Faulting styles observed in Pit 8. (**A**) Sketch (from photograph) of duplex-style faulting in the NNE wall of Pit 8 (see Fig. 1 for location). Bedding dips shallowly to moderately SW, and the duplex has an apparent top-to-the-NE shear sense, although the fault strikes slightly oblique (clockwise) to the axial trend of the dome. The insets schematically illustrate the various fault-timing criteria; these include (**i**) cleavage-truncation and rotation of cleaved (S_2) fault-breccia clasts (**Bx**), as well as (**ii**) bedding reactivation ($S_\mathbf{R}$) that crenulated S_2. (**B**) Reverse faulting that initiated along bedding and bifurcated upwards through the siltstone country rock (SW face of Pit 8). Associated with this fault are small disharmonic folds that have an orientation similar to that of F_4 folds, thus suggesting the fault formed during D_4. Massive quartz infill occurs along the bedding, particularly where local disharmonic folding of fine laminae, resulting in gaping, has occurred (Inset). (**C**) Reactivation of early normal faults during D_2/D_4 shortening to produce reverse faults. The faults lie parallel to S_1 and in outcrop some exhibited normal movement suggesting a possible formation resulting from local layer-parallel extension of sub-horizontal bedding during D_1 (see Section A). Other similarly oriented faults in the same outcrop exhibited reverse movement suggesting that the earlier normal faults were reactivated by horizontal shortening during D_2/D_4. (Location: B; SW face of Pit 8, Telfer Mine; Mine Grid - 12880mN 9490mE. C; N face of Pit 8, Telfer Mine; Mine Grid - 13035mN 9480mE).

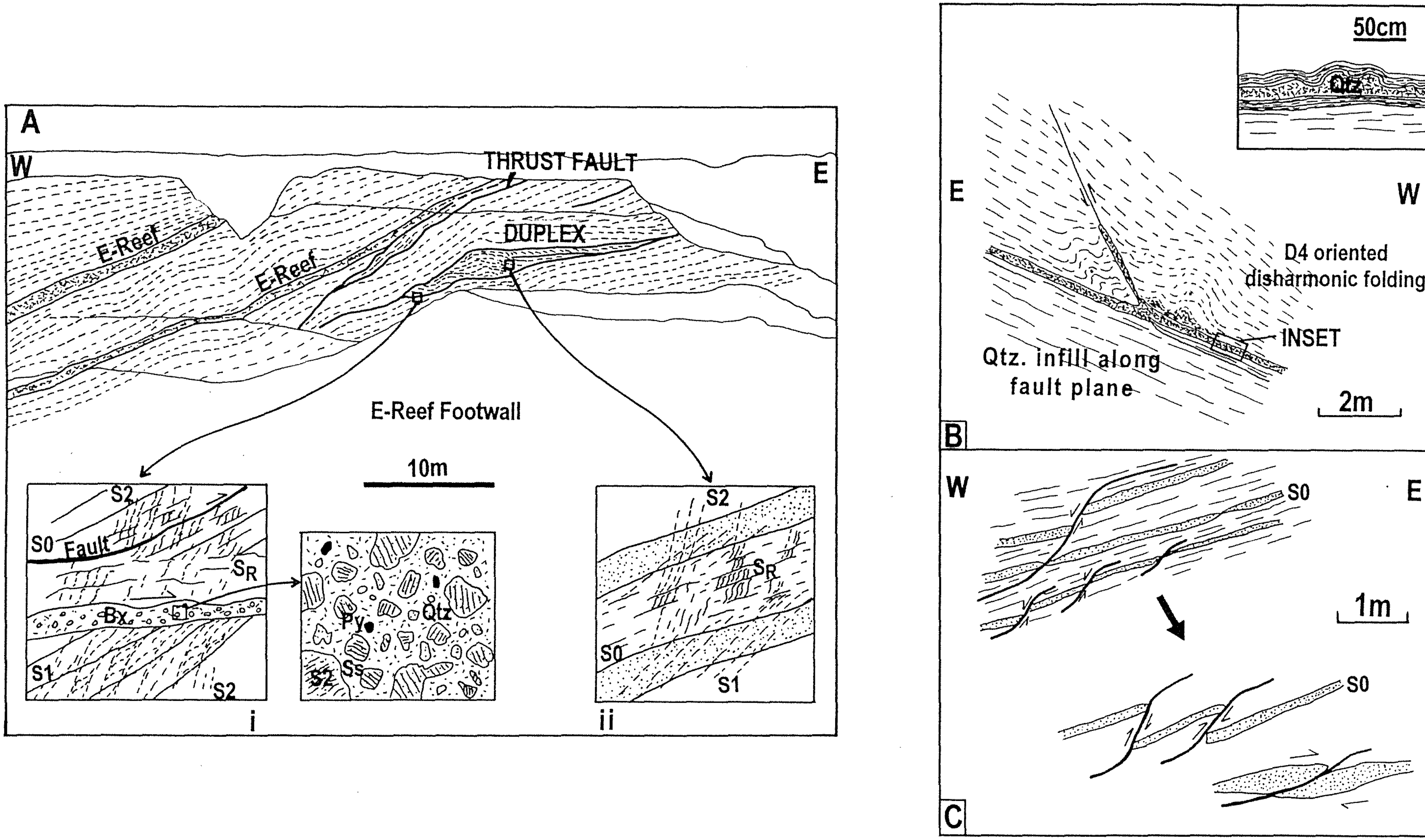
A
W
E
THRUST FAULT
DUPLEX
E-Reef
E-Reef
E-Reef Footwall
10m
S2
S0
Fault
SR
Bx
S1
S2
i
Py
Qtz
S2
Ss
S2
SR
S0
S1
ii
50cm
Qtz
E
W
D4 oriented
disharmonic folding
INSET
Qtz. infill along
fault plane
2m
B
W
E
S0
1m
S0
C

Figure 11: Structure contour map (**A**) and cross sections (**B** - overpage), of the upper Rim Sandstone contact in West Dome (redrawn from Hill, 1989) illustrating the gross geometry of the dome. The map illustrates the variably developed major and minor fold axes, and the asymmetric form of the dome. The cross sections, along the three grid lines shown in (A) illustrate the upper contact of both the Rim Sandstone (**RSM**) and Middle Vale Siltstone (**MVS**). Cross section scale : vertical = horizontal. Grid in (A) refers to the local mine grid; **GN** - Grid North. The contours are in metres above a reference level (RL).

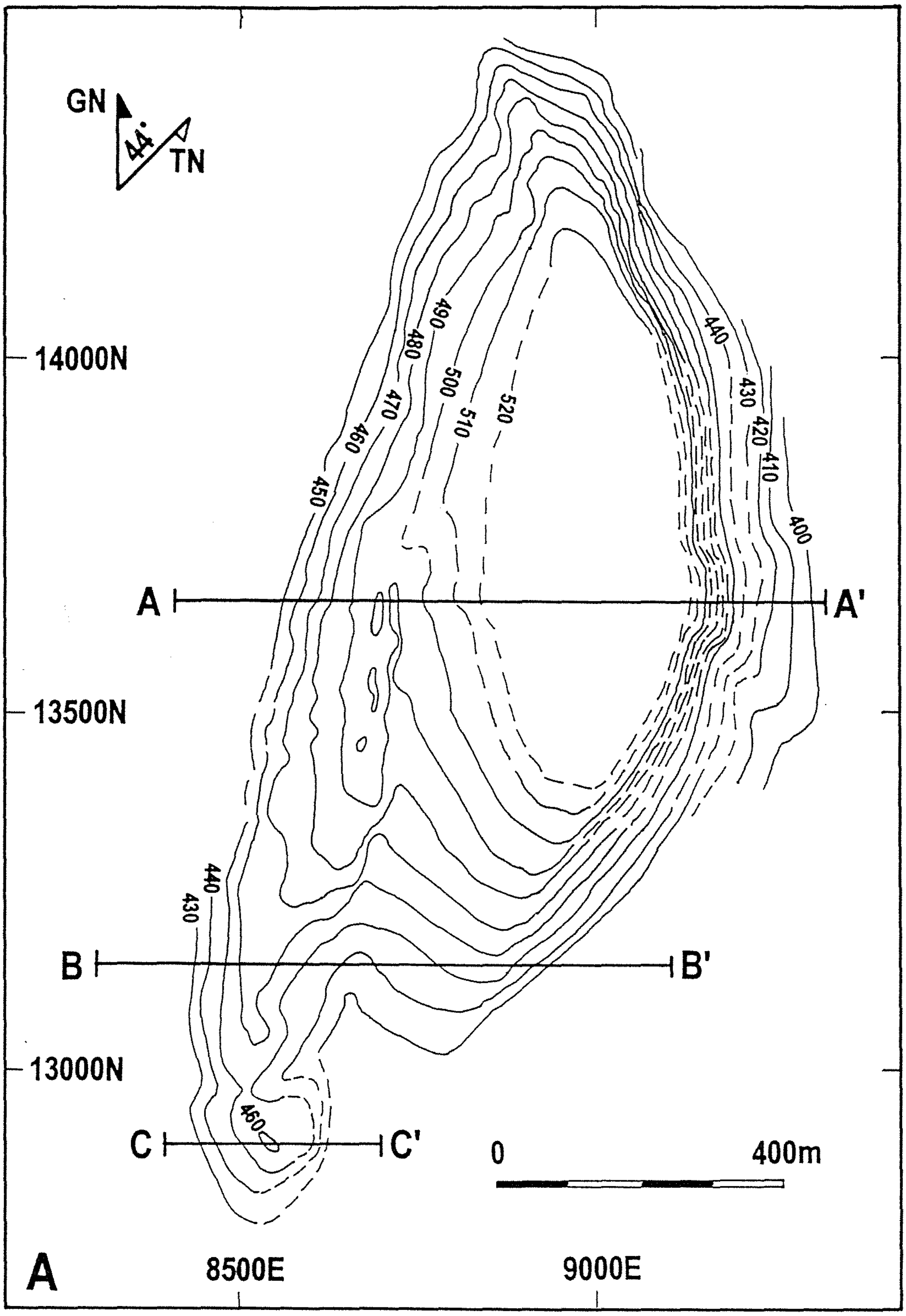
GN
44°
TN
14000N
13500N
13000N
8500E
9000E
A
A'
B
B'
C
C'
0
400m
400
410
420
430
440
450
460
470
480
490
500
510
520
A

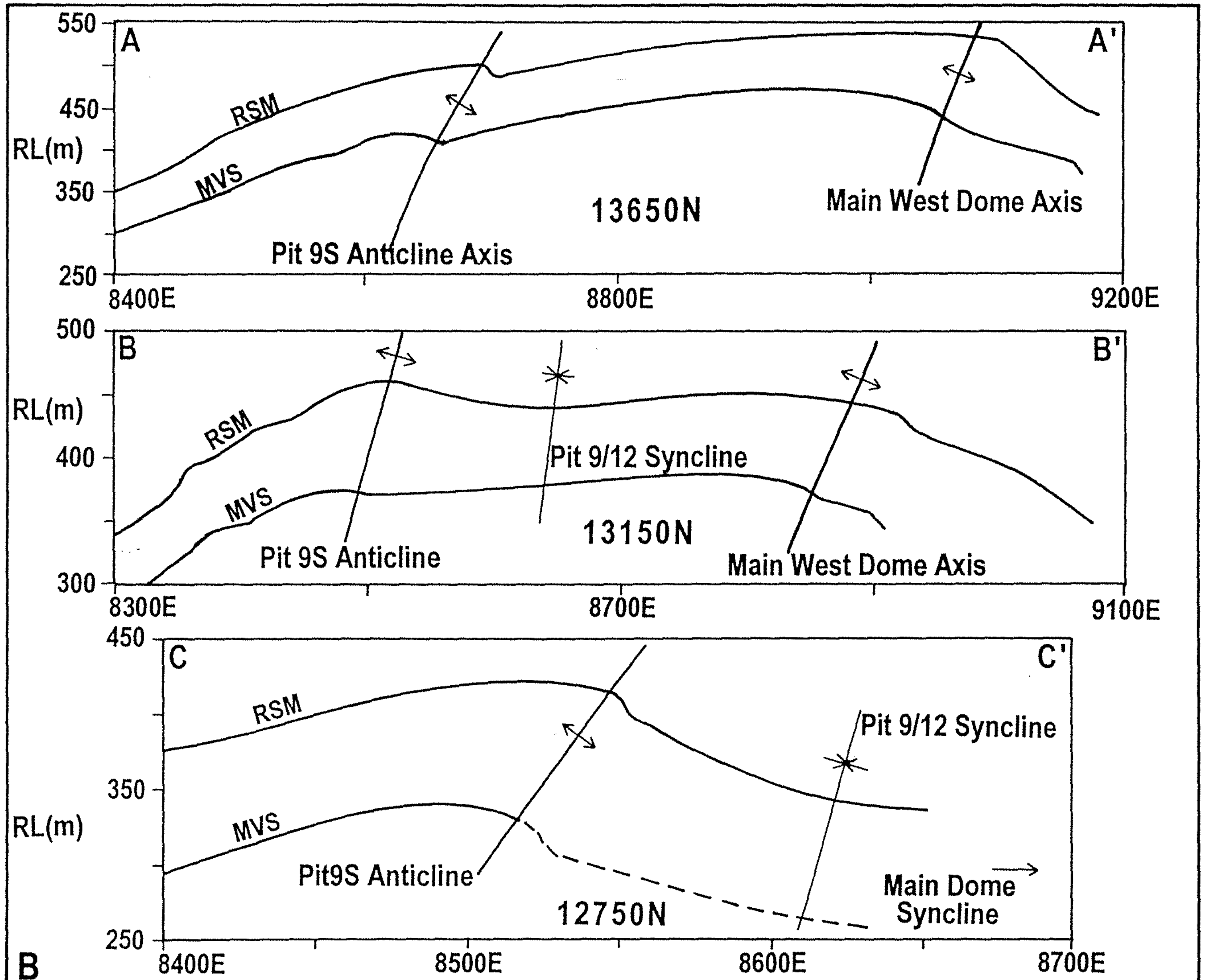

550
A
A'
450
RL(m)
350
250
RSM
MVS
13650N
Main West Dome Axis
Pit 9S Anticline Axis
8400E
8800E
9200E
500
B
B'
RL(m)
400
300
RSM
MVS
Pit 9/12 Syncline
13150N
Pit 9S Anticline
Main West Dome Axis
8300E
8700E
9100E
450
C
C'
RSM
Pit 9/12 Syncline
350
RL(m)
MVS
Pit9S Anticline
12750N
Main Dome
Syncline
250
8400E
8500E
8600E
8700E
B

Figure 12: Sketch of the main closure of West Dome observed just north of Pit 12 illustrating the locally disharmonic and asymmetric shape of the hinge, and the cleavage-bedding relationships on either side. The hinge is cut by medium- to high-angle reverse faults. The constant sub-vertical S_2 orientation across the hinge suggests that the asymmetry is due to strain intensification during D_2. (Location: NW face of Pit 12, Telfer Mine; Mine Grid - 13305mN 8945mE)

Figure 13: Sketch (drawn from field photograph) of a recumbent F_1 fold observed in the south-eastern face of Pit 10 on the NE limb of the main West Dome Anticline. (Location: SE face of Pit 10, Telfer Mine; Mine Grid - 13800mN 9170mE)

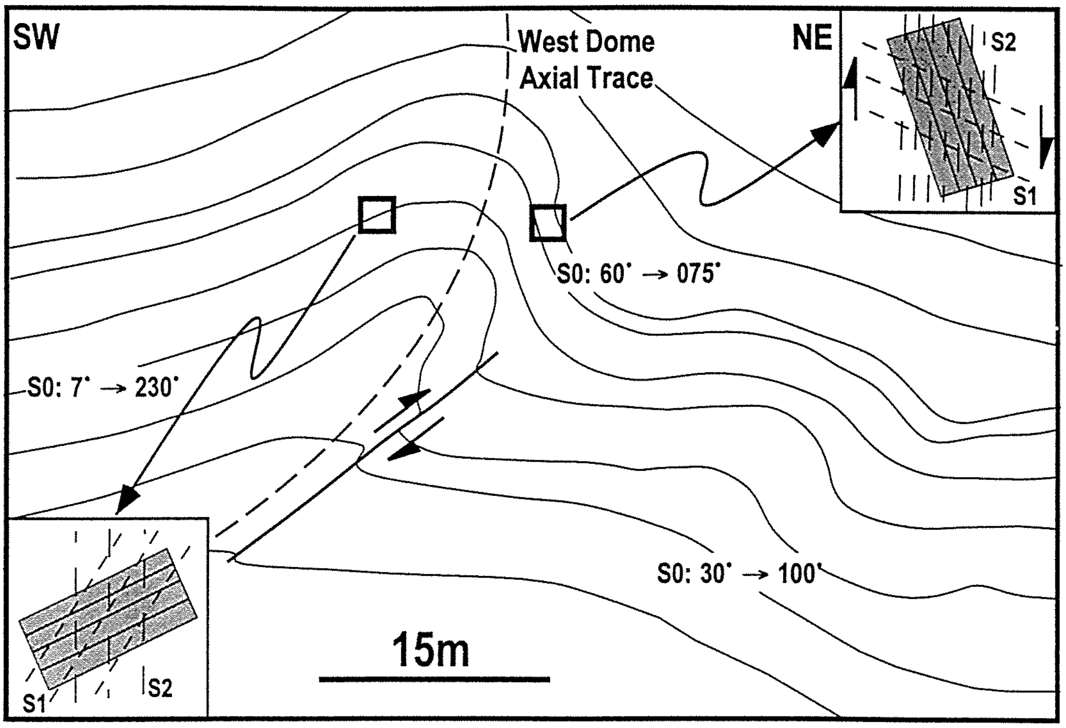
SW
West Dome
Axial Trace
NE
S2
S1
S0: 60° → 075°
S0: 7° → 230°
S0: 30° → 100°
S1
S2
15m

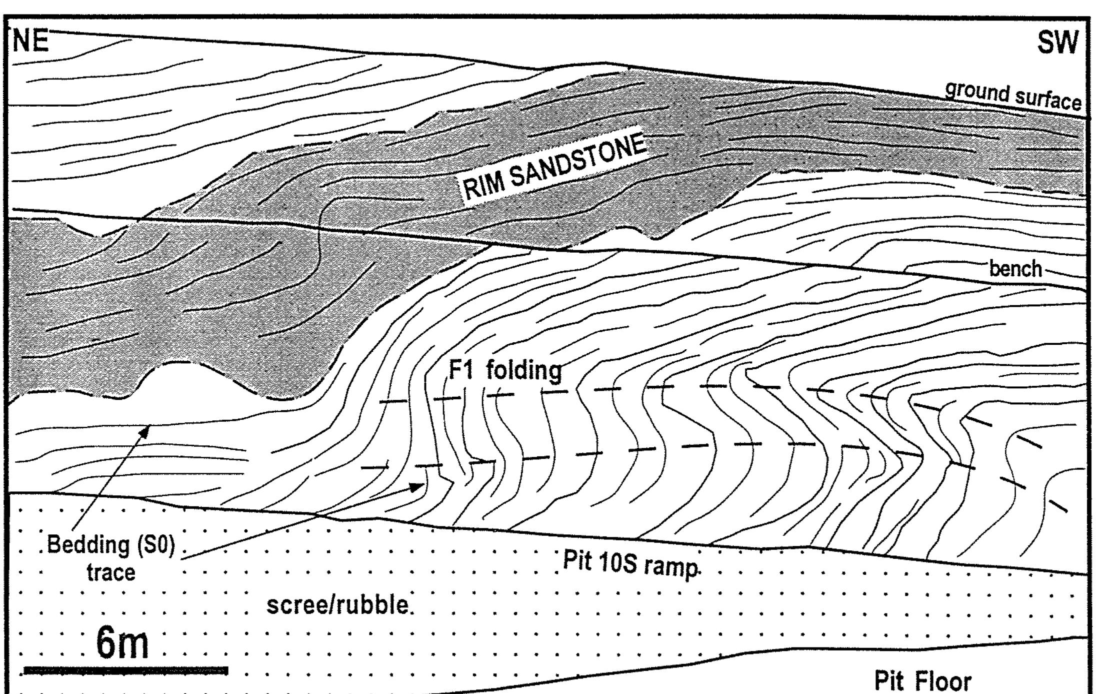
NE
SW
ground surface
RIM SANDSTONE
bench
F1 folding
Bedding (S0)
trace
Pit 10S ramp
scree/rubble
6m
Pit Floor

Figure 14: Schematic diagram illustrating bedding cleavage relations observed in the NE wall of Pit 10. (**A**) Preservation of a sub-horizontally plunging D_1 fold is suggested by cleavage (S_1) - bedding relationships (1, 2 & 3) that were observed in a traverse along the NE benches of Pit 10 (**B**), on the NE limb of the main West Dome Anticline (**C**). The D_1 fold lies in a position similar to the F_1 fold illustrated in Fig. 13.

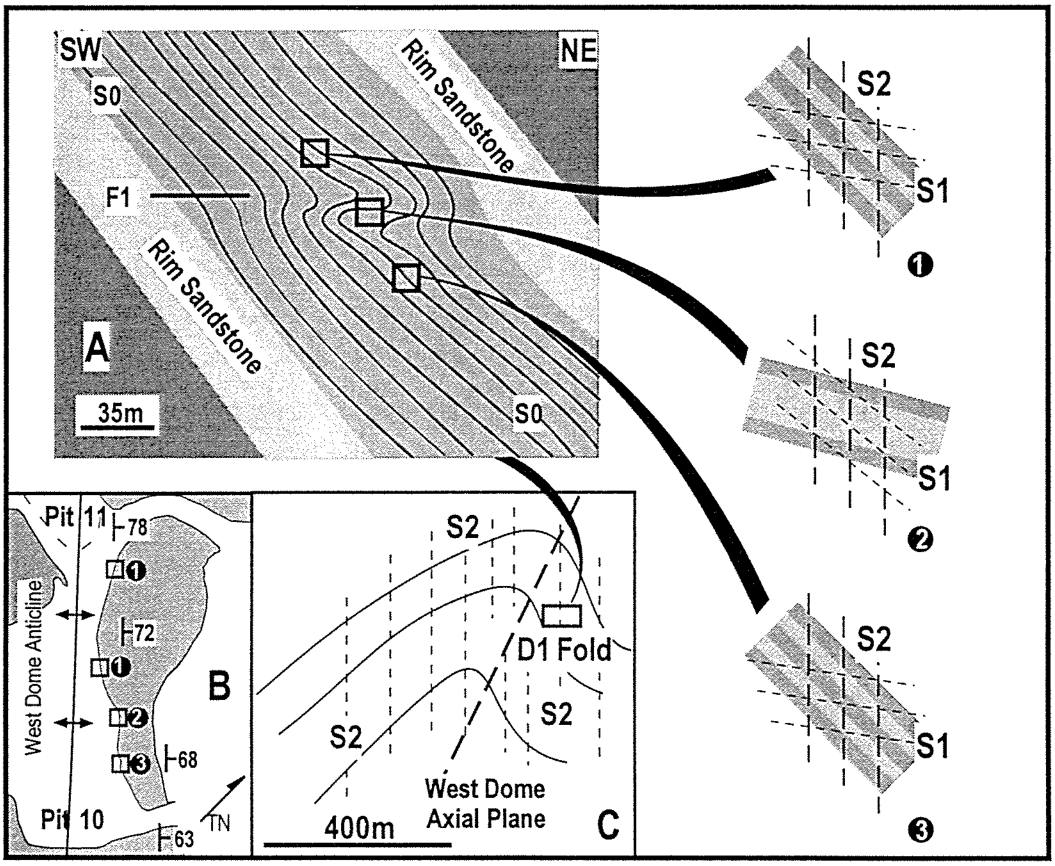

SW
NE
S0
F1
Rim Sandstone
Rim Sandstone
A
35m
S0
S2
S1
❶
S2
S1
❷
S2
S1
❸
Pit 11
78
West Dome Anticline
72
68
Pit 10
63
TN
B
S2
S2
D1 Fold
S2
S2
West Dome
Axial Plane
400m
C

Figure 15: Field sketches of various fold shapes/styles commonly observed in West Dome. (**A**) High angle reverse faults that initiate as bedding-parallel faults, and bifurcate upwards through the overlying strata. These commonly contain coarse-grained quartz that precipitated along the steepened fault planes. (**B**) Reverse faulting that produced small fault-propagation folds. (**C**) Concentric folding overlying a bedding-parallel reverse fault. (**D**) Mesoscale box folding in finely bedded strata. (**E**) Anticlinal folds in finely bedded strata illustrate the locally contorted character of bedding and irregular fold shapes that have resulted from complex multi-layer behaviour. (**F**) Asymmetric anticlinal folding with an overturned NE limb and associated curvature of the fold hinge. (**G**) Irregular intra-bedding monoclinal flexure. This is likely to represent an early fold phase that produced locally sub-vertical bedding, which was subsequently truncated by bedding reactivation (**R**) during D_2/D_4, and/or attenuation through synthetic D_3 shear. The flexure has the wrong vergence to be a D_1 fold. (**H**) Synformal D_2 fold with a small D_1 monoclinal flexure (outlined by brackets) preserved in the SW limb. Arrows parallel to F_2 axial plane illustrate the bulk fold movements, along the axial plane, during D_2. (**I**) Relict D_1 monocline (outlined by brackets) preserved in uniform NE dipping strata that are cut by high-angle reverse faults.

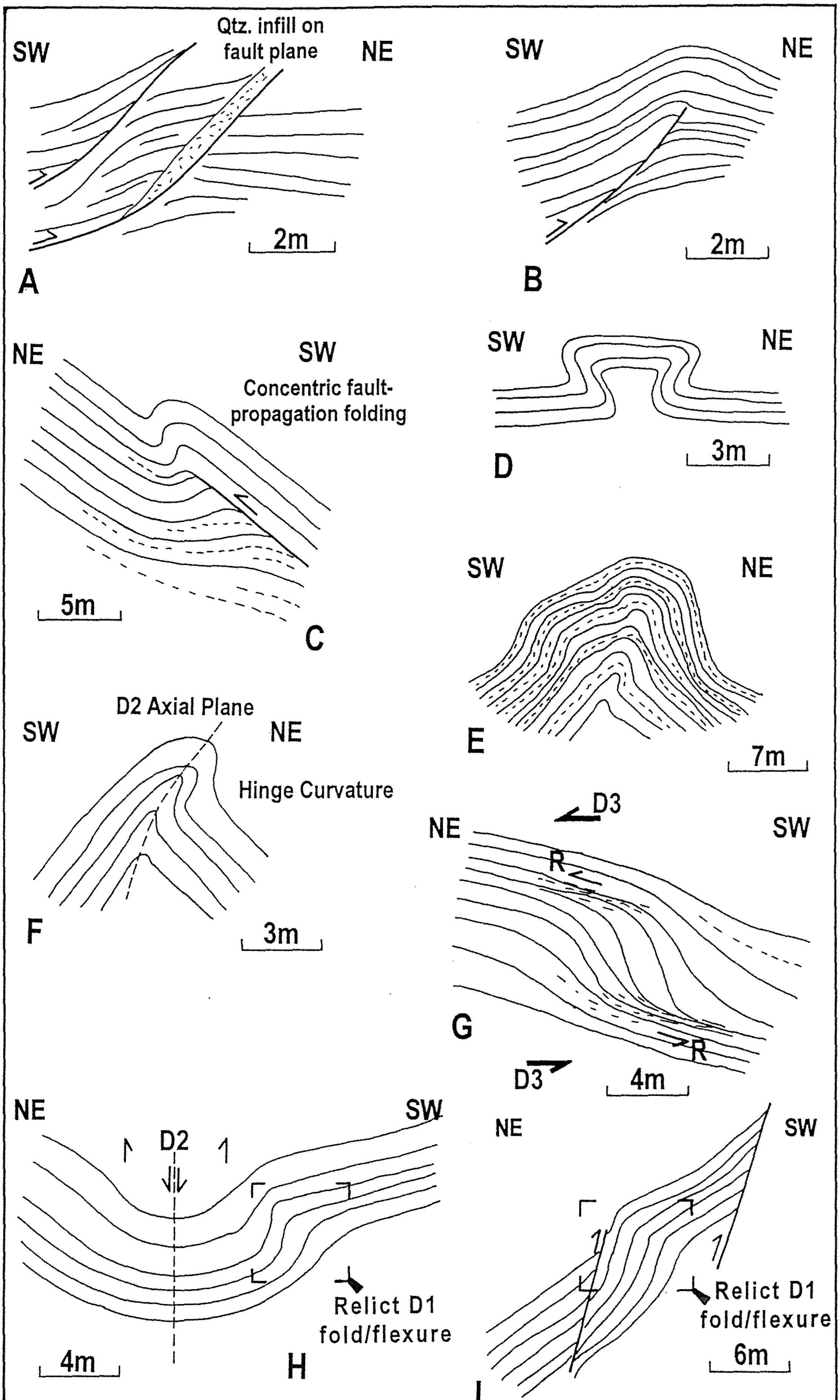

SW
Qtz. infill on fault plane
NE
2m
A
SW
NE
2m
B
NE
SW
Concentric fault-propagation folding
5m
C
SW
NE
3m
D
SW
NE
7m
E
D2 Axial Plane
SW
NE
Hinge Curvature
3m
F
D3
NE
SW
R
R
G
D3
4m
NE
SW
D2
Relict D1 fold/flexure
4m
H
NE
SW
Relict D1 fold/flexure
6m
I

Figure 16: Cross section of the Pit 9S anticlinal closure illustrating the large high-angle reverse Pit 9S fault zone that lies axial plane to the fold. Small boxes illustrate the S_2 -bedding relationships across the fault-fold structure (*solid lines* - bedding; *finely dashed lines* - S_2). These highlight the local overturning of the NE fold limb and the general vertical orientation of S_2 across the fold. The fault zone comprises anastomosing zones of gouge, disrupted bedding and strong brecciation that lies along the fold axial plane. At deeper levels the Pit 9S fault zone passes into the upper mineralised E-reefs (see text). (Location: SW face of Pit 9S, Telfer Mine; Centre of Fault Zone = Mine Grid - 12635mN 8550mE)

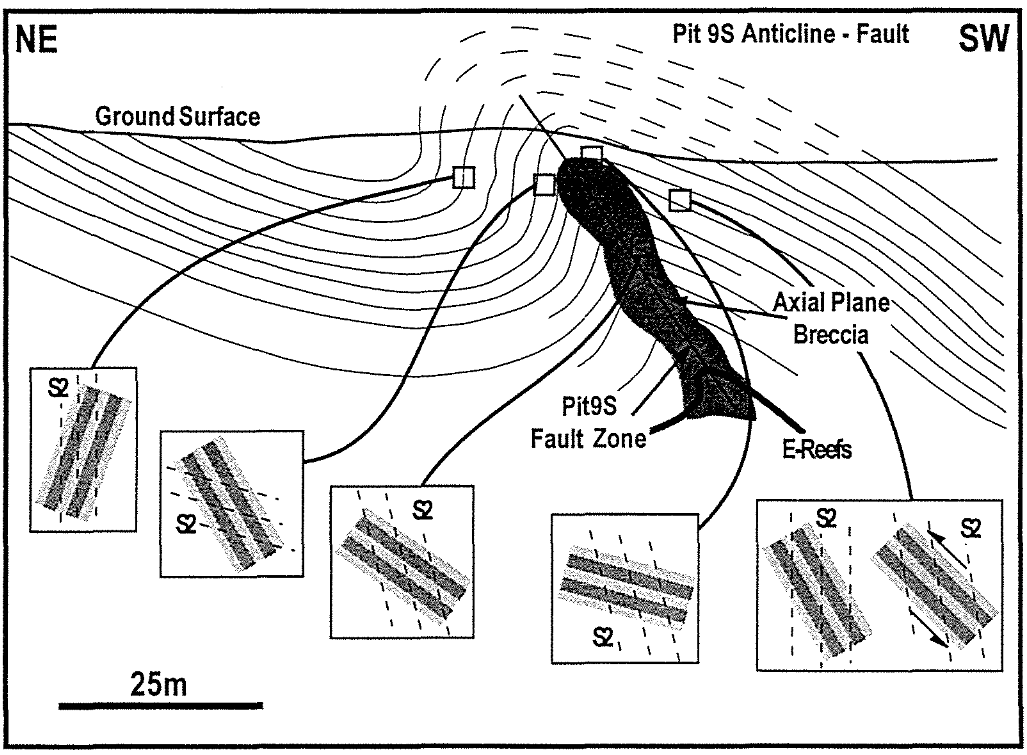
NE
Pit 9S Anticline - Fault
SW
Ground Surface
Axial Plane
Breccia
Pit9S
Fault Zone
E-Reefs
S2
S2
S2
S2
S2
S2
25m

Figure 17: Photograph of typical exposure of the Middle Vale Reef in underground mining operations. The reef is approximately 1.2m thick in this location and comprises massive quartz veining (**Qtz**), particularly along the lower contact (**LC**), within a finely laminated siltstone horizon. Coarse sulphide aggregates formed throughout the reef along with finer disseminated pyrite-quartz. However, much of the sulphide is now altered to chalcocite (**Chc**). Reefal margins are typically planar, although locally (particularly the lower one - LC) they become convolute. Photograph is looking NW, the roof of the drive is the hanging-wall (**HW**) and the scale bar represents 40cm. (Location: 610-South drive, Telfer Underground Operations).

Figure 18: Diagrammatic stratigraphic section of Middle Vale Siltstone, which encloses the Middle Vale Reef, on the SW limb of Main Dome in Pit 4. The Middle Vale Reef, which is comprised of massive and granular quartz-carbonate-sulphide, is enclosed within finely laminated units that are characterised by alternating sandstone and siltstone laminae. The quartz reef and associated veining often occur at the upper contacts of upward-fining sedimentary sequences. The finely laminated siltstone units lie between progressively (away from the reef) thicker and more massively bedded strata.

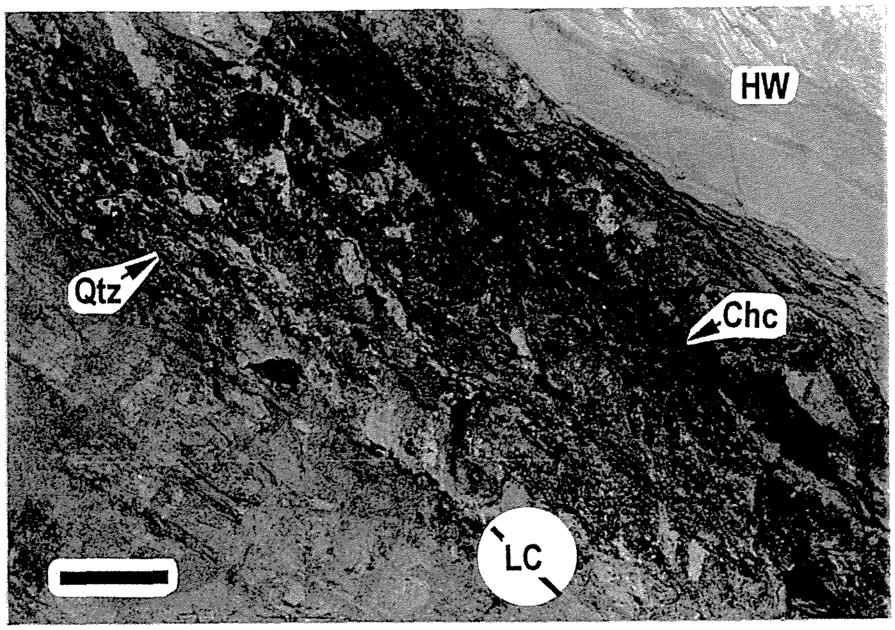
HW
Qtz
Chc
LC

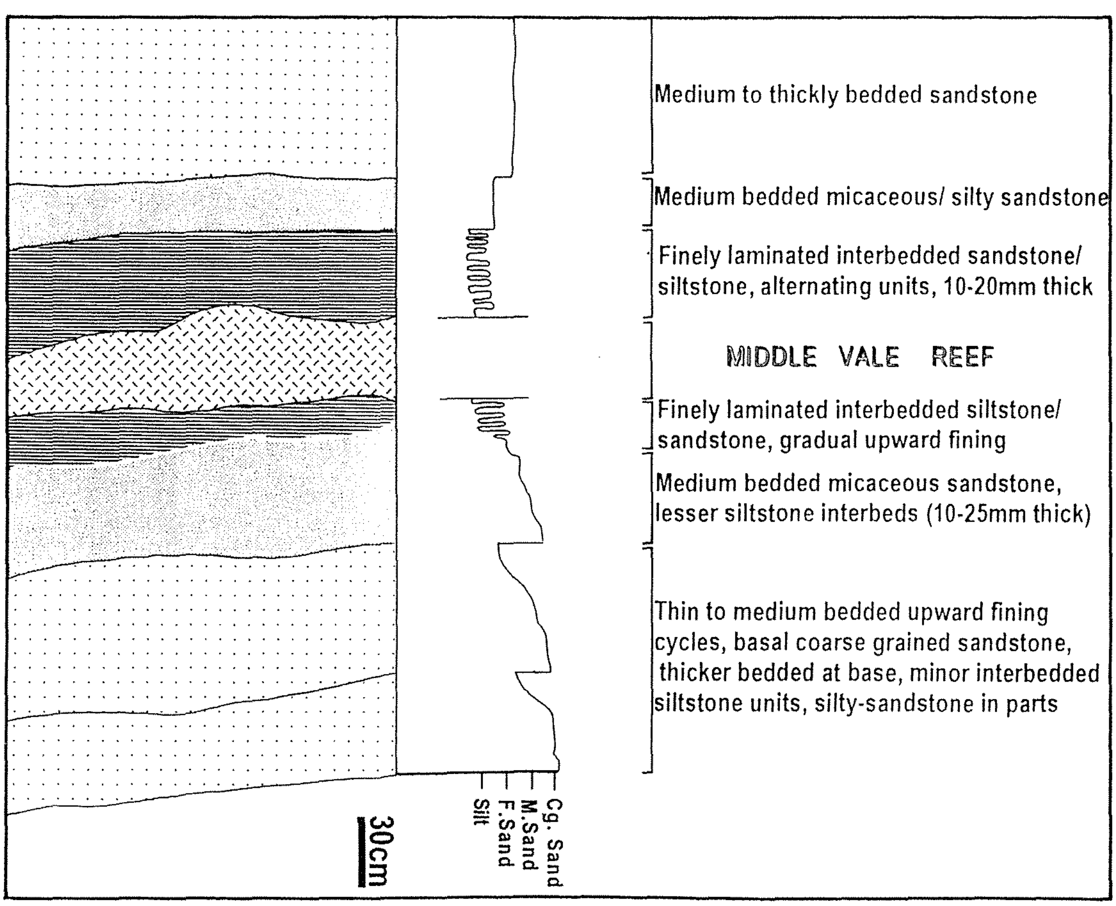
Medium to thickly bedded sandstone
Medium bedded micaceous/ silty sandstone
Finely laminated interbedded sandstone/ siltstone, alternating units, 10-20mm thick
MIDDLE VALE REEF
Finely laminated interbedded siltstone/ sandstone, gradual upward fining
Medium bedded micaceous sandstone, lesser siltstone interbeds (10-25mm thick)
Thin to medium bedded upward fining cycles, basal coarse grained sandstone, thicker bedded at base, minor interbedded siltstone units, silty-sandstone in parts
Cg. Sand
M.Sand
F.Sand
Silt
30cm

Figure 19: Photomicrograph of a sample from the lower margin of the Middle Vale Reef illustrating the replacive character of massive quartz veining/silicification. In hand specimen and outcrop the margin appears brecciated/granulated. However, the thin section reveals that smaller quartz grains (**Qtz**) lying in the matrix preserve fine inclusion trails parallel to bedding (**S_0**) indicating the quartz replaced bedding. This, coupled with the numerous fine dusty inclusions in the quartz, suggests that much of the massive quartz-vein component in the MVR is replacive. The thin section comes from an oriented sample whose orientation (marked) is 89° → 002° . (*JCU Catalogue No.* 48356)

Figure 20: Photograph of small-scale faulting (**F**) along the lower margin of the Middle Vale Reef that has thrust small wedges of bedding into the reef. Such faults would have provided ideal channelways for fluid infiltration into the reef as evidenced by the presence of fine-grained sulphides (pyrite-chalcopyrite) along the faults. The concentration of these faults along the lower reef margin suggests that fluid pressures reached supra-lithostatic levels during some stages of reef formation. The sample was oriented when collected and is photographed looking SE/SSE (SW to the right) at the lower margin of the Middle vale Reef. (*JCU Catalogue No.* 48357).

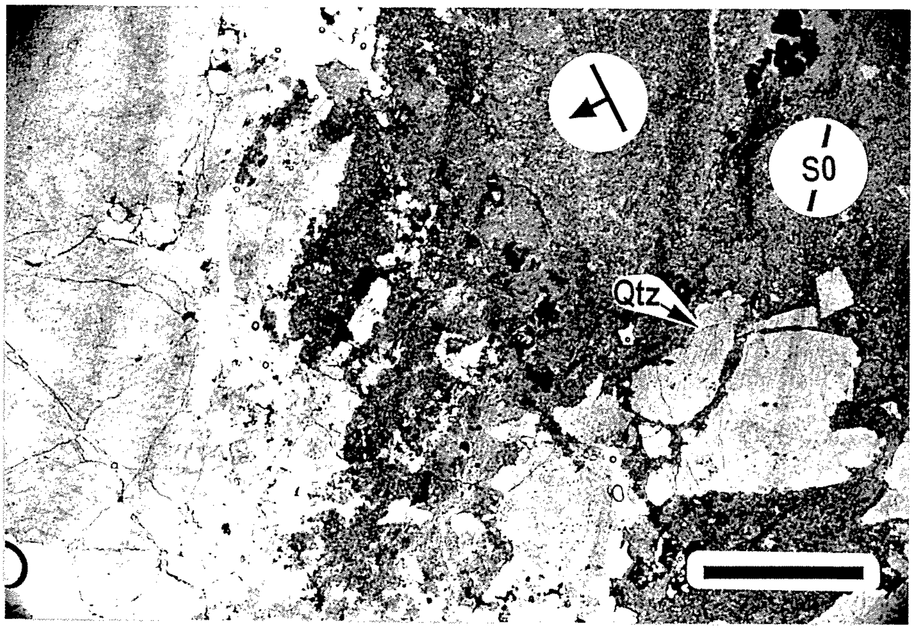
S0
Qtz

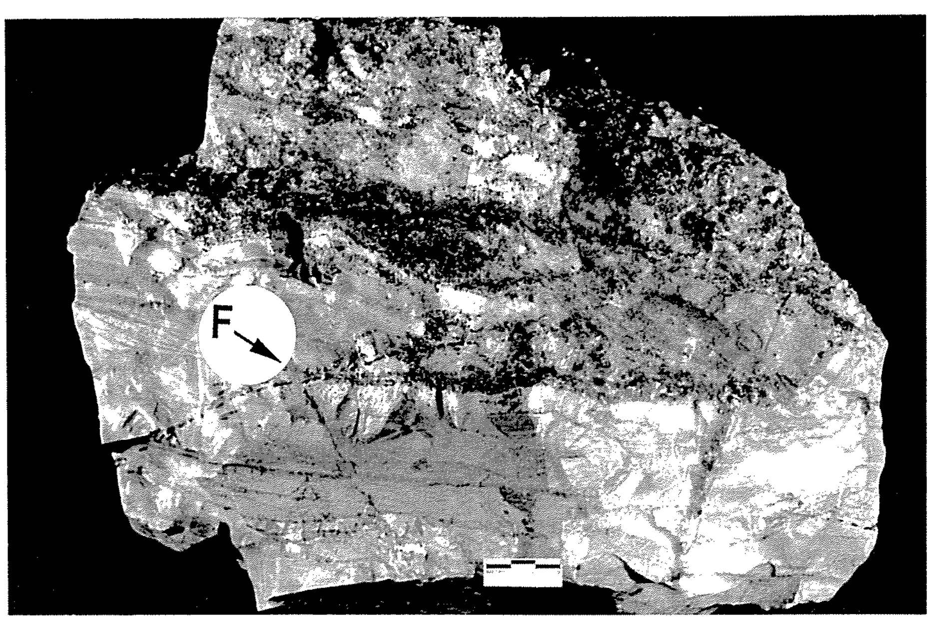
F

Figure 21: Diagram and photomicrographs illustrating textural zonation within the Middle Vale Reef (zones summarised in Table 4 in Text). The line diagram illustrates the three zones and their relative thickness. The photomicrographs illustrate the textural characteristics of each zone. (**Z1**) - Zone 1, the upper zone, comprises highly granular quartz that is commonly fractured and/or recrystallised, with associated fine-grained disseminated sulphide. Large sulphide grains are from an earlier phase of precipitation and, along with the quartz, have been deformed by repeated movement and cataclasis along the upper reef margin. (**Z2**) - Zone 2, the middle zone, comprises finer grained pyrite and aggregates that form laminae throughout the zone. Larger pyrite grains exhibit fine-grained quartz-fibre pressure shadows indicating strong layer-parallel deformation in this layer. (**Z3**) - Zone 3, the lower zone, comprises massive quartz (dusty, inclusion-full) that is highly strained and has been subsequently infilled with pyrite-chalcopyrite aggregates. Renewed deformation produced prominent quartz-fibre shadows on the larger angular and fractured sulphide grains. Scale bars in all photomicrographs are 2mm long, Z1 & Z2 are in plane polarised light and Z3 is under cross nichols. (Z1 - MVR SM-1; Z2 - MVR SM-2; Z3 - MVR LSZ-1: Newcrest Mining Pty. Ltd., Telfer Geology Dept., Telfer Gold Mine).

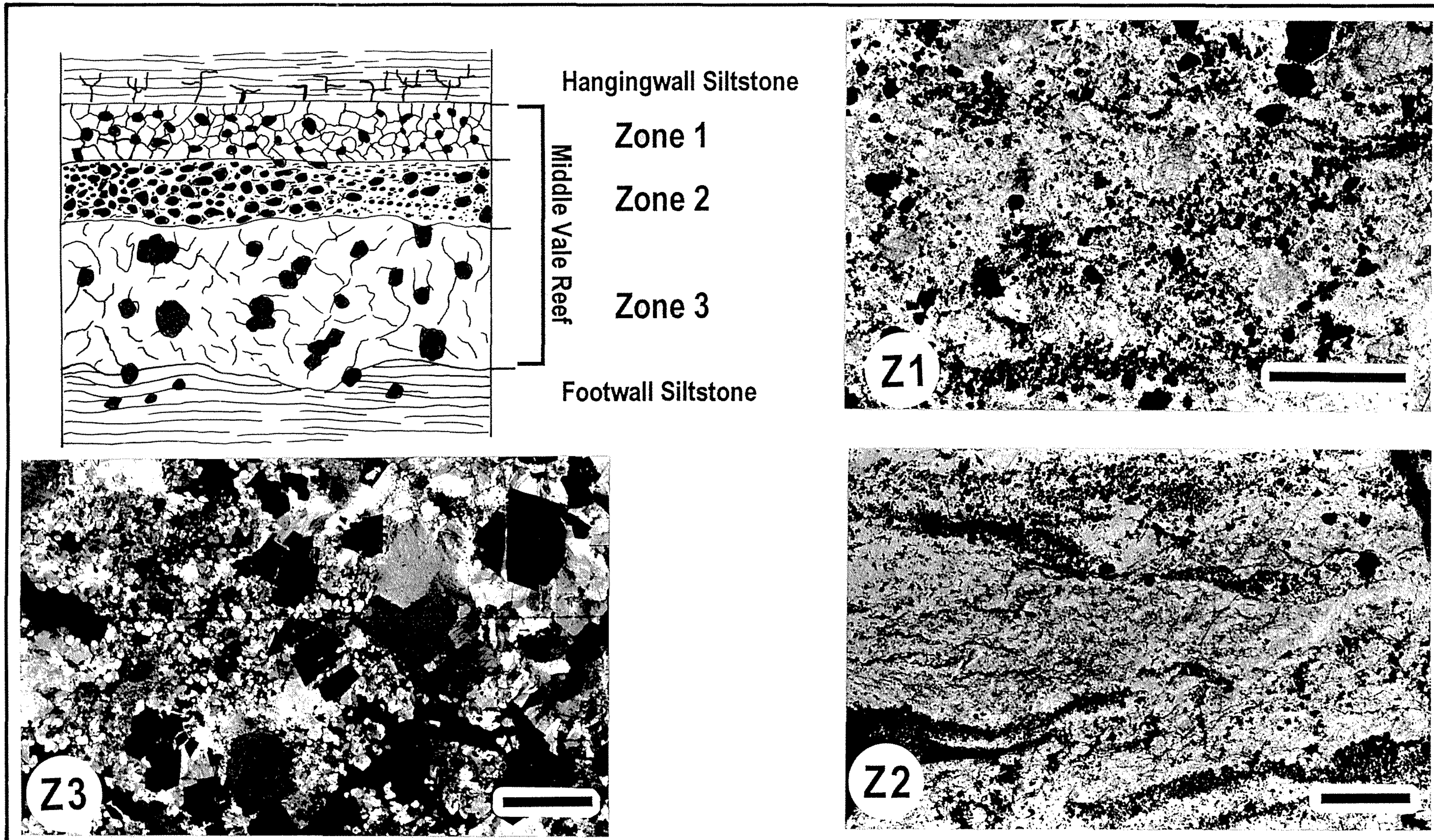
Hangingwall Siltstone
Zone 1
Zone 2
Zone 3
Middle Vale Reef
Footwall Siltstone
Z1
Z2
Z3

***Figure** 22*: Cross-sections through Pit 9S (13,000mN -mine grid) illustrating the geometry and styles of E-reef mineralisation. (**A**) The E-reef package formed immediately above the Rim Sandstone contact, as a series of stratabound reefs (E1A, E1 & E2). These thicken in the asymmetric hinge of the Pit 9S anticline, particularly along the more-steeply dipping, and locally overturned, NE limb. Underlying the sequence is a tabular stockwork zone comprising vein-hosted and disseminated mineralisation. (**B**) Textural variation across the E-Reef horizons which contain breccia along their length. This breccia predominates in tightened asymmetric hinge regions. On the limbs mineralisation/veining styles are more replacive. The development of discrete ore-bodies, known as "pods" (see text), is also illustrated. These preferentially developed in fold hinges and on steepened NE limbs, and consist of breccia-hosted mineralisation.

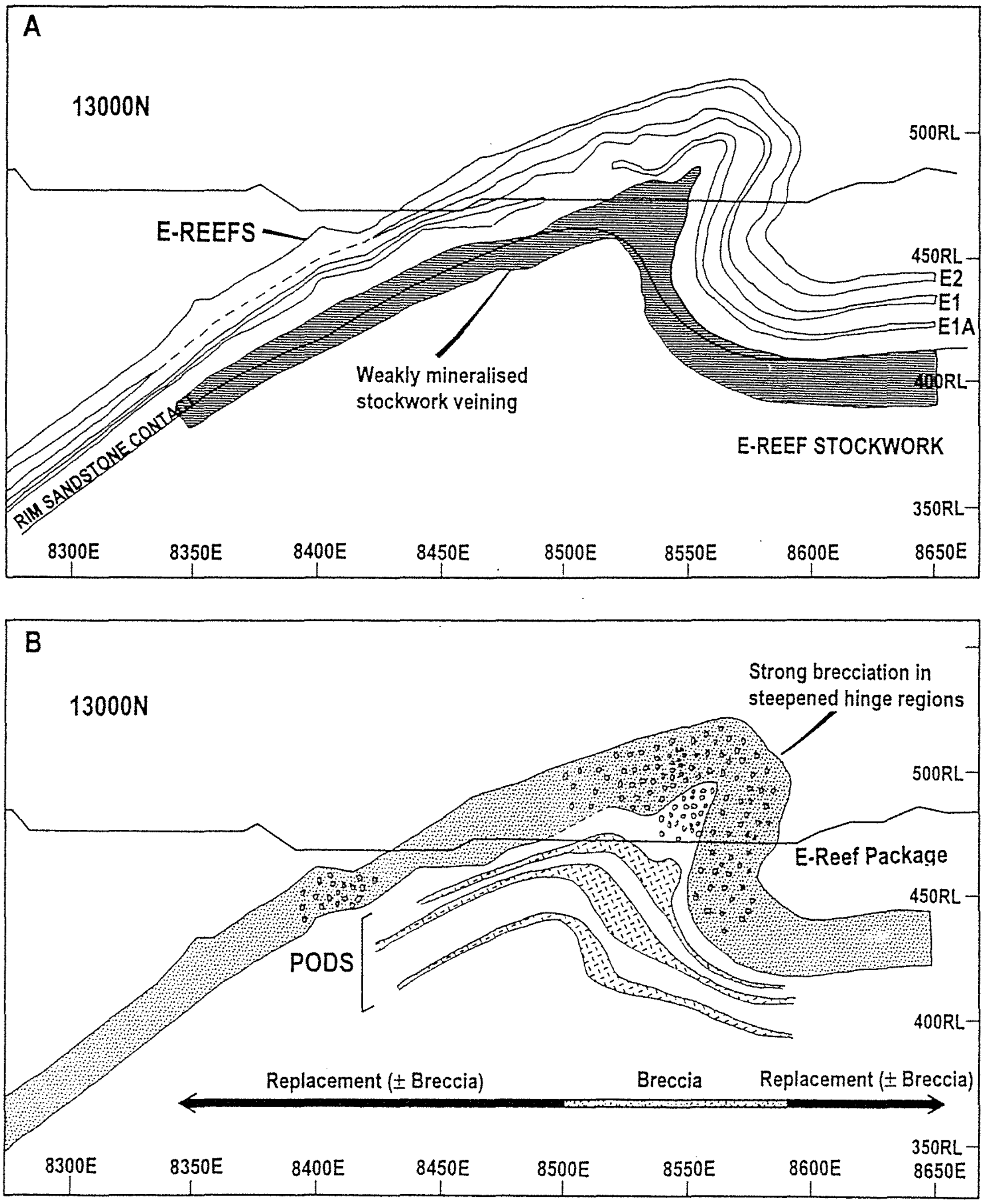
A
13000N
E-REEFS
500RL
450RL
400RL
350RL
E2
E1
E1A
Weakly mineralised
stockwork veining
RIM SANDSTONE CONTACT
E-REEF STOCKWORK
8300E
8350E
8400E
8450E
8500E
8550E
8600E
8650E
B
13000N
Strong brecciation in
steepened hinge regions
E-Reef Package
PODS
Replacement (± Breccia)
Breccia
Replacement (± Breccia)
500RL
450RL
400RL
350RL
8300E
8350E
8400E
8450E
8500E
8550E
8600E
8650E

Figure *23*: Map of West Dome illustrating the distribution of the various mineralisation styles. The major of these, the E-Reefs occur around the dome with individual reefs each developed at distinct stratigraphic levels. Also illustrated are the various pods, which occur as distinct bodies throughout West Dome. In Pit 10, pod mineralisation overlies the E-Reef package, whilst in Pit 9 the reverse occurs. The map-view position of disseminated/breccia hosted mineralisation associated with the West Dome Deeps shear zones and the location of sheeted vein arrays (Leeder Hills and Daves Vein) are also illustrated.

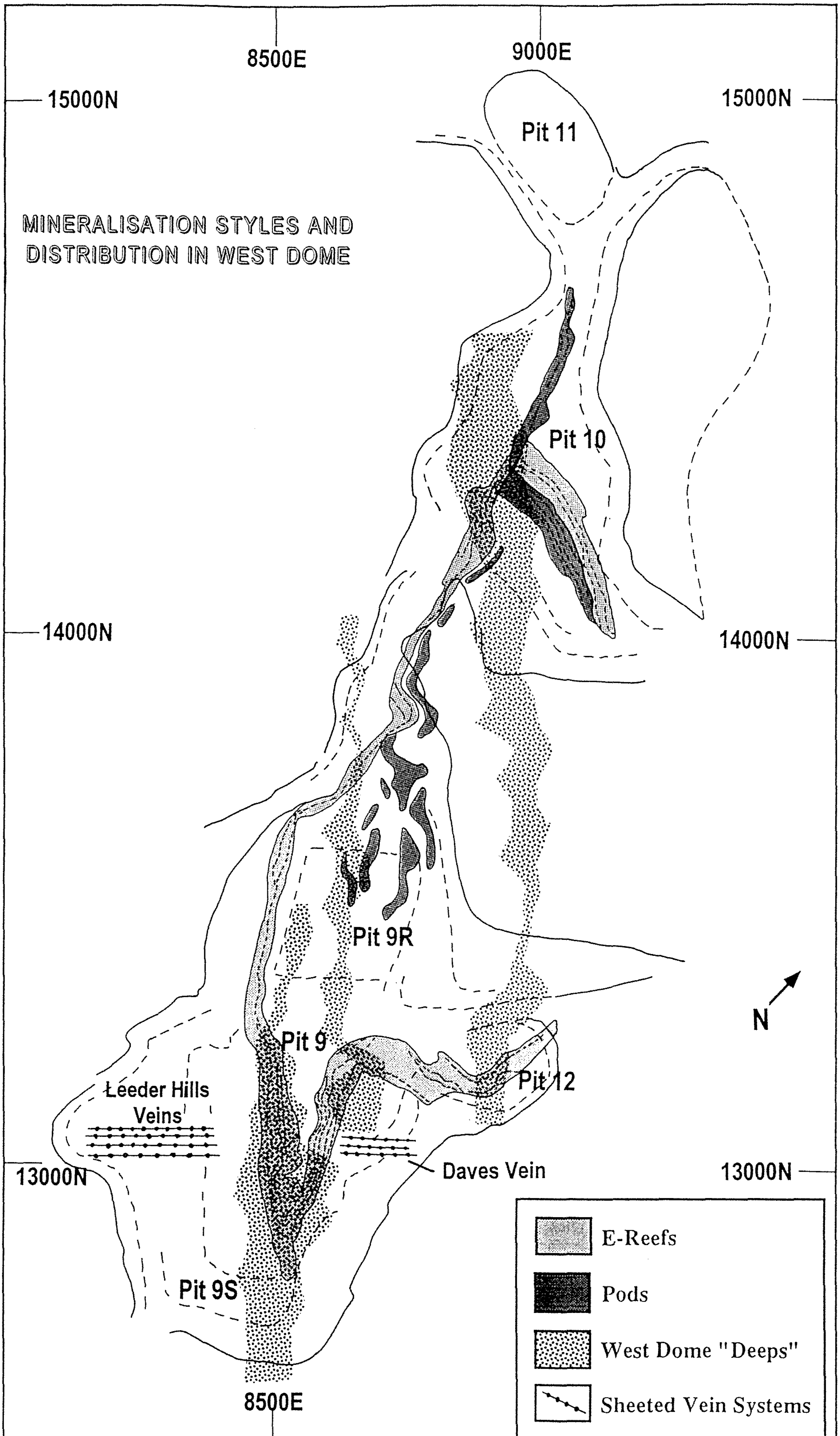

MINERALISATION STYLES AND
DISTRIBUTION IN WEST DOME
8500E
9000E
15000N
15000N
14000N
14000N
13000N
13000N
8500E
Pit 11
Pit 10
Pit 9R
Pit 9
Pit 12
Pit 9S
Leeder Hills
Veins
Daves Vein
N
E-Reefs
Pods
West Dome "Deeps"
Sheeted Vein Systems

Figure 24: Photograph of the M10 reef illustrating the markedly planar nature of the reef and it's margins (**UC** - upper contact; **LC** - lower contact). The reef contains thick quartz veining, that was successively infilled by dolomite (2 phases) and sulphide mineralisation. Thin stringer veinlets formed preferentially along the lower margin, and the reef is hosted within thinly bedded siltstone/sandy-siltstone units, which occur infrequently within the massive Malu Quartzite formation. The blotchy appearance in the adjacent wallrock is partly due to silicification (and consequent colour change) in the wallrocks, coupled with water from mining activity. **HW** - Hanging Wall; and the photograph is looking NW. (Location: RAW drive - Main Exploration Decline (see Fig. 1), Telfer Underground Operations).

Figure 25: Photograph of the M30 reef illustrating the presence of host-rock fragments and small asymmetric drag folds (**As.F**). These verge towards the Main Dome hinge and are consistent with flexural slip deformation during either D_2 and/or D_4. The reef was formed through variable infilling and replacive quartz-dolomite-sulphide mineralisation (marked) that pervaded this siltstone horizon. Wallrock margins of the M30 are sharply planar to slightly undulose. The photograph is looking SE with a hammer for scale. (Location: Main Exploration Decline (Fig. 1), Telfer Underground Operations).

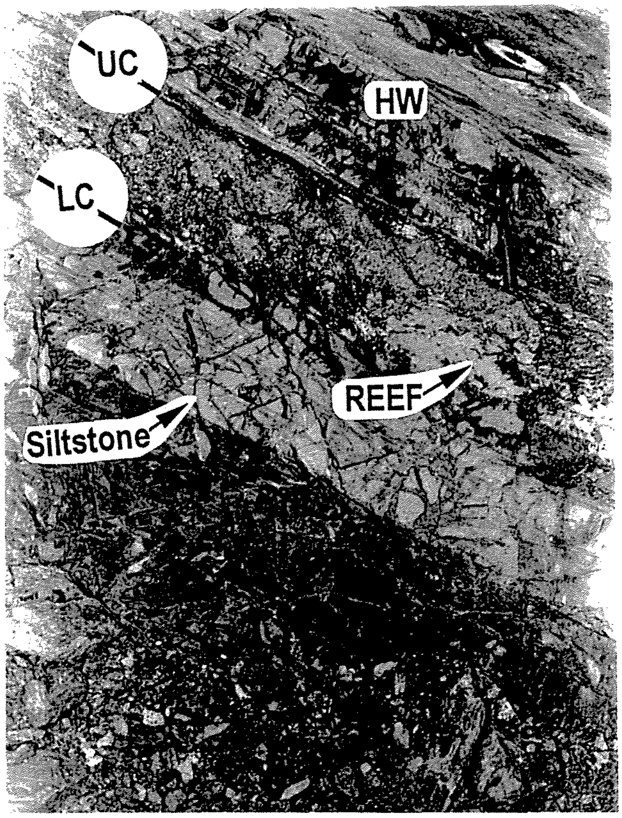
UC
HW
LC
REEF
Siltstone

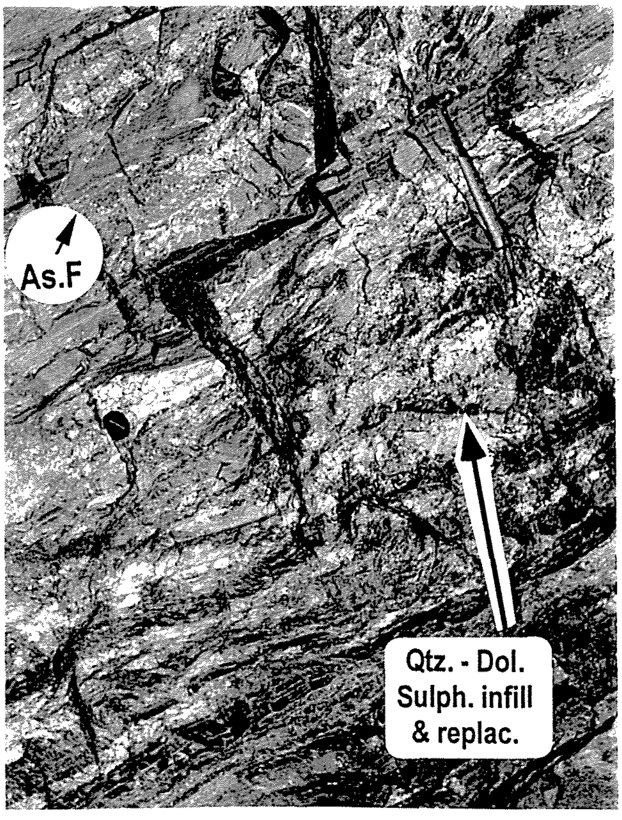
As.F
Qtz. - Dol.
Sulph. infill
& replac.

Figure 26: Schematic diagram summarising the geometry and textural relations of the I-Reef system identified through deep drilling of Main Dome. Three stratabound reefs, I10, I20 and I30 form within siltstone dominated sections of the Isdell Formation. These reefs occur at the contact between calc-arenites and overlying finely laminated siltstones. Faulting along the axial plane in the southern section is associated with spectacular brecciation, and a general thickening of the reefs is observed in tightened and refolded/rotated domal hinges. Away from the hinges mineralisation becomes replacement dominated. Mineralisation styles include quartz veining with associated sulphide alteration (**i**), breccia-hosted mineralisation (**ii**), massive dolomitisation (**iii**) and fine-quartz veining through wallrocks (**iv**). *Abbreviations*: **W** - wallrock; **Qtz** - quartz; **Dol** - Dolomite; **Py** - Pyrite.

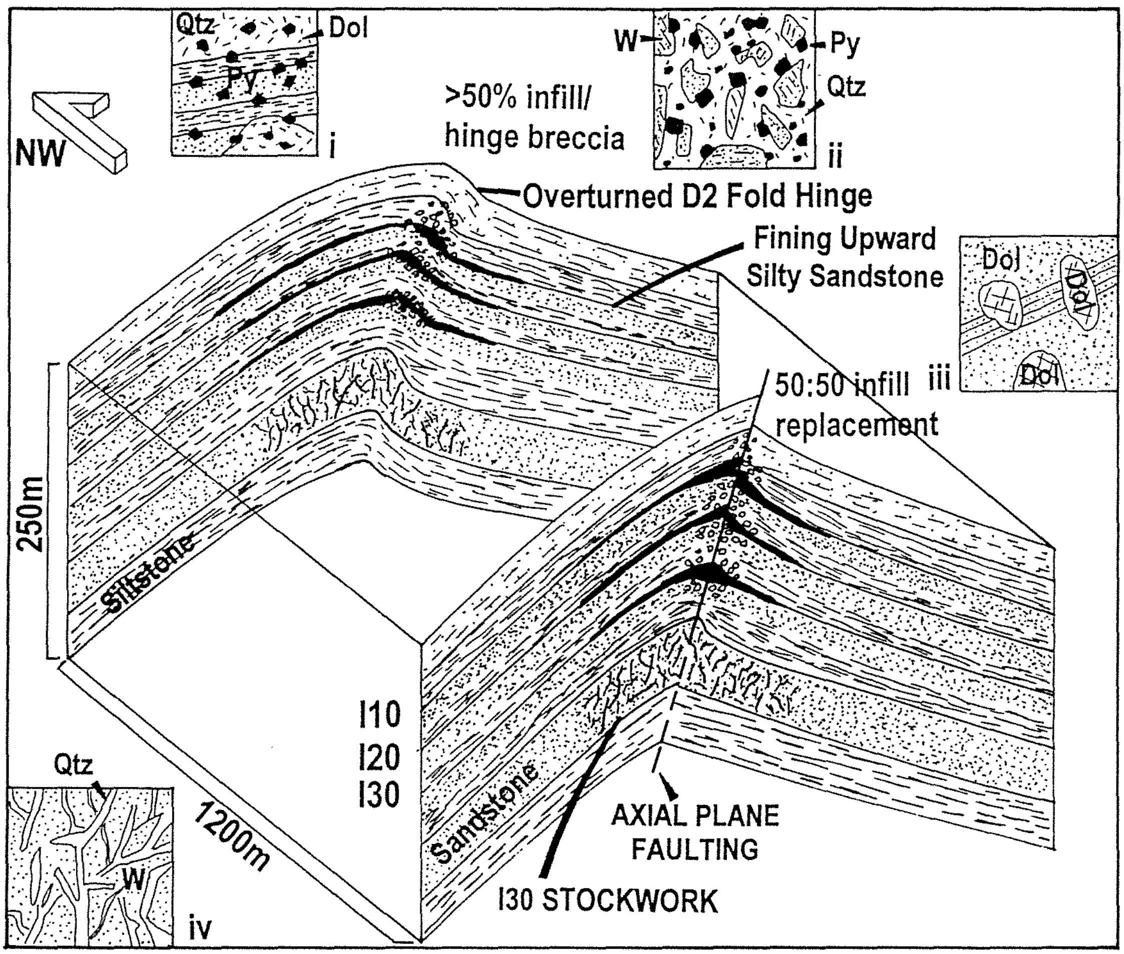

Qtz
Dol
Py
i
NW
>50% infill/
hinge breccia
W
Py
Qtz
ii
Overturned D2 Fold Hinge
Fining Upward
Silty Sandstone
Dol
Dol
Dol
iii
50:50 infill
replacement
250m
Siltstone
I10
I20
I30
Sandstone
AXIAL PLANE
FAULTING
I30 STOCKWORK
1200m
Qtz
W
iv

Figure *27*: Gold grade distribution in some Telfer reefs in Main Dome. (**A**) Thickness-grade contour diagram for the Middle Vale Reef in Main Dome (redrawn from unpub. data, Newcrest Mining). Within the reef, a higher grade N-S/NNW-SSE linear trend corresponds to a prominent veining direction (see text). A lesser E-W trend is also evident; this is approximately strike (reef) parallel. (**B**) Schematic geometry of high-grade zones within the M-Reefs (M10 and M30) on the NE limb of Main Dome. Two orientations are observed; both dip and strike (of the reefs) parallel. **NOTE:** The increased thickness-grade of the MVR in the south-eastern corner; this corresponds with a general asymmetry of grade across the Telfer Dome, with high grades in both the SE corner of Main Dome (illustrated) and NW corner of West Dome (not illustrated on this diagram).

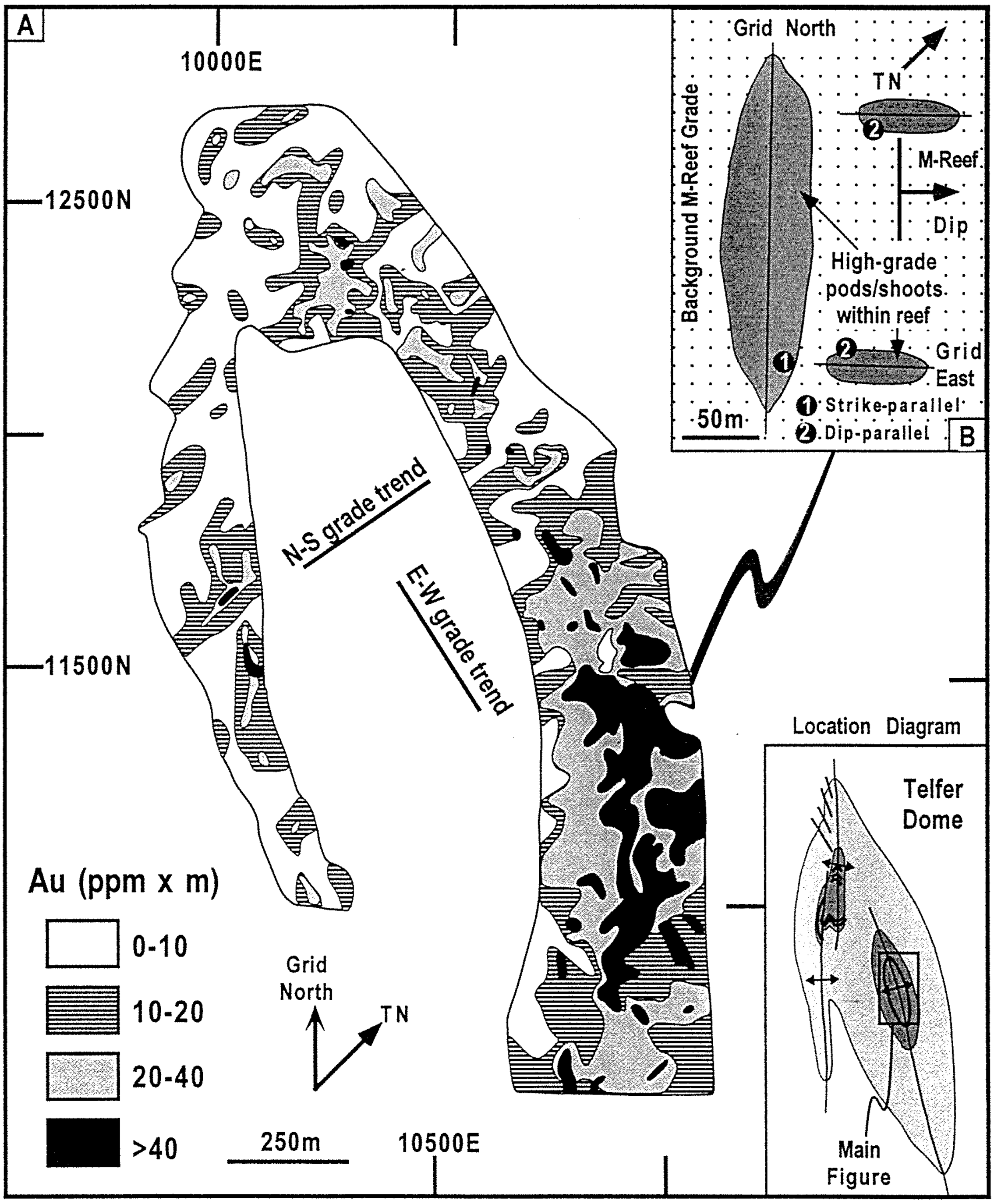

A
10000E
12500N
11500N
10500E
N-S grade trend
E-W grade trend
Au (ppm x m)
0-10
10-20
20-40
>40
Grid North
TN
250m
Grid North
TN
M-Reef
Dip
Background M-Reef Grade
High-grade pods/shoots within reef
Grid East
50m
1 Strike-parallel
2 Dip-parallel
B
Location Diagram
Telfer Dome
Main Figure

***Figure** 35*: Schematic summary of the mineralising effects of D_3. (**A**) Fold hinges were gaped, particularly the steepened NE limbs in asymmetric antiformal folds (**E** = extensional opening), by a combination of vertical shortening and NE directed horizontal movement during D_3, resulting in implosive brecciation (**B**). Antithetic reactivation of the SE limbs of antiformal folds (**D_{3R}**) would have caused steep structures, such as faults, to gape. (**C**) Reactivation of the SW limb during D_3 (**D_{3R}**) may also have produced opposing shear sense couples within silicified reefs. These would have arisen when synthetic shear (**SS**), acting in the quartz (light stipple) opposed antithetic shearing (**AS**) in marginal bedding, causing gaping along reef margins and quartz-sulphide (heavy stipple) addition. This process could occur at lateral terminations of silicified horizons thus extending the mineralised zone further up and down the fold limb. (**D**) Within Main Dome the stratabound reefs are thicker and best developed in the hinge and NE limb. The M-reefs developed preferentially through the hinge region, and on the NE limb. The I-reefs exhibit spectacular brecciation as the tighter hinge was rotated towards the NE and gaped during D_3. (**E**) Reef mineralisation on the NE limb was primarily produced through gaping of this limb during D_3. This arose from tensional opening/cracking of the silicified horizon (light stipple) causing infilling and replacive quartz-carbonate-sulphide mineralisation (heavy stipple). (**F**) Sulphide mineral addition to reef horizons on the SW limb may have occurred through antithetic reactivation of the enclosing bedding surface (**D_{3R}**) causing tensional microcracking in the quartz protolith and fracturing of the quartz-wallrock contact allowing ore-fluid infiltration.

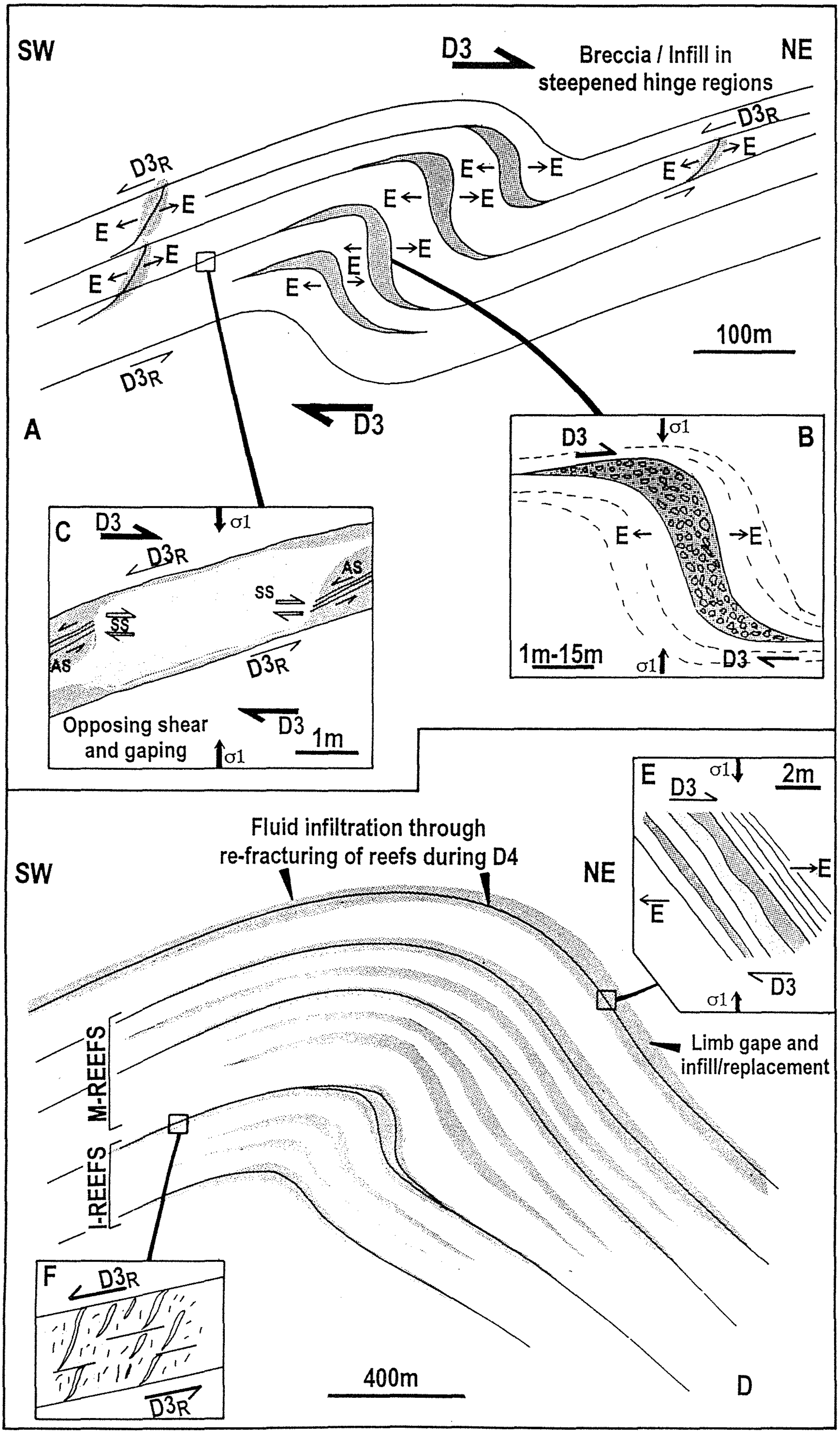

SW
D3
Breccia / Infill in steepened hinge regions
NE
D3R
E
100m
A
D3
B
σ1
1m-15m
C
SS
AS
Opposing shear and gaping
1m
Fluid infiltration through re-fracturing of reefs during D4
M-REEFS
I-REEFS
2m
Limb gape and infill/replacement
F
400m
D

Figure 36: Schematic summary of the effects of D_4 on mineralisation development. (**A**) Renewed shortening during D_4 would have caused further flexural slip and layer-parallel shearing along reefal horizons during reactivation of bedding (**D_{4R}**), as well as reactivating steep faults (in a reverse manner) and veins/fractures in tabular stockwork bodies. (**B**) In the asymmetric Telfer Dome the steeper dipping NE limb would have been preferentially reactivated (**D_{4R}**) during synthetic D_4 shear (**SS**). This culminated a progressive reef development that commenced with quartz (light stipple), followed by carbonate-sulphide (block stipple & opaque spots) during D_3 and new quartz-sulphide material along the upper reef during D_4 shearing (heavy stipple). (**C**) Shearing on the SW limb is likely to have been weaker, given its shallower dip, hence synthetic shearing deformation (**SS**) of the pre-existing reef (light stipple), coupled with reactivation (**D_{4R}**), would have caused limited material addition at reef contacts (heavy stipple). (**D**) Silicified-mineralised breccia pods (produced by D_3) would have been re-fractured by D_4 shortening and reactivation allowing further fluid infiltration. (**E**) In plan-view, the obliquity of D_4 stress across the Telfer Dome would have caused a weak sinistral transpression and subsequent intensification of strain into the NW and SE corners (stippled). In these areas, bedding reactivation and reefal deformation would have been enhanced (**F** & **G**) during D_4 synthetic shear (**SS**), causing an asymmetric grade enrichment across the dome. (**H**) Fault systems would also have been reactivated (sinistrally) by D_4 producing internal fracturing and breccia development (**Bx**) that hosted mineralisation (stippled).

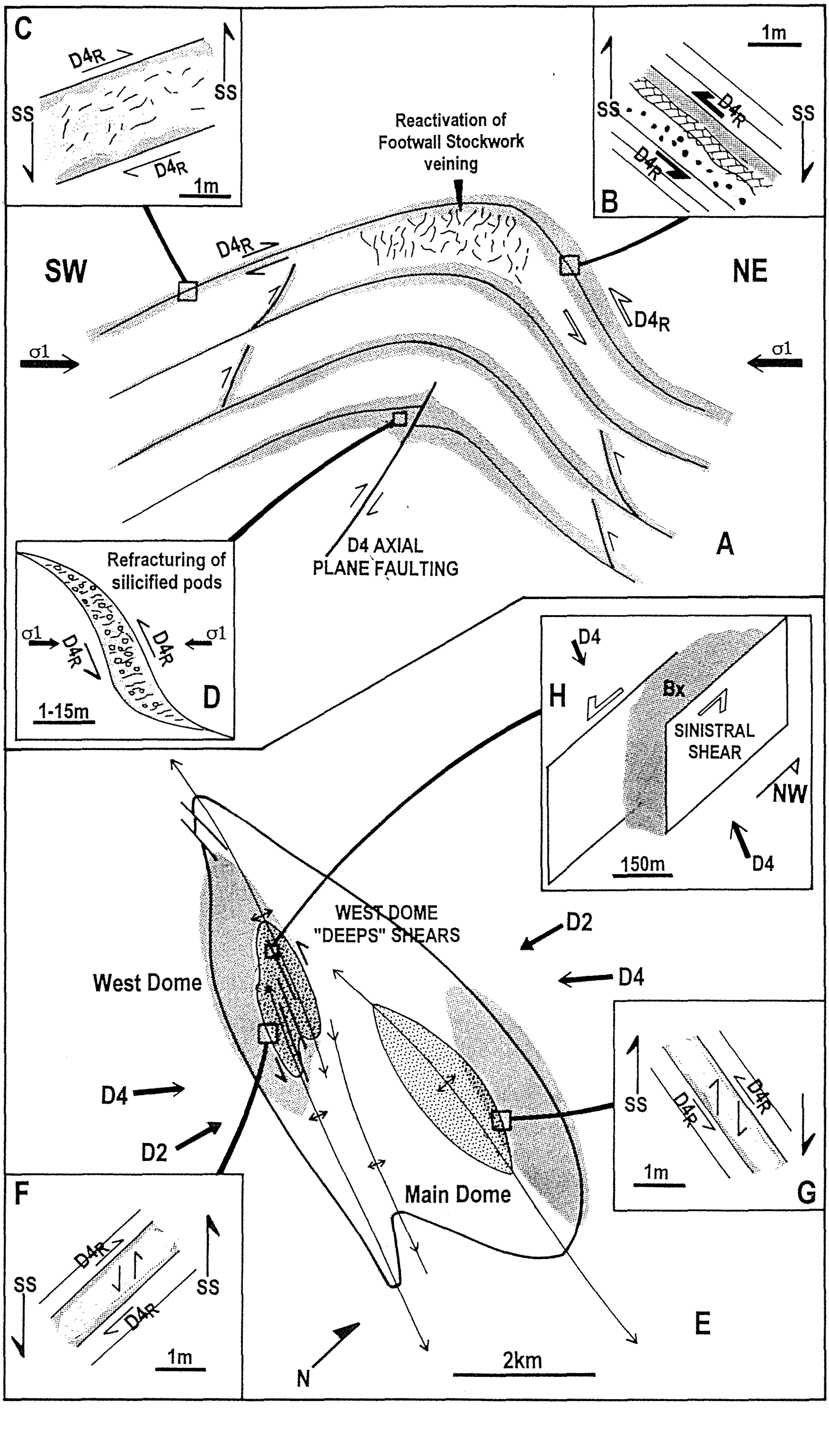

C
D4R
SS
SS
D4R
1m
1m
SS
D4R
D4R
SS
B
Reactivation of
Footwall Stockwork
veining
SW
NE
D4R
D4R
σ1
σ1
D4 AXIAL
PLANE FAULTING
A
Refracturing of
silicified pods
σ1
D4R
D4R
σ1
1-15m
D
D4
H
Bx
SINISTRAL
SHEAR
NW
150m
D4
WEST DOME
"DEEPS" SHEARS
D2
D4
West Dome
D4
D2
SS
D4R
D4R
SS
1m
G
Main Dome
F
D4R
SS
SS
D4R
1m
E
N
2km

Figure *37*: Tabular summary of the progressive development of the Telfer deposit during the various deformational events that were coeval with mineralisation (the two shaded were the major controlling events). Also illustrated are the likely effects of D_5 in producing further discrete bodies of mineralisation. Abbreviations **E** - extension; **WDD** - West Dome Deeps; **S** - shear.

Deformation	Effects	Schematic Relations
D_2	- forms the deposit host structure - silicification of mechanically favourable horizons during bedding/flexural slip. - these act as subsequent sites of nucleation for reef mineralisation - may unfold D_1 folds slightly causing "poddy" silicification	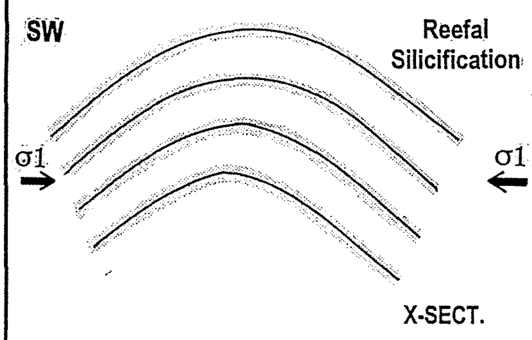
D_3	- gaping and implosive brecciation of steepened NE fold limbs and discrete pod development - potential back-limb replacement, and gaping of favourably oriented structures - opening of vertical veining arrays - marked development of mineralisation on relict D_1 fold short-limbs (NE side)	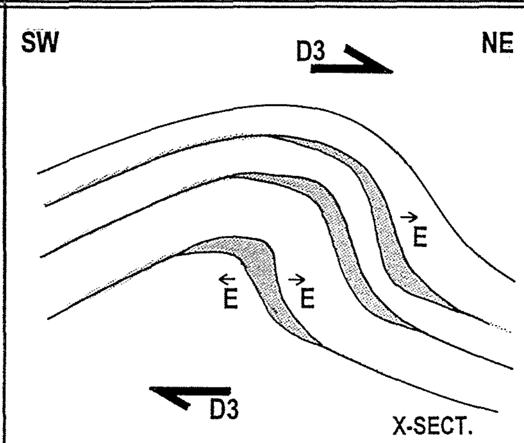
D_4	- tightening of the D_2-formed dome coupled with renewed flexural slip deformation along upper reef margins resulting in further mineral addition - asymmetric grade development across the dome as a result of oblique D_4 stress - mineralised shear/fault development/reactivation	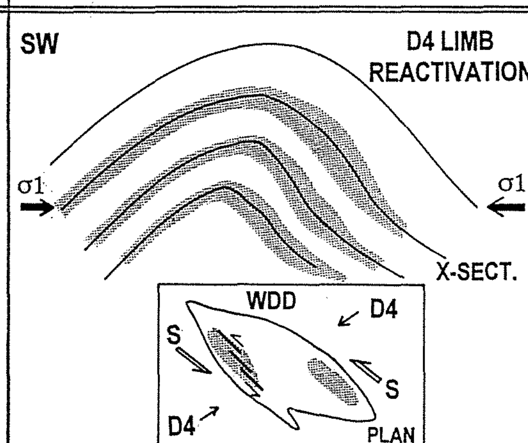
D_5 / D_{5b}	- sporadic mineralisation development associated with cross-cutting (high-angle) structures/trends - especially N-S trending features such as the Graben Fault - N-S trending extensional vein arrays - D_5 cross-folding may cause "poddy" reef grades and local mineralisation	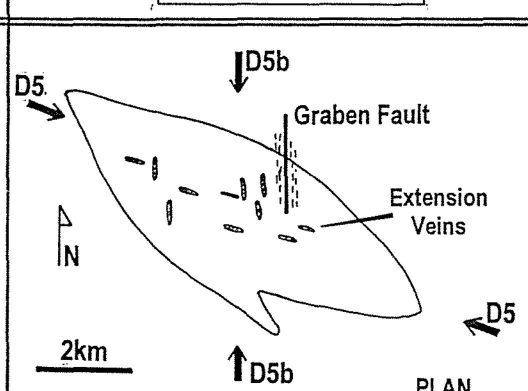

SECTION E

Exploration Models for Fold-hosted and Other Epigenetic Mineralisation Styles in the NE Paterson Province.

(FIGURES)

Figure 1: Interpretive solid geological map of the NE Paterson Province illustrating the prominent folding trends and dome/basin structure development. Larger anticlinoria and synclinoria are indicated by the laterally extensive fold axes, and within these smaller regional domal antiforms and synformal culminations developed. The positions of four seismic traverse lines (see text ; Fig. 2) are also shown, and the figure comprises data from Maps 2 & 2B. The overlay illustrates the locations of major mineralised occurrences and igneous intrusives in the district.

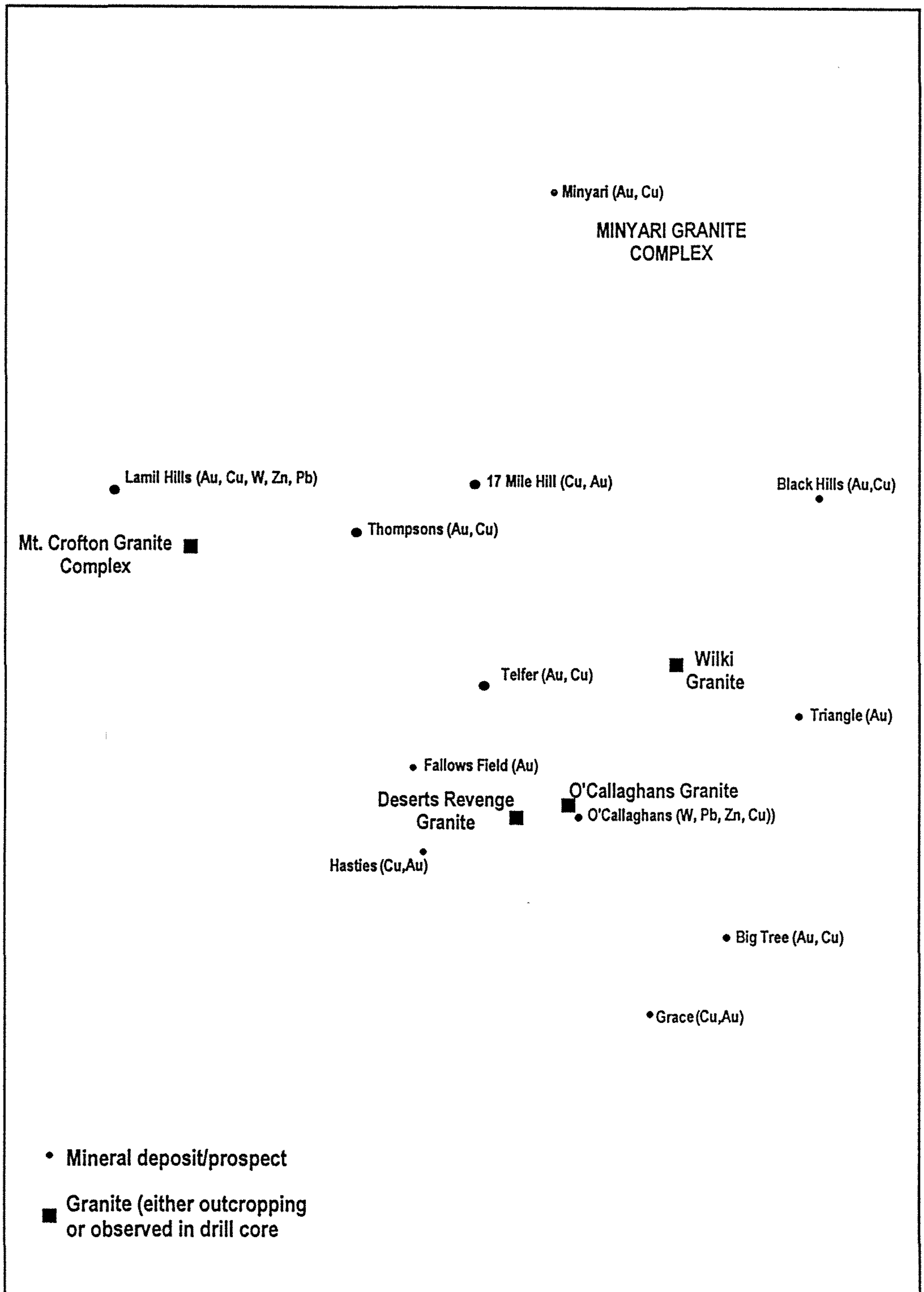

DISTRIBUTION OF MAJOR MINERALISED OCCURRENCES AND REGIONAL GRANITOIDS IN THE TELFER DISTRICT, W.A.

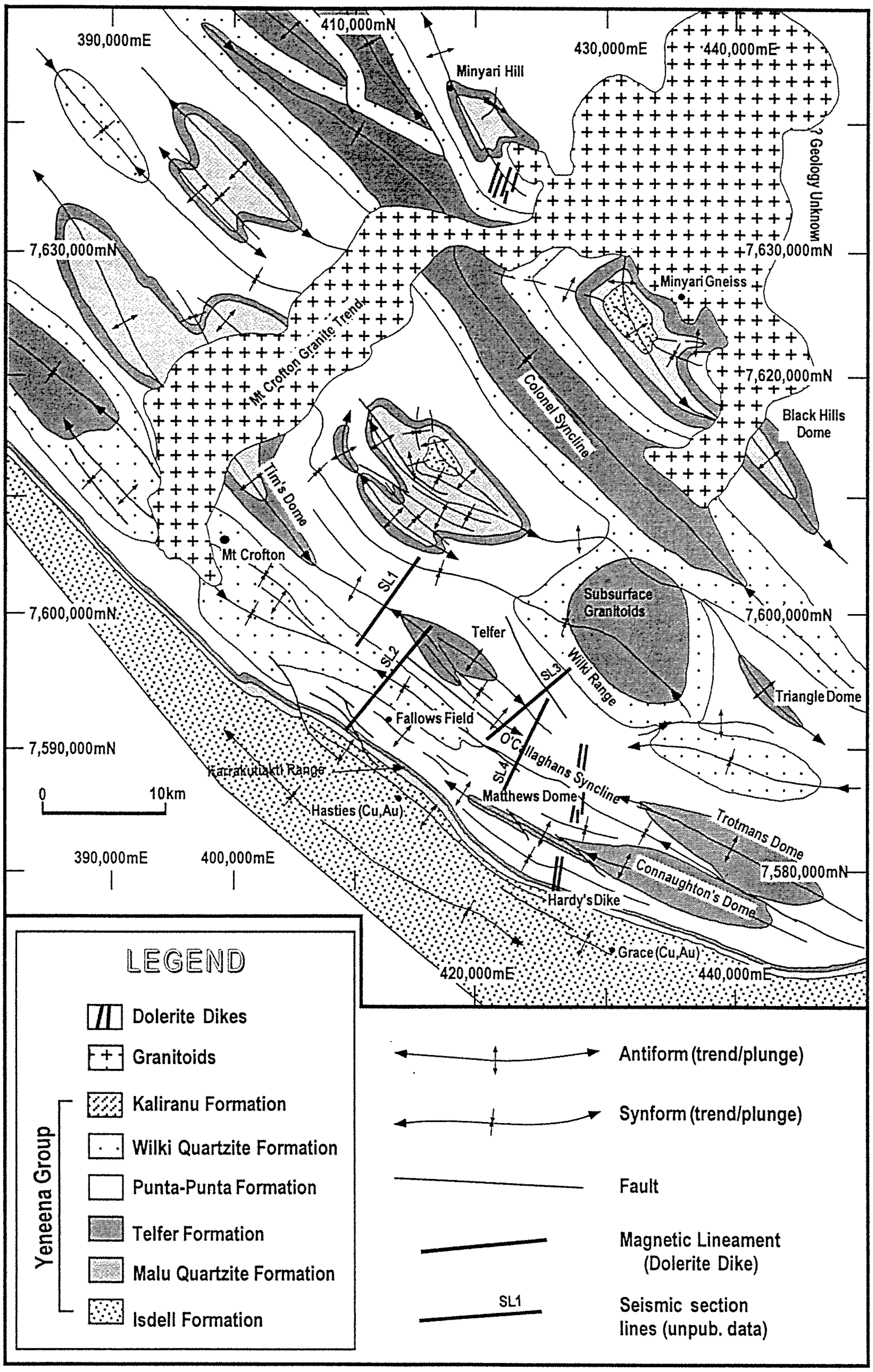

390,000mE
410,000mN
Minyari Hill
430,000mE
440,000mE
? Geology Unknown
7,630,000mN
Minyari Gneiss
Mt Crofton Granite Trend
7,620,000mN
Colonel Syncline
Black Hills Dome
Tim's Dome
Mt Crofton
SL1
Subsurface Granitoids
7,600,000mN
Telfer
SL2
SL3
Wilki Range
Triangle Dome
Fallows Field
7,590,000mN
O'Callaghans Syncline
SL4
Karrakutakti Range
Matthews Dome
0
10km
Hasties (Cu,Au)
Trotmans Dome
390,000mE
400,000mE
Connaughton's Dome
7,580,000mN
Hardy's Dike
Grace (Cu,Au)
420,000mE
440,000mE
LEGEND
Dolerite Dikes
Granitoids
Yeneena Group
Kaliranu Formation
Wilki Quartzite Formation
Punta-Punta Formation
Telfer Formation
Malu Quartzite Formation
Isdell Formation
Antiform (trend/plunge)
Synform (trend/plunge)
Fault
Magnetic Lineament (Dolerite Dike)
SL1
Seismic section lines (unpub. data)

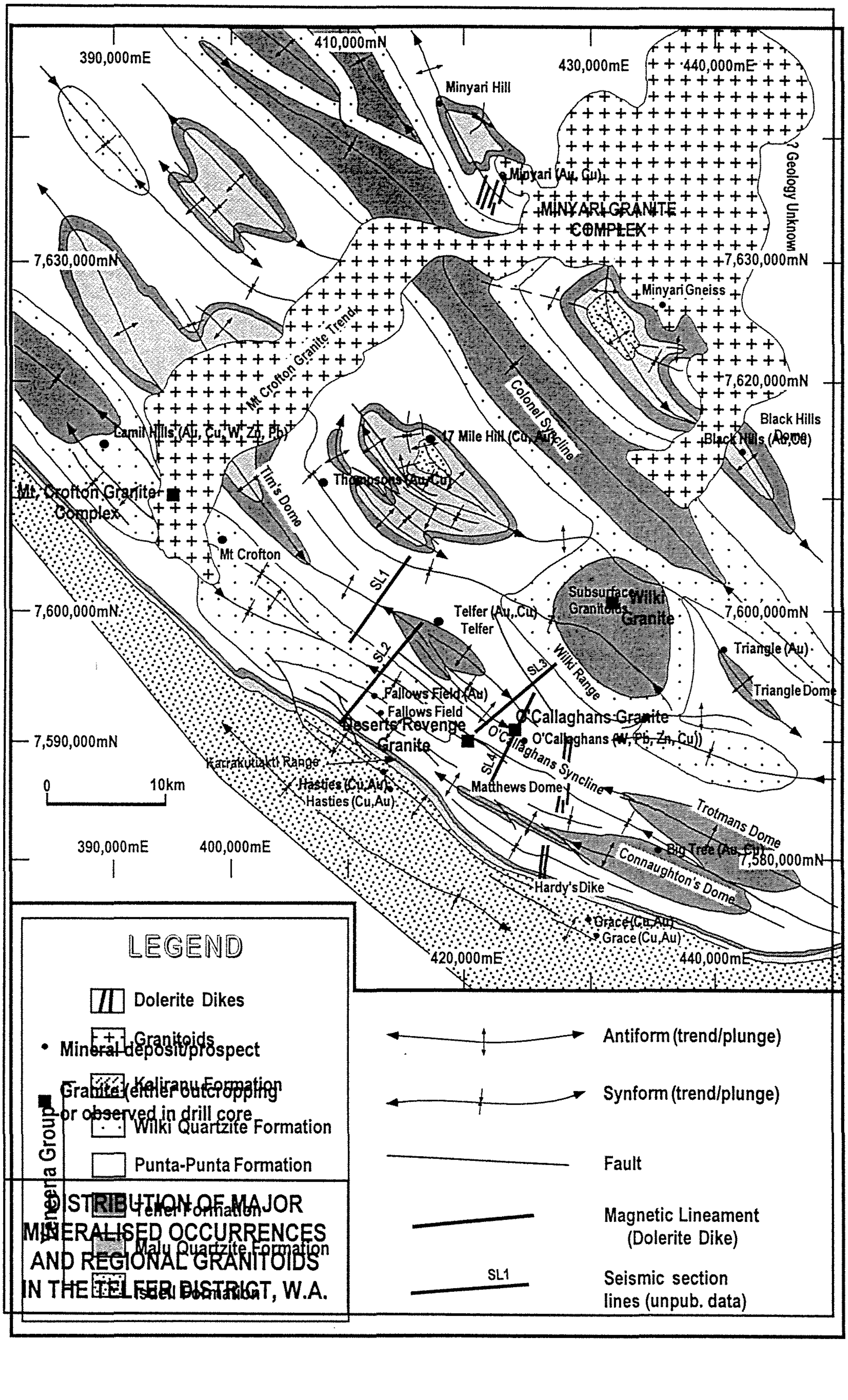

DISTRIBUTION OF MAJOR MINERALISED OCCURRENCES AND REGIONAL GRANITOIDS IN THE TELFER DISTRICT, W.A.

Figure 2: Interpretive cross sections illustrating regional fold styles, based on seismic surveys (data and sections - unpub. data, Newcrest Mining Pty Ltd) conducted along the four traverse lines illustrated in Fig. 1.

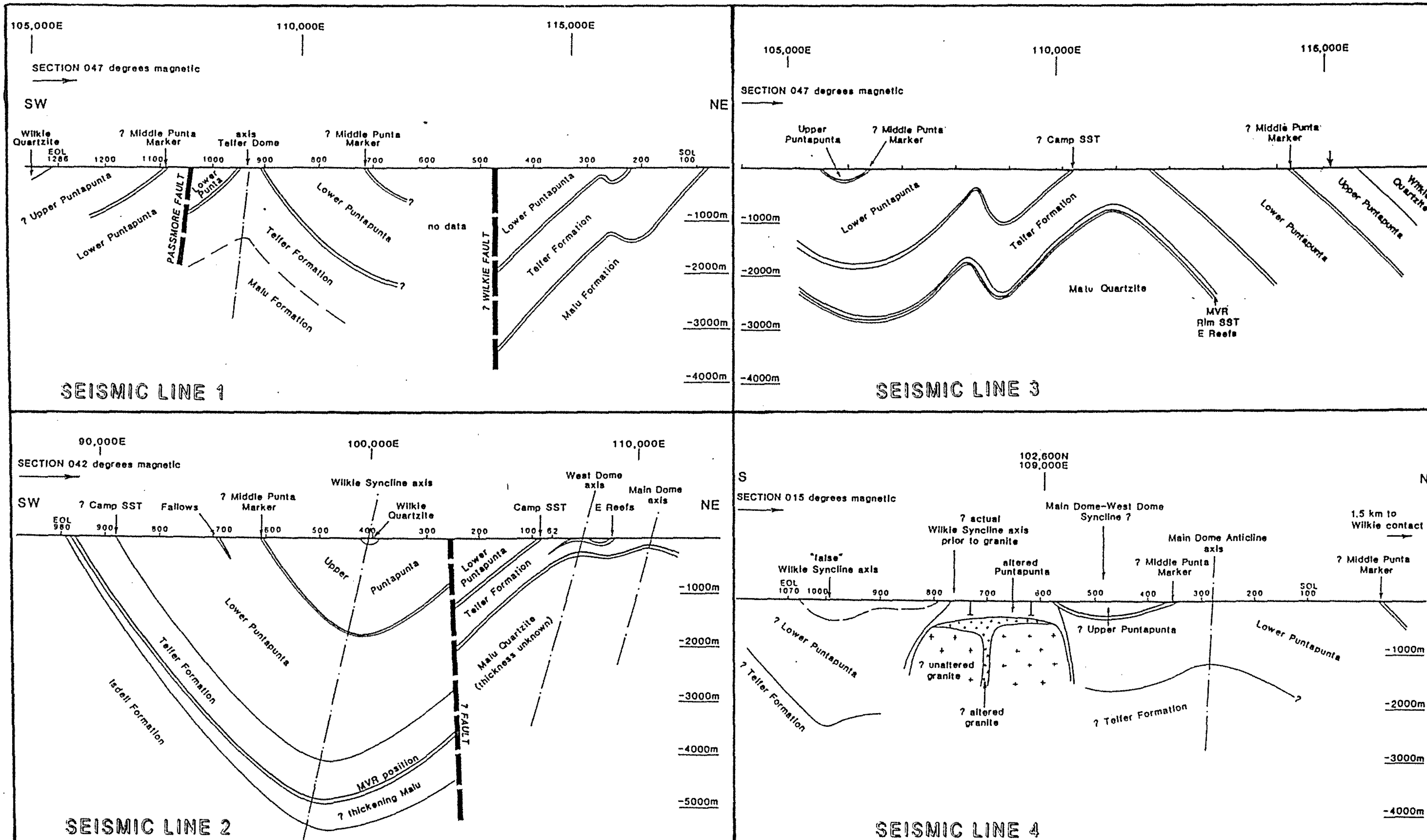

105,000E
110,000E
115,000E
SECTION 047 degrees magnetic
SW
NE
Wilkie Quartzite
EOL 1286
? Middle Punta Marker
axis Telfer Dome
? Middle Punta Marker
SOL 100
? Upper Puntapunta
Lower Puntapunta
PASSMORE FAULT
Lower Punta
Telfer Formation
Malu Formation
Lower Puntapunta
no data
? WILKIE FAULT
Lower Puntapunta
Telfer Formation
Malu Formation
-1000m
-2000m
-3000m
-4000m
SEISMIC LINE 1
105,000E
110,000E
115,000E
SECTION 047 degrees magnetic
Upper Puntapunta
? Middle Punta Marker
? Camp SST
? Middle Punta Marker
Lower Puntapunta
Telfer Formation
Malu Quartzite
MVR Rim SST E Reefs
Lower Puntapunta
Upper Puntapunta
Wilkie Quartzite
-1000m
-2000m
-3000m
-4000m
SEISMIC LINE 3
90,000E
100,000E
110,000E
SECTION 042 degrees magnetic
SW
NE
EOL 980
? Camp SST
Fallows
? Middle Punta Marker
Wilkie Syncline axis
Wilkie Quartzite
Camp SST
West Dome axis
E Reefs
Main Dome axis
Upper Puntapunta
Lower Puntapunta
Lower Puntapunta
Telfer Formation
Malu Quartzite (thickness unknown)
Telfer Formation
Isdell Formation
MVR position
? thickening Malu
? FAULT
-1000m
-2000m
-3000m
-4000m
-5000m
SEISMIC LINE 2
102,600N 109,000E
S
N
SECTION 015 degrees magnetic
? actual Wilkie Syncline axis prior to granite
Main Dome-West Dome Syncline ?
1.5 km to Wilkie contact
"false" Wilkie Syncline axis
altered Puntapunta
Main Dome Anticline axis
? Middle Punta Marker
? Middle Punta Marker
EOL 1070
SOL 100
? Lower Puntapunta
? Telfer Formation
? unaltered granite
? altered granite
? Upper Puntapunta
Lower Puntapunta
? Telfer Formation
-1000m
-2000m
-3000m
-4000m
SEISMIC LINE 4

Figure 3: Sketch map (taken from data presented in Map 2) of the large Wilki "ring" structure illustrating regional fold/cleavage and bedding trends. This structure comprises a circular shaped aggregate of outcrops of Wilki Quartzite Formation that dip steeply into the centre of the aggregates. Relict synformal and antiformal closures suggests that this structure initiated as a D_2 syncline. This is supported by regional (S_2) cleavage overprinting the central (NW & SE) limbs, which now lie almost perpendicular to the regional fold trend suggesting an early D_2 formation. D_2 fold axial traces anastomose around the structure suggesting that the syncline was subsequently disrupted through renewed shortening (either during D_2 or in D_4) around an internal rigid object. Very minor outcrops of coarse-grained monzogranite (Wilki Granite) and geophysical (magnetic) anomalies, coupled with garnetiferous schist that may constitute part of a contact aureole, suggest that one or more large igneous bodies (granitic) may lie in the centre.

Figure 4: Table summarising the various characteristics of regional granitoids in the NE Paterson Province (summarised from Goellnicht et al., 1991; Goellnicht, 1992). The locations of the granites are illustrated in Fig. 1. **NOTE:** * = SHRIMP dating conducted by D.Nelson, Geological Survey of Western Australia - I. Williams pers. comm.,1993; Hickman et al., 1994. # = μ - ^{238}U/^{204}**Pb** ratio

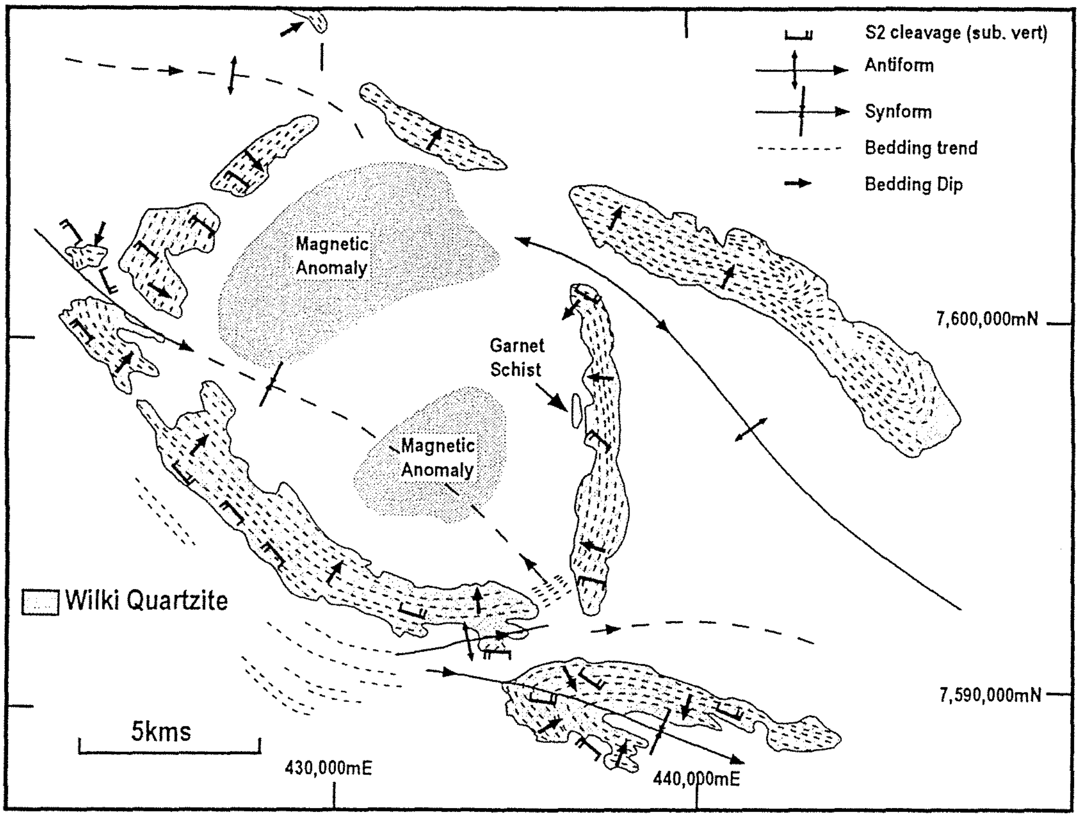

CHARACTERISTICS	MINYARI SUITE	O'CALLAGHANS	MT CROFTON
Localities	Minyari Granite complex (incl. Minyari Gneiss)	O' Callaghans Granite	Mt Crofton Granite, Deserts Revenge, Wilki Granite
Classification	Highly fractionated (≈71 wt% SiO_2) ilmenite bearing (reduced; crustal assimilations of carbon?) monzogranites, syenogranites,		Very highly fractionated (>74 wt% SiO_2) magnetite bearing (oxidised) monzogranites
Chemical Affinities	Metaluminous (Shand, 1943), calc-alkaline (Lameyre & Bowden, 1982), I type (Chappell & White (1974).		
Timing / Deformation	Early - Late tectonic: moderate tectonic (regional S2 parallel) foliation, weak solid-state deformation	Late-post tectonic : banding parallel to contact (flow-banding or tectonic?), weak solid state deformation	Late-post tectonic : weak undulose quartz extinction and solid-state deformation
Emplacement shape *(based on gravity interp.)*	**Large Plutons with deep root zones:** Minyari Granite Complex, O'Callaghans, Deserts Revenge. **Laccolithic bodies with narrow root zones:** Mt Crofton Granite complex, Wilki Granite		
Geochronolgy *(crystallisation age)*	642 ± 34 Ma - (Pb-Pb) 640 Ma - (U-Pb*)	617 ± 64 Ma - (Pb-Pb)	678 ± 36 Ma - (Pb-Pb) ≈ 619 Ma - (U-Pb*)
Source	Fractionated from partial melts of calc-alkaline I-Type lower crust, variably mixed with mantle derived partial melts. Lower crustal source may be heterogeneous comprising high $\mu^{\#}$ and low $\mu^{\#}$ rock types		
Tectonic setting/ discrimination	Calc-alkaline syn-post collisional granites (geochemistry - Pearce et al, 1984) suggest collision, possibly island arc; regional geology (as surmised by Goellnicht,1992) is suggestive of an intracratonic setting.		

Figure 5: Interpretive solid geology of the O'Callaghans Corridor. The corridor is marked by laterally continuous and elongate folds, including the O'Callaghans Syncline, a regional synclinorium. These folds contain domal culminations, including the large Trotmans-Connaughtons double-dome structure, which are commonly truncated by faulting parallel and sub-parallel to the regional trend. The regional trend is also markedly curvilinear, a feature interpreted to arise from shortening of the corridor around the large Wilki "ring" structure (see text~~, and above~~). The overlay illustrates the position of various geophysical anomalies across the corridor. Magnetic highs generally suggest a near-surface igneous body, possibly a stock or cupola, whilst the large gravity low is suggestive of a thicker and deeper lying granite.

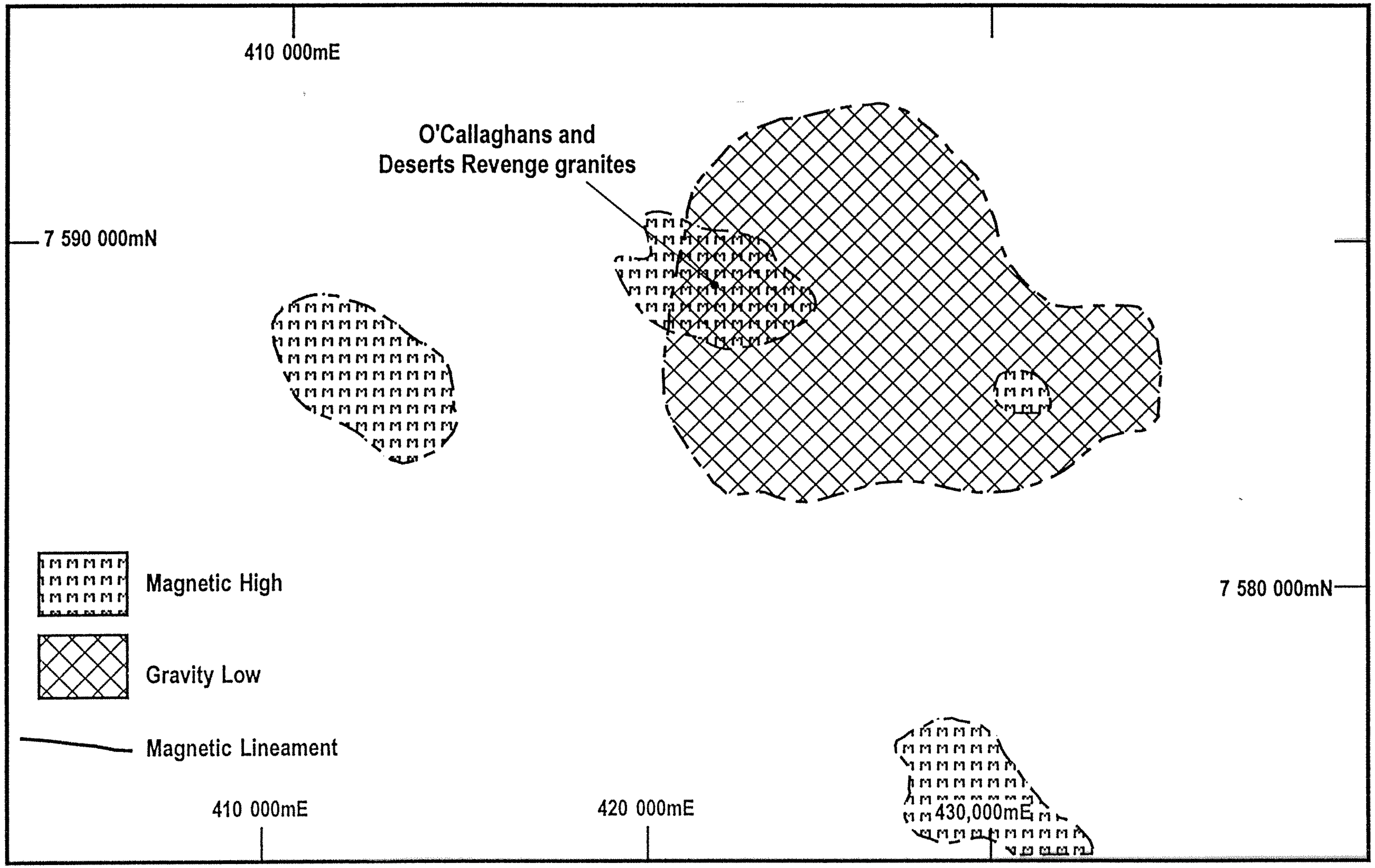

410 000mE
O'Callaghans and
Deserts Revenge granites
7 590 000mN
Magnetic High
Gravity Low
Magnetic Lineament
7 580 000mN
410 000mE
420 000mE
430,000mE

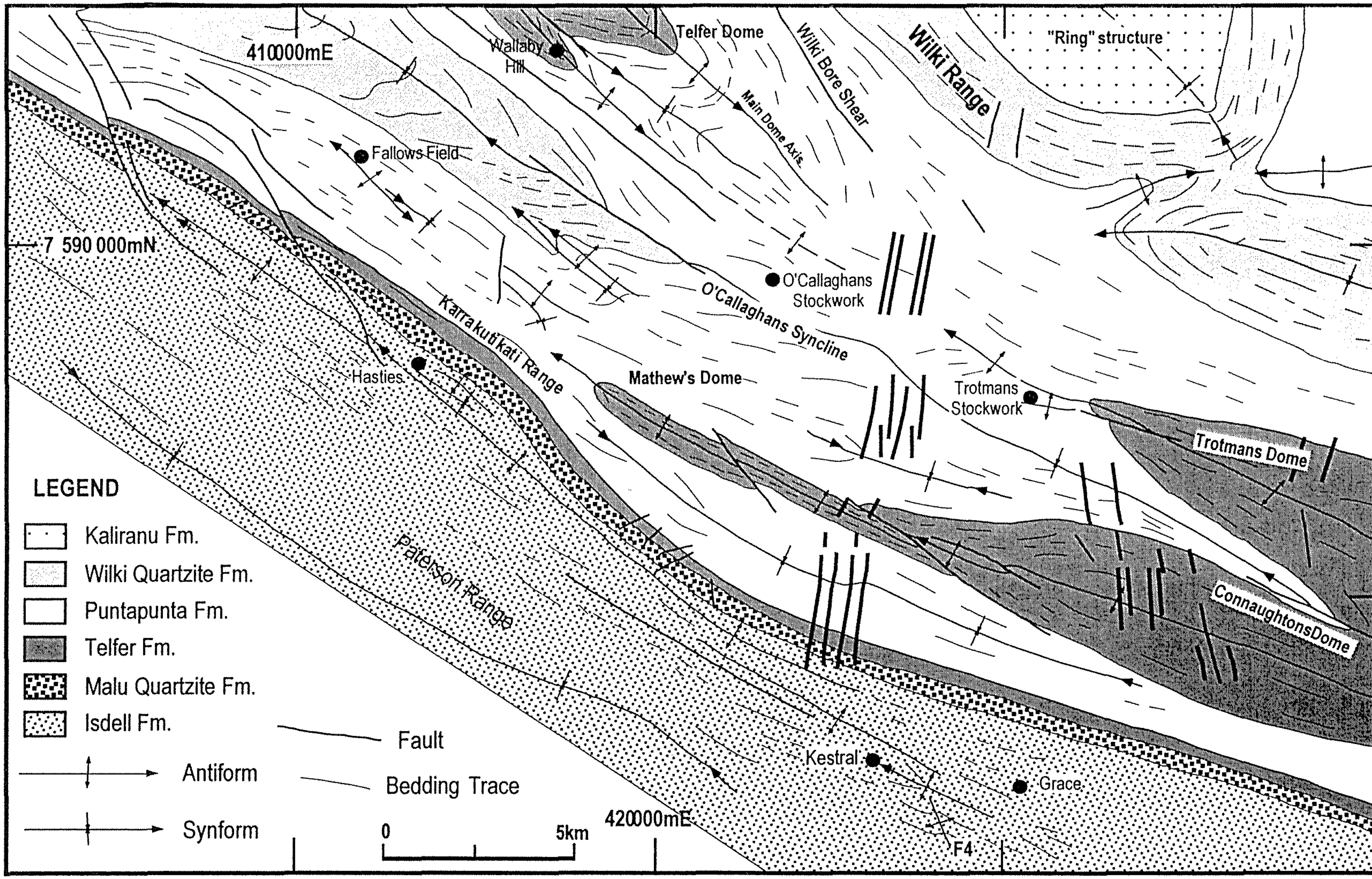

410000mE
Wallaby Hill
Telfer Dome
Wilki Bore Shear
Wilki Range
"Ring" structure
Main Dome Axis
Fallows Field
7 590 000mN
O'Callaghans Stockwork
O'Callaghans Syncline
Karrakutikati Range
Mathew's Dome
Hasties
Trotmans Stockwork
Trotmans Dome
Connaughtons Dome
Paterson Range
Kestral
Grace
F4
420000mE
LEGEND
Kaliranu Fm.
Wilki Quartzite Fm.
Puntapunta Fm.
Telfer Fm.
Malu Quartzite Fm.
Isdell Fm.
Fault
Bedding Trace
Antiform
Synform
0
5km

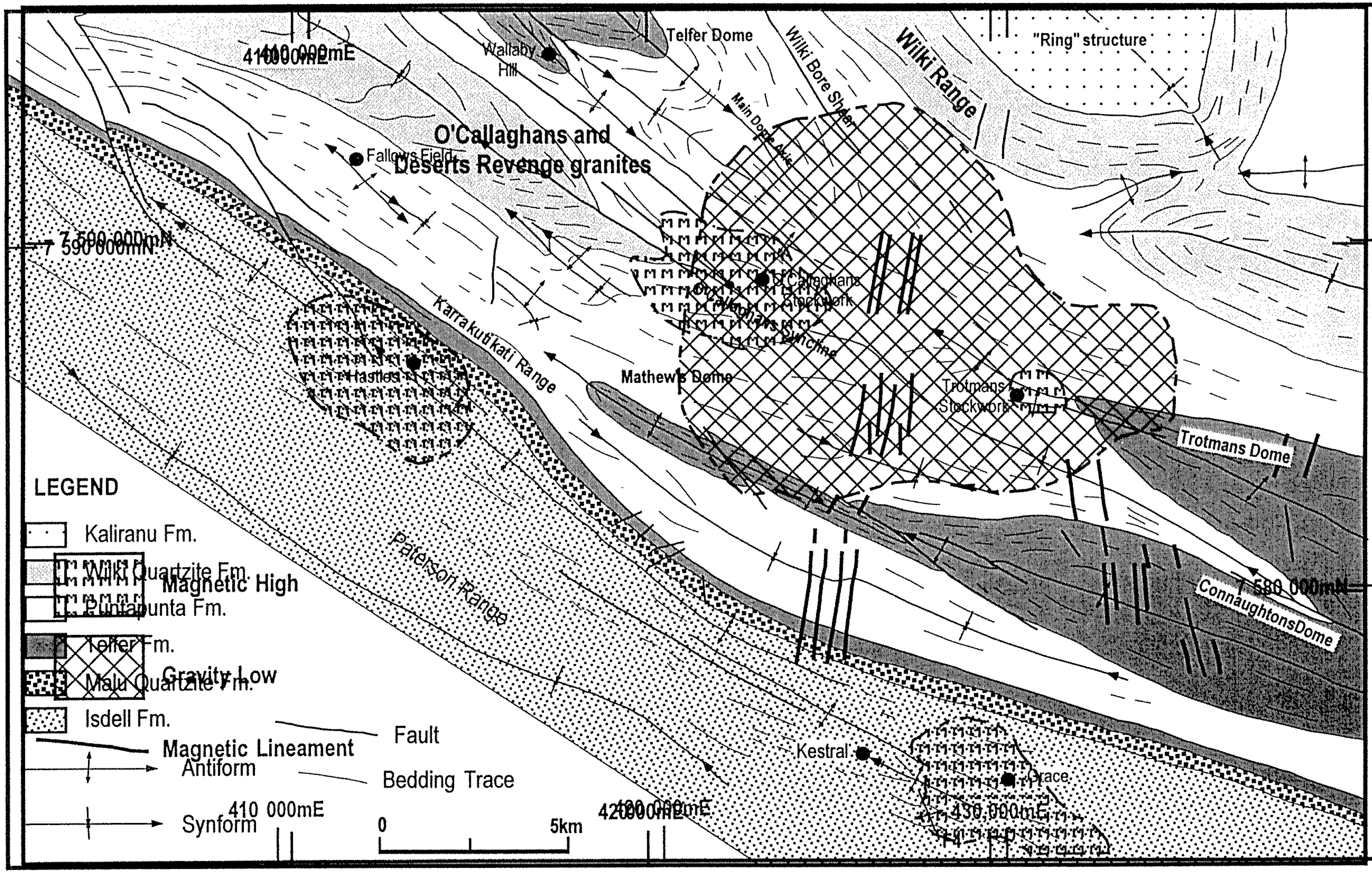

410 000mE
Telfer Dome
Wallaby Hill
Wilki Bore Shear
Wilki Range
"Ring" structure
Main Dome Axis
O'Callaghans and Deserts Revenge granites
Fallows Field
7 590 000mN
O'Callaghans Stockwork
Syncline
Karrakutikati Range
Hasties
Mathew's Dome
Trotmans Stockwork
Trotmans Dome
7 580 000mN
ConnaughtonsDome
Paterson Range
Kestral
Grace
430 000mE
420 000mE
LEGEND
Kaliranu Fm.
Wilki Quartzite Fm.
Magnetic High
Puntapunta Fm.
Telfer Fm.
Gravity Low
Malu Quartzite Fm.
Isdell Fm.
Fault
Magnetic Lineament
Antiform
Bedding Trace
Synform
0
5km

Figure 6: Sketch map of the Fallows Field area (main diagram, **A**), immediately NE of the Karakutikati Range (see Figs 1, 5 for location), illustrating the subtle bedding deflections, folding and faulting. These features are common throughout this area and are interpreted to represent late (D_4?) shuffling/faulting of the pre-folded and finely bedded sequence. (**B**) Schematic cross section of the asymmetric Fallows Field anticline, which formed as a parasitic fold on the SW limb of the O'Callaghans Syncline (Fig. 5; Map 2, 2B), illustrating the development of mineralisation (vein/breccia) within a competent carbonate unit in the core of the fold. (**C**) Plan view of the Fallows Field mine (Pit 13) along Section Line A - A` in (A), illustrating the oblique arrangement of stratabound pod mineralisation to the anticline hinge; two major pods, along with minor satellite bodies were developed.

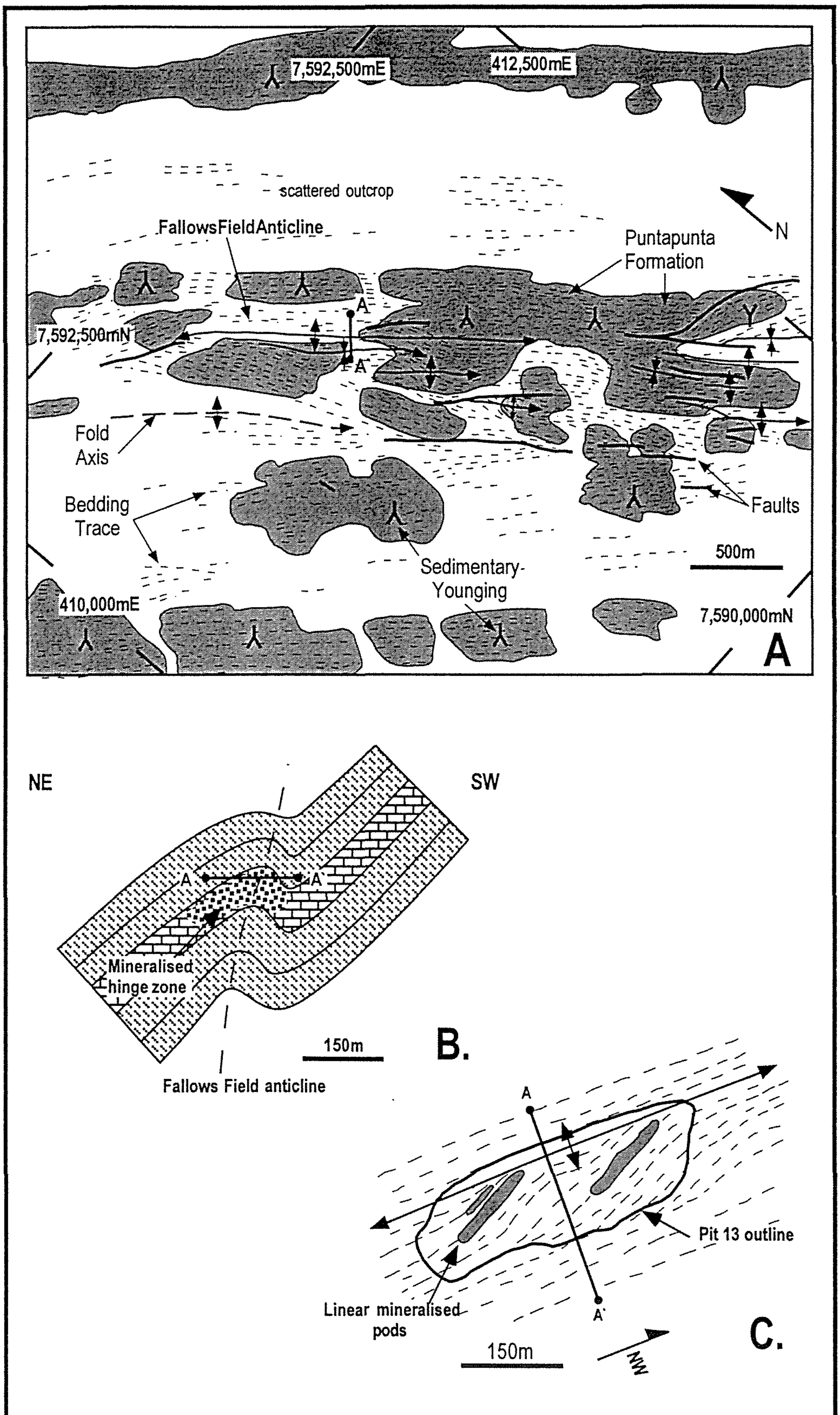
7,592,500mE
412,500mE
scattered outcrop
N
FallowsFieldAnticline
Puntapunta
Formation
A
A'
7,592,500mN
Fold
Axis
Bedding
Trace
Faults
500m
Sedimentary-
Younging
410,000mE
7,590,000mN
A
NE
SW
A
A'
Mineralised
hinge zone
150m
B.
Fallows Field anticline
A
Pit 13 outline
Linear mineralised
pods
A'
150m
NW
C.

Figure 7: Interpretative solid geology of the 17 Mile Hill Corridor. This area is dominated by the large Camp-Pajero-Thompsons East domal complex, which is sited on the NE of a major syncline that passes into the Wilki "ring" structure (see also above). In comparison with the O'Callaghans Corridor, this corridor is less elongate and truncated by regional faults. At the NW end of the corridor bedding and fold axes are sharply deflected against the Mt. Crofton Granite Trend. Similarly, in the SE regional fold axes wrap into the large Wilki "ring" structure.

Figure 8: Cleavage-bedding relationships observed in the D_2 Camp Dome that suggest potential refolding of a D_1 fold. (**A**) Cross section illustrating the cleavage-bedding geometries identified through drilling. Cleavage traces in core appear to fall into two groups; those low-angle to bedding (*e.g.* SW drill hole) and those at a high-angle (*e.g.* two central drill holes, upper levels), and on the NE limb cleavage is perpendicular to bedding and markedly discordant to the fold axial plane (**FAP**). The drill section line lies perpendicular to the Camp Dome axis (**B**) in the central regions of the dome. (**C**) Schematic diagram illustrating the control of an earlier fold phase on the geometry of the D_2 Camp Dome. A D_1 monoclinal fold (**i**), with shallow dipping axial plane cleavage (S_1), is refolded by D_2 (**ii**) producing an inclined axial plane, and two different cleavages that have variable angular relationships to bedding across the dome. Note the similarity between cleavage-bedding relationships in (i) on the short NE limb to those on the NE limb in (A). Note: some low-angle cleavage may be an artefact of fold-limb reactivation that rotated steeply-dipping cleavage (S_2) towards parallelism with bedding (small inset). On the SW limb both S_1 and S_2 have the same vergence with respect to bedding and therefore low-angle cleavage could either be S_1 or rotated S_2.

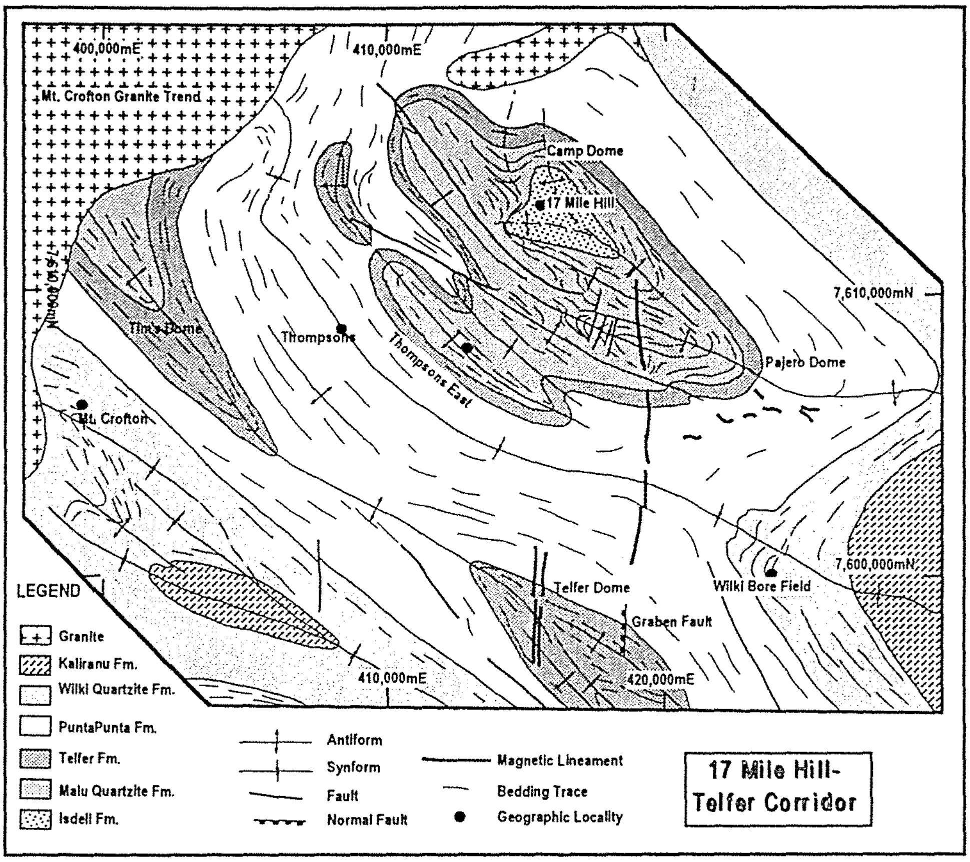

400,000mE
410,000mE
Mt. Crofton Granite Trend
Camp Dome
17 Mile Hill
7,610,000mN
Tim's Dome
Thompsons
Thompsons East
Pajero Dome
Mt. Crofton
7,600,000mN
Telfer Dome
Wilki Bore Field
Graben Fault
410,000mE
420,000mE
LEGEND
Granite
Kaliranu Fm.
Wilki Quartzite Fm.
PuntaPunta Fm.
Telfer Fm.
Malu Quartzite Fm.
Isdell Fm.
Antiform
Synform
Fault
Normal Fault
Magnetic Lineament
Bedding Trace
Geographic Locality
17 Mile Hill-
Telfer Corridor

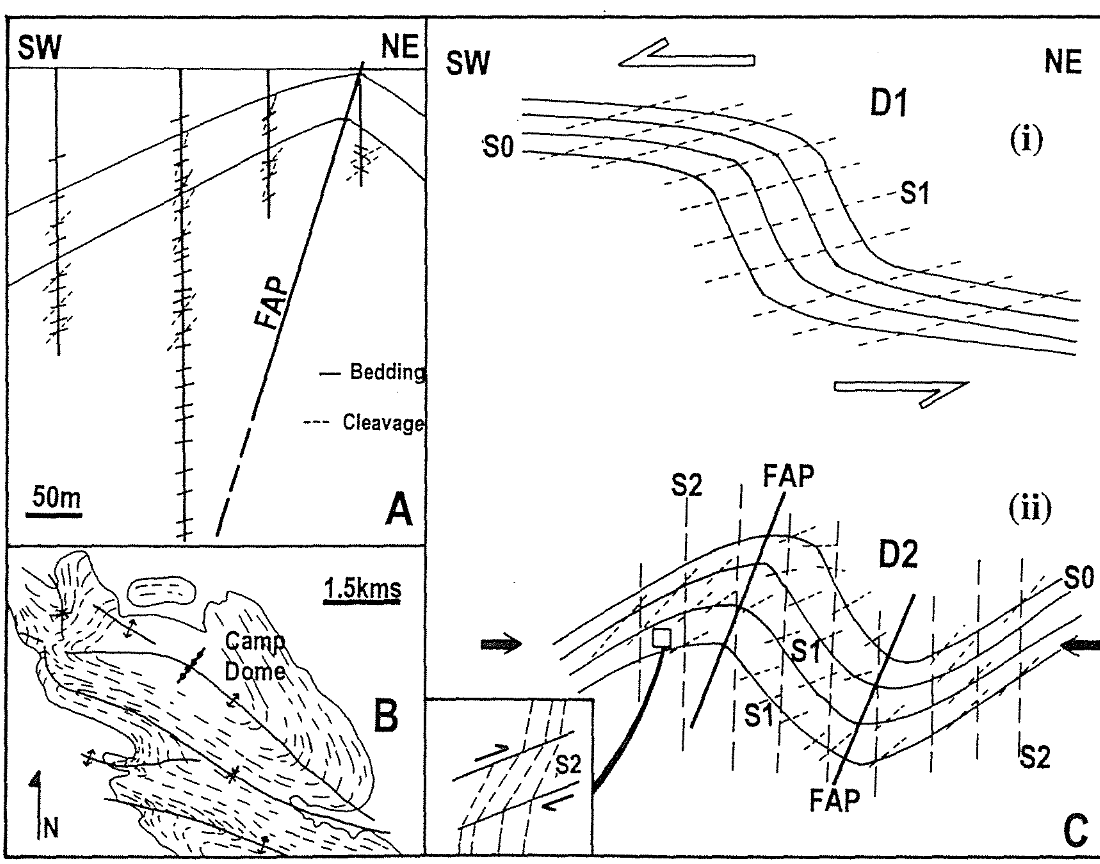

SW
NE
FAP
Bedding
Cleavage
50m
A
1.5kms
Camp
Dome
B
N
SW
NE
D1
(i)
S0
S1
S2
FAP
(ii)
D2
S0
S1
S1
S2
FAP
S2
C

Figure 9: Table summarising the various prospects and deposits identified in the NE Paterson Province (not including the Telfer deposit which is the subject of Sections C & D, and the Fallows Field deposit which is described in the text), the locations of which are given in Fig. 1. These represent the major identified mineral occurrences in which exploration activities have progressed beyond surficial geochemical/geological study. Numerous smaller prospects ("sniffs") also occur and these are commonly spatially associated with the major prospects.

Prospect	Type/Style	Metal Association	Alteration/Paragenesis
Big Tree	Stratabound quartz-vein hosted / Stockwork	**Au (±Cu,Bi)**	Quartz-chlorite-sericite-muscovite-carbonate (dolomite, ankerite, calcite) - pyrite - chalcopyrite
Black Hills	Skarn? / Qtz. vein hosted	**Au, Cu, As**	Quartz mosaic, muscovite & biotite metamorphic spotting; Dolerites (Plagioclase » K-feldspar; Pyroxene » chlorite, potassic alteration). Scapolite-quartz-sericite-pyrite (± tourmaline) alteration and veining.
Hasties	Breccia-quartz vein hosted/ Skarn?	**Cu (± Au)**	Quartz-dolomite-sulphides (pyrite, chalcopyrite)
Grace	Breccia-quartz vein hosted/ Skarn?	**Au (± As)**	Carbonate-albite-leucoxene-quartz-sulphide (pyrite)
Lamil Hills (Anomaly 1, 2,3)	Quartz vein hosted (An1) Skarn (An 2,3)	**Au (±Cu, Pb, Zn)** - Anomaly 1 **W, Zn, Pb, Cu, (± Mo, Sn)** - Anomaly 2,3	Lamil (An1) Silica-muscovite-tourmaline (rare)-rutile-minor silicified carbonate rhombs-pyrite. Lamil South (An.2,3)- contact metamorphic carbonate-diopside-scapolite-K-feldspar-albite-tremolite-sphene-phlogopite-talc-fluorite.
Minyari	Skarn/metasomatic replacement in fractures	**Au, Cu, As, Co (±Ni)**	Greisenisation (tourmaline, muscovite,biotite), retrogressed to chlorite-epidote-sericite, muscovite enrichment. Amphibole-albite-quartz-scapolite-biotite alteration/veining.
O'Callaghans	Skarn with associated stockworking	**W, Pb, Zn, Cu (± Mo, Sn)**	Pyroxene-amphibole-biotite-chlorite » quartz-carbonate-sulphide (± scheelite)
Thompsons	Stratabound quartz-vein hosted/ Stockwork	**Au, Cu (± Pb, Zn)**	Silica-sericite-carbonate (calcite and dolomite), minor tourmaline (locally intense) -rare biotite (alteration) » quartz-calcite-dolomite-sericite-pyrite veining.
Triangle	Qtz-vein hosted, stratabound?	**Au (±Cu)**	Pervasive sericite-silica (± pyrite) alteration haloes with quartz-tourmaline-sericite inclusions, around mineralised veins; quartz-tourmaline-sericite-carbonate-sulphide veining.
17 Mile Hill	Porphyry (replacement in fractures, quartz-vein hosted).	**Cu (±Au, Pb, Zn)**	Strong and zoned pervasive alteration. Upper zone; phyllic alteration (ser.-qtz-py) grades into potassic alteration (qtz-k felds-biotite-ser) that is strongest adjacent to veining. Chlorite-biotite-K-feldspar-pyrite-pyrrhotite-chalcopyrite alteration also associated. Discrete zones of intense silicification and limited greisenisation.

Figure 10: Schematic summary cross sections (looking NW) of the control that early folding phases (D_{EF}, D_1) may exert on D_2 fold and regional structural development. (**A**) Refolding of a low-angle D_1 thrust fault, or D_1 extensional fault (**B**), producing stratigraphic juxtaposition and subsequent thickening or thinning of individual formations. Two models that may explain the formation of the Karakutikati Range; a growth fault at a sub-basin boundary (**C**) or a SW verging ramp-flat or smooth trajectory thrust (**D**) refolded by D_2 and eroded to the present ground surface (**gs**); the position of the Karakutikati Range (**KR**) is stippled. An alternative model for formation of the Karrakutikati Range; (**E**) very early D_{EF} folding produces a broad antiformal warp across the Paterson Province, with the area studied lying on a NE dipping limb. (**F**) Inclined bedding on this NE limb is favourably oriented for monocline formation during D_1. (**G**) Refolding of a regional scale D_1 monocline during D_2 may have controlled the geometry and nucleation of D_2 folds, producing the Karakutikati Range as a relict short limb from a D_1 fold (stippled), and caused the adjacent syncline (O' Callaghans Syncline) and other D_2 folds to have SW inclined geometric axial planes. The initial inclination of strata by D_{EF} can also explain the constant angular relationship between S_1 and bedding (*e.g.* Section A), and implies that the Karakutikati Range units may have lain at higher crustal levels further SW, which have since been removed through erosion.

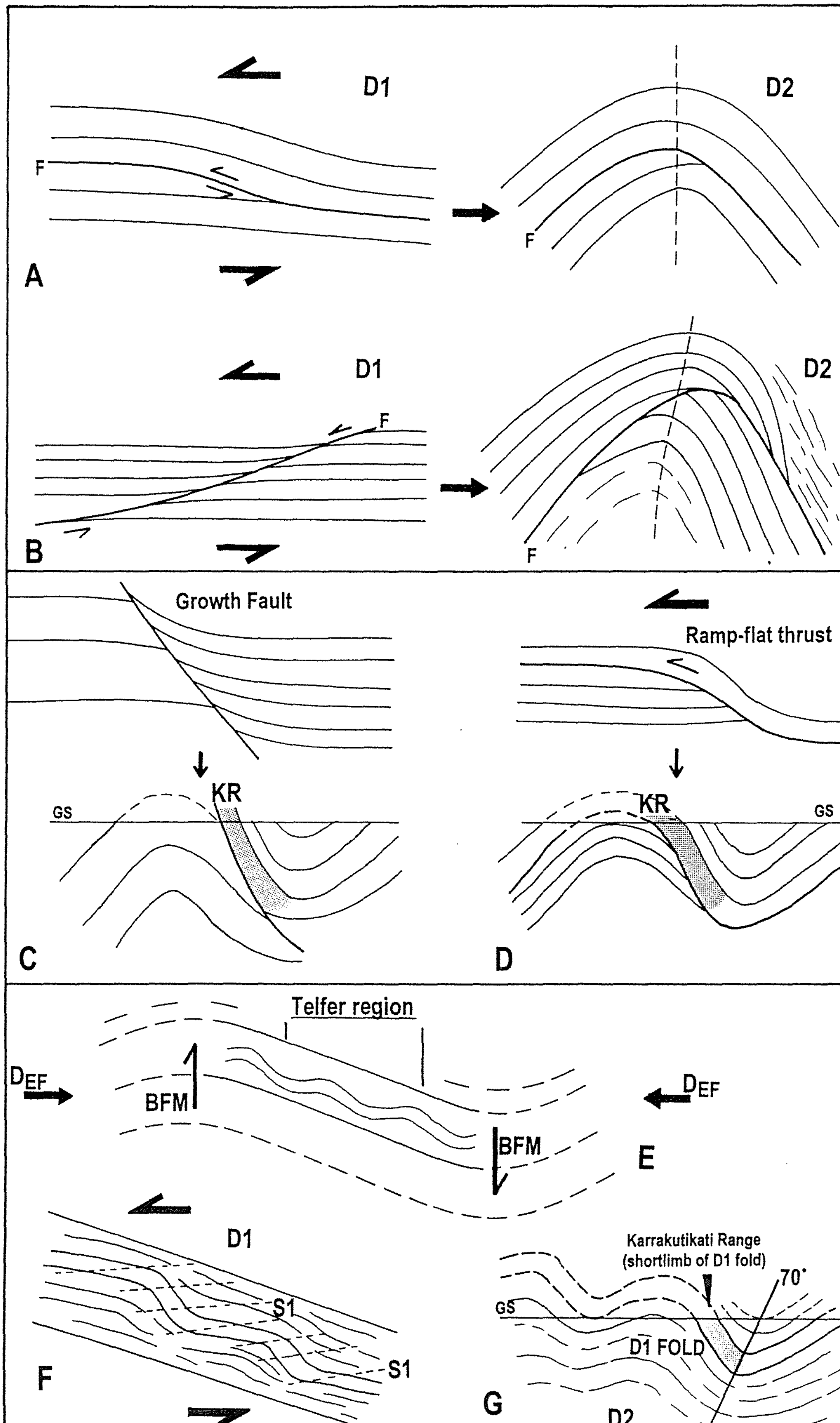
D1
D2
F
F
A
D1
D2
F
F
B
Growth Fault
KR
GS
C
Ramp-flat thrust
KR
GS
D
Telfer region
DEF
BFM
BFM
DEF
E
D1
S1
S1
F
Karrakutikati Range
(shortlimb of D1 fold)
70°
GS
D1 FOLD
G
D2

Figure 11: Schematic diagram illustrating new and re-initiated strike parallel faulting during subsequent oblique deformation in the NE Paterson Province. (**A**) Major folding (D_2) produced a dome & basin setting with some faulting, particularly intrabedding faults on fold limbs (inset) that exhibit mainly dip-slip movement. (**B**) Further shortening during D_4, oblique to the earlier-formed regional trend, produced a shortening (**Short.**) and a weak shearing (**Shear**) component. This weakly transpressive deformation developed bedding-strike parallel faulting that truncated the regional folds. These faults exhibit a combination of dip-slip and sinistral strike-slip (inset) movement. New faults would have partitioned in and around domal folds as these would have acted as "rigid" structural anisotropies.

Figure 12: Igneous architecture in the Telfer district and potential models for emplacement. Main diagram (**A**) illustrates the major igneous components, including the large Mt. Crofton Granite Trend, and elongate zones of low-density (defined by regional gravity data) that are interpreted to be root zones for some of the plutons. The long axes (**LA**) of these zones lie parallel to the prominent structural/bedding trend (fine dashed lines). The compressional directions for D_2 and D_5 are also illustrated. Two emplacement models/styles that may apply to the Mt. Crofton Granite Trend include; (**B**) brittle Andersonian-style crustal tensional opening (**E**) during orthogonal (D_2, D_4) deformation ***or*** (**C**) emplacement into a zone of shortening during D_5. (**D**) Structural trends in the NW end of the Camp Dome (location in A; also Figs 1 & 7) showing the high-angle D_5 cross-folding of D_2 folds adjacent to the Mt. Crofton Trend, which is suggestive of a local ductility increase during D_5 that may have been associated with a renewed phase of granite emplacement.

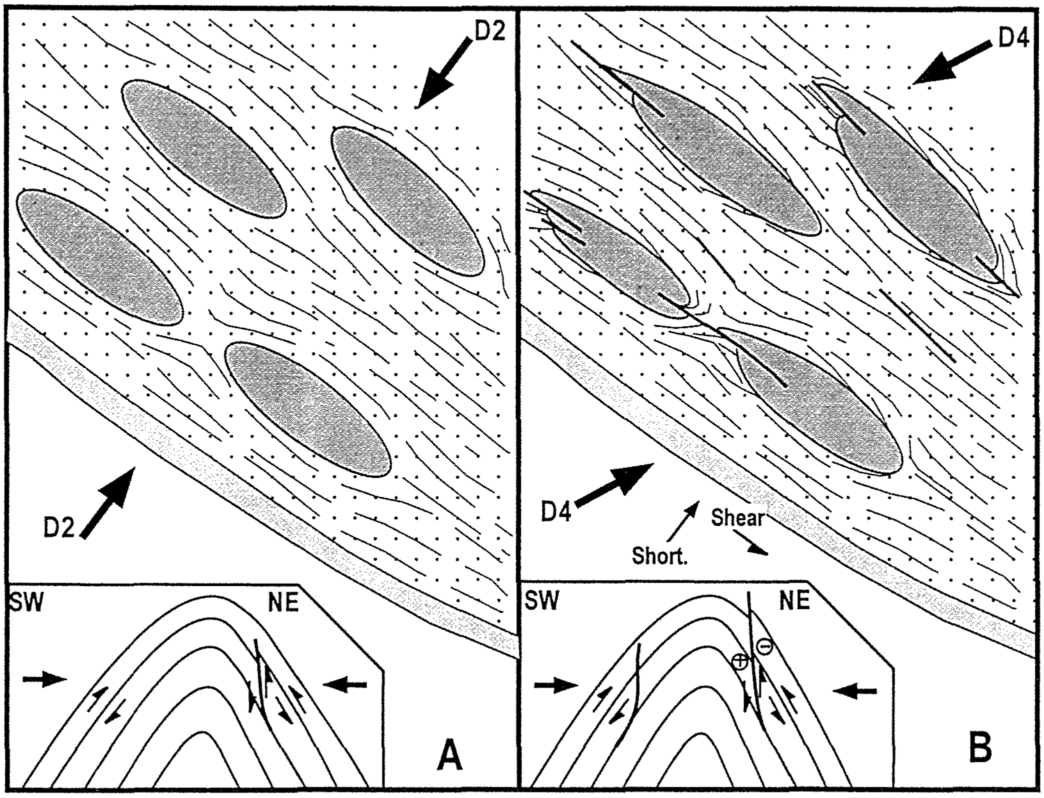
D2
D2
SW
NE
A
D4
D4
Short.
Shear
SW
NE
B

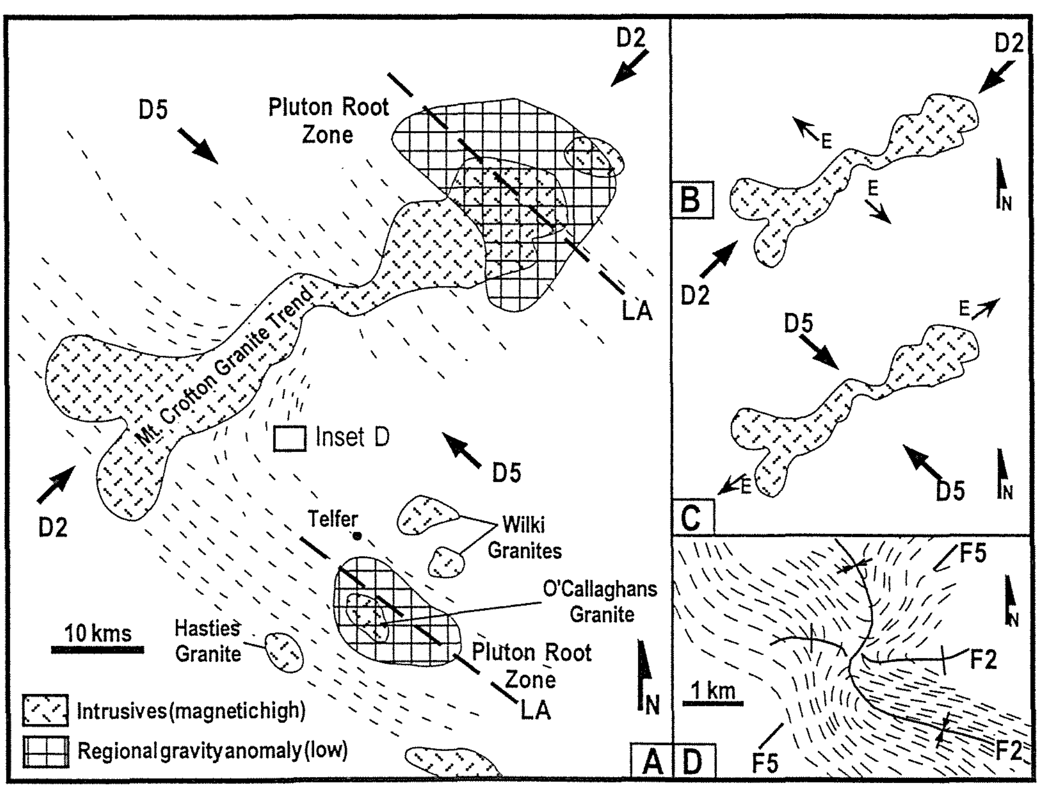
D2
D5
Pluton Root Zone
LA
Mt. Crofton Granite Trend
Inset D
D5
D2
Telfer
Wilki Granites
O'Callaghans Granite
10 kms
Hasties Granite
Pluton Root Zone
LA
N
Intrusives (magnetic high)
Regional gravity anomaly (low)
A
D2
E
E
B
D2
N
D5
E
C
E
D5
N
F5
N
F2
1 km
F5
F2
D

Figure 13: Summary of structural parameters for fold-hosted mineralisation in the NE Paterson Province. The effects of D_3 include; (**A**) preferential gaping of the NE limb and hinge regions resulting in concordant and hinge-hosted pods. (**B**) The inferred effects of coaxial D_3 deformation resulting in only limited gaping of both limbs, particularly those which are sub-vertical, and near-hinge regions. Deformation coaxiality is produced by local vergence reversals, opposite that of the overall deformation. (**C**) Gaping during D_3 may also be enhanced in domes that contain refolded D_1 folds as these produce a steeply dipping NE limb. Cleavage relationships (S_0-S_1) may assist the identification of this; these include cleavage at high-angle to bedding (**1**), or cleavage rotated towards parallelism with bedding (**2**) by D_2/D_4 strain. In both cases S_1 can be distinguished from S_2 in this limb position on the basis of vergence (*ie.* NE). (**D**) D_4 shortening (oblique) of a domal structure with preferential reactivation of high-strain zones (stippled, **HS**) on both the NW and SE corners (insets) and subsequent mineralised reef enhancement. (**E**) Veining styles that may develop through reactivation and renewed flexural slip include: (**i**) echelon and shear-extensional veining, (**ii**) hinge dilation (**iii**) re-fracturing of D_2/D_3 silicified hinge zones (**iv**) renewed reef development along fold limbs. (**F**) Oblique (to anticline axis) mineralised pod (dark stipple) geometry in the Fallows Field deposit resulting from sinistral transpressive D_4 strain (**T_P**) that developed within a competent carbonate unit (v. light stipple) in the anticline core. (**G**) Instantaneous strain ellipse for D_4 illustrating the veining geometries possible within the compressional (**-E**) field; these include tensional veins (**TVn**) and shear-extensional veins (**SEVn**). Note, bedding reactivation (**B_R**) occurs within the extensional field (**+E**) as predicted by Aerden (1993) for reactivation of foliations. The trace marked in the diagram corresponds to the bedding strike on the NW and SE corners of regional domes (ie. that which lies either side of the avergae fold trend - **AFT**). In this position, bedding lies within the extensional field.

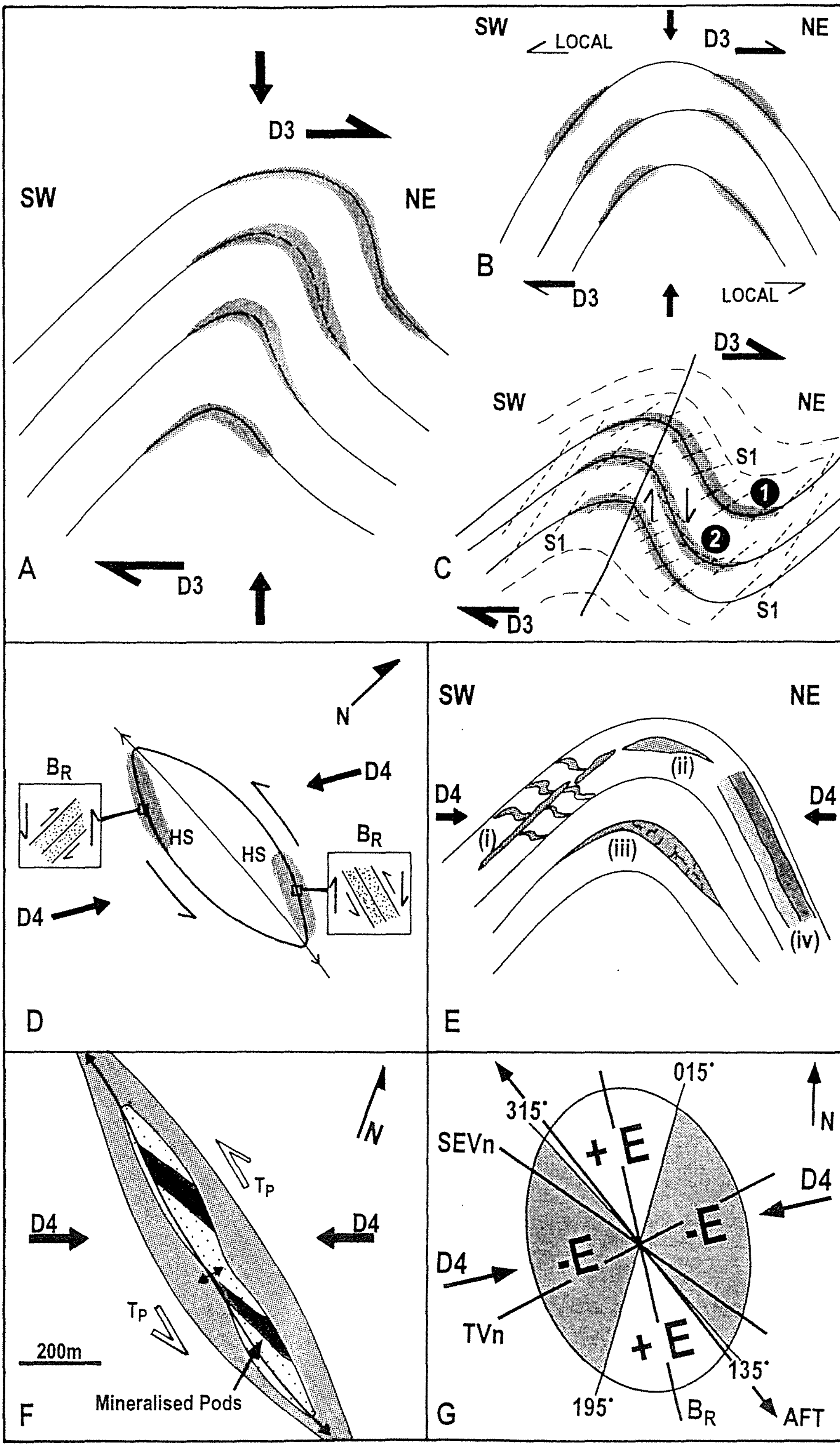

A
SW
NE
D3
B
LOCAL
D3
C
S1
1
2
D
N
D4
B_R
HS
E
(i)
(ii)
(iii)
(iv)
F
T_P
200m
Mineralised Pods
G
015°
315°
SEVn
+E
-E
TVn
135°
195°
AFT

Figure 14: Summary of the various shear- and fault-zone hosted deposit geometries possible in the NE Paterson Province during transpressive D_4 deformation (for shears/faults that lie parallel/sub-parallel to the regional trend). (**A**) Internal shear-zone vein geometries, including disseminated/cataclasite hosted (**1** - inset), en-echelon veins (**2**), which may exhibit a number of cross-cutting phases, and foliation-parallel shear lenses (**3**). (**B**) Dilational styles at left-stepping discontinuities on D_4 shear/fault systems; (**1**) tensional lenses/veins, (**2**) dilational jogs (+ implosive breccias); and (**3**) dilational (releasing) bends. (**C**) Tensional bridge development (after Gamond, 1987) in an overall sinistral movement zone, involving the initial formation of synthetic **R** reidal shears that are subsequently truncated by synthetic **P** shears producing tensional/dilational openings (stippled). (**D**) Tensional lense geometry in a D_4-formed or reactivated shear zone will depend on the dominant movement component; in D_4 this could be oblique, producing inclined openings (**1**), or horizontal producing vertical lenses (**2**).

Figure 15: Potential gaping geometries associated with proximal-granite mineralisation. (**A**) Synformal truncation against granite illustrating the potential for opposing shear couples between synthetic shear (**SS**) in granite and antithetic shear (**AS**) in reactivated layers with resultant gaping/dilation (stippled) at the contact, as well as along bedding. Also illustrated is D_3 gaping and extensional opening (**e**) of NE inclined strata. (**B**) As for (A) but for an antiformal fold, where opposing shear couples gape the contacts between granite and bedded rocks creating an ore-fluid trap for mineralisation (stippled). Mineralisation may also develop in stratabound positions through shearing (reactivation) of the beds. (**C**) Mineralisation styles produced by D_4 transpression (**D_{4TP}**) around a rigid granite body; these include shears/faults with dilational jogs (**1**) and lenses (**2**), as well as disseminated mineralisation and fluid focussing into pressure shadows. (**D**) Auriferous shear-structure development associated with dolerite dikes (**dl**) that were suitably oriented with respect to regional mineralising deformations; forms include internal fracturing/en-echelon veining (**1**) and auriferous shear-zones along dike margins (**2**).

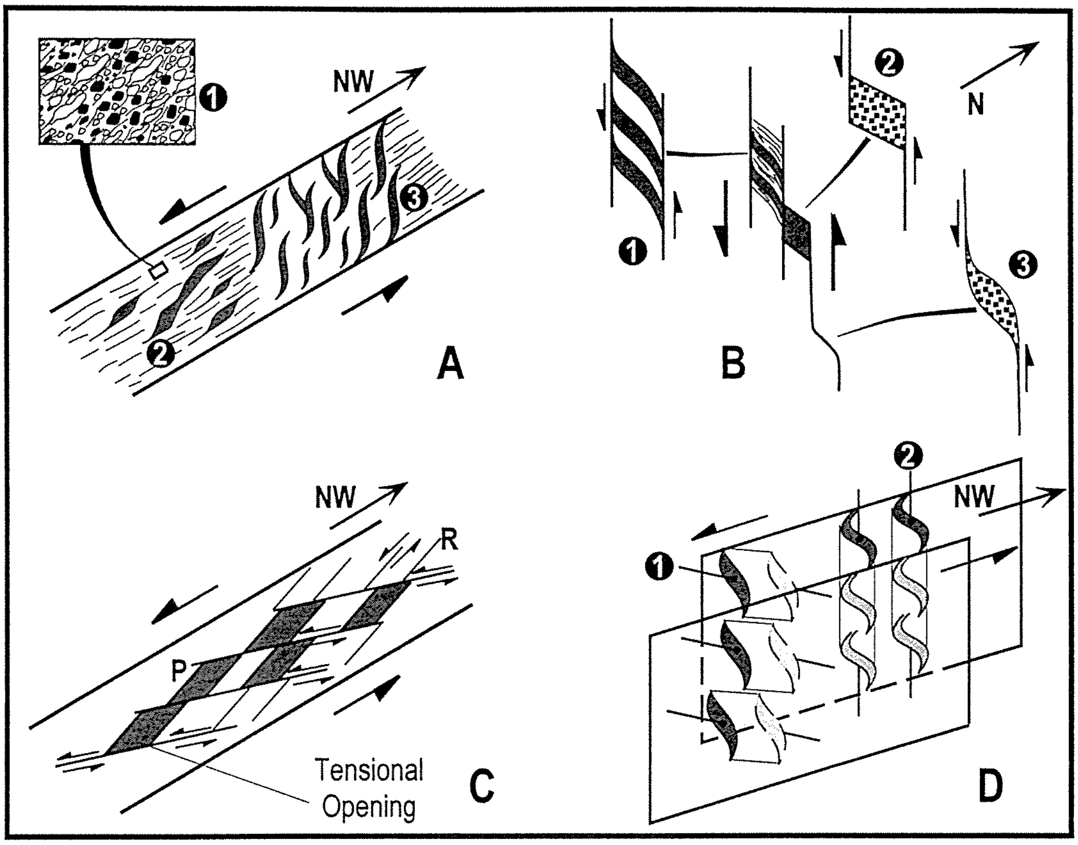
NW
A
B
N
NW
R
P
Tensional
Opening
C
D

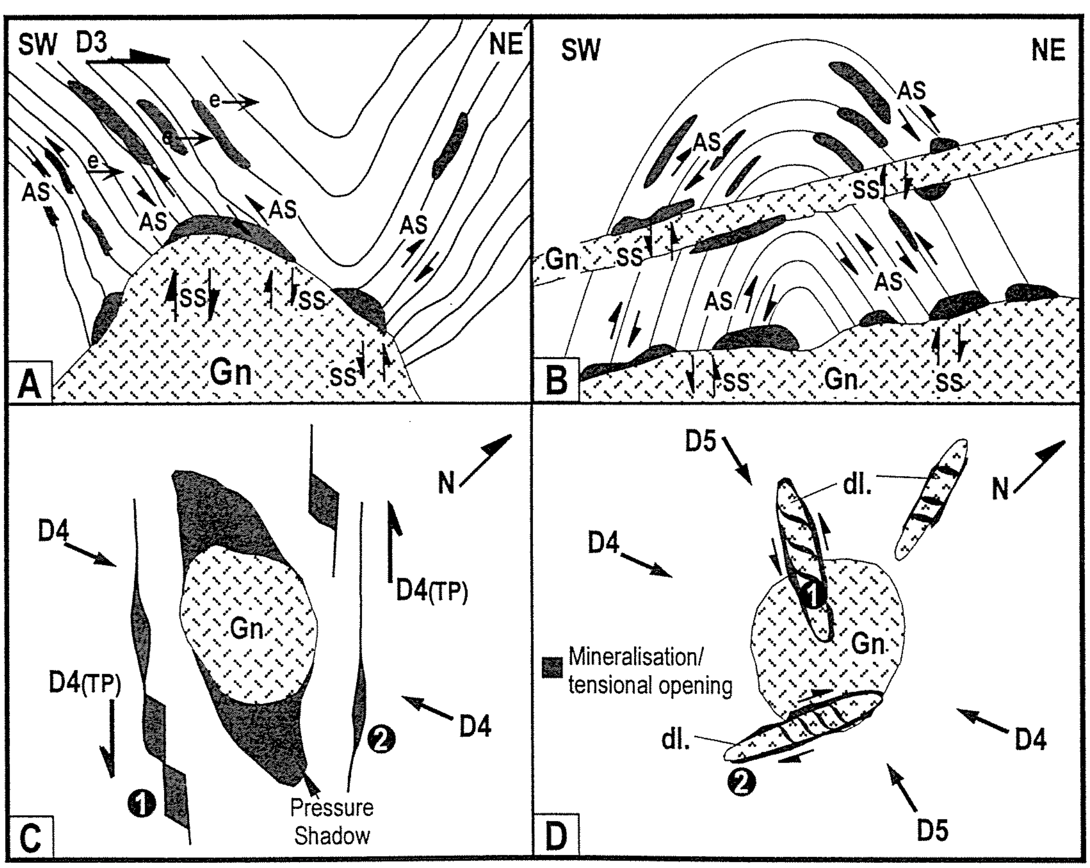
SW
D3
NE
e
AS
SS
Gn
A
B
N
D4
D4(TP)
Pressure
Shadow
C
D5
dl.
Mineralisation/
tensional opening
D

Figure 16: Flow-chart presenting the successive steps in an exploration strategy that utilises the conceptual structural models discussed in the text for targeting mineralisation occurrences within the NE Paterson Province. Shaded boxes represent structural geological parameters that need to be identified during the exploration process. The models cover both distal and proximal (to actively cooling granites) mineralisation, and summarise the effects of both D_3 and D_4.

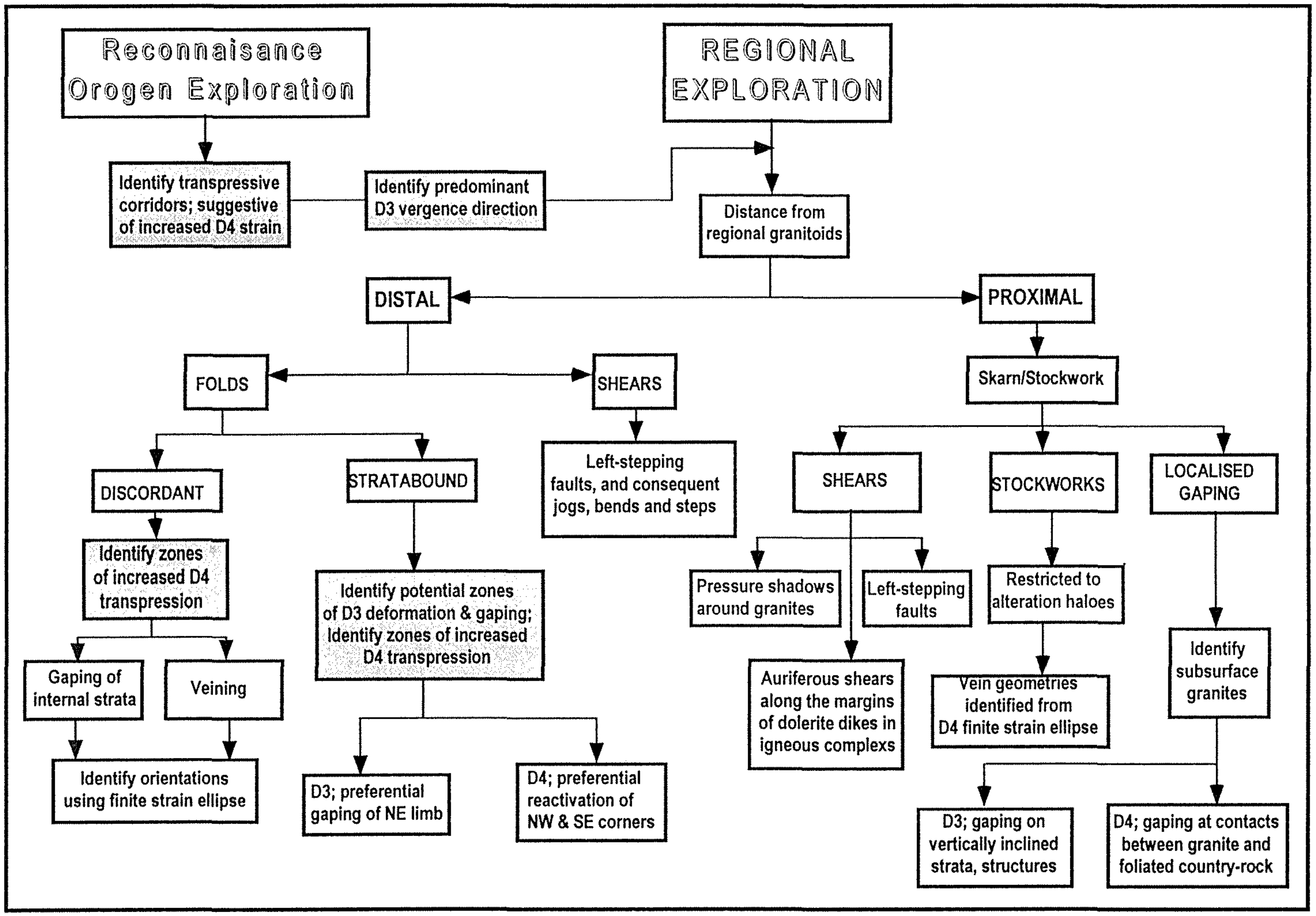
Reconnaisance
Orogen Exploration
REGIONAL
EXPLORATION
Identify transpressive corridors; suggestive of increased D4 strain
Identify predominant D3 vergence direction
Distance from regional granitoids
DISTAL
PROXIMAL
FOLDS
SHEARS
Skarn/Stockwork
DISCORDANT
STRATABOUND
Left-stepping faults, and consequent jogs, bends and steps
SHEARS
STOCKWORKS
LOCALISED GAPING
Identify zones of increased D4 transpression
Identify potential zones of D3 deformation & gaping; Identify zones of increased D4 transpression
Pressure shadows around granites
Left-stepping faults
Restricted to alteration haloes
Identify subsurface granites
Gaping of internal strata
Veining
Auriferous shears along the margins of dolerite dikes in igneous complexes
Vein geometries identified from D4 finite strain ellipse
Identify orientations using finite strain ellipse
D3; preferential gaping of NE limb
D4; preferential reactivation of NW & SE corners
D3; gaping on vertically inclined strata, structures
D4; gaping at contacts between granite and foliated country-rock

Figure 17: Cleavage-bedding relationships that can be used as indicators of D_2 domal fold geometry in the NE Paterson Province. (**A**) Schematic illustration of the various cleavage-bedding relationships around a D_2 antiform for S_1, S_2 (axial-plane cleavage) and S_3. Relationships for D_3 refolding are also illustrated (**iv**), as well as those for a refolded D_1 fold in the anticline core (INSET; (**v**)). All illustrations are looking NW. NOTE: (v) is similar to (i), however, this can be discerned by utilising sedimentary younging information. (**B**) The cleavage relationships in (A; i - v) represented in vertical drill-core intersections; looking NW and down-hole at oriented core. (**C**) Mesoscale fold vergence criteria, incorporating younging direction, for the five fold relationships (i - v) in (A). These folds may be observed on the surface or in drill-core. (**D**) Schematic illustration of how the overprinting relationship between S_1 and S_2 can be used to orient unoriented drill-core utilising the bedding inclination, strike-trend of S_2 and the relationship between S_0, S_1 and S_2 (see explanatory text on figure page). The cleavage relationships can be used to determine the basic bedding direction, which in combination with the strike of S_2 (used as a core reference structure) enables the position on the fold to be determined.

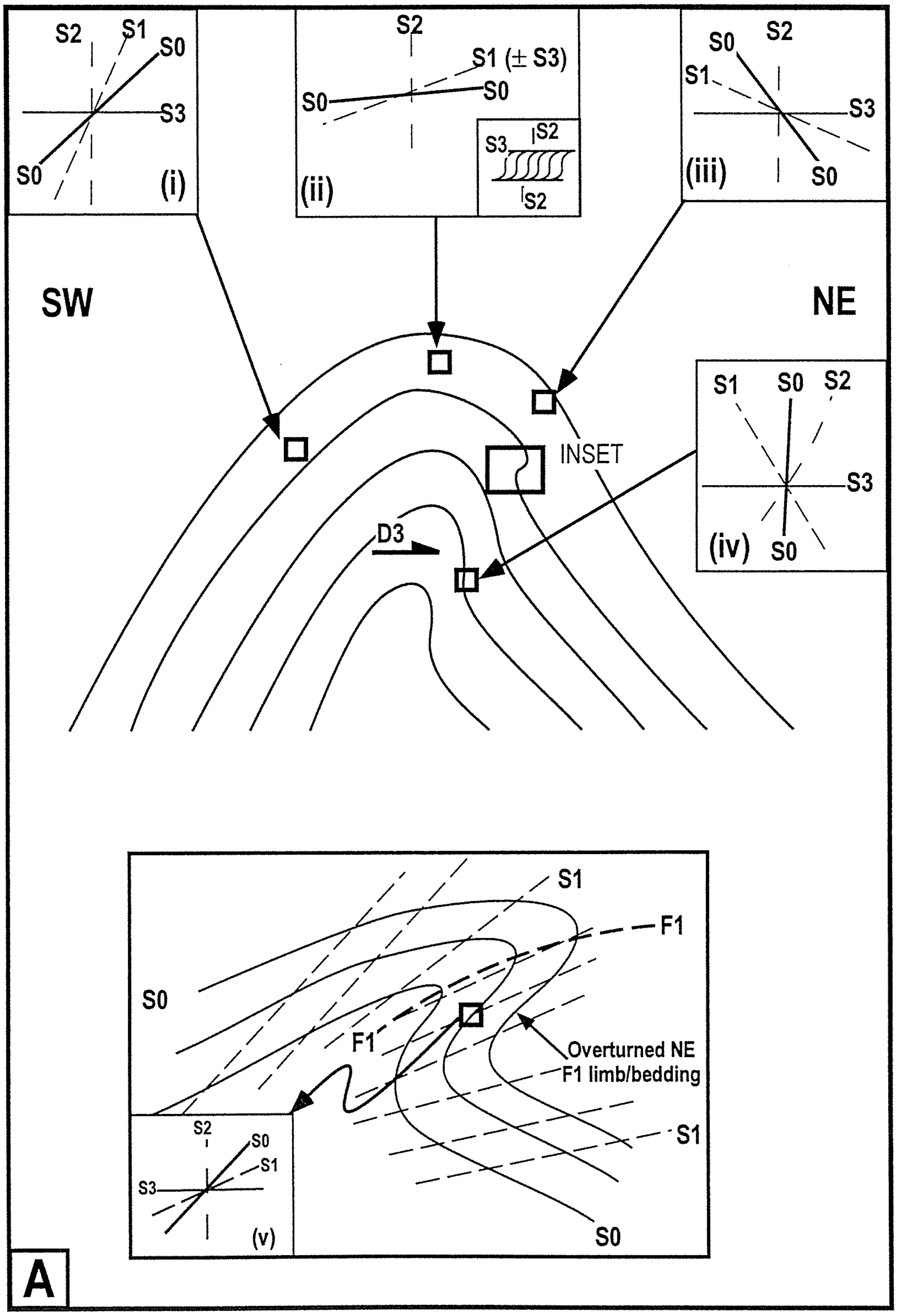

S2
S1
S0
S3
S0
(i)
S2
S1 (± S3)
S0
S0
S3
S2
S2
(ii)
S0
S2
S1
S3
(iii)
S0
SW
NE
S1
S0
S2
S3
(iv)
S0
INSET
D3
S1
F1
S0
F1
Overturned NE
F1 limb/bedding
S1
S2
S0
S1
S3
(v)
S0
A

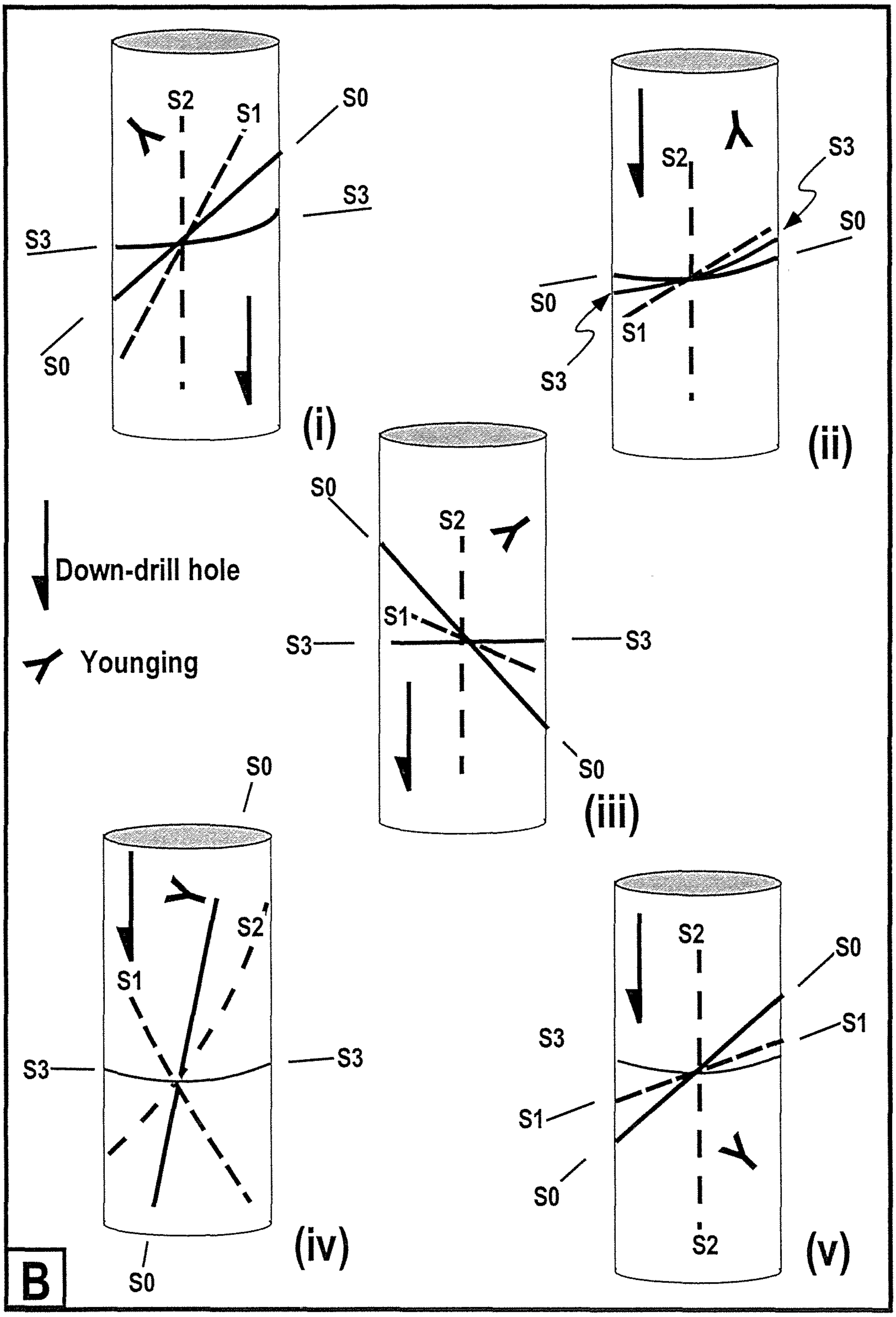
S2
S1
S0
S3
S3
S0
(i)
S2
S3
S0
S0
S1
S3
(ii)
Down-drill hole
Younging
S0
S2
S1
S3
S3
S0
(iii)
S0
S2
S1
S3
S3
S0
(iv)
S2
S0
S1
S3
S1
S0
S2
(v)
B

FIG. 17 Cont.

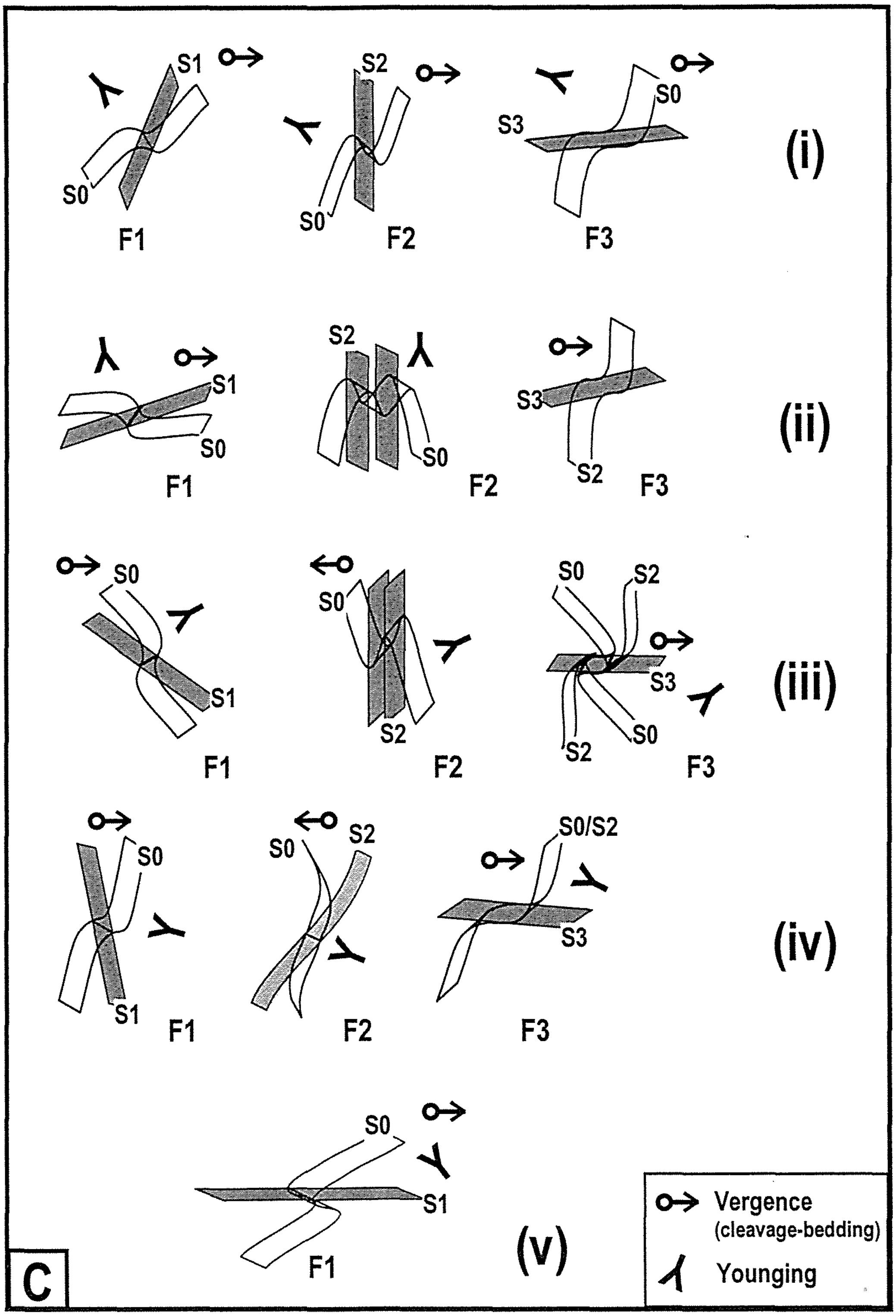

S1
S0
F1
S2
S0
F2
S0
S3
F3
(i)
S1
S0
F1
S2
S0
F2
S3
S2
F3
(ii)
S0
S1
F1
S0
S2
F2
S0
S2
S3
S2
S0
F3
(iii)
S0
S1
F1
S0
S2
F2
S0/S2
S3
F3
(iv)
S0
S1
F1
(v)
Vergence
(cleavage-bedding)
Younging
C

FIG. 17 Cont.

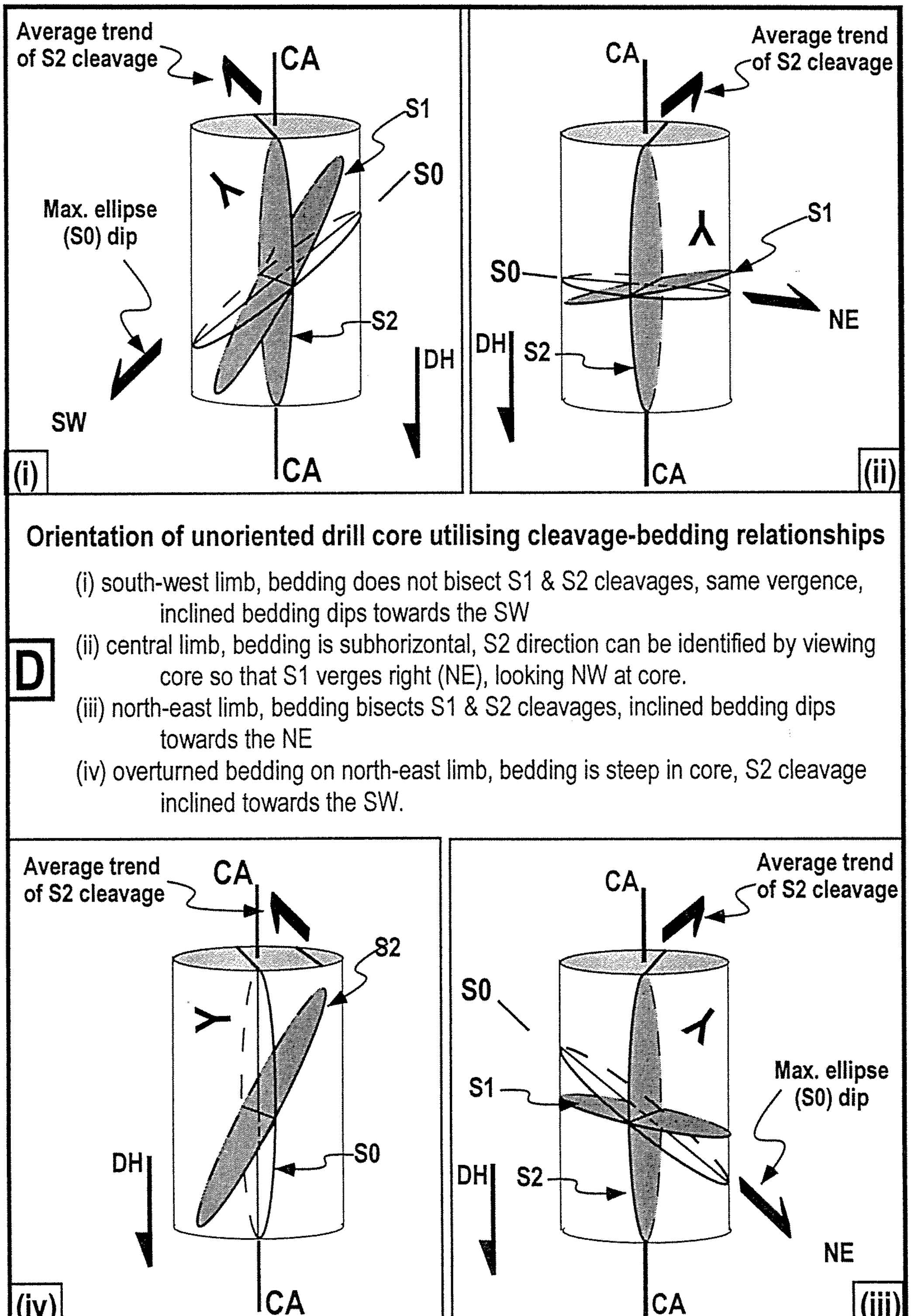

Average trend of S2 cleavage
CA
S1
S0
Max. ellipse (S0) dip
S2
DH
SW
CA
(i)
Average trend of S2 cleavage
CA
S1
S0
NE
DH
S2
CA
(ii)
Orientation of unoriented drill core utilising cleavage-bedding relationships
D
(i) south-west limb, bedding does not bisect S1 & S2 cleavages, same vergence, inclined bedding dips towards the SW
(ii) central limb, bedding is subhorizontal, S2 direction can be identified by viewing core so that S1 verges right (NE), looking NW at core.
(iii) north-east limb, bedding bisects S1 & S2 cleavages, inclined bedding dips towards the NE
(iv) overturned bedding on north-east limb, bedding is steep in core, S2 cleavage inclined towards the SW.
Average trend of S2 cleavage
CA
S2
S0
DH
CA
(iv)
Average trend of S2 cleavage
CA
S0
S1
Max. ellipse (S0) dip
DH
S2
NE
CA
(iii)

FIG. 17 Cont.

Figure 18: Diagrammatic summary map of the contrasting rock unit competencies across the area illustrated in Fig. 1, and their potential bearing on the development of high-D_4 strain corridors in which transpressive deformation would have intensified. Also illustrated are areas of sub-surface granitoid intrusion (as interpreted from magnetic geophysical data) where detachment models produced by opposing shear sense couples (see text for explanation) may occur.

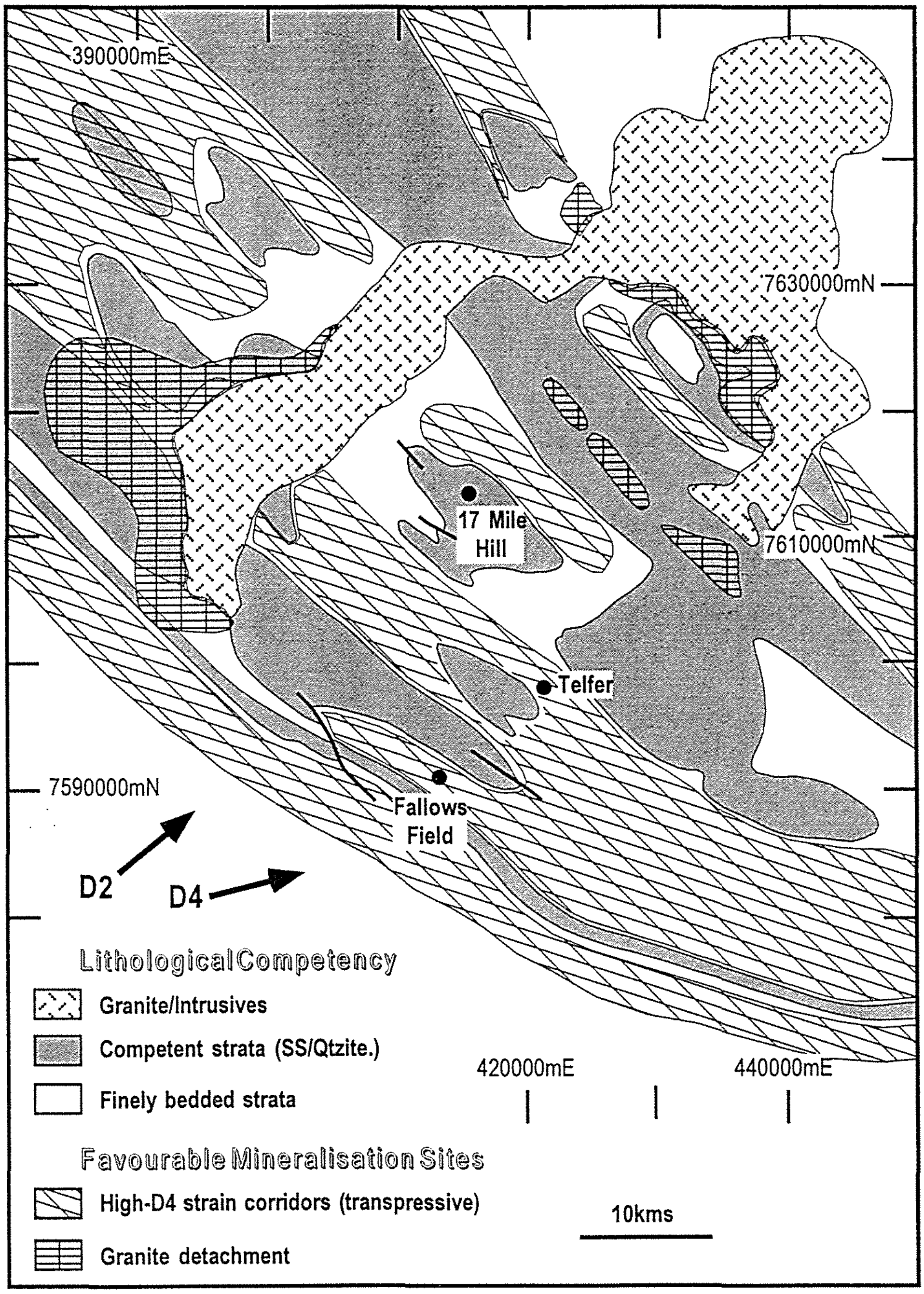
390000mE
7630000mN
7610000mN
7590000mN
420000mE
440000mE
17 Mile Hill
Telfer
Fallows Field
D2
D4
Lithological Competency
Granite/Intrusives
Competent strata (SS/Qtzite.)
Finely bedded strata
Favourable Mineralisation Sites
High-D4 strain corridors (transpressive)
Granite detachment
10kms

Figure 19 : Schematic diagram illustrating the role of macroscale regional folding on ore-fluid movement in dome-hosted deposit development. In all cases ore-fluids appear to rise into anticlinal crests. However, the scale of this is related to the position of such closures with respect to anticlinorium/synclinorium folding. (**A**) Small fold hosted deposits could occur in parasitic antiforms that lie on the NE limbs of anticlinorium (**1**), such as Fallows Field, due to the combined effects of D_3 (gaping) and D_4 on ore-fluid movement. Parasitic antiforms in the hinge of synclinorium (**2**), such as Thompsons, are likely to host only small amounts of mineralisation as ore fluids migrate away and upwards along adjacent anticlinorium limbs. Ore-fluids are likely to migrate to the crests of regional anticlinorium, hence regional domes lying in such positions (e.g. Telfer) could have the potential to host a much larger deposit (**3**). (**B**) Schematic block diagram illustrating the three dimensional ore-fluid migration paths expected in the doubly plunging NW-SE striking domal folds; ore-fluids are likely to rise towards anticlinal culminations along regional antiformal fold axes.

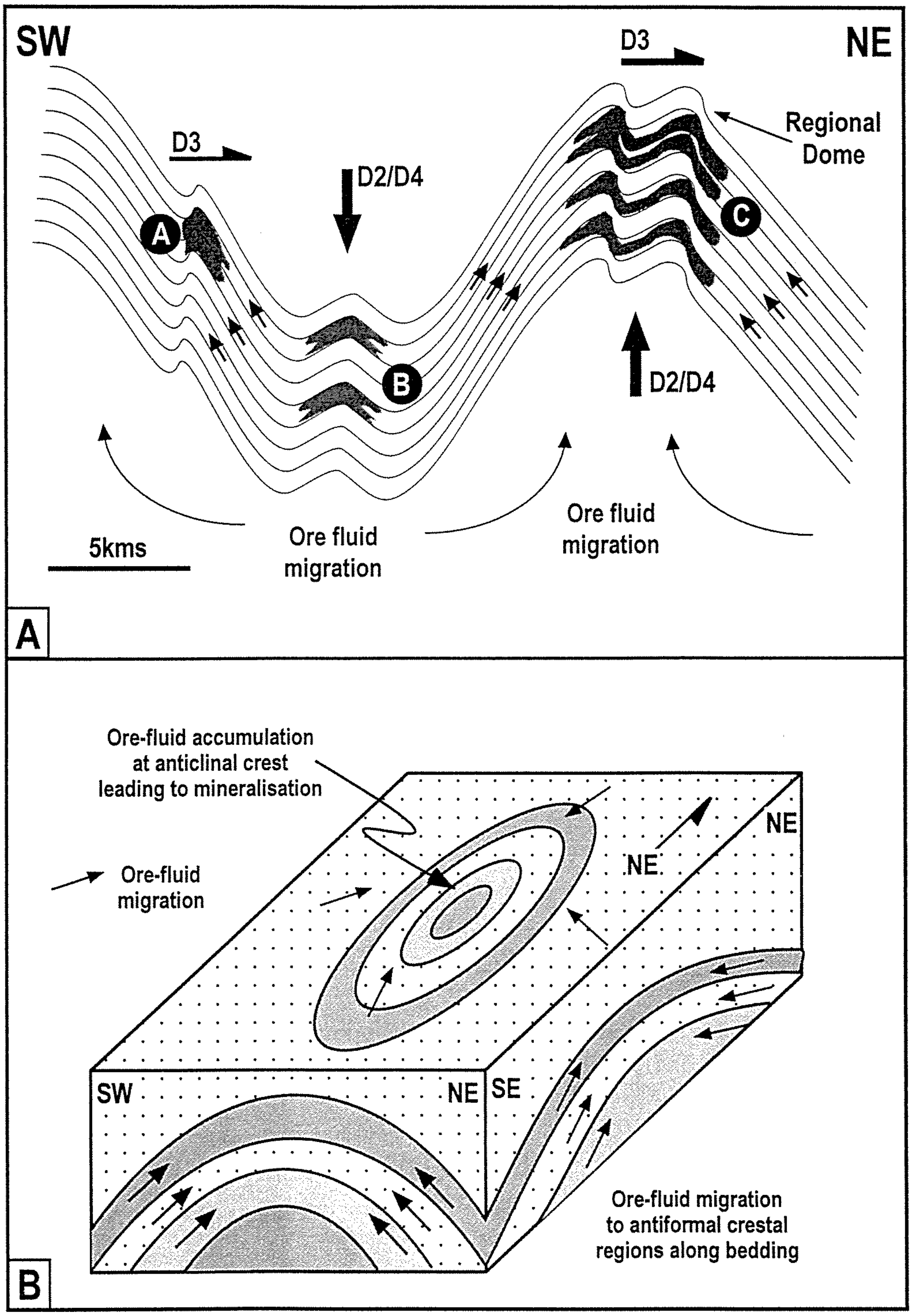
SW
NE
D3
D3
Regional Dome
D2/D4
D2/D4
A
B
C
5kms
Ore fluid migration
Ore fluid migration
A
Ore-fluid accumulation at anticlinal crest leading to mineralisation
Ore-fluid migration
NE
NE
SW
NE
SE
Ore-fluid migration to antiformal crestal regions along bedding
B

Appendix 1

Stereographic Data - Section A

Notes:

1. All planar data represented as poles
2. Plots generated on Stereonet v. 4.9 (© R. Allmendinger)

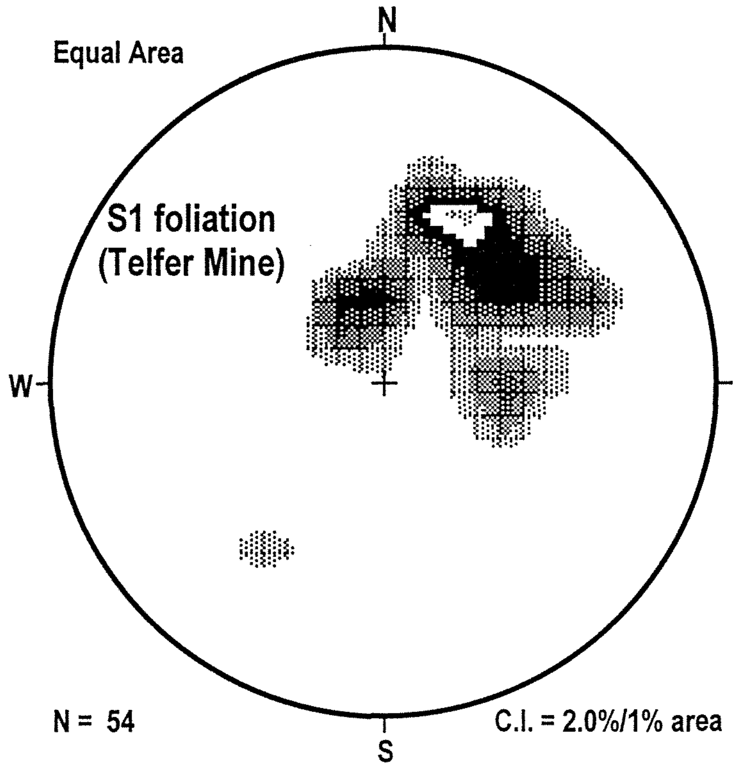
Equal Area
N
S1 foliation
(Telfer Mine)
W
E
N = 54
S
C.I. = 2.0%/1% area

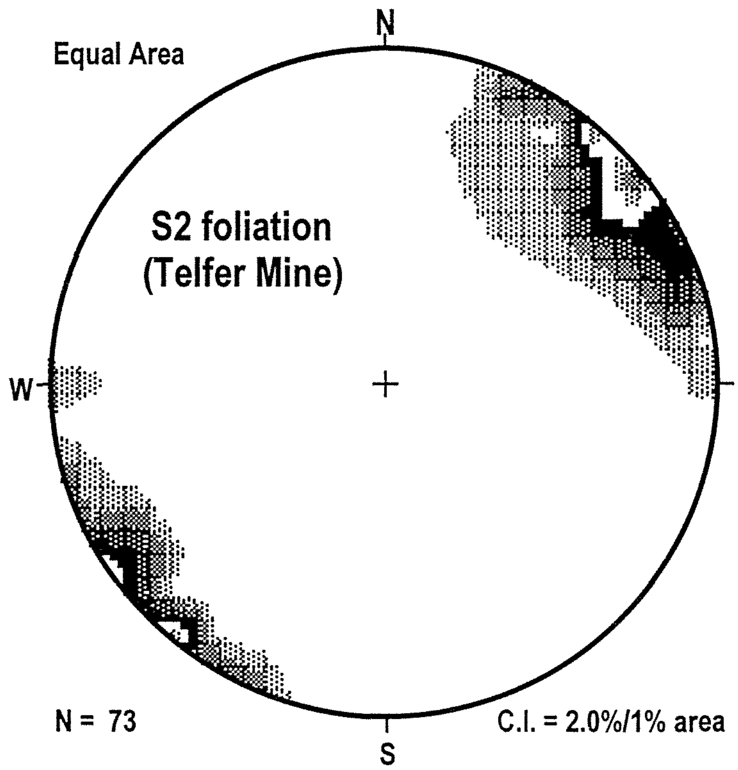
Equal Area
N
S2 foliation
(Telfer Mine)
W
E
N = 73
S
C.I. = 2.0%/1% area

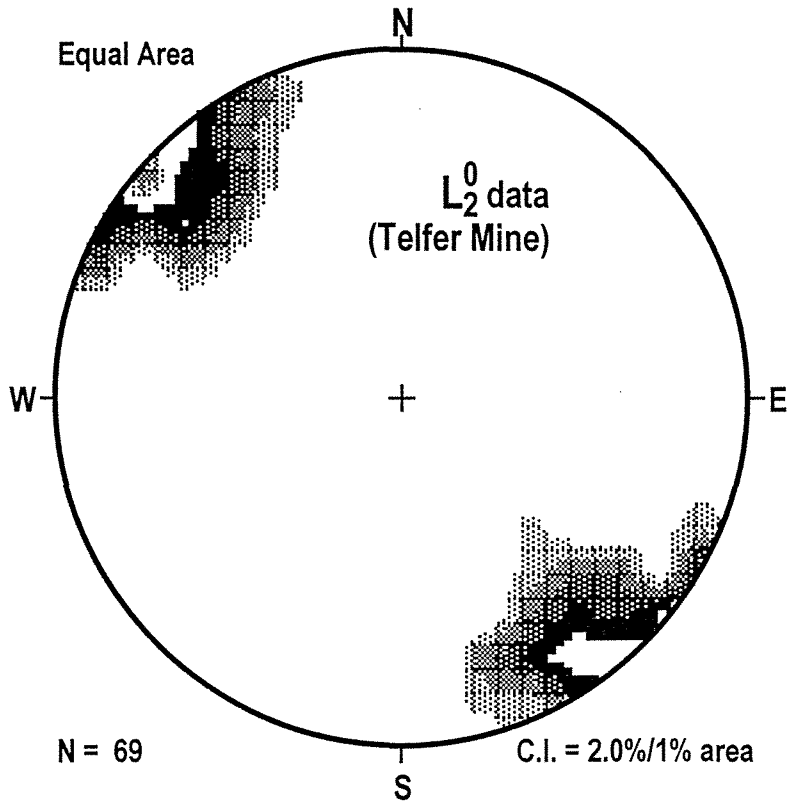
Equal Area
N
L_2^0 data
(Telfer Mine)
W
E
N = 69
C.I. = 2.0%/1% area
S

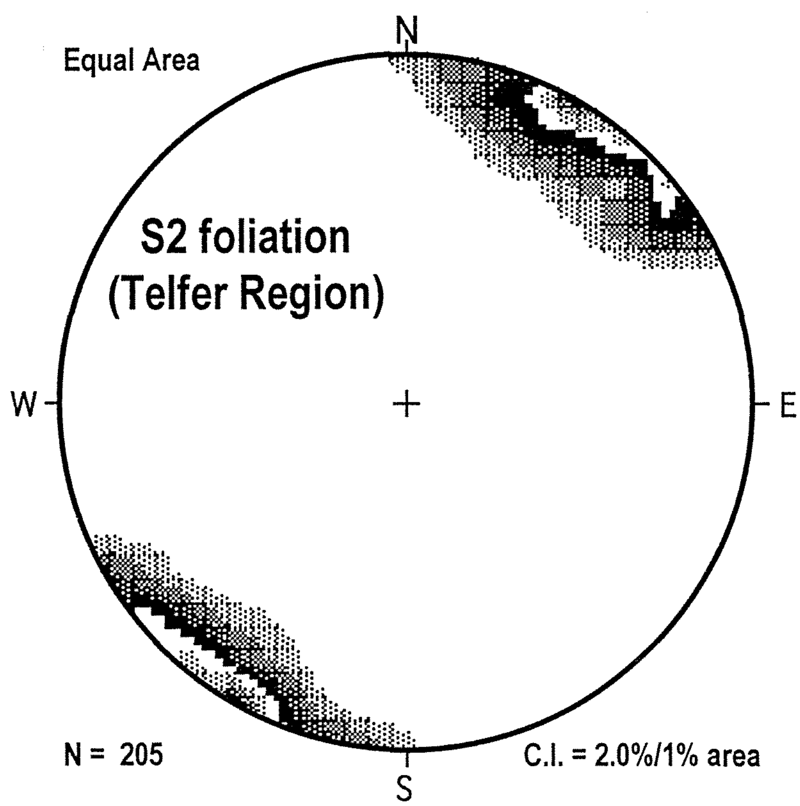
Equal Area
N
S2 foliation
(Telfer Region)
W
E
N = 205
C.I. = 2.0%/1% area
S

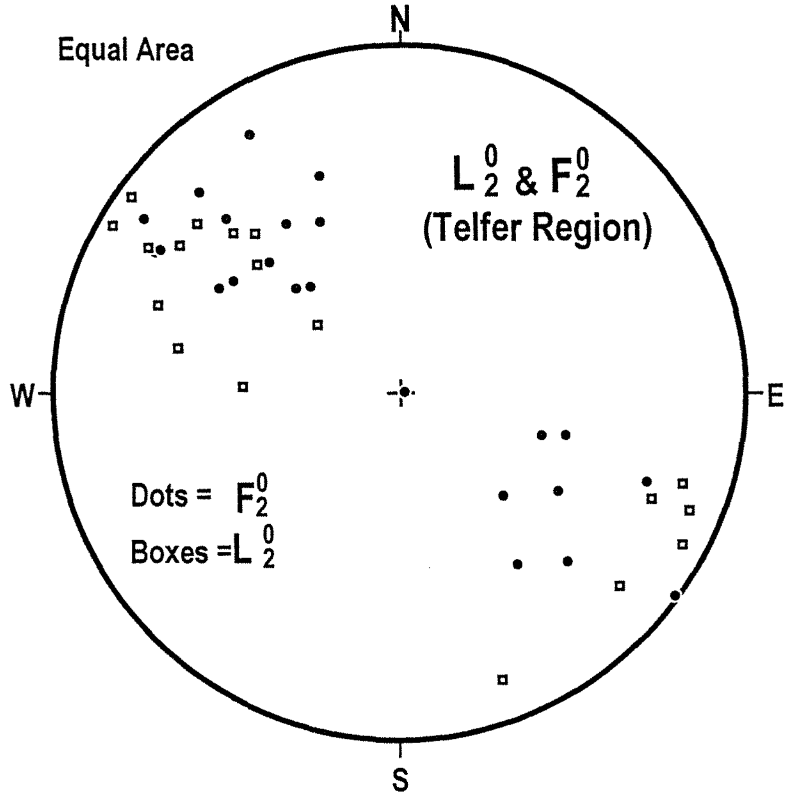
Equal Area
N
L_2^0 & F_2^0
(Telfer Region)
W
E
Dots = F_2^0
Boxes = L_2^0
S

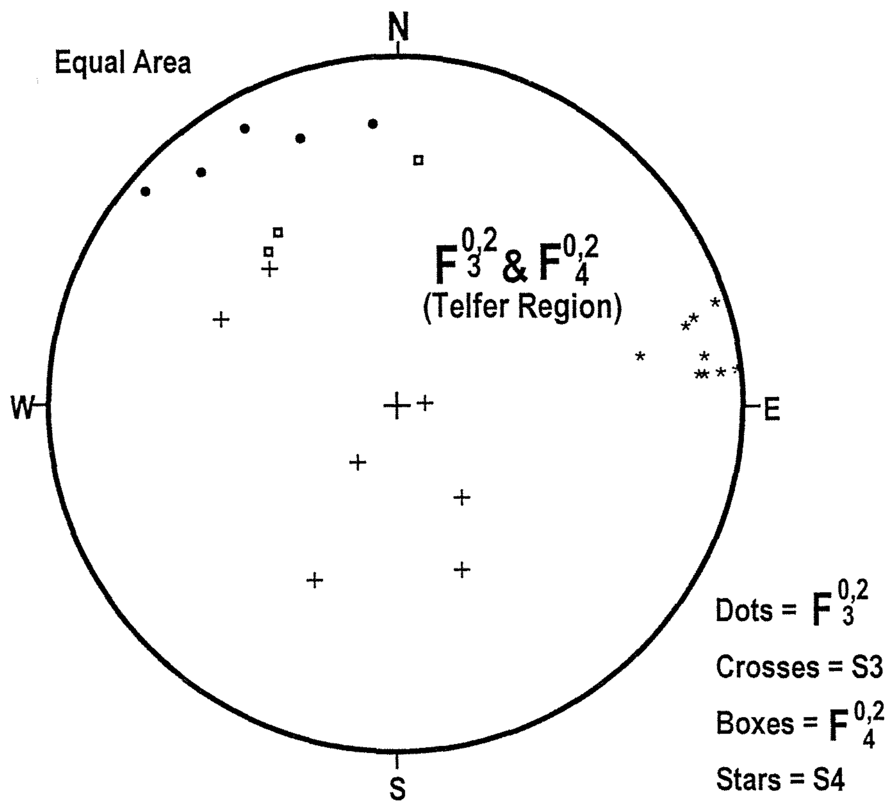
Equal Area
N
$F_3^{0,2}$ & $F_4^{0,2}$
(Telfer Region)
W
E
S
Dots = $F_3^{0,2}$
Crosses = S3
Boxes = $F_4^{0,2}$
Stars = S4

Appendix 2

Field Location Descriptions/Field Sketches

Stereographic Data - Section B

Notes:

1. All planar data represented as poles
2. Plots generated on Stereonet v. 4.9 (© R. Allmendinger)
3. D_6 data too limited to successfully plot/contour

LOCATION DESCRIPTIONS/STRUCTURAL DATA - SECTION B

Location 1 (385152mE 7559418mN)
Massive Coolbro sandstone (micaceous) that lies on the margins of a large anticlinorium overlying the northern end of the Rudall Metamorphic Complex. Bedding dips NE (S_0; 30° → 051°) and contains an early bedding-parallel cleavage/fissility that is overprinted by S_3 (82° → 039°). A possible weak sub-horizontal cleavage overprints S_3.

Location 2 (377011mE 7549951mN)
Steeply dipping trough cross bedded Coolbro sandstone (S_0; 80° → 068°) that is locally strongly cleaved (S_3; 85° → 059°). This cleavage is overprinted by a coarse sub-horizontal weakly differentiated crenulation (S_4; 8° → 352°), with a shear-sense/asymmetry on minor F_4 folds (F_4^0; sub-horizontal → 330°) indicating top-to-the SW tectonic transport. Minor F_6 kink folding with axial planes defined by fine dissolution seams (S_6; 82° → 287°) that overprint S_3 and S_4.

Location 3 (377829mE 7544432mN).
Shallow N-dipping bedding (Coolbro Sandstone) is cleaved by S_3 that is markedly inclined to the SW (S_3; 41° → 020°).

Location 4 (378308mE 7541842mN)
Strongly trough-crossbedded sandstone (Coolbro) dips steeply NE (S_0; 85° → 074°), and is locally overturned. Regional cleavage is vertical (S_3; 90° → 060°).

Location 5 (374289mE 7531975mN)
In Broadhurst Formation on the outer SW margin of the Rudall Inlier, regional folding (F_3) is commonly inclined and overturned (Chin et al, 1980). However, in this location F_3 folds are open and upright. Regional cleavage (S_3; 90° → 055°) is only weakly developed and vertical and the folds plunge shallowly NW (L_3^0; 10° → 328°).

Location 6 (383177mE 7527473mN)
Strongly penetrative regional (S_3) cleavage, in finely fissile Broadhurst Formation, is inclined to the SW (42° → 045°). S_3 is subsequently refolded by F_4 into coarse open monoclinal folds (Fig. A1) with a sub-horizontal axial plane (S_4; 8° → 012°; F_4^3; 8° → 295°). Shear sense on S_4, and vergence on F_4 folds, indicates a top-to-the SW

transport direction. F_4 monoclines are overprinted in their hinges by F_5 crenulations (S_5; 82° → 242°).

Location 7 (383467mE 7526689mN)
Finely fissile Broadhurst Formation exhibits a meso-scale D_4 fold, with a weak coarsely spaced and weakly differentiated axial plane cleavage (S_4; 20° → 028°). The F_4 fold verges NE, consistent with the shear-sense asymmetry on S_4. S_3 is folded around the F_4 fold, and locally is preserved in it's initial vertical orientation within quartz veins that lie sub-parallel to bedding. F_4 folding is both asymmetric and symmetric, the latter suggesting local coaxiality in D_4 at this location. F_4 folds are overprinted by fine vertical D_5 crenulations (S_5; 80° → 065°).

Location 8 (384352mE 7524859mN)
Within transitional units at the Broadhurst-Coolbro Formations contact, bedding dips towards the SW (S_0; 40° → 260°). Regional cleavage (S_3; 28° → 250°, L_3^0; 25° → 260°) dips shallower than bedding indicating that this is an overturned NE limb of a regional F_3 fold (Fig. A2) that is reclined to the NE. This overturning is probably the result of D_4, in which case the tectonic transport for D_4 at this location was top-to-the NE.

Location 9 (392732mE 7519113mN)
A thrust contact between basement (Rudall Metamorphic Complex) and Coolbro Formation (S_0; 57° → 040°). High angle reverse duplex style faults dip steeply towards the NE (Thrust Faults; 70° → 050°) indicating an overall SW directed thrusting motion. These faults cut the regional cleavage (S_3; 85° → 220°) and are therefore either late- or post-D_3. A mineral elongation (stretching) lineation on S_3 (L_3^3; 75°SW on 87° → 205°) plunges steeply down-dip suggesting bulk inhomogeneous tectonic shortening. Weak sub-horizontal crenulations of S_3 are observed (D_4/S_4; 8° → 002°); these exhibit a top-to-the SW vergence/crenulation asymmetry indicating SW directed tectonic transport. D_6 kinking and micro-folding/crenulations overprint everything, and their axial planes are marked by fine dissolution seams (S_6; 72° → 110°, 75° → 102°, F_2^0, F_6^2; 37° → 035°).

Location 10 (388263mE 7518749mN)
Coarse grained Coolbro Sandstone exhibits a very strong sub-horizontal coarsely differentiated crenulation foliation (Fig. A3; 10° → 020°), overprinting an earlier fabric. The sub-horizontal fabric may either be S_4 that overprinted S_3 (Fig. A3-**1**), ***or*** else may be flattened/inclined S_3 that is subsequently re-used by D_4 to produce a

composite S_3-S_4 foliation (Fig. A3 -2). In the latter case, the earlier fabric that is crenned is likely to be S_0 and/or S_2. The sub-horizontal foliation exhibits a top-to-the SW shear sense (crenulation asymmetry).

Location 11 (389830mE 7514827mN)
Similar to the above, medium-coarse grained Coolbro Sandstone in the hinge of an overturned regional anticline exhibits an exceptionally strong sub-horizontal fabric (S_3/S_4 7° → 148°), that is interpreted to be S_3 rotated towards the SW and re-used by D_4 (*e.g.* Fig. A3).

Location 12 (389644mE 7514540mN)
An overturned regional anticline (F_3) in Coolbro Sandstone with a steeply dipping SW limb that is locally overturned (Fig. A4). Folding plunges ≈20° to the NW, and regional cleavage (S_3; 60° → 030°) is markedly inclined. A weak sub-horizontal fabric is also observed (S_4; 27° → 048°) overprinting S_3.

Location 13 (392630mE 7514646mN)
Contact between Coolbro sandstone and Rudall Metamorphic Complex gneisses. The Coolbro Formation exhibits a strong schistosity (S_3?; 40° → 045°) that parallels the thrust contact. Internal porphyroclasts (relict gneiss cobbles) have been strongly shortened and boudinaged. Minor striations on the cobble surface indicate down-dip movement, and small asperities coupled with porphyroclast geometry confirm reverse (top-to-the SW) movement on the zone, which is consistent with the sense of overturning of regional (F_3) folds in the area.

Location 14 (392401mE 7513175mN)
Strong S_3 cleavage, in schistose Broadhurst Formation (S_0; 30° → 002°), is markedly inclined (S_3; 37° → 230) and folded into recumbent monoclinal folds (F_4; *e.g.* Fig. A1), with a sub-horizontal axial-plane. Vergence/shear asymmetry on F_4 folds is top-to the SW, consistent with the dominant F_3 inclination (see below) in the area. These are overprinted by weak upright crenulations (D_5/S_5; 85° → 242°, F_5^0, F_5^3; 40° → 330°). Regional scale folding through this area is moderately to strongly overturned towards the SW, with NE dipping axial planes, and subsequent shearing out of limbs (Fig. A5).

Location 15 (393544mE 7511348mN)
Within a lense of schistose Broadhurst Formation, which is thrust SW and interleaved with Choorun and Coolbro Formations. The formation in this location is extremely

well cleaved by a vertical slaty cleavage (S3; 90° → 015) that is axial plane to tight folds (F_3).

Location 16 (394490mE 7512698mN)
F_3 folding of Rudall gneisses, and gneissic fabric. F_3 folds in this area are markedly inclined and the lower limbs are commonly faulted out (*e.g.* Fig. A5), whilst the upper limbs exhibit lag faults and an overall lower strain.

Location 17 (411409mE 7541376mN)
At the outer edge of the Sunday Creek Syncline, bedding dips NE (S_0; 33° → 041°) and S_3 is markedly inclined (S_3; 38° → 218°). F_3 folding is sub-horizontal (L_3^0; 2° → 320°). A moderate dipping fabric overprints S_3 (S_4; 38° → 218°) and exhibits a top-to-the NE shear sense/asymmetry, that may be, given the inclination of S_4, a result of cleavage reactivation during rotation by D_5 (*e.g.* see also Loc. 20).

Location 18 (413433mE 7541890mN)
Within an anticlinal hinge (S_0; variable, 10° → 070°) in finely fissile Broadhurst Formation, an intense layer-parallel fissility and a low-angle fabric (S_2; 33° → 251°, 22° → 124° in S_0; 24° → 110°) are axial plane to monoclinal folds (D_2/F_2^0; 25° → 110°). These overprint rootless semi-isoclinal intrafolial folds that appear to have formed upright and been rotated by D_2 (see Figure 7 in main text). Both folding events are overprinted by S_3, which is commonly inclined (S_3; 60° → 195°, 72° → 203°)

Location 19 (416448mE 7541870mN)
Within the hinge region of a moderate sized anticline in the Sunday Creek Syncline, a strong fabric sub-parallel to bedding is crenulated by the regional cleavage (S_3; 87° → 042°). Locally, this earlier fabric lies closely parallel to bedding and is near- axial plane to intrafolial isoclinal folds, whose limbs are faulted off along bedding (Fig. A6). These isoclines are similar to those reported by Hickman & Clarke (1993), and are transected by S_3 cleavage. S_3 is overprinted by a coarse weak sub-horizontal folding event (F_4/S_4; 5° → 006°).

Location 20 (417457mE 7543322mN)
Strong S_3 fabric in schistose Broadhurst Formation is locally inclined (S_3; 65° → 043°), and is crenulated by F_4 (S_4; 45° → 241°). S_4 is uncharacteristically inclined, and exhibits a top-to-the NE shear sense. Its moderate dip suggests that a subsequent deformation, for which a crenulation is evident (see below), has rotated S_4 away from flat-lying, with subsequent reactivation of the fabric producing the observed shear

sense (Fig. A7). Consequently the shear sense on S_4 does not represent the true transport direction for D_4. Overprinting S_4 is a weak crenulation, only observed on one limb of the S_4 crenulations. The orientation of this crenulation was unable to be determined. 50m north coarse kink folding (F_6) overprints S_2 (S_6; 90° → 310°). These display a sinistral shear sense across individual kink planes which are marked by dissolution seams.

Location 21 (418217mE 7545044mN)
The outer margin of the Pirkil Anticline, which has an inclined axial plane (≈ 65,70° → NE), where the Broadhurst Formation is thrust SW along the NE dipping limb. The SW limb is locally overturned. S_3 axial plane cleavage is locally crenulated along bedding with an asymmetry consistent with late D_3 fold-limb reactivation. This in turn is overprinted by high-angle thrust faulting indicating that thrusting is late-post D_3. Small kinking/micro-folding (F_6) of the S_0 and S_2 surfaces is also observed, and these have axial planes (S_6; ≈ 70° → 340°) that are marked by fine dissolution seams. These structures, which have a sinistral shear asymmetry, may be related to nearby faulting (Alistair Clarke, pers. comm., 1993).

Location 22 (420044mE 7544969mN)
A low-angle NE dipping thrust surface in Broadhurst Formation is folded by D_3 (S_3; 83° → 028°). Small monoclinal flexures (D_2) appear to be associated with the thrusting phase. These verge NE, and have a strong coarsely spaced axial plane crenulation cleavage (S_2; 6° → 154°) which verges NE. The monoclines overprint small D_1 isoclines that have been rotated from an upright to recumbent orientation by D_2.

Location 23 (420069mE 7545596mN)
Metre scale D_4 folding of S_3 cleavage (F_4/S_4; 15° → 246° - top-to-the SW asymmetry/vergence) is overprinted by a weak sub-vertical open crenulation (D_5/S_5; 70° → 254°). S_3 is markedly inclined in this area (S_3; 20° → 215°).

Location 24 (420482mE 7545581mN)
Within finely fissile and strongly cleaved (S_3) Broadhurst Formation S_3 is inclined (S_3; 50° → 035°) and crenulated by D_4, into recumbent monoclines with a sub-horizontal axial plane (S_4). Crenulation asymmetry suggests a top-to-the SW shear sense, and thus tectonic transport, for D_4. F_4 hinges are overprinted a sub-vertical crenulation/fabric (D_5/S_5; 85° → 040°), which is approximately 15-20° anticlockwise from S_3.

Location 25 (418145mE 7542172mN)

Strong S_3 (S_3; 86° → 052°) cleavage in Broadhurst Formation, is coarsely spaced as a result of overprinting an fissility that is an earlier cleavage sub-parallel to bedding. S_3 has a sub-vertical mineral elongation (L_3^3; 85° → 049°).

Location 26 (419179mE 7540856mN)

Strong sub-vertical regional cleavage (S_3; 87° → 230°) overprints an earlier fabric (S_2; 35° → 047°) that is at a low angle to bedding (S_0; 22° → 057°).

Location 27 (418356mE 7537034mN)

Strongly penetrative sub-horizontal foliation (S_4; 13° → 185°, 3° → 135°) is axial plane to a small flexure (F_4^0; 2,5 → 130,140°) that crenulates bedding and S_3. The F_4 flexure verges, locally, to the NE, however at a meso-scale the overall vergence of D_4 at this location is towards the SW.

Location 28 (420557mE 7538010mN)

Near to the Sunday Creek airstrip, bedding dips NE (S_0; 63° → 045°) and regional cleavage is markedly inclined (S_3; 68° → 217°) and crenulated along bedding (Fig. A8). The shear sense is consistent with bedding reactivation during top-to-the NE directed D_4 deformation (Fig. A8) that would also have rotated S_3 into a shallower orientation. D_5 shortening would also have antithetically reactivated the S3 cleavage, giving the observed shear sense.

Location 29 (420693mE 7539134mN)

Regional antiform (F_3) hinge with finely laminated bedding and sub-vertical axial plane cleavage (S_3; 90° → 030°), the latter which moderately refracts around the closure.

Location 30 (421695mE 7536664mN)

Strongly cleaved Broadhurst Formation (S_3; 84° → 231°) on the SW limb of a syncline (S_0; 36° → 043°) exhibits a sub-vertical mineral elongation (L_3^3; 87°SW on S_3). Subsequent bedding reactivation and crenulation of S_3, with a shear asymmetry different to that expected during D_3, has occurred, and is interpreted to result from rotation and reactivation of the limb during SW directed D_4 deformation (see main text).

Location 31 (422183mE 7535852mN)

Along the SW edge of the Sunday Creek syncline, large quartz blows mark lensoid quartz bodies that are sited along high-angle thrust faults (F_3 axial-plane sub-parallel), which slice up F_3 folds throughout the Sunday Creek syncline. (S_0; 28° → 175°, S_3; 67°→ 214°).

Location 32 (422863mE 7535961mN)

Regional cleavage (S_3; 75° → 223°) has a variable dip, locally becoming markedly inclined to the SW, and crenulating an earlier fabric (S_2; 47° → 067°) that is sub-parallel to bedding (S_0; 42° → 051°). S_2 verges NE in this location. Pieces of float adjacent to outcrop exhibit S_3 cleavage overprinted by a coarse crenulation phase which is at high angle to S_3.

Location 33 (423763mE 7537473mN)

Markedly inclined regional cleavage (S_3; 49° → 243°) in sandy pelitic Broadhurst Formation. F_3 folds are similarly inclined and layering exhibits a prominent fissility comprising bedding and a very low-angle fabric (S_2?). Shear sense relationships along S_3 are consistent with synthetic shearing during D_3 (Fig. A9). The inclination of S_3 towards the NE suggests that it was rotated this way by D_4 deformation, thus suggesting that, at this locality, D_4 had a NE vergence. Subsequent reactivation of the fabric, in its inclined orientation, by renewed D_5 shortening could also contribute to the shear sense observed (Fig. A9). An alternative explanation is that the inclined foliation is actually S_4 rotated away from the horizontal by D_5 and thus subsequently reactivated with an antithetic sense (as for Loc. 20/Fig. A7).

Location 34 (395998mE 7546670mN)

Massive trough cross-bedded Coolbro Sandstone dips NE (S_0; 62° → 050°) and contains small D_2 monoclinal folds (F_2) with a weak axial-plane cleavage (S_2; 35° → 265°) and a moderate W plunge (F_2^0; 25° → 305°). These are overprinted by the regional cleavage (S_3; 87° → 215°).

Location 35 (415253mE 7525102mN)

Outcrop on the way to the Desert Queen Baths, exhibits high-angle SW verging thrusting that is common throughout the Rudall area. This thrusting post-dates crenulation of the regional cleavage (S_3; 86° → 218°, 81° → 035°) along bedding by fold limb reactivation during late-D_3 deformation, and is therefore either late- or post-D_3 deformation.

Location 36 (411643mE 7507755mN)

Outcropping Coolbro Sandstone, part of an outlier within the Rudall Metamorphic Complex, exhibits a markedly inclined S_3 foliation (S_3; 55° → 028°, 53° → 045°, 62° → 038°). Most regional foliation in Yeneena Group sediments within the Rudall Metamorphic Complex is similarly inclined.

Location 37 (425075mE 7515749mN)

Muscovite schist on the margins of the Rudall Metamorphic Complex gneisses, exhibits a strong schistosity (S_3; 81° → 034°, 90° → 210°) that is partially differentiated (*e.g.* stage 3-4 of Bell & Rubenach, 1983). Small fault planes cut S_3, and ductilely crenulate it (Fig. A10). These faults may either be related to a D_4 fabric and were subsequently steepened and reactivated by D_5; or may have initiated as Andersonian-style faults during horizontal D_3/D_5 shortening (Fig. A10).

Location 38 (438256mE 7507995mN)

Medium grained Coolbro Sandstone on the SE end of the Miles Ridge (S_0; 62° → 039°) exhibits an inclined regional cleavage (S_3; 68° → 200°, 61° → 196°, 42° → 200°).

Alistair's Sample

A sample (unoriented cleavage slab) showing three cleavages (Fig. A11). The regional foliation (S_3; main schistosity) is openly crenulated by S_4 (Fig. A11), which lies orthogonal to S_3. S_4 is subsequently overprinted by a further crenulation phase (S_5), evident on one limb of the S_4 crens (Fig. A11). The latter, which is at high angle to S_4, exhibits an approximate angular difference in trend from S_3 of 20°. Sample collected by Alistair Clarke, University of Western Australia.

NOTE:

- *Geographic coordinates for each location are in Australian Mapping Grid (AMG) notation, and were gathered using a global positioning system (GPS - Garmin).*
- *Location numbers do not necessarily reflect the order of examination.*

Figure A1: Recumbent D_4 monoclinal folding of S_3 cleavage (vertical away from the fold) with subsequent overprinting of the flat-limb by vertical D_5 crenulations.

Figure A2: Cleavage-bedding relationships (S_3 dips shallower than bedding) indicating overturning of regional (F_3) folding and S_3, interpreted to occur during sub-horizontal D_4 deformation, which in this example has a NE directed movement.

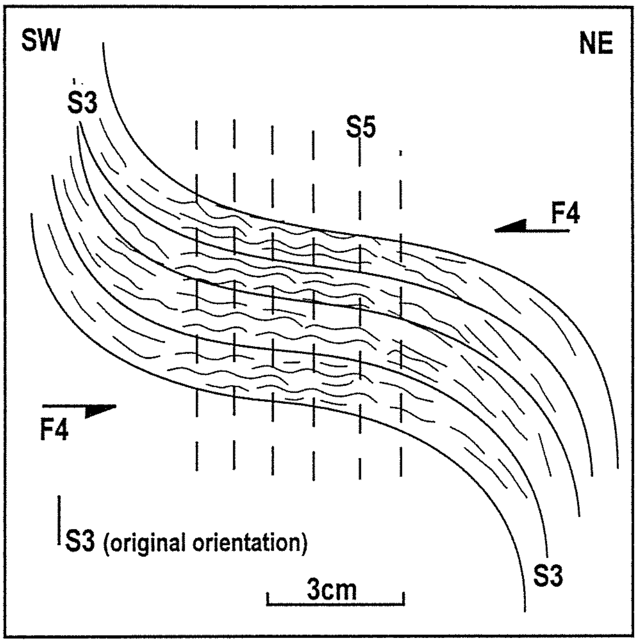
SW
NE
S3
S5
F4
F4
S3 (original orientation)
S3
3cm

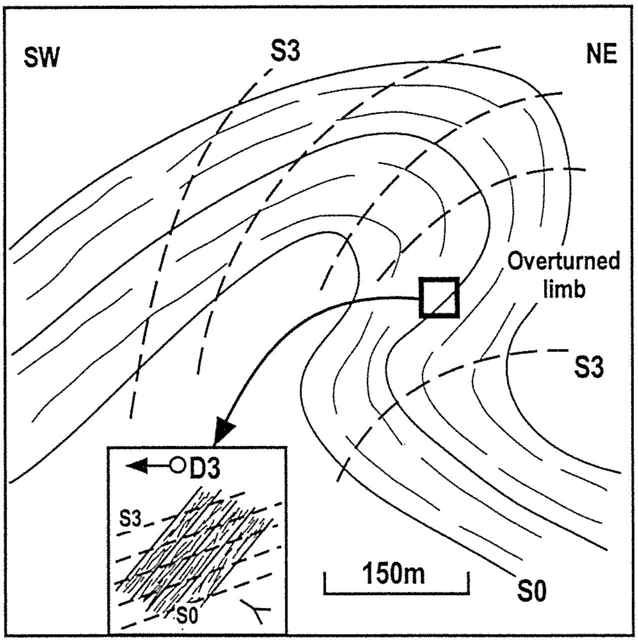
SW
S3
NE
Overturned limb
S3
D3
S3
S0
150m
S0

Figure A3: Two possibilities to explain strong flat-lying coarsely differentiated crenulation cleavage observed in the Coolbro Formation. The fabric may either be S_4 crenulating S_3, which crenulates S_0 and an earlier fabric, probably S_2, (**1**), *OR* could be strongly inclined S_3 which is subsequently reused by D_4 producing a composite S_2/S_4 foliation (**2**).

Figure A4: Inclination of S3 cleavage on the SW limb of an F_3 antiform, with corresponding steepening, and local overturning, of the SW limb.

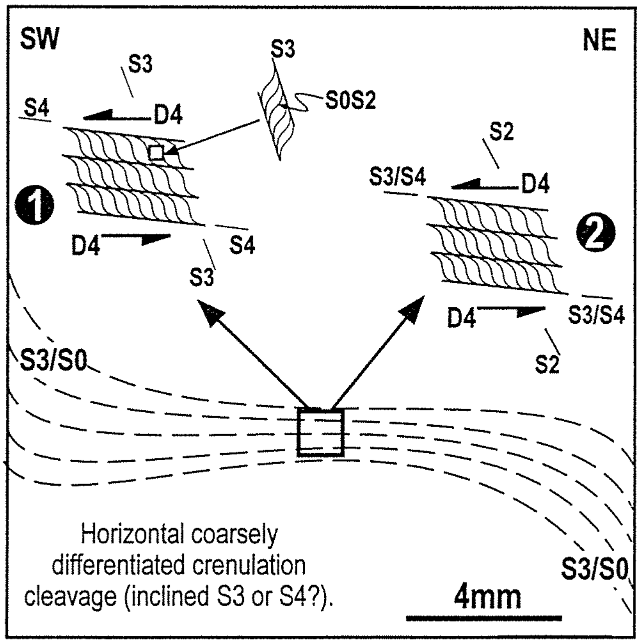
SW
NE
S3
S0S2
S4
D4
S2
S3/S4
D4
1
2
D4
S4
S3
D4
S3/S4
S2
S3/S0
Horizontal coarsely differentiated crenulation cleavage (inclined S3 or S4?).
S3/S0
4mm

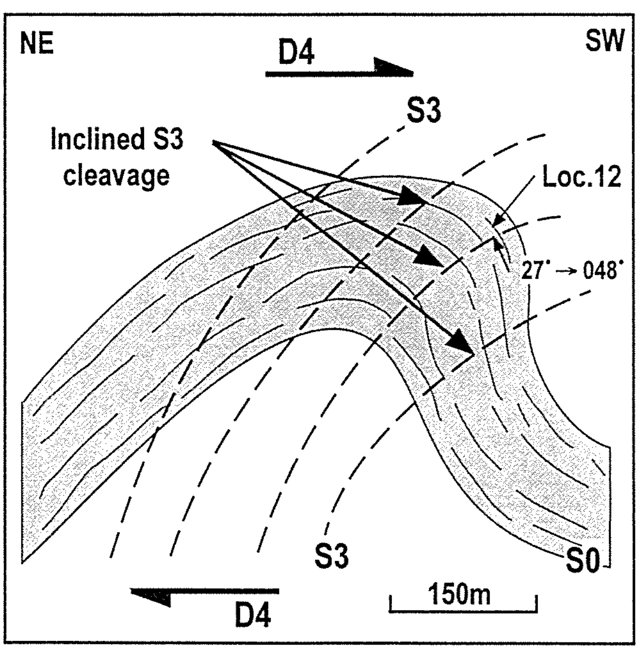
NE
D4
SW
S3
Inclined S3 cleavage
Loc.12
27° → 048°
S3
S0
150m
D4

Figure A5: F_3 fold style, in Yeneena Group sediments, along the south-western margin of the Rudall Metamorphic Complex. Folds are commonly inclined towards the SW with NE dipping axial planes, and leading limbs are often thrust-faulted. Cleavage relations suggest that faulting is either late- or post-F_3 folding.

Figure A6: Rootless intrafolial isoclines observed within graphitic shales in the Broadhurst Formation. In this exposure two differently verging isoclines are faulted off along bedding, the geometry of each suggesting a previous NE verging isocline. The isocline axial planes are near-parallel to bedding which shows a prominent fissility, and the isoclines are overprinted by S_3 cleavage.

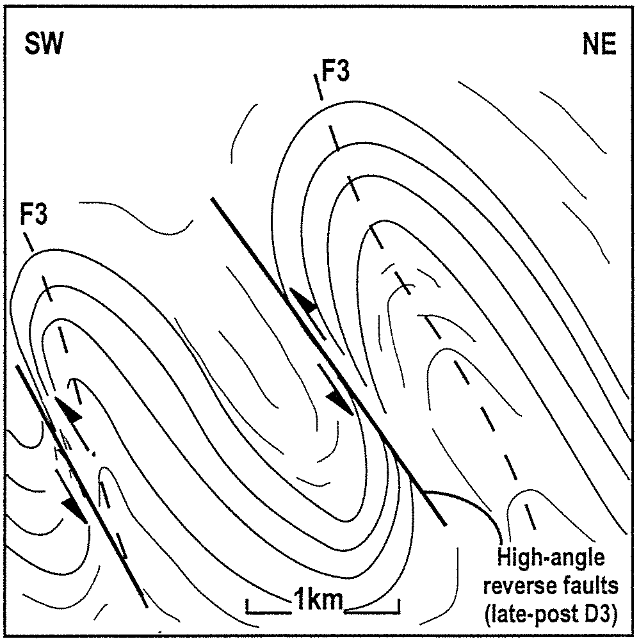
SW
NE
F3
F3
1km
High-angle
reverse faults
(late-post D3)

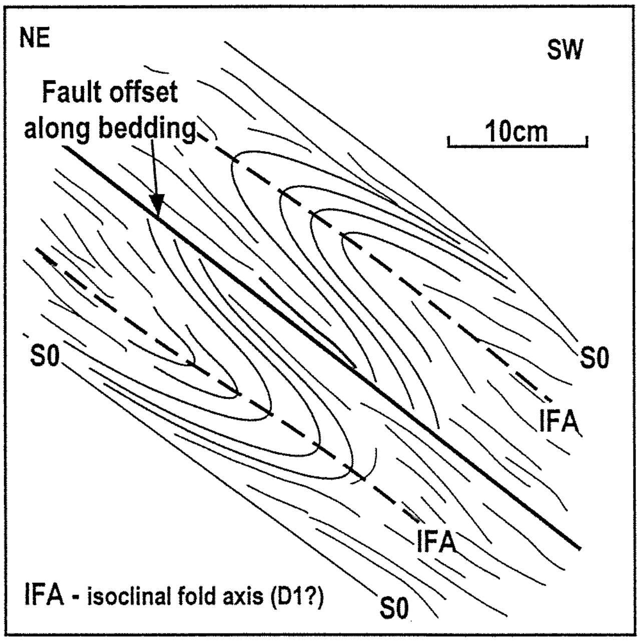
NE
SW
Fault offset
along bedding
10cm
S0
S0
IFA
IFA
IFA - isoclinal fold axis (D1?)
S0

***Figure** A7*: S_4 overprinting S_3 cleavage with a top-to-the NE shear sense on S_4 suggested by crenulation asymmetry. However, S_4 cleavage is markedly inclined, in contrast to most examples which are horizontal, suggesting a latter deformation (D_5? - unoriented crenulations observed in outcrop) may have rotated S_4; in the process reactivating it with an antithetic shear sense (ie. top-to-the NE).

***Figure** A8*: Bedding-cleavage relations suggesting subsequent D_4 deformation. A strong foliation (S_3) cuts bedding, but is inclined, and exhibits crenulation along the S_0 surface. Both can be explained through NE directed D_4 deformation that inclined S_0 and S_3, and caused antithetic reactivation of bedding that crenulated S_3. An alternative explanation is that S_3 was inclined by D_4, with reactivation of the fabric (and S_3 crenulation) during D_5.

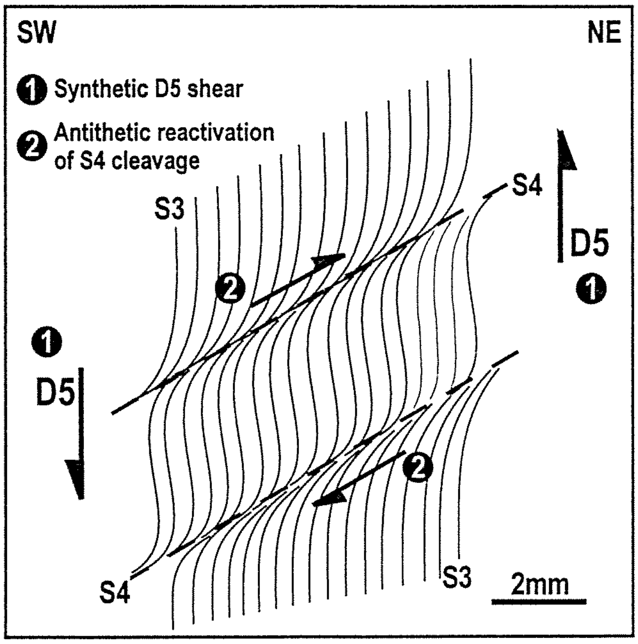

SW
NE
Synthetic D5 shear
Antithetic reactivation of S4 cleavage
S3
S4
D5
S4
S3
2mm

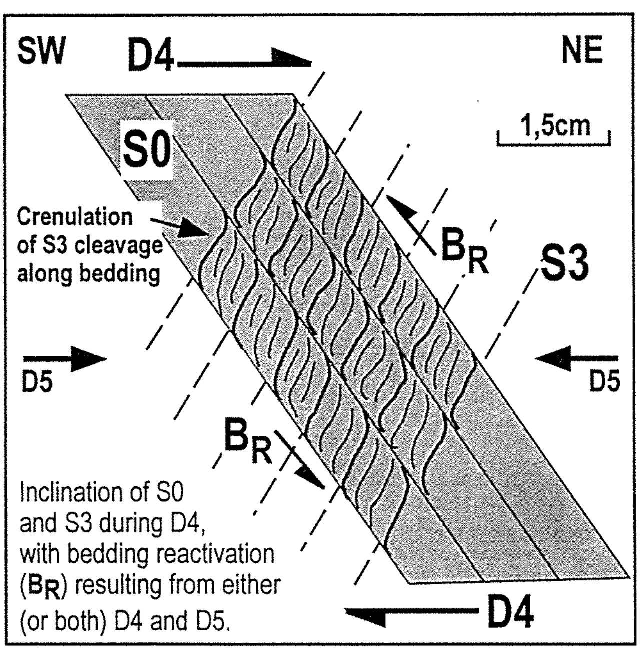

SW
D4
NE
S0
1,5cm
Crenulation of S3 cleavage along bedding
BR
S3
D5
D5
BR
Inclination of S0 and S3 during D4, with bedding reactivation (BR) resulting from either (or both) D4 and D5.
D4

Figure A9: Sketch of cleavage-bedding relations in pelitic Broadhurst Formation at Locality 33. A markedly inclined foliation, interpreted to be S_3, is broadly axial plane to contorted folding. Shear sense relationships across S_3 are consistent with synthetic shear during F_3 folding. S_3 could initially be inclined by D_4, and subsequently reactivated by D_5 with an antithetic shear-sense across the fabric. In this case D_5 folding is at a coarser scale than D_3.

Figure A10: Small inclined fault-planes that crenulate S_3 cleavage. These may form either as Andersonian faults during late D_3 or D_5, or else may nucleate on a pre-existing S_4 fabric, which during inclination by D_5 would reactivate and thus crenulate the S_3 fabric.

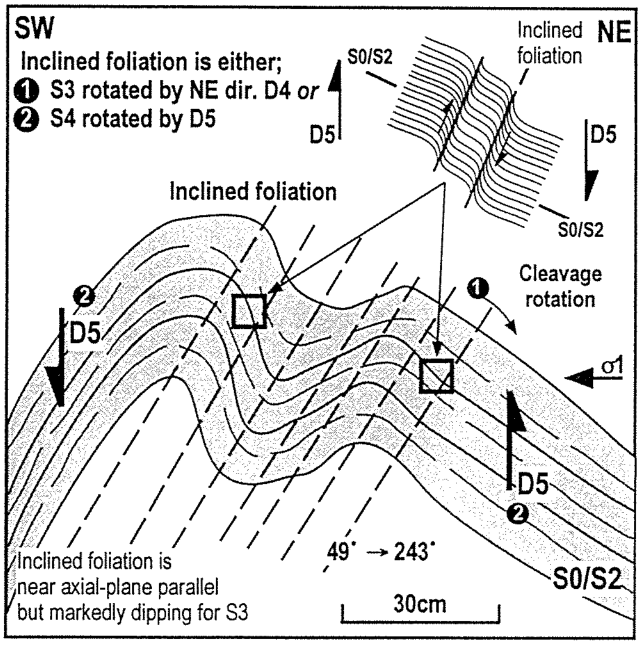
SW
NE
Inclined foliation is either;
1 S3 rotated by NE dir. D4 or
2 S4 rotated by D5
S0/S2
D5
Inclined
foliation
D5
S0/S2
Inclined foliation
Cleavage
rotation
2
D5
1
σ1
D5
2
49° → 243°
S0/S2
Inclined foliation is
near axial-plane parallel
but markedly dipping for S3
30cm

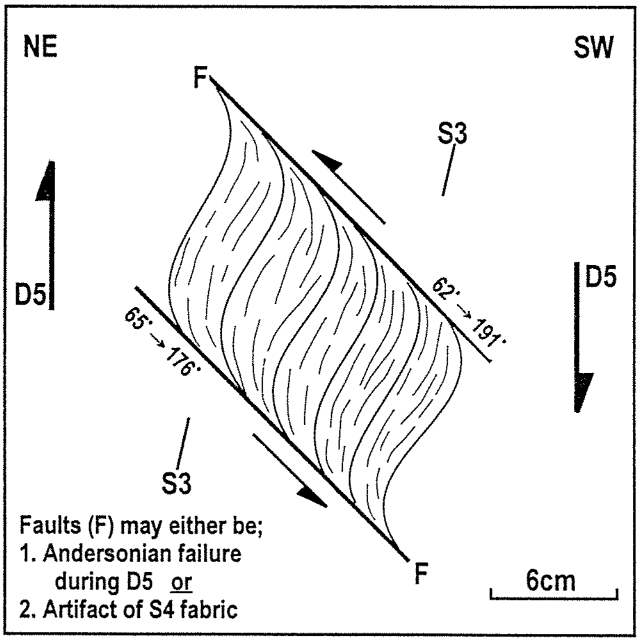
NE
SW
F
S3
D5
62° → 191°
D5
65° → 176°
S3
Faults (F) may either be;
1. Andersonian failure
during D5 or
2. Artifact of S4 fabric
F
6cm

Figure A11: Cleavage (S_3) slab of pelitic Broadhurst Formation, collected by Alistair Clark (University of Western Australia) in the Sunday Creek Syncline. The sample exhibits three overprinting cleavages, suggesting three separate deformation phases. (Line drawing from field photograph; the sample is unoriented).

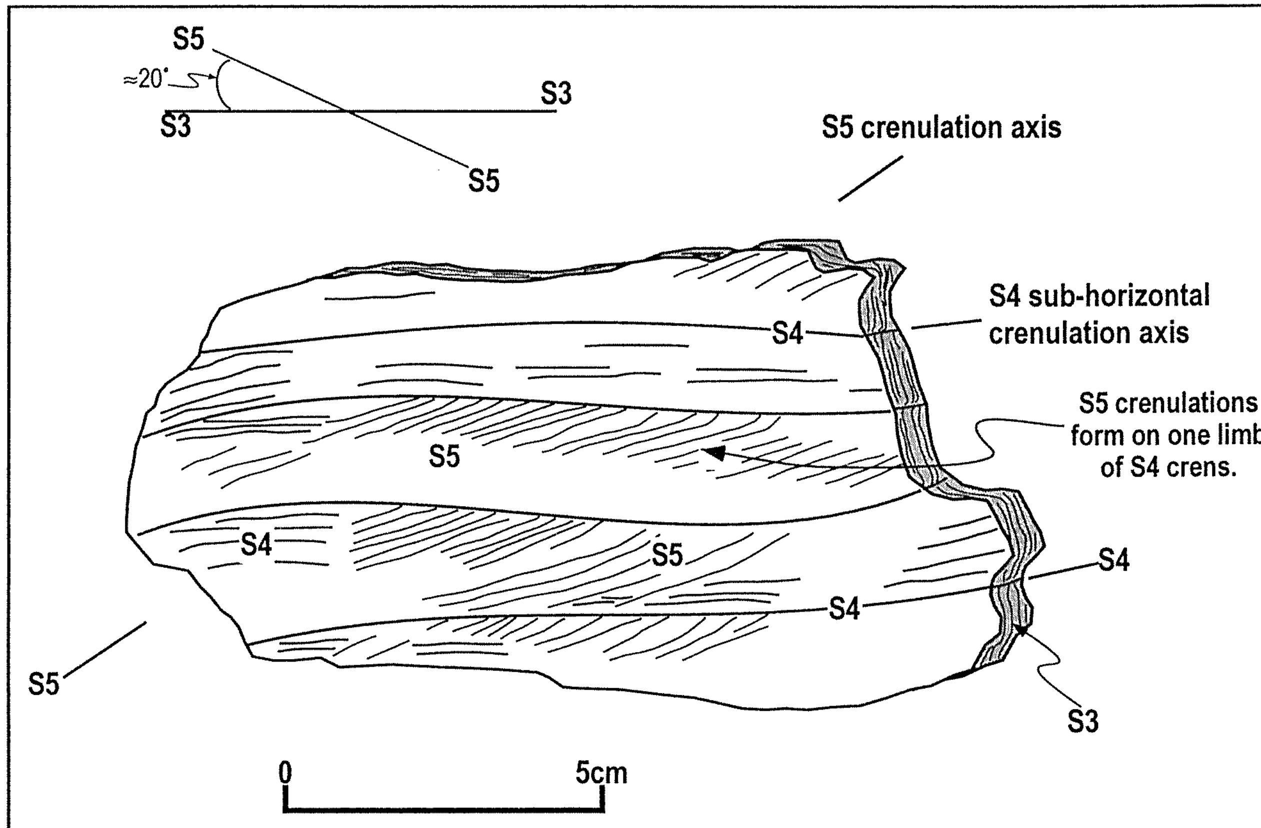
S5
≈20°
S3
S3
S5
S5 crenulation axis
S4
S4 sub-horizontal
crenulation axis
S5 crenulations
form on one limb
of S4 crens.
S5
S4
S5
S4
S4
S5
S3
0
5cm

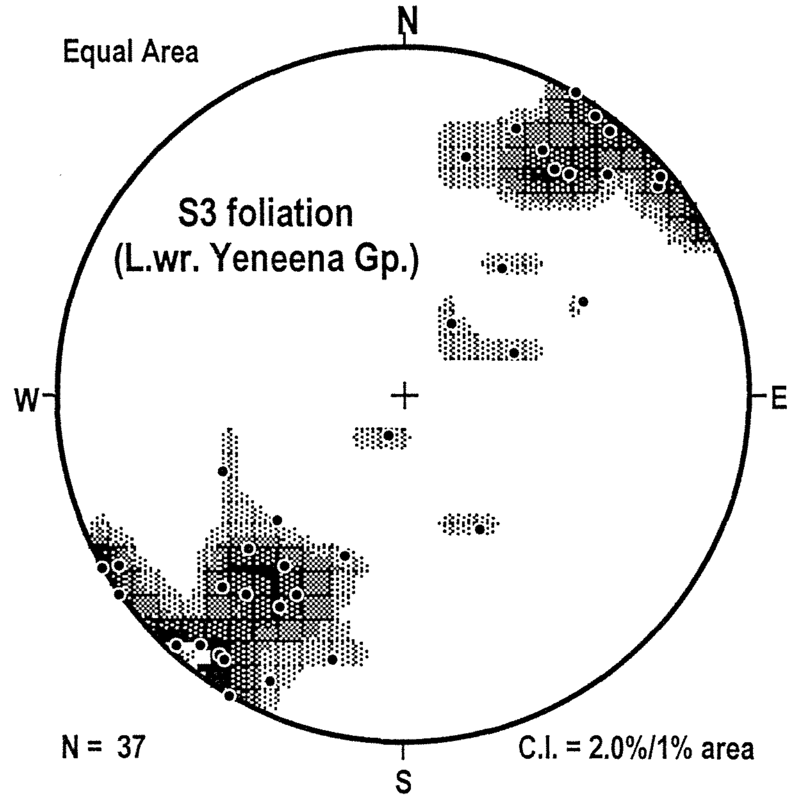
N
Equal Area
S3 foliation
(L.wr. Yeneena Gp.)
W
E
S
N = 37
C.I. = 2.0%/1% area

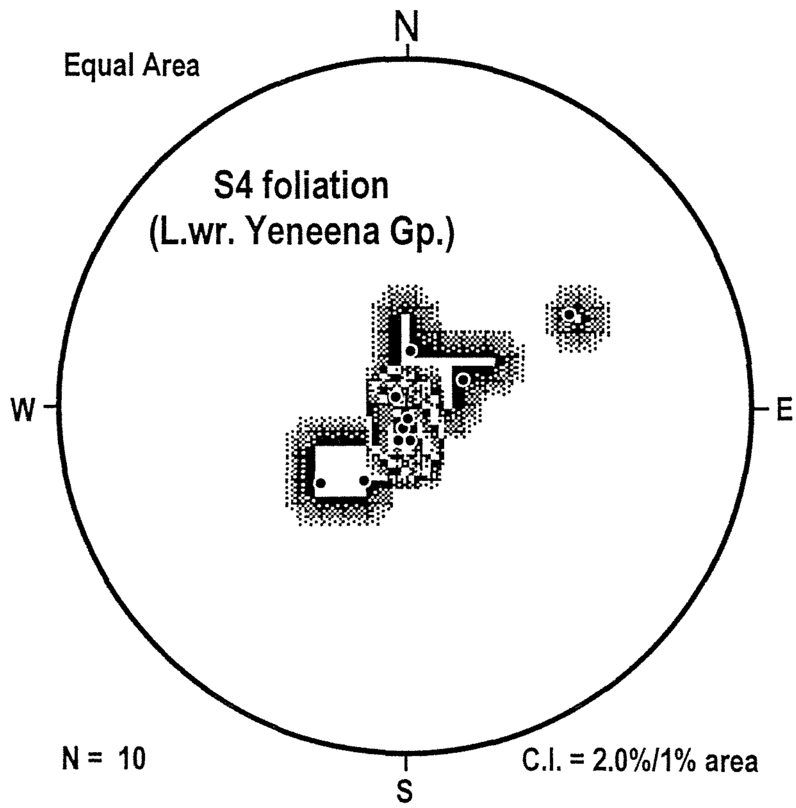
N
Equal Area
S4 foliation
(L.wr. Yeneena Gp.)
W
E
S
N = 10
C.I. = 2.0%/1% area

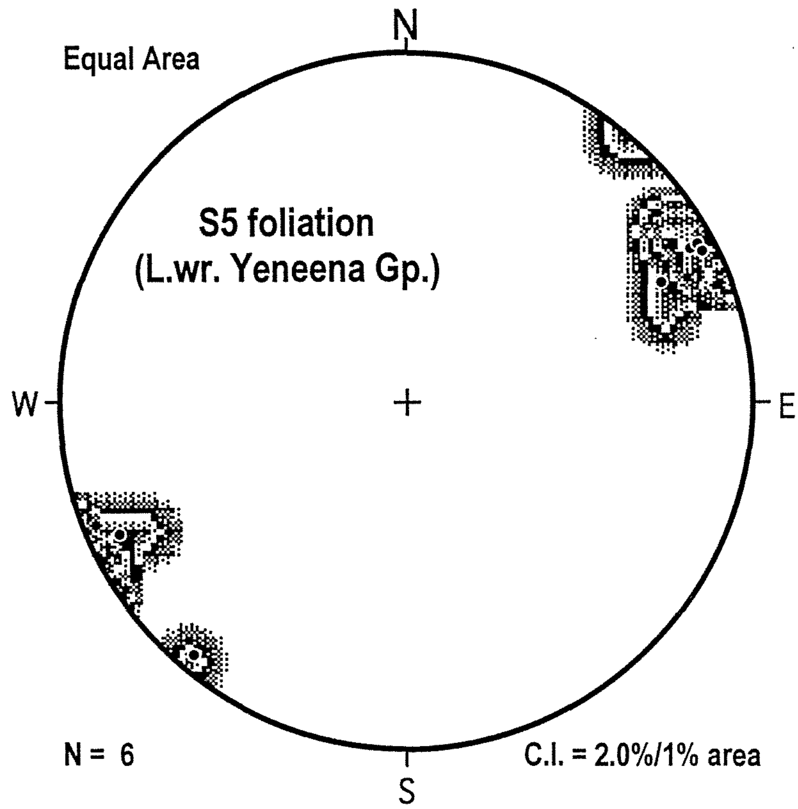

Equal Area
N
S5 foliation
(L.wr. Yeneena Gp.)
W
E
N = 6
S
C.I. = 2.0%/1% area

Appendix 3

Sample Catalogue (referred samples)

Catalogue of Referred Samples

JCU Catalogue No.	Sample No.	Location	Description / Comments
48341	*SH 134-200*	Hinge of a minor anticline Pit 10 - Telfer Mne-14020mN 9100mE	Pelitic unit from the Telfer mine exhibiting coarsely spaced S_1 cleavage. Oriented thin section cut in the vertical plane and trending 020-200°. (Structural notation after Section A).
48342	*R35*	Field Location 22 - Lower Yeneena Group (see appendix 2) (AMG - 7544969mN 420044mE	Sampled from the hanging-wall of a low-angle D_2 thrust fault zone in the Lower Yeneena Group. The thrust developed on the NE margin of the Pirkil Anticline in the Broadhurst Range region. (Structural notation after Section B).
48343	*R5-050*	Field location 24 - Lower Yeneena Group (see appendix 2) (AMG - 7545581mN 420482mE	Finely schistose Broadhurst Formation located in the Sunday Creek Syncline. The prominent schistosity is S_3, the regional foliation that is axial plane to regional folds. The sample shows a penetrative very coarsely spaced (≈ 7-15mm) S_4 crenulation cleavage (Structural notation after Section B).
48344	*R11*	Field Location 7 - Lower Yeneena Group (see appendix 2) (AMG - 7526689mN 383467mE	Finely schistose pelitic Broadhurst Formation on the SW margin of the Rudall Inlier. The sample contains a prominent sub-vertical schistosity (S_0) that is locally crenulated by D_4 with a sub-horizontal axial plane. (Structural notation after Section B).
48345	*R7 - 240*	Field Location 7 - Lower Yeneena Group (see appendix 2) (AMG - 7526689mN 383467mE	Finely schistose pelitic Broadhurst Formation on the SW margin of the Rudall Inlier. The unit is locally folded by D_4, which has rotated both S_0 and S_3 into a shallow dipping orientation resulting in a composite foliation. This prominent shallow-dipping schistosity is overprinted by coarse spaced D_5 crenulation (Structural notation after Section B).
48346	*MVR5-4*	Telfer U/G Operations 6-26 Drive (South end)	Finely laminated siltstone (Middle Vale Siltstone) from the lower margin of the Middle Vale Reef (MVR). Sporadic quartz veining of the MVR overprints the siltstone and in hand specimen has a brecciated appearance. Coarse-grained pyrite aggregates infill and replace the quartz-siltstone host. Fine-grained disseminated pyrite mineralisation occurs in the wallrock. (Orientation Mark is 10-177° (magnetic)).
48347	*MRC 295-1 (2)*	DDH - *MRC 295-1 (Dp. 139m)* Drillhole Coordinates: Mine Grid 12950mN 9600E	Coarse-grained albite-dolomite-quartz veining in the Middle Vale Siltstone underlying the Middle Vale Reef. Vein crystals grow perpendicular to the vein walls. Coarse-grained pyrite infills and replaces the vein assemblage along grain boundaries. The country rock is strongly altered to sericite-muscovite (lime-green colour). There is ≈ 10-20% disseminated pyrite mineralisation in the country-rock; forms include rounded aggregates and sub-hedral grains.

48348	*MRC-P/1*	DDH - *MRC-P (Dp. 105.4m)* Drillhole Coordinates: Mine Grid 11650mN 11900mE	Finely laminated Middle Vale Siltstone (grey -black) containing rhombic dolomite porphyroblasts. The porphyroblasts exhibit a fine core of quartz-sericite. The siltstone contains shale interbeds that are finely cleaved (S_2), and the porphyroblasts overprint this foliation. (Structural notation after Section A)
48349	*MRC 295-2 (2)*	DDH - MRC 295-2 (Dp. 86.4m) Drillhole Coordinates: Mine Grid 12950mN 9800mE	Cross bedded siltstone from the Median Sandstone Member of the Telfer Formation. Shale laminae are overprinted by coarsely spaced S_2, and overprinting this cleavage are fine-grained ovoid quartz-albite aggregates that are commonly replaced by pyrite. Disseminated pyrite mineralisation also occurs in the country-rock; this consists of rounded aggregates, 1-2mm in diameter. (Structural notation is after Section A).
48350	*M10-4*	Telfer U/G Operations M-Reef Exploration Decline (M10 reef- NW face)	The section exhibits the contact between massive reef quartz and siltstone country rock along the lower margins of the M10 reef. Massive quartz veining of the reef is fractured and infilled by grey ferroan dolomite, pyrite and chalcopyrite. The dark grey-khaki coloured siltstone wallrock contains thin veinlets along fractures and is very fine-grained disseminated sulphide mineralisation. (Orientation Mark is 66-114° (magnetic)).
48351	*M30-2*	Telfer U/G Operations M30 reef exploratory cross cut. (M30 Reef)	Dark grey to black, and finely laminated, siltstones of the M30 contain coarse-grained hydrothermal dolomite veins. The dolomite varies from white to white-pink coloured and formed extensional veins along laminae, as well as large aggregates that contain wallrock fragments. The siltstone country rock is extremely hard suggesting that it has been silicified. Two to three stages of hydraulic veining are evident in the sample.
48352	*A8*	DDH - *MRC 120-33 (W1)* (Dp. 823m)	Sampled from a sandstone unit in the Isdell Formation that was drilled into by the Main Dome Deep Drilling program. The sandstone has been extensively veined (coarse-grained quartz - grey ferroan dolomite). Infilling the veins, and replacing the country rock are small aggregates of chalcopyrite and very large aggregates of galena. Chalcopyrite infills and replaces the galena.
48353	*A1*	DDH - *MRC 120-33 (W1)* (Dp. 773.45m)	Finely laminated silty-sandstone unit of the Isdell Formation (drilled into by Main Dome Deep Drilling program). The sandstone is strongly silicified and was replaced by chalcopyrite-galena aggregates.
48354	*M10 - 1*	Telfer U/G Operations. M-Reef Exploration Decline.(M10 reef - NW face).	Massive quartz veining of the M10 reef. The quartz is fractured and infilled by fine-grained grey ferroan dolomite aggregates, as well as anhedral chalcopyrite aggregates. Minor amounts of chlorite formed with the chalcopyrite and occur as green selvedges along sulphide margins. The chalcopyrite aggregates also contain smaller euhedral pyrite grains.

48355	*MRC 295-2 (1)*	DDH - *MRC 295-2* (Dp. 86.4m) Drillhole Coordinates: Mine Grid 12950mN 9800E	Pale yellow-green coloured siltstone unit of the Median Sandstone Member in the Telfer Formation, with lesser interbedded shale units/lenses. The siltstone is weakly cleaved (S_2 is weakly visible in hand specimen). Shale units (dark grey) exhibit a prominent bedding fissility and a low-angle overprinting cleavage, S_3. S_3 is coarsely spaced. Metasomatic quartz-albite aggregates, which are ovoid shaped, overprint the rock matrix. These are replaced by fine-grained sulphides (pyrite mainly). A shale lense is extensively altered to dolomite and contains opaque material that may be graphite. (Structural notation after Section A).
48356	*MVR - 5*	Telfer U/G Operations 6-26 Drive (South end)	Sample of the upper contact of a quartz stringer that lies along the lower margin of the Middle Vale Reef (MVR). Massive quartz veining of the MVR overprints the finely laminated grey-khaki coloured Middle Vale Siltstone host. Coarse-grained pyrite aggregates infill and replace the quartz-siltstone host. Siltstone laminae along the quartz-contact exhibit an undulose character and are replaced by the massive quartz phase. Fine-grained disseminated pyrite mineralisation occurs in the wallrock. (Orientation Mark is 89 - 002° (magnetic)).
48357	*MVR - 8*	Telfer U/G Operations 6-26 Drive (North end)	Large sample from the lower margin of the MVR. The upper half of the specimen comprises massive white-clear quartz of the reef, which is variably infilled by sulphide aggregates that are now largely altered to digenite, with malachite halos. The lower half is the footwall siltstone (Middle Vale Siltstone) which is finely laminated and exhibits small trough cross-beds. The footwall is cut by low-angle faults that have thrust wedges of siltstone into the reef. The siltstone is replaced by disseminated sulphide mineralisation (that is altered to malachite), and contains small argillic veinlets.
48358	*QVN - 3*	Outer Siltstone Member - Main Dome Haul Road (NW end of Pit 7 - Telfer Mne. (12490mN 10150mE)	Sample comprises a piece of a massive-laminar bedding-concordant quartz vein that formed in the Outer Siltstone Member. The vein developed at the contact between a sandstone and siltstone (beds), and is variably massive, or displays thin laminations. The external surfaces of the vein exhibited slickenside and slickenfibre formation. Vein quartz is clear and the crystals are variably anhedral or sub-hedral.

Newcrest Mining Pty Ltd Samples - Held at the Geology Dept., Telfer Gold Mine, Telfer.		
MVR SM-1 MVR SM-2 MVR LSZ-1	Collected by C. Switzer as part of a suite from one location in the Middle Vale Reef (underground workings) that exposed three well defined textural zones. (specific location in the underground unspecified).	SM - 1: Semi massive zone along the upper margin of the Middle Vale Reef; exhibits fine-grained pyrite and granular quartz. SM - 2: Semi-massive pyrite and quartz from the middle of the MVR, exhibiting fine-grained pyrite that forms wispy laminae, with occasional larger rounded pyrites and associated quartz overgrowths. LSZ - 1: Lower zone of the MVR comprising massive white-clear coloured quartz that is fractured and infilled by pyrite-chalcopyrite aggregates.
ST 11	Sampled by S. Hewson from deep diamond drillhole MRC 095. (Dp. 910.7 - 910.8m)	Pervasively altered (sericite-dolomite) silty carbonate unit of the Isdell Formation cut by quartz-sulphide-muscovite veining and alteration.
ST 16	Sampled by S. Hewson from deep diamond drillhole MRC 095. (Dp. 959.4 - 959.5mm)	Coarse grained dolomite aggregate (euhedral crystals) with interstitial sulphides (mainly chalcopyrite).
ST 17	Sampled by S. Hewson from deep diamond drillhole MRC 095. (Dp. 959.85 - 959.9m)	Highly altered (sercite-dolomite) country rock (Isdell Formation) that is cut by fine hairline silica veinlets with associated alteration halos.
ST 18	Sampled by S. Hewson from deep diamond drillhole MRC 095. (Dp. 960.8 - 960.85m)	Altered Isdell Formation exhibiting coarse brecciation comprising large angular clasts supported in a grey-white dolomite matrix.

NOTE: ***Abbreviations***

AMG - Australian Mapping Grid
U/G - Underground
DDH - Diamond Drill Hole
Dp. - Drill hole depth
Mne - Mine